This page was intentionally left in blank


FCT
Fundação para a Ciência e a Tecnologia
MINISTÉRIO DA EDUCAÇÃO E CIÊNCIA


U.PORTO
FACULDADE DE FARMÁCIA
UNIVERSIDADE DO PORTO


imfacts


CESPU
COOPERATIVA DE ENSINO
SUPERIOR POLITÉCNICO
E UNIVERSITÁRIO


Northeastern University
Bouvé College of Health Sciences


INEB
Instituto de Engenharia Biomédica

Ana Vanessa Hortas do Nascimento

Innovative functional polymer therapeutic nanotechnologies for siRNA delivery in lung cancer

Thesis Submitted in fulfilment of the requirements to obtain the PhD degree in Pharmaceutical Sciences, Pharmaceutical Technology Specialty

Tese do 3.º Ciclo de Estudos Conducente ao Grau de Doutoramento em Ciências Farmacêuticas na Especialidade de Tecnologia Farmacêutica

Work developed under supervision of Prof. Dr. Bruno Sarmento and co-supervision of Prof. Dr. Hassan Bousbaa and Prof. Dr. Domingos de Carvalho Ferreira

February, 2016

(Ana Vanessa Hortas do Nascimento)

“'Always Look On The Bright Side Of Life”

by Monty Python

“A longa noite escura é gêmea da manhã“

by João Neiva de Sousa

I dedicate this thesis to the five beloved people
who bravely fought cancer while I was on this journey.

I would like to dedicate it to my best friend A.S., my uncle J.T. and my godfather A.F.,
for teaching me the awesome power of determination.

To my uncle Q.N. and dear D.S., who recently lost her battle,
for teaching me the value of living for the moment, each and every day…
the here, the now…

Acknowledgments

I would like to to acknowledge the Fundação Ciência e Tecnologia (FCT), Portugal, for my Ph.D. grant no. SFRH/BD/69271/2010.

During my stay in Boston, this study was supported by the National Cancer Institute's Alliance for Nanotechnology in Cancer Nanotechnology Platform Partnership (CNPP) grant U01-CA151452.

I also thank to CESPU - Cooperativa de Ensino Superior Politécnico e Universitário (grant #: 02-GCQF-CICS-2011N), from the European Regional Development Fund (ERDF) through the Programa Operacional Factores de Competitividade (COMPETE), to Portuguese funds through FCT in the framework of the project PEst-C/SAU/LA0002/2013, and co-financed by North Portugal Regional Operational Programme (ON.2 - O Novo Norte) in the framework of project SAESCTN-PIIC&DT/2011, under the National Strategic Reference Framework (NSRF).

I would like to thank my supervisor Professor Bruno Sarmento for allowing me to go on this journey. For all the support and commitment to the development of this work, especially since this work was not a smooth ride :)

I would like to express my gratitude to my co-supervisor and my friend for the past 10 years (TIME flies!), Professor Hassan Bousbaa for giving me the opportunity to work in an excellent and stimulating academic environment. I have to thank all his incessant support, willingness, understanding and guidance into this great adventure. Their mentorship always kept me in the right direction and helped me overcome all possible adversities.

To my co-supervisor Professor Domingos de Carvalho Ferreira for believing in my capabilities and for accepting the challenge of participate and supervise this work and the present thesis.

I would like to express my heartfelt gratitude to Professor Mansoor Amiji for his continuous guidance, encouragement, inspiration and assistance. He has been a role model for a scientist, mentor, and teacher for me since I first arrived in Boston.

I am very thankful to the Department of Pharmaceutical Sciences, School of Pharmacy, Bouvé College of Health Sciences at Northeastern University, Boston, USA; Instituto de Investigação e Formação Avançada em Ciências e Tecnologias da Saúde (IINFACTS), Instituto Superior de Ciências de Saúde do Norte (ISCS-N) - Cooperativa de Ensino Superior Politécnico e Universitário (CESPU), Gandra, Portugal, for providing me the wonderful opportunity to join their department as PhD student and for their support to this work.

I would like to express my gratitude to all the people and institutions that receive me, help me and support me during the performance of this work.

To my dear friends in Boston, thank you for all the hospitality and friendship. Thank you for being my home away from home.

Para não correr o risco de me esquecer o nome de alguém vou agradecer no geral. Obrigada a todas as pessoas do grupo orientado pelo Professor Bruno Sarmento, os presentes e os que por cá passaram, pelas inúmeras trocas de impressões, correções e comentários ao trabalho mas também pela diversão e companheirismo.

Cassilda, obrigada pela tua amizade, por estares sempre disponível para me ajudar e por teres sempre uma palavra amiga e positiva nos momentos mais difíceis.

Muito obrigada às meninas do grupo orientado pelo Professor Hassan, "OUR CESPU FAMILY", Nilza, Joana F., Sandra, Joana T., Vânia, mas também a Joana Nunes e Ana Henriques, que sempre foram o meu escape saudável para manter a minha sanidade mental :)

Muito obrigada a todas as pessoas colaboradoras da CESPU que direta ou indiretamente contribuíram para esta tese. Um especial OBRIGADA à Isabel, Paula e Zélia por muito aturarem as minhas maluqueiras e por serem seres humanos incríveis que sempre tiveram disponíveis para me ajudar, seja nos meus pedidos para alguma experiencia mirabolante, seja quando apenas precisava de umas boas gargalhadas…

Muito obrigada à Doutora Elizabete Loureiro pelo apoio incansável e pelas muitas horas de boa conversa, boa disposição a tentar descomplicar a vida :)

Dedico também ao Manu, pois foi o meu pilar durante anos. Acreditou nas minhas capacidades, "empurrou-me" para o Doutoramento mas acima de tudo "empurrou-me" Boston pois sabia que iria ser uma oportunidade única para o meu projeto de doutoramento. Obrigada por tudo.

As pessoas mais importantes da minha vida, a minha FAMÍLIA! Os meus pais, os meus irmãos, a minha irmã, a minha avó e o meu querido avô, que infelizmente já não se encontra entre nós mas que sempre me fez acreditar em mim… Aos meus pais, por todos os sacrifícios e pelo amor ao estudo que sempre me incutiram. Por terem acreditado, desde cedo, que eu podia chegar mais além e me terem ensinado a nunca desistir dos meus sonhos… Por estarem sempre presentes a meu lado, com o seu apoio incondicional e sem os quais seria impossível ultrapassar inúmeros desafios. Se hoje estou a terminar esta tese devo-o a vocês e aos valores que me ensinaram. AMO MUITO

Aos meus Bro´s, Pedro e Artur e Sis, Kidinha, obrigada por me aturarem nos bons e maus momentos pois sei que consigo ser muito chata :) Obrigada pelas palhaçadas, diversão, companheirismo, amizade! Apesar de todas as confusões, discussões e estarmos sempre a pegar uns com os outros são estas coisas que fazem cada um de vocês únicos e é por essa razão que vos AMO MUITO… Kidinha, obrigada por seres a minha confidente, ouvires os meus desabafos e tentares pores algum juízo nesta cabeça…

Dedico também à minha avozinha que na sua inocência me proporcionou muitas gargalhadas, muitas memórias divertidas…Um beijinho enorme BóBó…

Ao longo do meu doutoramento tive a oportunidade de conhecer pessoas fantásticas que me marcaram e que vou recordar para sempre. Foi uma jornada que, como todas as outras na vida, me proporcionou momentos muito bons e momentos muito difíceis. Os momentos bons vão ser recordados para sempre com muito carinho e saudade. Os momentos mais difíceis vão ser recordados com orgulho, pois certamente contribuíram para o meu crescimento pessoal e profissional. Na reta final desta etapa sinto que me tornei numa pessoa mais resiliente, confiante, tolerante e perseverante. Não podia deixar de agradecer a todas as pessoas que contribuíram para o sucesso deste meu percurso.

Existem três pessoas que nunca conseguirei retribuir todo o amor, amizade, carinho e ensinamentos sábios que me dedicaram. Foram o meu suporte quando mais precisei, sempre que precisei… Fosse feriado, domingo, madrugada… Sempre estiveram a meu lado a puxarem por mim e a fazerem-me acreditar em mim mesmo quando eu não acreditava… Não podia estar mais agradecida por ter o privilégio de vos poder chamar de AMIGOS... Amit, João e Patrícia AMO-VOS DE CORAÇAO…

Pati, obrigada por rires comigo nos bons momentos. Obrigada por chorares comigo nos momentos mais difíceis, por enxugares as minhas lágrimas e me dares a mão e mostrares o caminho…

Obrigada a quem me virou as costas, pois hoje sei o seu valor e sou uma pessoa mais forte… Muito obrigada a quem ficou a meu lado durante a tempestade, pois hoje reconheço o verdadeiro valor da amizade e amor…

Obrigada a todos…

Thank you all…

Abstract

Lung cancer is the second common malignancy in both men and women and the leading cause of cancer-related deaths worldwide. More than 220,000 individuals are diagnosed with a form of lung cancer and over 150,000 patients will die of the disease each year. One of the most challenging aspects of lung cancer therapy is the development of multidrug resistance and metastatic dissemination to other parts of the body.

RNA interference has emerged as a powerful strategy in cancer therapy to down-regulate specific genes associated with tumor progression and resistance. Mad2 is an essential mitotic checkpoint component required for accurate chromosome segregation during mitosis, and its complete abolition leads to cell death. However, intracellular delivery of small interfering RNA (siRNA) to specific tumor site is a major challenge that needs to be overcome before this experimental technique can be routinely used as a clinically viable therapeutic strategy.

We have developed an epidermal growth factor receptor (EGFR)-targeted chitosan system for silencing the Mad2 gene as a strategy to efficiently induce cell death in EGFR overexpressing human A549 non-small cell lung cancer cells (NSCLC). EGFR-targeted nanoparticles were formulated and characterized for size, charge, morphology, and encapsulation efficiency. Qualitative and quantitative intracellular uptake studies by confocal imaging and flow cytometry, respectively, showed time-dependent enhanced and selective intracellular internalization of EGFR-targeted nanoparticles compared to non-targeted system. Targeted nanoparticles showed nearly complete depletion of Mad2 expression in A549 cells contrasting with the partial depletion in the non-targeted system. Accordingly, Mad2-silencing induced apoptotic cell death was confirmed by cytotoxicity assay and flow cytometry.

Additionally, the biodistribution of the nanoparticles was assessed qualitatively and quantitatively in cisplatin (DDP) sensitive and resistant lung cancer xenograft model. The targeted nanoparticles showed a consistent and preferential tumor targeting ability with rapid clearance from the plasma to infiltrate and sustain within the tumor up to 96 h. They exhibited a 6-fold higher tumor targeting efficiency compared to the non-targeted nanoparticles.

Furthermore, we investigated the *in vivo* gene knockdown, therapeutic efficacy, and safety profile of the targeted and non-targeted formulations. This system was tested as a single therapy and in combination with cisplatin in drug sensitive (A549-WT) and resistant (A549-

DDP) subcutaneous tumor models of NSCLC. We verified that the combination treatment of cisplatin with siMad2-loaded EGFR-targeted CS nanoparticles delayed the tumor growth significantly in cisplatin-resistant tumors. In addition, this treatment was found to be devoid of toxic effects, as confirmed by the results of the following parameters: body weight gain; biochemical markers of hepatic and renal function; histopathology of liver/kidney/spleen tissues. Collectively, our results highlight the noteworthy potential that this strategy holds promise for the treatment of aggressive cancers.

We believe that the development of efficient and versatile drug delivery platforms to overcome the physical and biological obstacles in cancer therapeutics is an area of great concern, and novel materials are actively sought for such applications. For these reasons, we have designed a nanoparticle system with different functional blocks with that can be "mixed and matched" to attain desired characteristics in a delivery vector. We have applied the combinatorial design to chitosan (CS), where the polymer backbone has been modified with (i) polyethylene glycol, (ii) EGFR-binding peptide, and (iii) lipid derivatives of varying chain length to encapsulate hydrophobic drugs. Cisplatin is one of the most potent chemotherapy drugs broadly administered for cancer treatment. Cisplatin is a hydrophilic drug, and in order for it to be encapsulated in the developed nanosystems, it was modified with lipids of varying chain length. The library of four CS derivatives and six platinum derivatives was self-assembled in aqueous medium and evaluated for physicochemical characteristics and cytotoxic effects in platinum-sensitive and resistant lung cancer cells. The results show that the lipid-modified platinate encapsulation into CS nanoparticles significantly improved cellular cytotoxicity of the drug. In this work, we have also reinforced the idea that CS is a multifaceted system that can be as successful in delivering small molecules as it has been as a nucleic acids carrier.

Keywords: Chitosan nanoparticles, Epidermal Growth Factor Receptor, *mad2* gene, RNA interference, cisplatin, Non-Small Cell Lung Cancer

,

Resumo

O cancro do pulmão é o segundo tumor maligno mais comum em homens e mulheres e a principal causa de mortes relacionadas com cancro em todo o mundo. Mais de 220.000 pessoas são diagnosticadas com uma forma de cancro de pulmão e mais de 150.000 pacientes morrem da doença a cada ano. Um dos aspetos mais desafiadores da terapia contra o cancro de pulmão é o desenvolvimento de resistência a múltiplas drogas e disseminação metastática para outras partes do corpo.

O RNA de interferência tem emergido como uma poderosa estratégia na terapia contra o cancro para regular negativamente genes específicos associados com a progressão do tumor e resistência. Mad2 é um componente essencial do checkpoint mitótico, necessário para a segregação cromossómica durante a mitose, e sua completa abolição leva à morte celular. No entanto, a entrega intracelular de *small interfering RNA* (siRNA) ao local específico do tumor consiste num grande desafio que necessita de ser ultrapassado antes desta técnica experimental poder ser rotineiramente utilizada como uma estratégia terapêutica viável clinicamente.

Desenvolvemos um sistema de quitosano (CS) direcionado para o recetor do fator de crescimento epidérmico (EGFR) para o silenciamento do gene *mad2* como uma estratégia para induzir eficientemente a morte celular em células humanas de cancro do pulmão de não-pequenas células (NSCLC), A549 que sobre-expressam EGFR. Nanopartículas EGFR-dirigidas foram formulados e caracterizadas em termos de tamanho, carga, morfologia e eficiência de encapsulação. Estudos de internalização intracelular qualitativos e quantitativos, por microscopia confocal e citometria de fluxo, respetivamente, demonstraram em função do tempo, uma internalização melhorada e seletiva das nanopartículas EGFR-dirigidas em relação às partículas alvo não-dirigidas. As nanopartículas alvo dirigidas demonstraram depleção quase completa da expressão de Mad2 em células A549 contrastando com a depleção parcial no sistema não-dirigido. Consequentemente, a morte celular por apoptose, induzida pelo silenciamento de Mad2 foi confirmada por ensaio de citotoxicidade e citometria de fluxo.

Adicionalmente, a biodistribuição das nanopartículas foi avaliada qualitativamente e quantitativamente em modelos de cancro do pulmão sensíveis e resistentes à cisplatina (DDP). As nanopartículas alvo dirigidas demonstraram uma capacidade de direcionamento específico e acumulação consistente preferencial pelo tumor com rápida remoção do plasma para o tumor até 96 h. Estas exibiram uma eficiência de direcionamento para o tumor de 6 vezes mais elevada que nanopartículas alvo não-dirigidas.

Além disso, investigou-se o silenciamento genómico *in vivo*, a eficácia terapêutica e o perfil de segurança das formulações alvo e não-alvo dirigidas. Este sistema foi testado como terapia única e em combinação com cisplatina em modelos de tumores subcutâneos de NSCLC sensíveis (A549-WT) e resistentes (A549-DDP) a cisplatina. Verificou-se que o tratamento de combinação de cisplatina com nanopartículas de CS EGFR-dirigidas contendo siMad2 atrasou significativamente o crescimento de tumores resistentes à cisplatina. Além disso, este tratamento demonstrou ser desprovido de efeitos tóxicos, tal como confirmado pelos resultados dos seguintes parâmetros: monotorização do peso corporal; marcadores bioquímicos da função hepática e renal; histopatologia dos tecidos do fígado / rim / baço. Coletivamente, os nossos resultados destacaram o potencial desta estratégia e o facto de que esta consiste numa possível terapêutica promissora no tratamento de cancros agressivos e resistentes.

Acreditamos que o desenvolvimento de plataformas eficientes e versáteis para a entrega de fármacos para superar os obstáculos físicos e biológicos na terapêutica contra o cancro é uma área de grande preocupação, e novos materiais são ativamente procurados para tais aplicações. Por estas razões, projetamos um sistema de nanopartículas com diferentes blocos funcionais para que pudessem ser "misturados e combinados" para atingir as características desejadas como vetor de entrega. Aplicou-se o desenho combinatório ao quitosano, em que a espinha dorsal do polímero foi modificada com (i) polietilenoglicol, (ii) péptido de ligação ao EGFR e (iii) derivados de lípidos de cadeia de comprimento variável para encapsular fármacos hidrofóbicos. A cisplatina, é um dos quimioterápicos mais potentes e amplamente administrados no tratamento do cancro. A cisplatina é um fármaco hidrofílico, e para que ele a ser encapsulado nos nanosistemas desenvolvidos, esta molécula foi modificada com lípidos de cadeia de comprimento variável. A biblioteca de quatro derivados de CS e seis derivados de cisplatina foi quanto às características físico-químicas e os efeitos citotóxicos em células sensíveis e resistentes à cisplatina de cancro do pulmão. Os resultados demonstram que o encapsulamento de cisplatina modificada com lípidos em nanopartículas de CS melhorou significativamente a citotoxicidade celular do fármaco. Neste trabalho, queremos também reforçaram a ideia de que o CS é um sistema multifacetado que pode ser tão bem sucedido na entrega de pequenas moléculas como tem sido como de ácidos nucleicos.

Palavras-chave: Nanopartículas de quitosano, recetor do fator de crescimento epidérmico, gene *mad2*, RNA de interferência, cisplatina, cancro do pulmão das não pequenas células

Table of Contents

ACKNOWLEDGMENTS VII

ABSTRACT XI

RESUMO XIII

TABLE OF CONTENTS XV

LIST OF FIGURES XIX

LIST OF TABLES XXIII

LIST OF ABBREVIATIONS XXV

THESIS OUTLINE AND ORGANIZATION XXVII

CHAPTER 1: STATE-OF-ART 1

NON-SMALL CELL LUNG CANCER (NSCLC) 3

1. INTRODUCTION 3

2. CURRENT MOLECULAR TARGETS FOR NSCLC THERAPY 5

MITOSIS 16

1. CELL CYCLE 16

2. MITOSIS 17

3. KINETOCHORE TO MICROTUBULE ATTACHMENT 18

4. MITOTIC REGULATION 19

5. MITOTIC CHECKPOINT AND CANCER 24

RNA INTERFERENCE 29

1. INTRODUCTION 29

2. RNAI MECHANISM 29

3. RNAI VERSUS ANTISENSE APPROACH 31

4. SIRNA VS. SHRNA 31

5. RNAI-BASED ANTI-CANCER THERAPY 32

6. CHALLENGES OF RNAI AS THERAPEUTIC PLATFORM 35

7. CHITOSAN-BASED NANOSYSTEMS 37

CHAPTER 2: OBJECTIVE AND SPECIFIC AIMS 41

CHAPTER 3: *IN VITRO* MAD2 CHECKPOINT GENE SILENCING USING EGFR-TARGETED CHITOSAN NANOPARTICLES IN NON-SMALL CELL LUNG CANCER MODEL 45

1. INTRODUCTION 47

2. EXPERIMENTAL METHODS 49

2.1 Materials 49

2.2 Synthesis of Chitosan Derivatives 50

2.3. Preparation and Characterization of siRNA-Encapsulated Chitosan Nanoparticles 50

2.4 Stability of Chitosan-siRNA Nanoparticles 51

2.5 Cell Culture and Transfection 52

2.6 Qualitative Analysis of Cellular Trafficking By Confocal Microscopy *52*
2.7 Quantitative Cellular Uptake Studies by Flow Cytometry *53*
2.8 Assessment of EGFR-Specific Cellular Internalization *53*
2.9 In Vitro Gene Silencing Efficiency *54*
2.10 Determination of Mad2 Protein Expression Levels by Flow Cytometry *55*
2.11 Cell Viability Analysis *55*
2.12 Data Analysis *55*
3. RESULTS 55
3.1 Characterization of siRNA Encapsulated CS Nanoparticles *55*
3.2 Stability against Rnase digestion *61*
3.3 Qualitative analysis of nanoparticle uptake and cellular trafficking *61*
3.4 Quantitative cellular uptake by flow cytometry *62*
3.5 Evaluation of targeted receptor internalization *64*
3.7 In vitro Mad2 gene silencing in A459 NSCLC cells *66*
3.8 Determination of Mad2 protein levels in A549 NSCLC cells *67*
3.9 cell viability analysis with siRNA-encapsulated CS nanoparticles *67*
3.10 cellular apoptosis studies with siRNA-encapsulated CS nanoparticles *70*
4. DISCUSSION 72
5. CONCLUSIONS 76

CHAPTER 4: BIODISTRIBUTION AND PHARMACOKINETICS ANALYSIS OF EGFR-TARGETED CHITOSAN NANOPARTICLES FOR DELIVERY OF MAD2 SILENCING SIRNA IN DRUG SENSITIVE AND RESISTANT NON-SMALL CELL LUNG CANCER MODELS 79

1. INTRODUCTION 81
2. MATERIALS AND METHODS 83
2.1 Materials *83*
2.2 Cisplatin sensitive and resistant cell lines and tumor models *83*
2.3 Synthesis of chitosan derivatives *84*
2.4 Chitosan labeling with NIR dye for in vivo imaging *84*
2.5 siMad2-loaded chitosan nanoparticles *85*
2.6 Whole body and ex vivo NIR imaging *85*
2.7 Quantitative analysis of siMad2 in blood and tissues *86*
2.8 Quantitative pharmacokinetic analysis *86*
2.9 Data analysis *87*
3. RESULTS AND DISCUSSION 87
3.1 Whole body and ex vivo qualitative biodistribution studies *87*
3.2 Plasma pharmacokinetic analysis *90*
3.3 Tumor and other tissue pharmacokinetic analysis *92*
3.4 Evaluation Of The Tumor Targeting Efficiency *96*
4. CONCLUSIONS 97

CHAPTER 5: OVERCOMING CISPLATIN RESISTANCE IN NON-SMALL CELL LUNG CANCER WITH MAD2 SILENCING SIRNA DELIVERED SYSTEMICALLY USING EGFR-TARGETED CHITOSAN NANOPARTICLES 99

1. INTRODUCTION 101
2. EXPERIMENTAL SECTION 103
2.1 Materials 103
2.2 Cell Lines 104
2.3 Synthesis and characterization of pegylated chitosan and epidermal growth factor receptor-targeted chitosan derivatives 104
2.4 Nanoparticle formulation and characterization 105
2.5 In vitro cytotoxicity studies for cisplatin in combination with siRNA therapy 105
2.6. Human Lung Adenocarcinoma Xenograft Tumors 106
2.7 In vivo mad2 gene knockdown in A549 WT and A549-DDP tumor model 106
2.8 In vivo efficacy studies for the combination treatment of Mad2 siRNA/chitosan conjugates and cisplatin solution 107
2.9 Measuring Body Weight Changes, Liver and Kidney Enzyme Levels Quantification, White Blood Cells Count and Platelets 108
2.10 Histopathological Analysis 108
2.11 Statistical analysis 108
3. RESULTS AND DISCUSSION 108
3.1 Characterization of chitosan- siRNA nanoparticles 108
3.2 Mad2 knockdown potentiates cisplatin effects and sensitizes Cisplatin-Resistant Lung Cancer Cells in vitro 109
3.3 Mad2 gene silencing in tumor bearing mice 111
3.4 In vivo efficacy assessment of siMad2/cisplatin combination treatment 112
3.5 In vivo safety profiles 113
CONCLUSIONS 118

CHAPTER 6: *COMBINATORIAL-DESIGNED EPIDERMAL GROWTH FACTOR RECEPTOR-TARGETED CHITOSAN NANOPARTICLES FOR ENCAPSULATION AND DELIVERY OF LIPID-MODIFIED PLATINUM DERIVATIVES IN WILD-TYPE AND RESISTANT NON-SMALL-CELL LUNG CANCER CELLS* 121

1. INTRODUCTION 123
2. EXPERIMENTAL SECTION 125
2.1 Materials 125
2.2 A549-WT and A549-DDP resistant NSCLC cell lines 125
2.3 Synthesis and characterization of CS derivatives 126
2.4 Synthesis and characterization of lipid-modified platinum derivatives 127
2.5 Formulation and characterization of control and targeted nanoparticles 127
2.6 Analysis of cell-kill in wild-type and resistant NSCLC cells 129
2.7 Cellular apoptotic response 129
2.8 Data analysis 130

3. RESULTS AND DISCUSSION 130
3.1 Characterization of the CS derivatives 130
3.2 Characterization of the platinum derivatives 133
3.3 Characterization of the platinum encapsulated chitosan nanoparticles 134
3.4. In vitro cell-kill efficacy in wild-type and resistant NSCLC cells 137
3.5 Cellular apoptosis studies 142
CHAPTER 7: GENERAL CONCLUSIONS 151
REFERENCES 157

List of Figures

Figure 1: Distribution of the expected cases and deaths for the 5 most common cancers in Europe 2012 in males (a) and females (b). 4

Figure 2: Signaling pathways and tyrosine kinase receptors involved in the tumorigenesis of NSCLC. 5

Figure 3: The cell cycle engine of mammalian cells. 18

Figure 4 : Overview of protein complexes that build the kinetochore in animal cells. 20

Figure 5: Bi-orientation and kinetochore attachment errors. 20

Figure 6: Model of spindle assembly checkpoint signalling. 23

Figure 7: Defects in SAC activity can contribute to aneuploidy and tumorigenesis. 26

Figure 8: Models for targeting mitosis as an anticancer strategy 26

Figure 9: Small regulatory RNAs are non-coding RNA molecules that silence target RNAs in a sequence-specific manner.. 30

Figure 10: Chitin and Chitosan structure 37

Figure 11: Schematic diagram 49

Figure 12: ^{1}H-NMR spectrums. 58

Figure 13: Effect of N/P ratio on the siRNA encapsulation efficiency (A), size (B) and charge (C) of nanoparticles formulated with targeted and non-targeted LMW and HMW chitosan. 59

Figure 14: TEM image of chitosan/siRNA nanoparticles at a N/P ratio of 50/1 (A) NT-LMW, (B) T-LMW, (C) NT-HMW and (D) T-HMW.. 60

Figure 15: RNase stability of siRNA in the CS/PLA/siRNA complexes.. 61

Figure 16: Cell uptake and intracellular trafficking of siMad2-Cy5 encapsulated in chitosan nanoparticles modified with Alexa 488nm. 63

Figure 17: Quantitative relative intracellular uptake study of non-targeted and targeted siRNA loaded CS nanoparticles by flow cytometry in A549 cell line.. 65

Figure 18: Quantitative relative intracellular uptake study collected by flow cytometry of non-targeted and targeted siRNA loaded CS nanoparticles in A549 and NIH-3T3 cell line 65

Figure 19: EGFR expression levels in NIH-3T3 and A549. 65

Figure 20: Effect of different percentages of EGFR-P modified chitosan in the targeted formulation, on the relative uptake. 68

Figure 21: Down-regulation of Mad2 expression by siMad2 loaded non-targeted and targeted CS nanoparticles in A549 cell line (A) dose-dependent gene silencing 48 h post-dosing and (B) time-dependent gene silencing with 50 nM siMad2 administration. 68

Figure 22: Mad2 protein levels in A549 cells. 69

Figure 23: Time-dependent cytotoxicity for A549 cells (A) and HPAEpiC (B) upon incubation with 50nM of siScramble loaded in CS-derivatives in a N/P ratio of 50/1. 69

Figure 24: Time-dependent cytotoxicity studies in (A) A549 cells and (B) HPAEpiC upon incubation with 50nM of siMad2 loaded in CS-derivatives. 71

Figure 25: Apoptosis assay using Annexin V-PI staining after exposure of A549 cells to 50nM siMad2 loaded in CS nanoparticles and lipofectamine as positive control. 71

Figure 26: Whole body and ex vivo optical imaging of near-IR labeled chitosan/siMad2 nanoparticles in mice A549-WT tumor bearing mice for up to 96 h. 89

Figure 27: Plasma concentrations of siMad2 (%ID/mL) ± SD versus time (h) in A549-WT (A) and A549-DDP (B) tumor models, after IV injection of NTG and TG nanoparticles at 3 mg/kg equivalent siRNA. 91

Figure 28: Plasma exposure to siMad2 over the duration of the study. AUClast +SE (in h*%ID/mL of plasma) for A549-WT and A549-DDP tumor models, after IV injection of NTG and TG nanoparticles at 3 mg/kg equivalent siRNA.. 92

Figure 29: Biodistribution in tumor and major organs.. 93

Figure 30: Tissues exposure to siMad2 over the duration of the study. 95

Figure 31: Targeting efficiency.. 97

Figure 32: In vitro Mad2 expression in the A549 WT and A549 DDP cell line. 110

Figure 33: Knockdown efficiency of siRNA targeting Mad2 in NSCLC tumor bearing mice. 113

Figure 34: Effect of the combination of cisplatin treatment and Mad2 silencing on growth of sensitive and resistant A549 tumor bearing mice. 115

Figure 35: Safety profile. 116

Figure 36: Histological sections after H&E staining of liver, kidney, and spleen from mice from different treatment of (A) A549 WT and (B) A549 DDP tumor bearing mice. 118

Figure 37: Schematic diagram 125

Figure 38: 1H-NMR spectrum for the CS derivatives (CS4, CS6, CS8, CS10) obtained by the modification of chitosan (CS) with lipids with different carbon chain lengths. 131

Figure 39: FTIR spectra of CS and CS6 132

Figure 40: ^{1}H NMR spectrum (DMSO-d_6) for cisplatin derivative DDP_{10}. 133

Figure 41: ^{13}C NMR spectrum (DMSO-d_6) for cisplatin derivative DDP_{10}. 134

Figure 42: ^{195}Pt NMR spectrum (DMSO-d_6) for cisplatin derivative DDP_{10}. 134

Figure 43: Mass spectrum of the DDP_{10} derivative.. 135

Figure 44: Nanosight DLS measurement of the DDP_8 and DDP_{10} nanoparticles. 136

Figure 45: HPLC chromatograms used to determine pro-drug encapsulation efficiency. 139

Figure 46: Transmission electron microscopy images of epidermal growth factor receptor-targeted chitosan nanoparticles. 142

Figure 47: Caspase-3 expression level in A549-WT(A) and A549-DDP resistant (B) non-small cell lung cancer cells after 24 hours treatment with platinum derivatives, both in solution and encapsulated in CS8 nanoparticles, at their IC50 concentrations. 143

Figure 48: Analysis of cell death effect of cisplatin and lipid-modified platinum (DDP) derivatives encapsulated in CS8 hydrophobic derivative at their IC50 concentration. 145

Figure 49: Annexin V-PI analysis for Apoptotic population of A549-DDP cells. 146

Figure 50. TUNEL staining images of (A) A549-WTand (B) $A549^{DDP}$ cells treated with lipid-modified platinum derivatives CS formulations. 148

List of Tables

Table 1. Mitotic checkpoint core proteins and their most significant properties, interactions and functions 22

Table 2: RNA interference based therapeutics in clinical trials 34

Table 3: Major obstacles for therapeutic efficacy of siRNA without modifications 36

Table 4: Particle size, polydispersity index (PDI), zeta potential and siRNA encapsulation efficiency of chitosan/siRNA nanoparticles at a N/P ratio of 50/1. 60

Table 5: NIR dye-loaded CS nanoparticles characterization 88

Table 6: Plasma PK parameters calculated by non-compartmental analysis using Phoenix® WinNonLin® software. 92

Table 7: Ratio of the last time-point concentration (C_{last}) versus the maximum concentration reached over the duration of the study (C_{max}), expressed in % (SD).. 94

Table 8: CS nanoparticles characterization (particle size, zeta-potential, and siMad2 encapsulation efficiency) of CS/siRNA nanoparticles at a N/P ratio of 50/1. 109

Table 9: IC50 values of free cisplatin treatment, 48h post-transfection with siMad2 encapsulated in TG or NTG nanoparticles in A549-WT (A) and A549-DDP (B) cells..... 110

Table 10: Physical Characterization of Combinatorial-Designed Control and Epidermal Growth Factor Receptor-Targeted Chitosan Nanoparticlesa..... 136

Table 11: Retention Times of Cisplatin and Lipid-Modified Platinum Derivatives 137

Table 12: IC50 values of platinum derivatives in solution or encapsulated in EGFR-targeted chitosan nanoparticles. 140

Table 13: Cell-kill efficacy as measured by IC50 values of values of platinum derivatives encapsulated in solution or encapsulated in CS8 nanoparticles that were tested for cellular apoptosis studies. 144

List of Abbreviations

APC/C - anaphase-promoting complex/cyclosome
CS - chitosan
DDP - cisplatin
EGFR - epidermal growth factor receptor
EPR - enhanced permeability and retention
Gm - geometric mean
HMW - high molecular weight
LMW - low molecular weight
Mad2 - mitotic arrest deficient 2
MPS - mononuclear phagocyte system
N/P - nitrogen/phosphate ratio
NMR - nuclear magnetic resonance
TEM - transmission electron microscopy
NSCLC - non-small cell lung cancer
NTG and NT - non-targeted
PEG - poly-ethylene glycol
RNAi - RNA interference
siMad2 - Mad2 siRNA
siRNAs - small interfering ribonucleic acids
qRT-PCR - quantitative real-time polymerase chain reaction
WT - wild type
WHO - world health organization
MDR - multi-drug resistance
TK - tyrosine kinase
ASCO - American Society of Clinical Oncology
VEGF - vascular endothelial growth factor
PDGF - platelet-derived growth factor
FGF - fibroblast growth factor
CIN - chromosome instability
MPS1 - Monopolar spindle 1 kinase
Cdk - Cyclin-dependent kinases
MPF - mitosis-promoting factor
RISC - RNA-induced silencing complex
IC50 - half maximal inhibitory concentration
LD50 - half maximal lethal concentration
AUC_{∞} - area under the time-concentration curve from time zero to infinity
CL - total body clearance
C_{last} - concentration at the last time-point

C_{max} - maximum observed concentration

HL - Half-life of the log-linear terminal part of the curve

MRT - mean residence time

SE - standard error of the mean

Vss - volume of distribution at the steady-state

Thesis outline and organization

This thesis is organized in **5 chapters** reflecting the progression of research objectives.

- **Chapter 1** consists in a bibliographic review centered on recent knowledge of targeted therapies for NSCLC treatment, such as targeting mitotic components. A particular emphasis has been put on RNA interference technology as an anti-cancer therapy and the contribution of nanocarriers in dramatic improvement of RNAi efficacy.

- The project aims and goals are described in detail in **Chapter 2.**

- **Chapter 3** reflects the optimization of chitosan-based nanoparticle formulation to encapsulate siRNA targeting the mitotic protein Mad2; and subsequently, the study of its *in vitro* efficiency

- **Chapter 4** describes the biodistribution and pharmacokinetics analysis of EGFR-targeted chitosan nanoparticles in drug sensitive and resistant NCSLC models

- **Chapter 5** reproduces the *in vivo* efficacy and safety studies towards NSCLC therapy when administered in combination with cisplatin.

- **Chapter 6** describes a parallel project that was focused on exploring chitosan as a carrier for hydrophobic drugs by modifying it with lipid chains where lipid-modified cisplatin was chosen as the model hydrophobic drug to critically study effect of lipid chain length on drug formulation and subsequent in vitro activity in drug-sensitive and resistant NSCLC cells.

- The overall conclusions are presented on **Chapter 7.**

Most information presented in the 5 chapters that constitute this thesis has been already submitted to international peer review, via publication in scientific journals - according to the following list:

- Nascimento AV, Bousbaa H, Ferreira D, Sarmento B. Non-small cell lung carcinoma: an overview on targeted therapy. Current drug targets. 2015 Dec 1;16(13):1448-63.

- Andrade F, Antunes F, Nascimento AV, Baptista da Silva S, das Neves J, Ferreira D, Sarmento B. Chitosan formulations as carriers for therapeutic proteins. Current drug discovery technologies. 2011 Sep 1;8(3):157-72.
- Silva P, Barbosa J, Nascimento AV, Faria J, Reis R, Bousbaa H. Monitoring the fidelity of mitotic chromosome segregation by the spindle assembly checkpoint. Cell proliferation. 2011 Oct 1;44(5):391-400.
- Nascimento AV, Singh A, Bousbaa H, Ferreira D, Sarmento B, Amiji MM. Mad2 checkpoint gene silencing using epidermal growth factor receptor-targeted chitosan nanoparticles in non-small cell lung cancer model. Molecular Pharmaceutics. 2014 Sep 26;11(10):3515-27.
- Nascimento AV, Singh A, Bousbaa H, Ferreira D, Sarmento B, Amiji MM. Combinatorial-designed epidermal growth factor receptor-targeted chitosan nanoparticles for encapsulation and delivery of lipid-modified platinum derivatives in wild-type and resistant non-small-cell lung cancer cells. Molecular Pharmaceutics. 2015 Nov 17;12(12):4466-77.
- Nascimento AV, Gattacceca F, Singh A, Bousbaa H, Ferreira D, Sarmento B, Amiji MM. Biodistribution and pharmacokinetics of Mad2 siRNA-loaded EGFR-targeted chitosan nanoparticles in cisplatin sensitive and resistant lung cancer models. Nanomedicine. *(in press)*
- Nascimento AV, Singh A, Bousbaa H, Ferreira D, Sarmento B, Amiji MM. Overcoming cisplatin resistance in non-small cell lung cancer with Mad2 silencing sirna delivered systemically using EGFR-targeted chitosan nanoparticles. Cancer Research. *(submited)*

CHAPTER 1

State-of-art

The information presented in this chapter was partially published in the following publications:

- Nascimento AV, Bousbaa H, Ferreira D, Sarmento B. Non-small cell lung carcinoma: an overview on targeted therapy. Current drug targets. 2015 Dec 1;16(13):1448-63.

- Andrade F, Antunes F, Nascimento AV, Baptista da Silva S, das Neves J, Ferreira D, Sarmento B. Chitosan formulations as carriers for therapeutic proteins. Current drug discovery technologies. 2011 Sep 1;8(3):157-72.

- Silva P, Barbosa J, Nascimento AV, Faria J, Reis R, Bousbaa H. Monitoring the fidelity of mitotic chromosome segregation by the spindle assembly checkpoint. Cell proliferation. 2011 Oct 1;44(5):391-400.

Non-Small Cell Lung Cancer (NSCLC)

1. INTRODUCTION

Cancer is a leading cause of death worldwide, accounting for 7.6 million deaths (around 13% of all deaths) in 2008 (1). Lung cancer is the most frequently occurring cancer in the world and has a very low 5-year survival rates, and for these reasons, lung cancer should be considered as a major public health problem. In Europe, lung cancer is the second most common cancer in men and the third most common cancer in women (Figure 1) (1). In terms of mortality, lung cancer is the third leading cause of death in high-income countries and the most deadly type of cancer, with 1.38 million deaths (18.2% of the total) (2). Worldwide, it is the leading cause of death in smokers and accounts for more deaths than any other cancer in both men and women (3). Lung cancer is related with a poor overall prognosis but, across all ages and irrespective of histologic subtype, women tend to live longer than men for reasons that are not yet understood.

The classification of lung cancers is based on pathologic features visible on light microscopy and it provides a basis for epidemiology, prognosis and therapeutic approach. The most recent classification of the World Health Organization (WHO) has been widely accepted and it divides lung cancers into two major groups, small cell (SCLC) and NSCLC (4). The non-small cell cancer group is subdivided in adenocarcinoma, squamous cell carcinoma, large cell carcinoma, and variants. Approximately 40% of all lung cancer cases are adenocarcinomas and 25-30% are squamous cell carcinomas (5). Large cell cancer makes up 10% of all cases, while SCLC accounts for 20% of all cases.

In the last 30 years, many attempts have been made to unravel the genetic bases of lung cancer. Tumor suppressors, including Rb and p53, were shown to be frequently inactivated in lung cancer (6), mostly due to deletion or hypermethylation (7). Several oncogenes are found activated in lung cancer, including K-ras, c-myc, N-myc, and L-myc, with a crucial role in cancer establishment (8). Finally, autocrine growth factors have been implicated in the onset of lung cancer, with the epidermal growth factor receptor (EGFR) playing a pivotal role in the development of the disease.

With the available therapeutics, the 5-year relative survival rate for patients with lung cancer is less than 15% (9). This instigates a huge demand for new and more potent therapies focusing on molecular mechanisms that offer great promise in this regard.

A promising strategy is to use RNA interference (RNAi). RNAi is a sequence-specific and post-transcriptional gene silencing mechanism, capable of the elucidating molecular

mechanisms that underpin both normal biology and human disease. The application of RNAi technology both *in vitro* and *in vivo* has tremendous potential as a therapy for various diseases especially since it allows to switch off the causative genes. Although substantial obstacles still exist for RNAi-based cancer therapeutics, several RNAi studies have successfully reached clinical stage. In this review, we will highlight the current understanding of molecular targets and latest advances in therapies for lung cancer, and will also address the current status of RNAi-based cancer therapeutics.

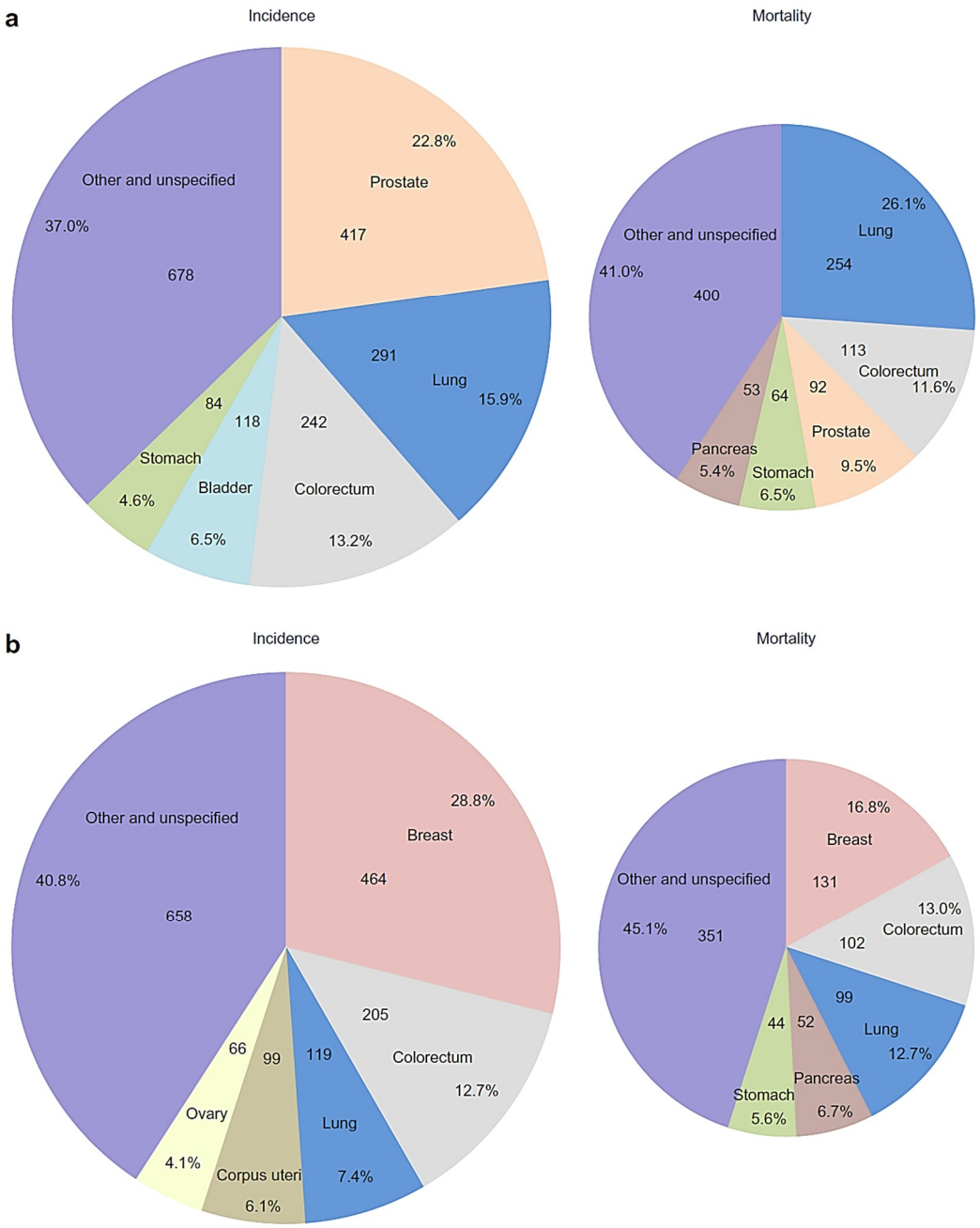

Figure 1: Distribution of the expected cases and deaths for the 5 most common cancers in Europe 2012 in males (a) and females (b). For each sex, the area of the segment of the pie chart reflects the proportion of the total number of cases or deaths (1).

2. CURRENT MOLECULAR TARGETS FOR NSCLC THERAPY

The best treatment option to NSCLC continues to be the complete surgical resection, which offers a 40% 5-year survival rate. However, 75% of patients have an advanced or metastatic form of lung cancer at the time of diagnosis and are unsuitable for surgery (8). In these cases, platinum-based chemotherapy drugs are the standard therapy but they imply severe toxicity and can result in multi-drug resistance (MDR) of NSCLC cells (10). In the search for new therapies, molecularly targeted drugs have appeared as an emerging platform for lung cancer therapy in the last decade (Figure 2).

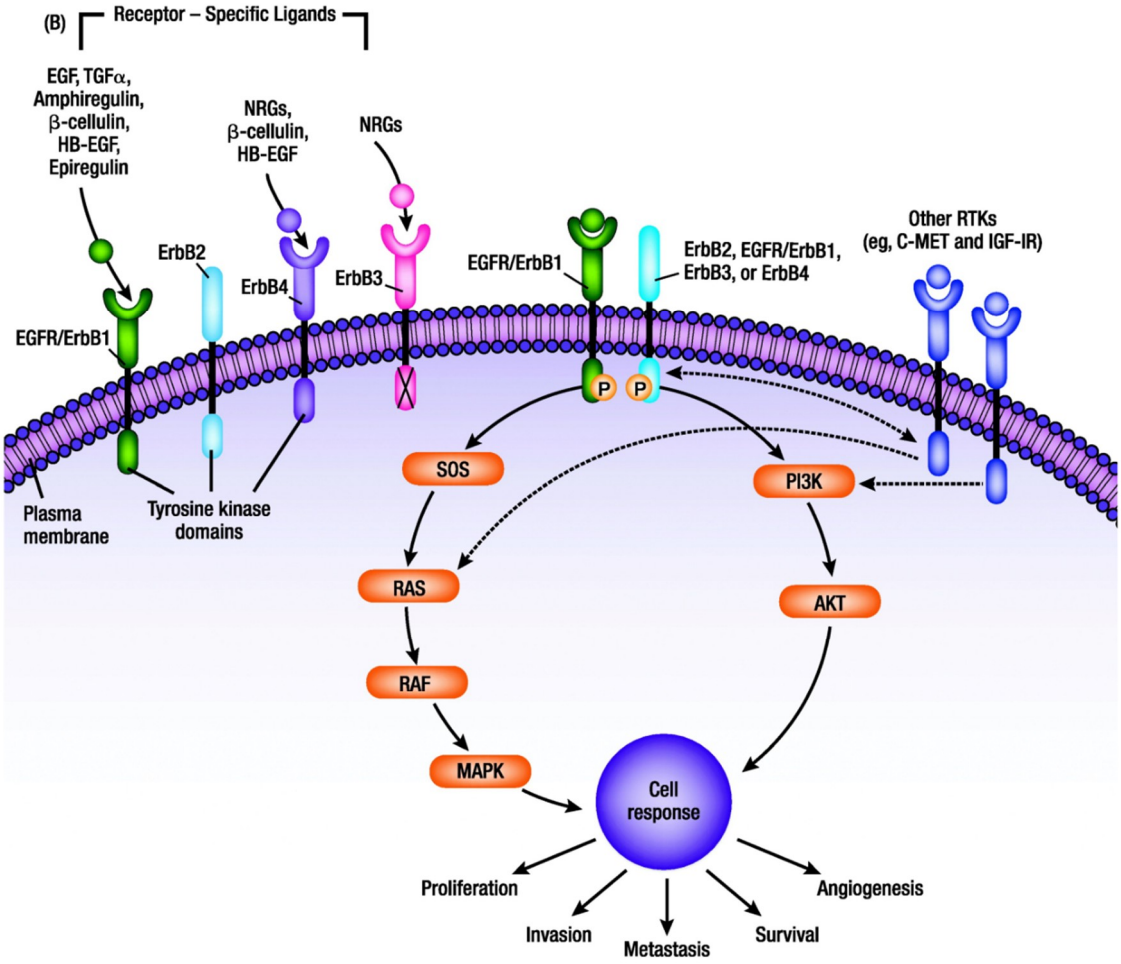

Figure 2: Signaling pathways and tyrosine kinase receptors involved in the tumorigenesis of NSCLC. Akt, protein kinase B; EGF, epidermal growth factor; EGFR, epidermal growth factor receptor; HB, heparin binding; IGF-1R, insulin-like growth factor 1 receptor; MAPK, mitogen-activated protein kinase; NRG, neuregulin; NSCLC, non-small cell lung cancer; P, phosphate; PI3K, phosphatidylinositol-3-kinase; Raf, v-raf 1 murine leukemia viral oncogene homolog 1; Ras, retrovirus-associated DNA sequences; RTK, receptor tyrosine kinase; SOS, Son of sevenless; TGF, transforming growth factor. (11)

Accordingly with National Cancer Institute Dictionary of Cancer Terms, these targeted drugs or other substances are able to block the growth and spread of cancer by interfering with specific molecules involved in tumor growth and progression (12). Patients selected for such

treatment on the basis of specific features of their tumor are currently benefiting from such agents. Although targeted drugs may block important pathways, lung cancer is a heterogeneous disease with multiple mutations and, as such, it is highly unlikely for neoplasic establishment and development to be dependent on a single signaling pathway (13). Consequently, several targeted therapies have been introduced into clinical trials, both as single and multiple agents or combined with other conventional treatment modalities (13). Continuous advances in our understanding of the molecular biology of cancer and mechanisms of tumorigenesis have empowered a constant discovery of potential molecular targets and the development of novel 'targeted therapies'.

2.1 Receptor Tyrosine Kinase Signalling

Epidermal Growth Factor Receptor

EGFR, also known as human epidermal receptor 1 (HER1) or ErbB1, is the founding member of the ErbB family of four structurally related receptor tyrosine kinases (RTKs): EGFR (ErbB-1), HER2/c-neu (ErbB-2), HER3 (ErbB-3), and HER4 (ErbB-4) (14). EGFR signaling activates two of the most important pathways in solid tumors, the RAS/RAF/MEK/MAPK pathway and the PI3K/AKT/mTOR pathway, which jointly endorse cancer cell proliferation, cell growth, invasion, apoptosis, and tumor angiogenesis.

Overexpression of EGFR is very common in NSCLC patients (40%-80%), and is associated with advanced tumor stage, resistance to standard therapies, and poor patient prognosis (15). Enhanced ligand production by cancerous cells, EGFR overexpression on cancer cell membranes and activating mutations on EGFR and related genes, represent different ways by which EGFR can be deregulated (16). EGFR has revealed to be one of the most relevant targets for NSCLC treatment (17). Strategies to block such pathway include tyrosine kinase inhibitors (TKIs) and monoclonal antibodies.

TKIs are small molecules that inhibit the phosphorylation and activation of EGFR and the downstream signaling pathway by blocking ATP assembly to the EGFR intracellular tyrosine kinase domain (18). EGFR TKIs have a narrow efficacy in unselected patients but are very effective in EGFR-mutated patients who frequently have certain clinical characteristics (adenocarcinoma, non-smoking history, Asian ethnicity, female gender) (8). In 2003 and 2004, the first generation of TKIs, gefitinib (AstraZeneca, London, UK) and erlotinib(Genzyme, Boston, MA, USA), were approved for the treatment of NSCLC (19). They are orally bioavailable synthetic anilinoquinazolines which selectively and reversibly inhibit the kinase activity of EGFR (20). Somatic activating mutations between *EGFR* gene exons 18 and 24, which code for tyrosine kinase (TK) domain, frame deletions in exon 19 (45%-50% of all somatic EGFR mutations), and the L858R missense mutations in exon 21

are positively associated with a strong patient response to erlotinib and gefitinib (21, 22). The use of EGFR TKIs as the favorite option for a first-line situation in metastatic EGFR mutation-positive patients with NSCLC has been supported by large phase III studies (23). Actually, gefitinib frontline use on patients with activating EGFR mutations has been recommended by the American Society of Clinical Oncology (ASCO) Clinical Practice Guidelines 2009. For those cases where EGFR mutation is absent or unknown, cytotoxic chemotherapy is recommended (24). Despite the success of first-generation TKIs, novel second-generation TKIs are urgently required, as new mutations have emerged (e.g. T790M, exon 20) and shown to be treatment resistant (25).

A number of second-generation agents have been developed and are currently undergoing clinical trials and include compounds that irreversibly inhibit both EGFR and HER2 ((11). One of those agents is afatinib (BIBW 2992; Boehringer Ingelheim; Ingelheim, Germany), a novel anilinoquinazoline derivative that irreversibly and powerfully targets the intrinsic kinase activity of all active ErbB receptor family members (26). A phase II LUX-Lung 2 trial was done in patients with the activating EGFR driver mutations (deletion 19 and L858R) that failed to respond to first-line chemotherapy (27). The trial showed that afatinib had a positive activity and 66% of the patients had an objective (complete or partial) response. The results were more disappointing, with an objective response seen in 39% of the patients, with other EGFR mutations, including T790M. Two different clinical trials are being conducted: one where afatinib is being compared with cisplatin/pemetrexed in the first-line treatment of advanced NSCLC patients with activating EGFR mutations; the other one also encloses advanced NSCLC population with EGFR mutations but aims to compare afatinib to cisplatin/gemcitabine (11). Dacomitinib (PF-00299804, Pfizer, New London, CT, USA) is a HER inhibitor with affinity for EGFR, HER2, and HER4, that has also shown activity in NSCLC (28). A phase III clinical trial comparing Dacomitinib with placebo in patients who did not respond to chemotherapy in currently under progress (11).

The efficacy of tumor-aimed monoclonal antibodies has been associated with the number of copies of the corresponding gene in the tumor in question, while the sensitivity to small molecules has been primarily correlated with mutations altering the receptor's catalytic domain (29). Cetuximab (IMC-C225, Erbitux, ImClone Systems Inc, New York City, NY, USA) is a human-mouse chimeric immunoglobulin G1 class monoclonal antibody that targets EGFR extracellular domain in the ligand-binding region (30). Cetuximab was initially registered for clinical practice for the treatment of advanced colorectal cancer and then for head and neck cancer. While being investigated as a first-line treatment of patients with advanced NSCLC, cetuximab was able to inhibit the growth of human NSCLC cell lines (31). The use of cetuximab has been also analyzed in advanced NSCLC patients as a

monotherapy or in combination with chemotherapy (32). The response rate to cetuximab in a single-agent regime was approximately 4.5% in recurrent EGFR-expressing NSCLC, while it increased to 25-35% when administered in combination with platinum-based chemotherapy (33). National Comprehensive Cancer Network practice guidelines for advanced/metastatic NSCLC recommend cetuximab in combination with platinum-based chemotherapy (32). Future patient selection based on predictive biomarkers will enhance the emerging clinical profile of this agent. Other HER family-targeted antibodies (e.g. trastuzumab) have failed to demonstrate clinical benefit in NSCLC, either as a monotherapy or in combination with chemotherapy (28).

Angiogenesis pathway

Angiogenesis is a hallmark of cancer and is crucial for tumor growth and metastasis. Cancer cells have the ability to induce blood vessel formation by secreting pro-angiogenic factors, such as vascular endothelial growth factor (VEGF), platelet-derived growth factor (PDGF) and fibroblast growth factor (FGF). Cell activation, proliferation, migration, and survival are intimately related to several signaling cascades, including RAF-MEK-ERK and PI3K pathways, which are activated through the recognition of VEGF by its receptor (29). Increased VEGF expression is found in a variety of human tumors, including NSCLC (34). One way to block angiogenesis pathways is by inhibiting VEGF receptor with ligand antibodies (e.g. bevacizumab) or TKI (e.g. sunitinib, sorafenib and valatinib).

Bevacizumab (Genentech, San Francisco, CA, United States), a recombinant humanized anti-VEGF monoclonal antibody, recognizes all isoforms of VEGF ligands and was the first commercially available angiogenesis inhibitor (35). In Europe, first line therapy includes the combination of bevacizumab with carboplatin plus paclitaxel or in addition to platinum based chemotherapy (22). A recent meta-analysis of four randomized phase II and III studies evaluating the effectiveness of adding bevacizumab to platinum-doublets in the treatment of NSCLS has demonstrated an improved outcome. Platinum-doublets consist in a combination of platinum-based (cisplatin, carboplatin) chemotherapy with a second agent like docetaxel, paclitaxel, vinorelbine, gemcitabine, etc. The safety of bevacizumab was also demonstrated through several studies aiming the treatment of NSCLC patients with treated central nervous system metastases, as results confirmed a favorable drug safety profile (36).

Sunitinib (SUGEN, Redwood City, CA, USA) is an oral, small-molecule, multi-targeted RTK inhibitor (37). Sunitinib has shown an 11.1% overall response rate in phase II studies but, when tested with other chemotherapeutic agents, its toxicity was fairly undesirable (38). Phase III trials tested sunitinib as single treatment or in conjugation with erlotinib (39).

Sunitinib plus erlotinib did not improve overall survival compared with erlotinib alone.Treatment-related toxicities were severe in combination therapy including rash/dermatitis, diarrhea, and asthenia/fatigue (39). Similar to sunitinib, sorafenib targets a spectrum of membrane receptors, including VEGFR-1 and -2. In contrast to its successful phase II trials, phase III studies on sorafenib conjugated with other chemotherapeutic agents showed no clinical benefit (37, 40).

Up-regulation of other angiogenesis pathways has been suggested as a resistance mechanism of tumor cells. Through alternative expression of another angiogenic factor, tumors may circumvent the inhibition of a single angiogenic protein (41). Therefore, TKIs that can block several receptors, such as PDGFR and FGFR, may be more effective. Having that in consideration, several agents have been developed such as axitinib, a TKI of VEGFR-1, VEGFR-2, VEGFR-3, PDGFR and c-kit (Pfizer, New York City, NY, USA), and BIBF 1120, an inhibitor of VEGFR, FGFR, and PDGFR (Boehringer Ingelheim, Ingelheim, Germany) (42, 43). Axitinib, a small molecule indazole derivative is an oral, potent, and selective kinase inhibitor and is currently being studied in multiple solid tumors. A phase II trial tested axitinib in monotherapy, aiming the treatment of advanced NSCLC. Results showed a median overall survival of 14.8 months and a progression-free survival of 4.9 months, which represent better outcomes than those obtained with other TKIs in monotherapy. Moreover, the treatment was well tolerated, being fatigue, hypertension, and hyponatremia the only frequent adverse effects registered (43). BIBF 1120 is an indolinone derivative that inhibits mitogen-activated protein kinase (MAPK) and Akt signaling pathways, resulting in the inhibition of cell proliferation and apoptosis (44). Phase I/II trials with BIBF 1120 indicates promising efficacy and a favorable safety profile in patients with advanced NSCLC (42). Phase I clinical trials investigated the effects of BIBF 1120 when combined with paclitaxel and carboplatin in first-line patients with advanced NSCLC and have demonstrated an acceptable safety profile (45). The novel generation of cancer therapies is now composed of multi-targeting agents, and several approaches aiming the inhibition of both EGFR and VEGF in the treatment of NSCLC are taking place (46).

Other receptor tyrosine kinases

The Insulin-like growth factor (IGF) pathway is a multicomponent cellular network that mediates growth, differentiation and developmental processes, and is also implicated in numerous metabolic events. It comprises two main receptors (IGF-1R and insulin receptor [IR]) and three main ligands (IGF-1, IGF-2 and insulin) (47). Growth deficits and cancer development are examples of pathologies interrelated with the deregulation of the IGF pathway, which leads to activation of major intracellular signaling cascades, including the RAS/RAF/MAP kinase and the PI3K pathway (48). Similar to other RTK, the main

categories of targeted therapy to inhibit IGF-1R signaling are small molecules and monoclonal antibodies. Deterioration of glucose metabolism can result from indiscriminate blocking of this receptor family, since its kinase domain has approximately 85% homology to the IR (49). Although it was initially a concern, it was later accepted that targeting both IGF-1R and IR may actually be beneficial in order to prevent adaptive resistance (50). Several small molecules and antibodies against IGF-1R are currently under preclinical and early clinical stages, such as ganitumab (Amgen, Thousand Oaks, CA, USA), AVE1642 (ImmunoGen Inc., Waltham, MA, USA) and BIIB022 (Biogen Idec., Weston, MA, USA) (51-53).

An emerging molecular target being tested in clinical trials is the RTK MET. C-Met is a proto-oncogene that encodes for a heterodimeric transmembrane RTK, known as MET or hepatocyte growth factor (HGF) receptor (HGFR). When binding to its ligand, HGF, MET activation leads to cell growth, survival, motility, invasion and angiogenesis (54). Despite multiple controls, pathway deregulation occurs in a variety of neoplasms. Many NSCLC patients (60-80%) overexpress c-MET, whereas only 20% display c-MET mutations (55). Since MET hyperactivation initiates the PI3K/Akt pathway independently of EGFR activation, EGFR inhibitors are ineffective for the treatment of c-MET amplification derived cancers (55). Therefore, designing therapeutic solutions aiming MET itself could become clinically relevant for patients unable to positively respond to gefitinib or erlotinib. NSCLC cell lines overexpressing MET showed to be very sensitive to PHA665752 (Pfizer, New York City, NY, USA), a selective inhibitor of MET kinase (56). Subsequent studies in patients with lung cancer, both resistant to EGFR TKIs and with MET amplification, demonstrated that treatment with PHA665752 could restore gefitinib sensitivity.

SCH 900105 (AVEO Pharmaceuticals, Cambridge, MA, USA), a humanized anti-HGF antibody with specificity for free HGF; cabozantinib (Exelixis Inc., South San Francisco, CA, USA), a MET and VEGFR2 inhibitor; tivantinib (Arqule Inc., Woburn, MA, USA), selective cMET inhibitor; and BMS-777607 (Bristol-Myers Squibb, New York City, NY, USA), a small-molecule MET kinase inhibitor, are currently under investigation and represent some strategies to prevent MET signaling (57-60).

2.2 RAS/RAF/MEK/MAPK Pathway

Ras is a protein superfamily of inner-membrane associated small GTPases, related to the Ras protein subfamily the members of which are H-Ras, K-Ras, and N-Ras. By acting as molecular switches connecting extracellular signals with nuclear transcription factors, they regulate key signaling pathways involved in normal cell differentiation, proliferation, and survival (61). The *Ras* oncogenes are often aberrantly activated in lung cancer due to *Ras*

mutations or growth factor receptor (GFR) overexpression, playing a crucial role in tumorigenesis (62, 63). Mutations on the *K-Ras* gene have been found in 20%-30% of NSCLC, pre-dominantly in smokers who have adenocarcinoma, and are believed to play a key role in this malignancy (64). Most of these mutations (90%) occur on exon 12 or exon 13 and are related with decreased sensitivity to EGFR TKI therapy (65).

Additionally to TKIs, several novel targeted drugs for this pathway are currently in pre-clinical and clinical tests in different types of cancer, such as GSK1120212 (GlaxoSmithKline, Brentford, UK), a selective inhibitor of MEK1; AS703026 (Merk Serono, Darmstadt, Germany), a selective inhibitor of MEK1/2; selumetinib (AstraZeneca, London, UK), a selective inhibitor of MEK1/2; and salirasib (Kadmon Corporation, New York City, NY, USA), a Ras inhibitor (66-71). A phase II study of the Ras-MAPK signaling pathway inhibitor TLN-4601 (Thallion, Dorval, QC, Canada) was conducted in patients with glioblastoma, but it showed to be ineffective when administered as monotherapy (72).

2.3 PI3K/AKT/Mtor Pathway

The serine/threonine kinase Akt has a critical regulatory role in diverse cellular processes, including cell growth, cell proliferation, angiogenesis, and protein synthesis. Akt cascade is activated by RTKs, integrins, B and T cell receptors, cytokine receptors, G protein coupled receptors, and other stimuli. PI3K/Akt/mTOR pathway activation in human cancers has been associated with resistance to anti-EGFR drugs, which has increased the interest in describing alterations in this pathway to optimize EGFR therapy (73). Several occurrences can contribute to this event: activation of upstream RTKs (including EGFR and PDGFR); constitutively activation of Akt; mutations in *PIK3CA*, which expresses the catalytic subunit of PI3K; altered expression of PTEN protein, which inhibits the PI3K/Akt pathway; among others (74, 75). Due to the potential to shut down survival pathways while targeting this pathway, therapeutic agents are being explored to determine pathway-activating mutations and to restore sensitivity to upstream signaling targeted agents (73, 76). First generation mTOR inhibitors (e.g., rapamycin) have essentially cytostatic anti-tumor activity and can only inhibit mTORC1, but second generation agents being tested can inhibit mTORC1 and mTORC2. These agents have shown promising antitumor activity in clinical trials (77, 78). Inhibition of mTORC2 will also affect the activation of Akt (55). RNA interference technology (see below) has also been tested against this pathway, leading to promising results (79). Small interfering RNA (siRNA) oligonucleotides that specifically inhibit mTOR have been evaluated *in vitro* and resulted in increased apoptosis and in the inhibition of proliferation/migration in NSCLC cells. Inhibition of PI3K enhances sensitivity of NSCLC cells to radio- and chemotherapy, as shown by preclinical studies with the PI3K inhibitor

LY294002 (Semafore Pharmaceuticals; Westfield, IN, USA), which is currently being tested in phase I trials (80).

2.4 Eml4-Alk

The anaplastic lymphoma kinase (ALK) is a member of the insulin superfamily of RTKs and acts as a dominant oncogenic driver following chromosomal rearrangements. It has been shown, in a specific subset of NSCLC patients, that ALK translocations instigate aberrant activation of downstream oncogenic signaling pathways such as MAP kinase, PI3-kinase, and signal transducers leading to cell proliferation, invasion, and inhibition of apoptosis (81, 82). EML4-ALK translocation consists of ALK fusion with echinoderm microtubule-associated protein-like 4 (EML4), is found in 3%-6% of all NSCLC cases, and is associated with resistance and poor response to EGFR TKIs (83). Crizotinib (PF02341066, Xalkori, Pfizer, New York City, NY, USA) has shown promising activity in phase I/II trials and was recently approved for the treatment of ALK-positive NSCLC (84).

2.5 Apoptotic Pathway

In recent years, apoptosis has become an appealing target for lung cancer therapy. This pathway is mainly structured by a balance between proapoptotic (Bax, Bak, Bad, and Bim) and antiapoptotic (Bcl-2, Bcl-xL, Bcl-w, and Mcl-1) factors (85). In 10%-35% of NSCLCs and 75%-95% of SCLCs, B-cell lymphoma 2 (Bcl-2) is overexpressed, conferring resistance to cytotoxic chemotherapy, radiotherapy, and monoclonal antibodies (86, 87). Clinical studies have shown that Oblimersen sodium (Genasense), an antisense oligonucleotide targeting Bcl-2, reduces Bcl-2 production in lung cancer cells, thereby increasing cell sensitivity to standard anticancer treatments. Small molecule inhibitors of antiapoptotic proteins as ABT-737 (ABBOTT, ABBOTT park, IL, USA), an inhibitor of the Bcl-2, Bcl-xL, and Bcl-w proteins, and AT-101 (Ascenta Pharmaceuticals Inc., San Diego, CA, USA), a Bcl-2 inhibitor, have demonstrated single-agent preclinical activity against NSCLC (88, 89).

Survivin, an antiapoptotic protein that regulates both programmed cell death and mitosis, has prognostic value for NSCLC patients since its expression and subcellular localization is associated with an increase in the risk of disease recurrence, resistance to radiotherapy and death (90, 91). YM155 (Astellas Pharma, Chūō, TKY, Japan), a novel small-molecule suppressor of Survivin has been evaluated in a monotherapy phase II trial in advanced NSCLC and showed reasonable antitumor activity, stabilizing the disease in 37.8% of patients (92). Data obtained from this trial suggests that YM155 may not be effective in monotherapy. Still, it could be useful if conjugated with other chemotherapeutic agents. Therefore, further multimodality studies should be performed. siRNA against Survivin has also demonstrated therapeutic potential by increasing apoptosis of H460 and A549 lung

cancer cells after radiotherapy and suppressing the growth of the transplanted lung cancer in mice (93, 94).

2.6 Histone Deacetylase and Heat Shock Proteins

Histone deacetylase are a class of enzyme responsible for removing acetyl groups on lysine residues from histones allowing tighter interaction between these and the DNA (95). These enzymes are believed to be involved in the repression of tumor suppressor genes and in the activation of transcriptional factors involved in tumorigenesis at different stages of cancer development (96). Histone deacetylase inhibitors cause cell cycle arrest and apoptosis by upregulating the intrinsic apoptotic pathway (97). Additionally, they can also enhance the cytotoxic effects of radiation and synergistically promote the effects of chemotherapy (98, 99). Suberoylanilide hydroxamic acid and trichostatin A, two histone deacetylase inhibitors, have recently proved to be able to sensitize NSCLC cancer cells to ionizing radiation (100). Vorinostat, another compound that inhibits histone deacetylases, has also been evaluated in combination with the novel proteasome inhibitor marizomib in a Phase I trial in lung cancer patients, resulting in a highly synergistic antitumor activity (101).

Heat shock proteins (Hsp), or stress proteins, are another class of proteins with therapeutic interest. Hsp are involved in essential cellular mechanisms as protein assembly, cell division, apoptosis, protein trafficking, cell signaling, prevention of unwanted protein aggregation, etc. (102). Hsp90 inhibitors have emerged as a class of promising drugs to target multiple oncogenic pathways. Hsp90 is upregulated in response to stress and also maintains the activity and stability of key oncogenic signaling proteins (103). Geldanamycin (Synta Pharmaceuticals, Lexington, MA, USA), an Hsp90 inhibitor, has shown promising effects in clinical trials, although its extremely low water solubility and severe hepatotoxicity have hindered its development as effective therapeutics (104, 105). Therefore, some improved analogues have been developed, including Tanespimycin (Kosan Biosciences INC, Bay Center Place Hayward, CA, USA)and Retaspimycin hydrochloride (Infinity Pharmaceuticals, Cambridge, MA, USA) (106).

2.7 Mitotic Inhibitors

Cell cycle deregulation is a common hallmark of cancer cells, and targeting the cell division cycle in cancer cells has been the aim of several therapeutic strategies. Antimitotic chemotherapy remains the most effective approach in the clinical treatment of a variety of human cancers. Cytotoxic platinum-doublet chemotherapy that includes antimitotic agents is a current standard therapy in advanced NSCLC. Traditional anti-mitotic agents include the microtubule toxins such as taxol, other taxanes and the vinca alkaloids, all of which have proven to be successful, but with significant toxicity (107). These drugs avert a

functional spindle leading to spindle assembly checkpoint (see below) activation and anaphase delay (108). After mitotic arrest, cells may undergo two different pathways, cell death or mitotic slippage (109). Slippage refers to a process where cells exit mitosis and begin a new cycle with twice the DNA content (110). These cells can arrest in G1 phase, undergo cell death, or continue cell cycle progression increasing the potential for tumorigenesis (111). However, severe side effects, like myelosuppression and neurotoxicity and the frequent development of resistance to these drugs have limited their use and motivate the search for alternative antimitotic drugs (112). Innovative targeted strategies are now evaluating the inhibition of critical activities, such as cyclin-dependent kinase 1, Aurora, spindle kinesins or polo kinases (113, 114).

Aurora kinases and Polo-like kinase 1

Mitotic kinases are deregulated in a multiplicity of tumor cells, suggesting their potential role in tumorigenesis and making them a tempting target for molecular therapies(115). Plk1 (polo-like kinase 1) and Aurora kinases represent a highly conserved family of serine/threonine kinases that ensures a correct spindle assembly during mitosis, heading to an accurate segregation of the chromosomes into daughter cells. Due to their recognition as potential targets for cancer chemotherapy, around thirty Aurora kinase inhibitors have reached different stages of pre-clinical and clinical development (116). Inhibiting Aurora B kinase in combination with radiation has recently proven to be a promising strategy in NSCLC cell lines (113). Concerning Plk1 activity, small-molecules and phosphopeptide inhibitors have been recently developed due to their potency and specificity against Plk1 (117). Blocking these targets' activity might not necessarily end in cell death; instead, cells can undergo mitotic slippage and exit mitosis without proper segregation of sister chromatids and cytokinesis, exhibiting multiple nuclei and polyploidy (118). Several inhibitors have been developed against this protein family and, recently, administration of siRNA against PLK-1 has shown promising results and demonstrated that PLK-1 is a suitable target for advanced NSCLC therapy (117-119).

CENP-E

Inhibitors of kinesin motor proteins, which are vital for spindle assembly and chromosomes movement during mitosis, have showed to be promising mitosis-specific agents to treat a variety of human neoplasm (114). CENP-E (centromere protein E) is an essential plus end-directed microtubule motor, present only in cells undergoing mitosis, and is a fundamental protein for the congression and alignment of chromosomes by moving unattached kinetochores towards the metaphase plate along kinetochore microtubule bundles, termed K-fibers (120). Cell cycle arrest and apoptosis are two consequences of

the inhibition of CENP-E activity, which can act as tumor suppressor and represent an attractive antimitotic target (121). Several CENP-E inhibitors, such as GSK923295A and GSK923295 (GlaxoSmithKline, Brentford, UK) have reached clinical trial stage (122, 123).

Eg5 Kinesin

Eg5 is a member of the kinesin superfamily of microtubule-based motors, and plays an essential role in the proper separation of centrosome and bipolar spindle assembly and maintenance, being upregulated in many tumor cells (124). Among patients with advanced NSCLC, Eg5 overexpression tended to be associated with a poorer outcome in terms of overall survival (125). A cell cycle arrest at mitosis is achieved through the inhibition of Eg5, which leads to the establishment of monoastral microtube arrays, followed by apoptosis (126). Mayer et al. discovered monastrol, the first small molecule able to inhibit Eg5, but since then several other inhibitors have been reported and some are being tested in clinical trials, both as single and in combination with other agents, although none in NSCLC (127, 128).

Ubiquitin-proteasome system

The ubiquitin-proteasome system is an intracellular multicatalytic complex that plays a central role in regulating the degradation of proteins involved in the cell cycle, DNA transcription and repair, apoptosis, angiogenesis and cell growth. Proteasome inhibition is a focus of intense research and therapeutic development since it is a critical pathway for the proliferation and survival of cancer cells. Clinical trials in advanced NSCLC have being investigating the use of bortezomib (Millennium Pharmaceuticals, Inc., Cambridge, MA, USA), a proteasome inhibitor, in combination with pemetrexed (Princeton University, Princeton, NJ, USA), ainhibitor of precursor purine and pyrimidine nucleotide synthesis, and cetuximab (13). Bortezomib causes downregulation of the antiapoptotic protein Bcl-2 in NSCLC and induces apoptosis in SCLC. In current phases I and II studies, bortezomib has shown very encouraging results in combination with chemotherapy (129). An extensive diversity of natural and synthetic proteasome inhibitors have been described and grouped into five groups: peptide aldehydes, peptide vinyl sulfones, peptide boronates, peptide epoxyketones, and β-lactones (lactacystin and its derivatives). From those only the ones that have shown chymotrypsin-like activity, similar to bortezomib, have reached clinical trials state (130).

Spindle assembly checkpoint pathway

The spindle assembly checkpoint (SAC) is a surveillance mechanism that assures the accurate segregation of chromosomes during mitosis, by ensuring proper bipolar attachment of each chromosome to the mitotic spindle (131). A deregulated SAC pathway

has been frequently described in different cancers, including NSCLC, in association with chromosome instability (CIN) (132). A weak SAC activity has been associated with aneuploidy and tumorigenesis, while complete SAC abrogation culminates in massive chromosome missegregation and cell death (133). Strategy to eliminate SAC activity has not been applied to lung cancer, not even with other mitotic proteins. Many genetic alterations have been associated with tumorigenesis and tumor progression in NSCLC, but the precise mechanisms behind these alterations remain unknown. One of those alterations, CIN, suggests improper allocation of the two chromatids of a chromosome to the two daughter cells during mitosis (134). Up to 40% of lung cancer cell lines have been shown to have SAC defects and are viable. Killing these cells by completely abolishing SAC could be a promising anti-cancer strategy. Studies conducted in colon carcinoma cells, showed that knockdown of MAD2 in vivo was associated with acute chromosome missegregation and resulted in a reduced tumor growth (135). Monopolar spindle 1 kinase (MPS1) intervenes in the chromosome alignment and kinetochore-microtubule interaction and due to its critical role in SAC signaling it could represent a promising therapeutic target. Colombo et al. have identified a MPS1 small-molecule inhibitor causing massive aneuploidization leading to cell death and tumor growth inhibition in xenograft models (136). Targeting SAC proteins in NSCLC, as well in other types of cancer appears as an unexplored promising new concept for cancer therapy.

MITOSIS

1. CELL CYCLE

Cell reproduction occurs by an evolutionarily conserved process named cell cycle. The cell division cycle is an orderly sequence of events terminating in mitosis and the production of two daughter cells, governed by a complex network of regulatory proteins . The somatic cell cycle may be divided into two main stages: the M (Mitosis) phase and the interphase, which corresponds to the period between two M phases. Interphase encompasses three phases: G1 (*gap 1*), S (synthesis) and G2 (*gap 2*). In G1 phase cell increases the size and DNA and RNA might be synthesised in order to prepare DNA replication in the next phase. In S phase, DNA synthesis takes place, increasing its content, and the cell becomes tetraploid (4n), instead of diploid (2n). After chromosome replication, the cell enters the G2 phase. In this phase, a rapid cell growth and protein synthesis occurs in order to prepare the cell for mitosis. In the M phase, the cell originates two new identical daughter cells, each of them owning a diploid set of chromosomes. This second major phase of the cell cycle is divided in two fundamental events: nuclear division (mitosis) and cytoplasmic division (cytokinesis).

Afterwards, each daughter cell immediately enters G1, having the opportunity to repeat the cycle or, alternatively, to pull out from the cycle into the G0 phase, a quiescence state, for an indefinite or permanent period of time (e.g., when nutrient supply is not favorable). In a developed multicellular organism, most cells are in G0 phase (Non-dividing cells), although retaining the opportunity to reactivate and re-enter the cell cycle in G1 phase at any time.

Cell cycle progression is regulated by, the protein family of Cyclins that interact with and activate the Cyclin-dependent kinases (Cdk), a family of serine/threonine protein kinases (137, 138). Each Cdk associates in a complex with a specific Cyclin and this association determines which proteins will be phosphorylated by the complex (Figure 3). Each phase of the cycle begins with a progressive increase in a specific Cyclin concentration, and terminates with its protease-mediated degradation. This degradation of Cyclin terminates its action and imprints a one-way direction to the cell cycle.

2. MITOSIS

Mitosis is an elaborated and highly regulated process by which a cell gives rise to two genetically identical daughter cells. Mitosis is a continuous event that occurs through five different stages that reflect general changes in cytoplasmic and chromosome structure: Prophase, Prometaphase, Metaphase, Anaphase and Telophase. Early mitosis initiates with Prophase which is marked by chromatin condensation, originating recognizable chromosomes. The classic four arm structure resides in a pair of sister chromatids held together by restricted area attached to each other at the centromere, where specific proteins bind and form the kinetochore - the structure at which spindle microtubules attach. It is also during this phase that previously duplicated centrosomes, the MTOCs (Microtubule Organizing Centres), begin to separate to opposite sites and define the future poles of the mitotic spindle. In the next stage, Prometaphase, the nuclear envelope breaks down and consequently, microtubules from opposite poles overcome all the cytoplasmic space, fully organize the mitotic spindle and start to attach to kinetochores of dispersed chromosomes, done by a ‘search and capture’ process.

Metaphase is achieved when kinetochore pairs of all chromosomes are bound to microtubules from opposite poles, assuming a bipolar orientation and an equatorial localization. Sister chromatid cohesion is then swiftly lost as they migrate to opposite poles of the spindle which marks the transition from metaphase to anaphase. At anaphase, it is possible to distinguish two periods, anaphase A, characterized by chromosome migration towards the poles, and anaphase B, characterized by the spindle poles moving apart as a result of spindle elongation. In the last stage, Telophase, chromatin decondenses, the

nuclear envelope is reconstituted into two identical nuclei and a contractile ring, which is composed of actomyosin fibers that extend around the equator of the dividing cell and then grips inward until they contact a group of microtubules that run between the poles, resulting in a structure connecting the future two daughter cells - the midbody.

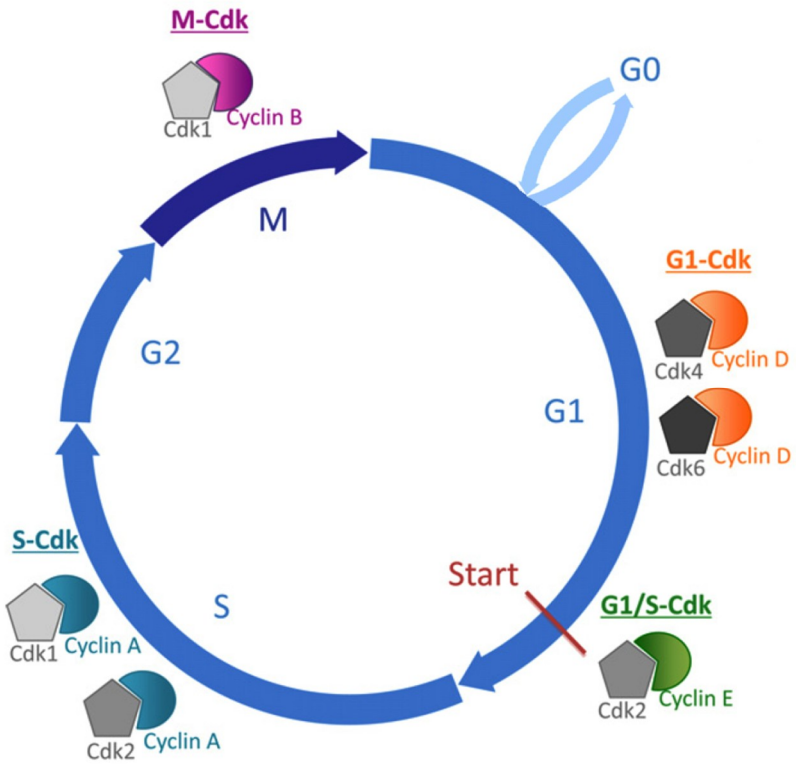

Figure 3: The cell cycle engine of mammalian cells. The cell cycle is driven by the sequential association of Cdks and cyclins: in G1 (growth phase): cyclin D, Cdk 4 and 6; in S (DNA synthesis phase): cyclin A, Cdk 1 and 2; in G2 (gap phase): cyclin A, Cdk 1; in M (mitosis phase): cyclin B, Cdk 1. Each Cdk-cyclin complex is thus specific of a phase of the cycle. The decision to enter a new cycle, or to arrest proliferation, is taken in G1. Prolonged, or "terminal", exit from the cycle is often denoted as G0 (Adapted from 139).

3. KINETOCHORE TO MICROTUBULE ATTACHMENT

After nuclear envelope break-down at the prophase to prometaphase transition, microtubules of the mitotic spindle initiate attachment to chromosomes at kinetochores. This specialized chromatin structure is the major site of microtubule-chromosome attachment by linking the centromere to the plus ends of microtubules originating from a spindle pole. This approximately 75-100 nm multiprotein structure has been exhaustively studied in the past few years in terms of its components and structural organization (140). An overall description of kinetochore structure and protein composition is given in Figure 4. Microtubules are polymers of α/β-tubulin dimers composed of 12-15 filaments arranged in hollow 25-nm diameter cylinders. Their length is variable as it alternates between growth and shrinkage phases, in a phenomenon generally known as "dynamic instability". Since

tubulin dimers are arranged in a fixed determined orientation, microtubules exhibit structural polarity, which influences movements along the spindle (132).

Chromosome attachment begins with the binding of a kinetochore to the lateral surface of a microtubule aided by the “search and capture” mechanism. This interaction initiates the movement of attached chromosomes towards one spindle pole where conversion from lateral to end-on attachment occurs (141, 142). The interaction with microtubules from the opposite pole (bi-orientation) allows chromosomes to localize near the spindle equator and to form a dynamic arrangement referred to as the metaphase plate.

During the process of chromosome bi-orientation, four possible kinetochore-microtubule attachments can be occur: monotelic attachment when one kinetochore is attached to microtubules from one spindle pole and its sister unattached; syntelic attachment when both kinetochores of a chromosome are attached to microtubules from the same spindle pole; merotelic attachment when a kinetochore is attached to both poles; and amphitelic attachment or bi-orientation, when each of the two opposing sister kinetochores is associated to microtubules originating from the proximal pole (Figure 5). Bi-orientation attachment is the only configuration that ensures accurate chromosome segregation at anaphase.

4. MITOTIC REGULATION

The control of mitosis is crucial and is mainly coordinated by two post-translational and intimately connected mechanisms: protein phosphorylation and proteolysis (143). Many of the major morphological changes that define mitosis are under the regulation of protein phosphorylation by serine/threonine kinases such as the Cdk1 (previously known as Cdc2) in association with Cyclin A and Cyclin B (144). Expression of Cyclin B peaks late in S phase and remains high during G2 and mitosis, establishing a complex with Cdk1 named Mitosis-Promoting Factor (MPF). Cyclin B-Cdk1 activation is fundamental to initiate the M phase and is also continuously required to trigger key mitotic events such as Nuclear Envelope Breakdown, centrosome separation, chromosome condensation, spindle assembly, APC/C (Anaphase-Promoting Complex or Cyclosome) activation and anaphase spindle elongation (145). The Ubiquitin-mediated proteolysis of Cyclin B, and consequently the inactivation of MPF, marks mitotic exit and cytokinesis (143). Besides these regulatory mechanisms of mitosis, cells have also developed a control mechanism that guarantees accurate chromosome segregation by preventing mitotic exit until each and every chromosome is attached in a bipolar fashion to the mitotic spindle. This machinery is called mitotic checkpoint or Spindle Assembly Checkpoint (SAC).

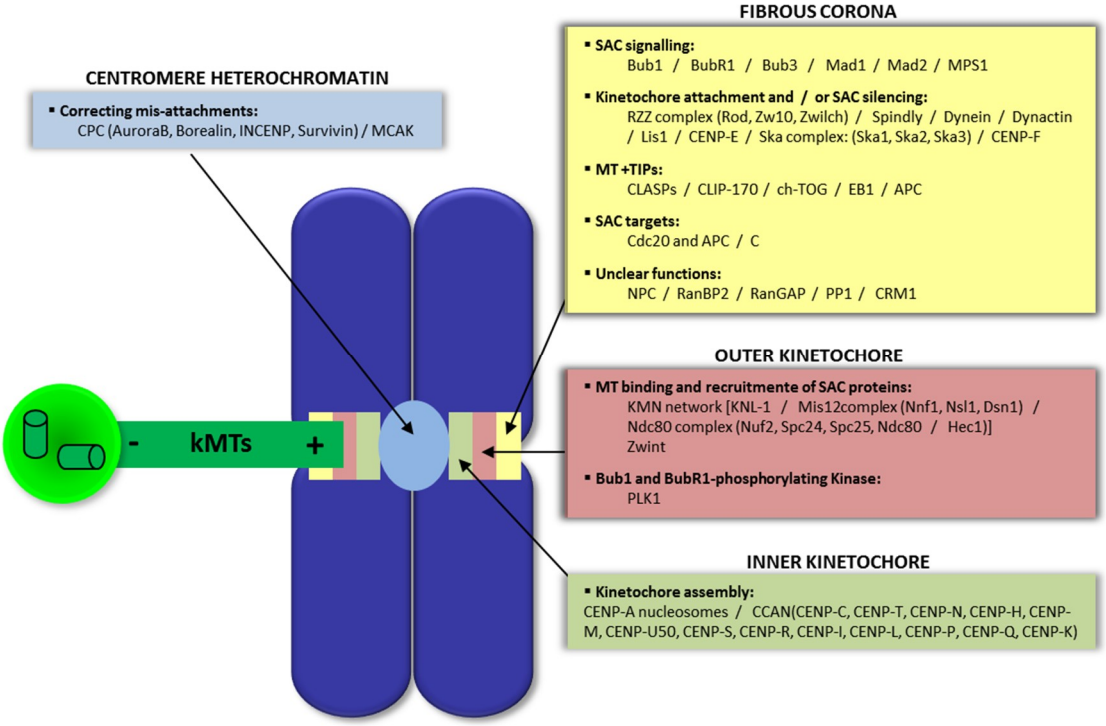

Figure 4 : Overview of protein complexes that build the kinetochore in animal cells. The kinetochore is built on the centromere as a trilaminar protein-rich structure: the inner kinetochore, the outer kinetochore and the fibrous corona. Proteins that compose each kinetochore layer are grouped by function (APC/C, anaphase promoting complex/Cyclosome; Bub1-BubR1-Bub3, budding uninhibited by benzimidazole; Cdc20, cell division cycle 20; CENP, centromere protein; CLASP, CLIP-associating protein; CLIP170, cytoplasmic linker protein-170; CPC, chromosome passenger complex; EB1, end-binding protein-1; INCENP, inner centromere protein; kMTs, kinetochore microtubules; LIS1, lissencephaly-1; Mad1-Mad2, mitotic-arrest deficient; MCAK, mitotic centromere-associated kinesin; MPS1, monopolar spindle-1; MT, microtubules; NPC, nuclear pore complex; PLK1, polo-like kinase-1; RanBP2, Ran-binding protein 2; RanGAP, Ran-GTPase-activating protein; RZZ, Rod (rough deal); SAC, spindle assembly checkpoint; Ska1-3, spindle and kinetochore-associated proteins; Zw10, zeste white 10 - Zwilch complex; Zwint, Zw10 interactor (132).

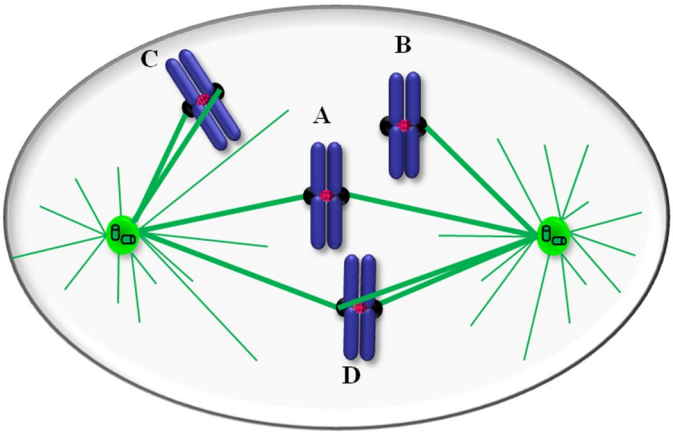

Figure 5: Bi-orientation and kinetochore attachment errors. (A) In amphitelic attachment, sister kinetochores are correctly attached to microtubules emanating from opposite poles of the spindle, leading to chromosome bi-orientation. (B) In monotelic attachment, the chromo-some is mono-oriented as one kinetochore is attached to the microtubules from one spindle pole, while its sister is unattached. (C) In syntelic attachment, the chromosome is mono-oriented but, in this case, both sister kinetochores are attached to microtubules from the same spindle pole. (D) In merotelic attachment, one sister kinetochore is attached to microtubules from both spindle poles, the chromosome is improperly bi-oriented and, if left uncorrected, can produce an anaphase lagging chromosome. (132).

4.1 Spindle Assembly Checkpoint

Key components and mechanism of action

The SAC is a surveillance mechanism that delays the onset of anaphase until all chromosomes are properly attached and bi-oriented on the microtubule spindle (146). Although there is still many discussion concerning which parameter is monitored by the mitotic checkpoint, the most accepted theory is the one that states that this mechanism senses either kinetochore- microtubule attachment and tension across sister kinetochores. This theory is reinforced by the fact that tension is generated by forces upon kinetochore-microtubules attachment and that this attachment needs tension to promote stable connections (147-149). SAC maintains cells in mitosis by preventing Cyclin B and securin from being targeted by the E3 ubiquitin ligase APC/C and degraded in the proteasome. Several conserved components of the SAC are involved, such as the core SAC components Mad1, Mad2, BubR1 (Mad3 in yeast, worms and plants), Bub1 and Bub3 (Table 1) (150, 151).

Mps1 protein also plays a significant role in SAC activity, besides its initially identified role as a requirement for the proper assembly of bipolar spindles (152, 153). Mps1 activity rises during mitosis and dynamically localizes to kinetochores, having the ability to dimerize and is autoactivated by cross-phosphorylation (154, 155). Mps1 directly phosphorylates the inner centromere protein Borealin and, subsequently, increases Aurora B activity. Its activity directs a number of checkpoint proteins including Mad1 to unattached kinetochores (156).

The unattached kinetochores rapidly promote the association of Bub1, BubR1, Bub3, Mad1 and Mad2 to the kinetochore. Mad2 is a conserved mitotic checkpoint protein that is thought to monitor microtubule attachment at the kinetochore, and can adopt two distinct conformations, open (O) and closed (C) (Figure 6) (157-159).

During interphase, most Mad2 exists in the O-conformation, although, localizing at the nuclear envelope, a small amount assumes the C-conformation assembled with Mad1 (159, 160). At prometaphase, Mad1:C-Mad2 complexes are found in unattached kinetochores and are believed to act as an instigator of conversion into C-Mad2 (161). C-Mad2 bounds to Cdc20, leaves the kinetochores and it is thought to catalyse O-Mad2/C-Mad2 conversion in the cytoplasm leading to signal transduction and amplification (162). Mad2 and Cdc20 together with the subcomplex BubR1:Bub3 promote a “wait anaphase” signal by generating the mitotic checkpoint complex (MCC), which prevents APC/C activation by sequestering Cdc20 (163, 164). The *Bub* family is believed to sense spindle tension.

Table 1. Mitotic checkpoint core proteins and their most significant properties, interactions and functions

Protein	Characteristics	Known ligands	Role in the SAC	Ref.
Bub1	122 kDa mitotic kinase	Bub3, SV40 T-large antigen, Blinkin	Part of the MCC complex. Localizes to Kinetochores. Inhibits Cdc20 by phosphorylation. Required for recruiting other checkpoint proteins. Kinase activity is not required for checkpoint arrest.	(165-167)
BubR1	120 kDa mitotic kinase	CENP-E, Bub3, Cdc20, Blinkin	Part of the MCC complex. Localizes to Kinetochores. Part of APC/C inhibitory complex. Directly binds to Cdc20 and inhibits APC/C activity. Yeast Mad3, the functional equivalent of BubR1.	(165, 166, 168)
Bub3	37 kDa	Bub1, BubR1	Part of the MCC complex. Localizes to Kinetochores. Part of APC/C inhibitory complex. Localizes Bub1 and BubR1 to kinetochores.	(169, 170)
Mad1	83 kDa	Mad2	Directly recruits Mad2 to unattached kinetochores. Localizes to nuclear pores and unattached kinetochores. Binds to Bub1 and Bub3 upon checkpoint activation in budding yeast.	(171)
Mad2	23 kDa	Mad1, Cdc20, CMT2/p31^{comet}	Inhibits APC/C by binding to Cdc20. Part of the MCC complex. Occurs in two conformations ('closed' C-Mad2 on binding Mad1 or Cdc20, or 'open' O-Mad2 when unbound). Localizes to nuclear pores and unattached kinetochores	(157, 159)
Mps1	97 kDa mitotic kinase	Mad1, Proteins SPB	Essential to centrosome duplication. Required for recruitment of Mad1, Mad2 and CENP-E to the kinetochore. Localizes to nuclear pores, centrosomes and Kinetochores	(153, 156)

Although it is widely accepted that Bub1 contributes to the communication between the mitotic checkpoint pathway and the kinetochore-microtubule network, its role in SAC is still very controversial the actual mechanism (165, 172).

As soon as chromosomes undergo bipolar attachment and are fully align at the metaphase plate, the mitotic checkpoint is quickly silenced. Regarding SAC silencing, a few mechanisms have been suggested, including: removal of checkpoint components from the attached kinetochore towards spindle poles by the microtubule motor complex dynein to cease MCC action; p31comet binding to Mad2, leading to Cdc20 dissociation from Mad2; Cdc20 multi-ubiquitination in a APC- or UbcH10-dependent way; and, more recently, a distinct regulatory network that includes the protein phosphatases PP1 and PP2A (173-182). In either case, SAC silencing leads to APC/C activation that in turn, targets Securin and Cyclin B for proteolysis. Securin is an inhibitor of a protease known as Separase, which

is mandatory to cleave the Cohesin complex that embraces sister chromatids together, and ultimately, Cohesin ring break is necessary to accomplish anaphase. In regard to Cyclin B, its degradation inactivates Cyclin B-Cdk1 complexes and consequently leads to mitotic exit.

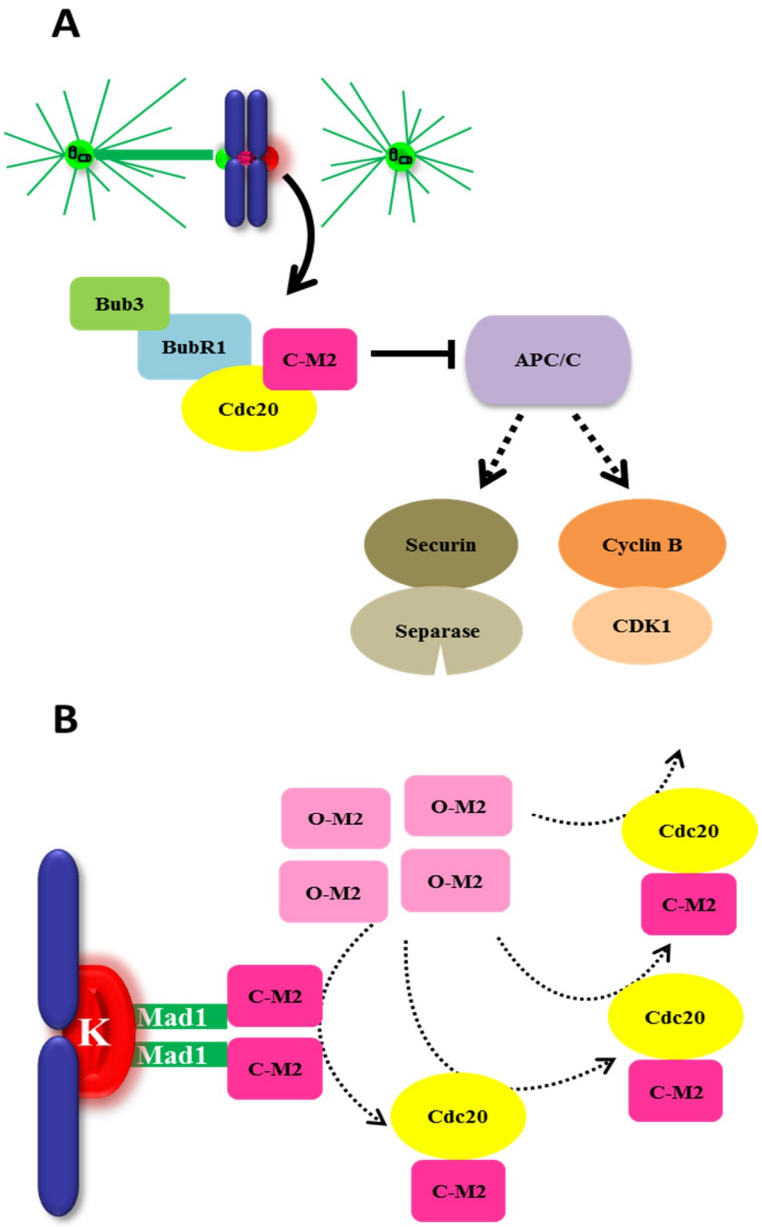

Figure 6: Model of spindle assembly checkpoint signalling. (A) Unattached kinetochore serves as a platform for SAC proteins BubR1, Bub3, and Mad2 to generate the mitotic checkpoint complex that binds to Cdc20 preventing it from activating APC⁄C, the E3 ubiquitin ligase that targets Securin and Cyclin B for degradation by the 26S proteasome, thereby inhibiting anaphase onset. (B) According to the Mad2 template model, a constitutively closed conformation of Mad2 (C-M2) bound to Mad1 serves as receptor at the unattached kinetochore for cytosolic open form of Mad2 (O-M2) to switch this latter to C-Mad2 bound to Cdc20. C-Mad2⁄ Cdc20 complex acts as a structural equivalent of Mad1⁄ Mad2 to convert more O-Mad2 into Cdc20 bound C-Mad2 in the cytosol, leading to signal amplification (132).

5. MITOTIC CHECKPOINT AND CANCER

Disordered mitotic passage frequently results in chromosome missegregation, essentially irreversible, which at high rates describes a phenomenon called chromosomal instability (CIN). CIN is a common feature of many cancers and it correlates with poor patient prognosis and drug resistance (183). CIN can lead to an abnormal number of chromosomes, termed aneuploidy, but not all aneuploid cells display CIN as some cells are aneuploid with a stable karyotype. The high frequency of aneuploidy in cancer and the awareness of aneuploidy as a possible cause of tumorigenesis were reinforced by analyses of the Mitelman Database, a major repository of cytogenetic information on human cancers, with results from over 60,000 cases (184, 185).

The impaired functioning of several cellular pathways has been associated with the increasing rate of chromosome gains and losses upon mitosis. Such pathways include: SAC dysfunction, centrosome abnormalities, defects in the attachment of chromosomes to spindle microtubules and chromosome cohesion defects (131, 186, 187). In this review, we will focus on how a defective SAC may contribute to chromosome missegregation.

The spindle assembly checkpoint is a key signaling pathway that should prevent cells from prematurely segregating their chromosomes and, as a result, preclude CIN. A single unattached kinetochore was proven to be enough to postpone anaphase onset until the last kinetochore is attached to the spindle. On the other hand, a complete silencing of the mitotic checkpoint results in massive chromosome loss, cell death and embryonic lethality (112, 188). However, a weakened mechanism, largely widespread among tumor cells, can cause premature anaphase, chromosome instability and aneuploidy (Figure 7) (189, 190). These effects have been studied in mice heterozygous for Mad1, Mad2, Bub3, Bub1 or BubR1, conditions which led to subtle rates of chromosome instability, compatible with cell viability (191-196). In agreement, is the case of patients with the premature chromatid separation (PCS) syndrome, also referred to as mosaic variegated aneuploidy (MVA) (197). This rare genetic disorder has been linked to mutations in the BUB1B locus and a high rate of cancer development, frequently within the first 3 years of life.

As a result, many studies have been conducted in order to find mutations on checkpoint components in human cancers that could explain SAC deregulation, and, although somatic mutations were detected and proven to be associated with chromosome segregation and cancer progression, it does not seem to be a common contributor for aneuploidy (189, 190). However, altered expression levels of SAC genes appear to be much more recurrent, and both under and overexpression were reported (190). A lower expression can be explained by the results obtained in mice heterozygous for SAC components (191, 193, 195, 196). On

the contrary, how an increased expression can be related to aneuploidy remains unknown. Nevertheless, some theories have been proposed; for instance, it is possible that overexpression could represent a cellular compensation for deficiencies in other molecular components of the SAC (198). Regardless the controversy surrounding SAC contribution to tumorigenesis and cancer, the involvement of SAC molecular elements in diverse cellular processes beyond chromosome congression, should be taken into account (160, 199, 200) How post-translational modifications of SAC elements could contribute to chromosome instability should also provide important information (201), especially when concerning CIN cancer cell lines that appear to have normally functioning checkpoints (202).

5.1 Therapeutic Targeting of the Mitotic Checkpoint Pathway

Antimitotic chemotherapy remains the most effective approach in the clinical treatment of a variety of human cancers. The most commonly used drugs are microtubule-targeting agents, which are classified in two main groups: microtubule-destabilizing drugs, that restrain microtubule polymerization (ex: vinca alkaloids); and microtubule-stabilizing agents, that intensify microtubule polymerization (ex: taxanes) Figure 8) (112). Vinka alkaloids such as vincristine, vinblastine, and vinorelbine, are often used for solid and haematological malignancies, such as NSCLC and Hodgkin and non-Hodgkin lymphoma (112, 124). Taxanes such as docetaxel and paclitaxel are frequently used as adjuvant on advanced breast, ovarian and head and neck cancer (124). On both classes these drugs avert a functional spindle leading to SAC activation and anaphase delay (108). After mitotic arrest, cells may undergo two different pathways, cell death or mitotic slippage (109). Slippage refers to a process where cells exit mitosis and begin a new cycle with twice the DNA content (110). These cells can arrest in G1 phase, undergo cell death or continue cell cycle progression increasing the potential for tumorigenesis (111). Apart from that, severe side effects, like myelosuppression and neurotoxicity and the frequent development of resistance to these drugs have limited their use and motivate the search for different antimitotic drugs (112).

SAC is an essential cell cycle checkpoint for cell survival and inducing lethal instability by targeting this mechanism is an innovative strategy in cancer therapy (203). Inhibitors of kinesin motor proteins, which are vital for spindle assembly and chromosomes movement during mitosis, show to be promising in this regard (114). CENP-E is an essential plus end-directed microtubule motor, present only in cells undergoing mitosis and is a fundamental protein for the alignment of chromosomes by moving unattached kinetochores towards the metaphase plate along kinetochore microtubule bundles, termed K-fibers (120).

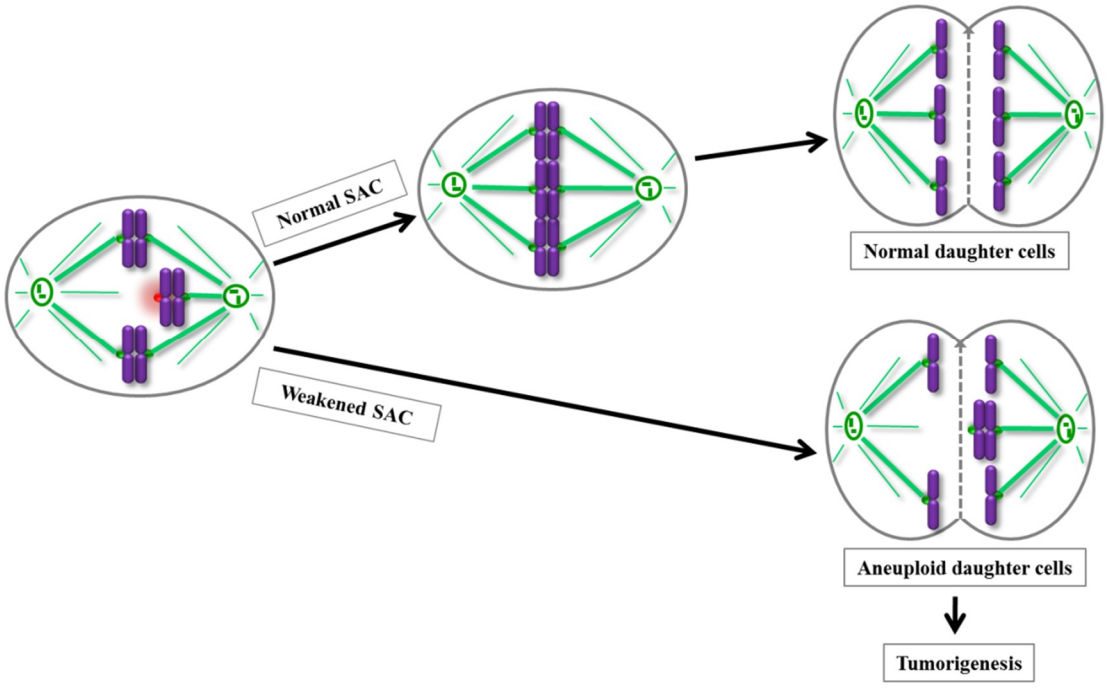

Figure 7: Defects in SAC activity can contribute to aneuploidy and tumorigenesis. Chromosome missegregation is prevented in cells with a fully functional SAC. In cells with weakened SAC activity, the residual checkpoint activity can still ensure the accuracy of chromosome segregation. However, occasional missegregations may escape from SAC control and lead to aneuploidy, which may contribute to tumorigenesis (131).

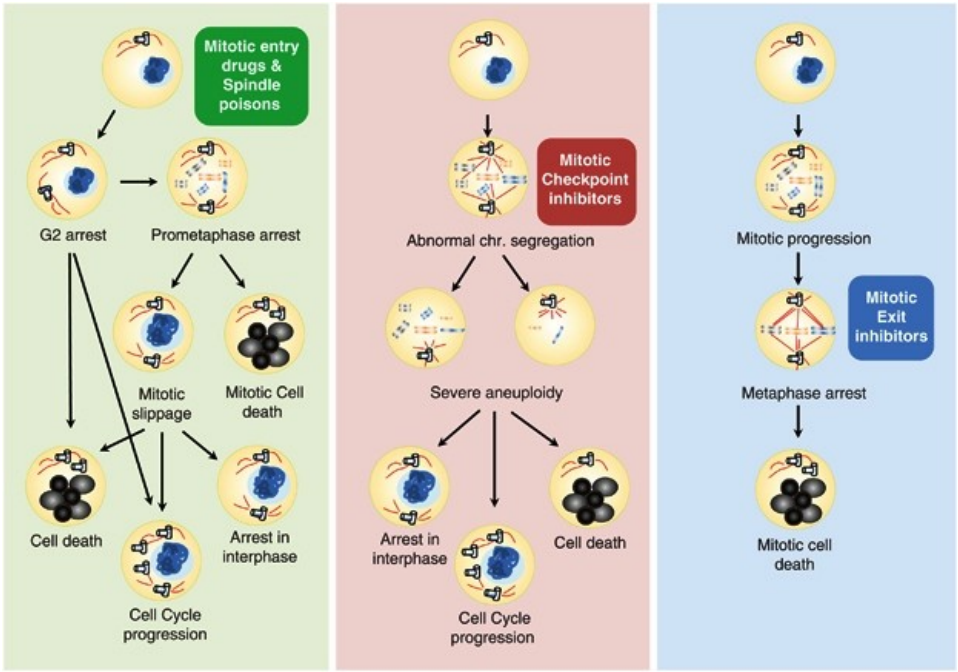

Figure 8: Models for targeting mitosis as an anticancer strategy. Treatment with mitotic entry inhibitors or spindle poisons leads to G2 or prometaphase arrest that eventually may end up in apoptosis during interphase or mitosis. However, cells may escape entering into a new cell cycle. Depending of the status of genes such as p53, pRb or p38, these cells may arrest before entering S phase, die or continue proliferating. Targeting mitotic checkpoint regulators, such as BubR1, Mps1 or Mad2, leads to severe levels of aneuploidy. Cells containing numerical chromosome aberrations can similarly either arrest in the subsequent G1 phase, progress through the cell cycle or undergo cell death. Inhibiting mitotic exit (e.g., by targeting APC/C-Cdc20) causes a permanent metaphase arrest by preventing cyclin B1 degradation, thus irreversibly leading to mitotic cell death (133)

CENP-E provides a link between chromosome/microtubule attachments and SAC by modulating BubR1 function (204). Cell cycle arrest and apoptosis are two consequences of the inhibition of CENP-E activity, which can act as tumor suppressor and represent an attractive antimitotic target (121). Several CENP-E inhibitors have been studied and a few have reached phase I of clinical trials (122, 205, 206).

In addition to CENP-E, Eg5 is a plus-end-directed kinesin 5-family protein, essential for the assembly and organization of the mitotic spindle and thought to bind antiparallel microtubules and slid them apart. Eg5 suppression results in the formation of characteristic monoaster spindles followed by mitotic arrest and apoptosis (207). The first small-molecule inhibitor being identified was monastrol, a cell-permeable molecule that arrests cells in mitosis, but since then, several Eg5 inhibitors have been analyzed and reached clinical trials (208). In spite of the initial expectation and the limited toxicity profile, only partial responses have been observed, suggesting that these agents should be used in combination with other cytotoxic drugs (114).

Mitotic kinases are deregulated in a multiplicity of tumor cells, suggesting their potential role in tumorigenesis and making them a tempting target for molecular therapies(115). PLK1 (polo-like kinase 1) and Aurora kinases represent a highly conserved family of serine/threonine kinases that ensures a correct spindle assembly heading to an accurate segregation of the chromosomes into daughter cells. There are three human Aurora kinases, Aurora A, B and C. Aurora A is the most extensively studied member and is required for bipolar spindle formation. Its suppression leads to cell cycle arrest and monopolar mitotic spindles, as it happens in Plk1 inhibition. Aurora B is required for chromosome segregation and cytokinesis and, thus, its inhibition culminates in a premature exit from mitosis, leading to polyploidization (209). In addition, inhibition of Aurora B kinase activity prevents BubR1 kinetochore localization after a reduction in centromeric tension. Aurora C is the less extensively investigated member and it appears to be important during mitosis, where it assumes a centrossomal localization and functions very similarly to Aurora B (210). An association between Aurora C and cancer has not been established until now. Due to their recognition as potential targets for cancer chemotherapy, around 30 Aurora kinase inhibitors have reached different stages of pre-clinical and clinical development (116). Concerning Plk1 activity, small-molecules and phosphopeptide inhibitors have been recently developed due to their potency and specificity against Plk1 (117). Blocking these targets' activity might not necessarily end in cell death; instead, cells can undergo mitotic slippage and exit mitosis without proper segregation of sister chromatids and cytokinesis, exhibiting multiple nuclei and polyploidy.

Another important mitotic kinase is Mps1, which is required for proper chromosome segregation during mitosis. Due to its function in mitosis, Mps1 is an appealing target for anti-cancer therapies. Mps1 reduced levels have showed to increase tumor cells, but not normal cell, sensitivity to paclitaxel, resulting in severe chromosome segregation errors and subsequently, in cell death (156). Although several chemical inhibitors of human Mps1 kinase activity led to promising results, none has fulfilled clinical premise (136, 211).

Mitotic slippage and its consequences occurs in the presence of an active SAC and it's thought to be trigger by cyclin B destruction (109). Considering the interest in stabilizing cyclin B concentrations in order to prevent mitotic exit, the E3 ubiquitin ligase APC/C has also been evaluated as potential cancer drug target. APC/C depletion, by RNA interference (RNAi), results in a prolonged mitotic arrest and increases cell sensitivity to chemotherapeutics (212). A small molecule called TAME was discovered, which prevents APC/C activation but still allows cyclin B degradation (213). This reflects the difficulties in targeting ubiquitin ligases. With the same purpose, experiments have been made in order to promote Cdc20 inhibition by RNA interference or genetic elimination (214). Mitotic arrest, vast apoptotic cell death and tumor regression resulted from Cdc20 removal (215). These results reinforce that targeting mitotic exit may be an excellent adjuvant for other mitotic drugs.

The SAC core proteins Mad2 and BubR1 bear the potential to be successful targets of several therapeutic strategies since their abnormal expression has been reported in countless types of malignancies (216-218). When downregulated, these proteins showed to increase cell proliferation and drug resistance although the responsible mechanism has not been fully evaluated (131, 219). On the contrary, their knockdown is consistently lethal, due to colossal chromosome loss, culminating in the inhibition of tumor progression (188, 191). A more recent work has described a natural diterpenoid, Pharicin A, capable of inhibiting BubR1 (220). During the last decade, a regulatory mechanism for gene expression in eukaryotic cells has gained particular attention. RNA interference has emerged as a powerful tool for modulating gene expression, including Mad2 and BubR1 expression (221, 222). A new class of anti-mitotic compounds has been emerging and continues to highlight the importance of increasing our knowledge on these pathways, so that it can be reflected in cancer drug development.

RNA INTERFERENCE

1. INTRODUCTION

RNA interference (RNAi) is a well characterized mechanism of eukaryotic gene regulation but also a defense mechanism to foreign RNA like from viruses and transposable elements (223). It has been a major focus of research since it allows to determining and dissecting the function of specific proteins and treatment of diseases caused by overexpression of specific genes (224, 225). The main advantage of RNAi when compared to approaches based on small molecules, antibodies or proteins, is that this approach can focus in any target, including the ones that do not fit into the so-called "drugable target classes", provided that the nucleotide sequence of the target gene of interest is known. Other benefits on using RNAi include high degrees of efficiency, specificity and efficacy, uncomplicated synthesis and manufacture, and high cross species reactivity (224).

RNAi, with its valuable advantages, has provided an enormous potential as a therapeutic tool given the ability to target and silence specific genes. As most of diseases embroil some sort of deregulated gene, including cancer, metabolic and genetic disorders, virus infections, they all become a possible target for RNAi-based therapeutics.

2. RNAI MECHANISM

RNA interference is mediated by the RNA-induced silencing complex (RISC) and by short double stranded RNA molecules that have about 20-30 nucleotides and can be found naturally in organisms or synthetically produced to target a specific gene (

Figure 9) (226). RNAi mainly occurs via two types of RNA molecules: small interfering RNAs (siRNAs) and microRNA (miRNA). miRNAs are endogenous non-coding single-stranded RNAs that mediate post-transcriptional gene silencing from endogenous transcripts. siRNAs can be produced from a long double-stranded RNA, of endogenous or exogenous origin, by the enzymatic activity of the RNase III enzyme Dicer. Synthetic siRNAs have a 2-nucleotide 3’ overhangs that copycats Dicer products. siRNAs produced by Dicer-mediated cleavage are incorporated into the RISC. The RISC complex is a multi-protein complex with nuclease activity that uses the antisense strand of the siRNA to target complementary mRNA for subsequent site-specific cleavage and degradation (227). The RISC complex is then recovered for further cleavage/degradation cycles. The mRNA cleavage is the result of the endoribonuclease activity of the RISC subunit, Argonaute 2 (228). Although there are additional RISC components, their roles in RNAi are not clearly known.

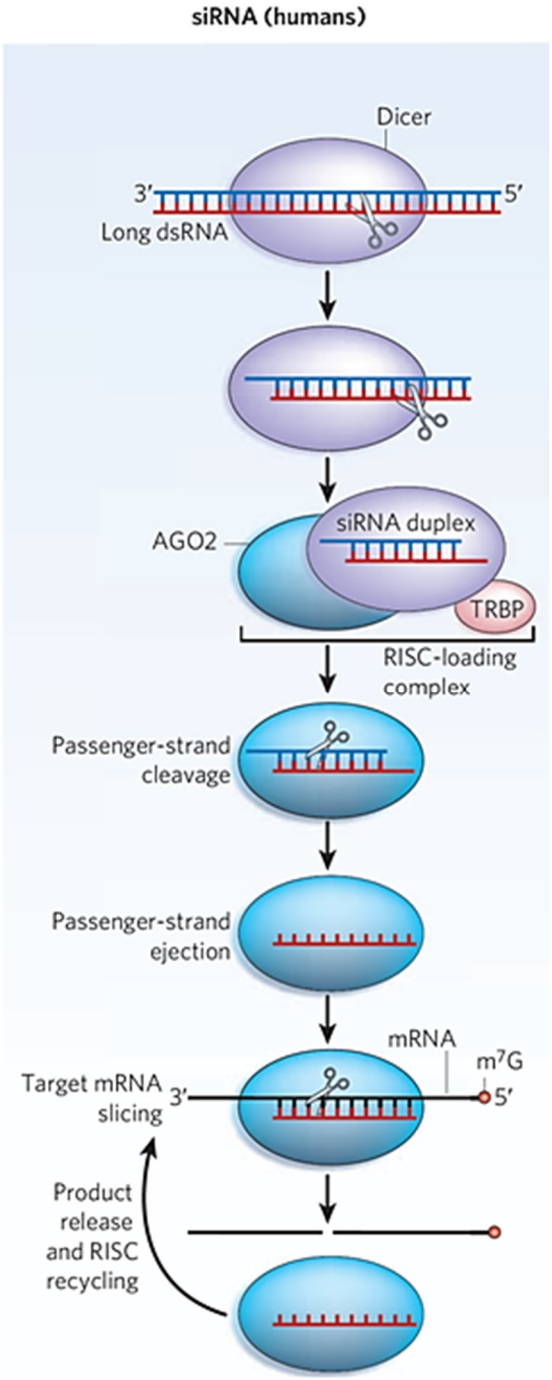

Figure 9: Small regulatory RNAs are non-coding RNA molecules that silence target RNAs in a sequence-specific manner. siRNAs, mediate RNAi by downregulating target RNAs through slicing; that is, by endonucleolytic cleavage These small RNAs are derived from long double-stranded RNA (dsRNA) molecules that result from RNA virus replication, convergent transcription of cellular genes or mobile genetic elements, self-annealing transcripts or experimental transfection. The endonuclease Dicer functions as a molecular ruler to cleave the dsRNA at 21-25-nucleotide intervals. After Dicer-mediated cleavage, one strand of the siRNA duplex (the guide strand) is loaded onto an Argonaute protein at the core of an RNA-induced silencing complex (RISC). (For simplicity, in the figure, the RISC is represented just by an Argonaute protein.) Argonaute loading takes place in the RISC-loading complex, a ternary complex that consists of an Argonaute protein, Dicer and a dsRNA-binding protein (known as TRBP in humans). During loading, the non-guide (passenger) strand is cleaved by an Argonaute protein and ejected. The Argonaute protein then uses the guide siRNA to associate with target RNAs that contain perfectly complementary sequence and then catalyses the slicing of these targets. After slicing, the cleaved target RNA is released, and the RISC is recycled for another round of slicing. (Adapted from 229).

3. RNAI VERSUS ANTISENSE APPROACH

The use of antisense oligonucleotides is another method of gene knockdown; however it relies on ribonuclease H (RNAse H)-dependent cleavage of mRNA. Antisense oligonucleotides refers to short, single-stranded DNA or RNA sequences that are designed to be synthetic analogues of natural nucleic acids that specifically bind to a target mRNA. Similar to RNAi technology, antisense approach works reducing translation of target protein using the cell machinery leading to a greatly potent down-regulation of gene expression. Since their first applications in 1978, several chemical modifications have been proposed in order to improve antisense oligonucleotides stability *in vitro* and *in vivo*, but still maintaining their activity (230). Two of the most common modifications include the addition of phosphorothioate bonds and 2′-O-methyl-modified nucleotides (231).

This last modification has successfully been used in clinical trials (232). Small antisense RNA may culminate on the same effect though it displays a much lower efficiency comparing to RNAi. Due to their charge and nature, generally both kind of molecules do not cross cell membranes efficiently on their own and therefore need to be specially formulated for most applications.

4. SIRNA VS. SHRNA

siRNAs are the most frequently used oligonucleotides in RNAi-based therapeutics, although there are two more different classes, miRNAs and short hairpin RNAs (shRNAs) (233). These three have different efficiencies and specificities, but all share the intervention of RISC in their RNAi pathways in mammals. siRNA and shRNA are originated from exogenous molecules. While siRNAs are delivered to target cells as 20-30 base duplexes using a RNA-based strategy, shRNAs are expressed from plasmids or viral vectors in a DNA-based approach, originating longer RNA hairpin transcripts that are intracellularly converted into siRNA (234). shRNAs are more frequently used in laboratory studies since they allow permanent gene silencing. shRNAs have a higher potential of being a successful therapeutic strategy since they result in a permanent potent gene silencing in a single treatment (235). However, shRNAs lose their main advantage to RNA-based approach when cell death is the main result of target gene knockdown. Another disadvantage of shRNA consists on the potential sequence-specific off-target effects due to structural similarities with miRNAs (236).

5. RNAI-BASED ANTI-CANCER THERAPY

The discovery of RNAi has prompted many innovations in the medical field. RNAi has been extensively analyzed aiming at two main purposes: elucidation of gene functions and as therapeutics. By knocking down a single gene at a time and studying the outcome, RNAi technology allows us to identify the genes responsible for the loss of that specific function or a particular disease, but also to detect synthetic interactions between genes due to redundancy of gene function in complex organisms (237). These can point out important targets for therapeutics. Theoretically, RNAi could be applied to treat or stop progression of any disease, including brain disorders such as Huntington's and Alzheimer's, hereditary maladies, genetic and viral diseases, and cancer. In fact, several of them have already progressed from bench to bedside with several RNAi-based drugs undergone through clinical trials (238). From now on, we will focus on the therapeutic potential of RNAi in cancer treatment.

RNAi therapeutics can be used to concurrently target multiple genes in different cellular pathways involved in tumor development and also be manipulated as an individually personalized anticancer drug (239). siRNA and shRNA have been extensively employed, with favorable outcomes in silencing key targets like oncogenes, proteins with different functions, including enzymes, cell cycle regulators, cytokines, etc., and that are critical for tumor cell growth, metastasis, angiogenesis and chemoresistance (240, 241). On the basis of their effectiveness, the most promising ones have been presented in a large number of preclinical studies involving mouse xenograft models. Tumor cell proliferation is one of the most significant predictor of prognosis for different types of cancer. Tumor necrosis factor ligand (TNF) superfamily member 13, also known as a proliferation-inducing ligand (APRIL) is a member of the TNF ligand family. This protein has been shown to be capable of inducing the tumor proliferation (242). In the *in vivo* study of Wang and co-workers, after intratumoral injection of APRIL siRNA, the grafted human colorectal tumor had its growth and metastasis inhibited as well as increased apoptosis and necrosis (243).

Signal transducer and activator of transcription (STAT) proteins are activated by many cytokines and growth factors and play a key role in cell survival, proliferation, and differentiation. Constitutively activated STAT leads to induction of an anti-apoptotic pathway and has been reported in a number of malignant cell lines and human cancers (244). STAT3, a member of this family, is a point of convergence for many oncogenic pathways directly contributing to tumorigenesis, invasion, and metastasis (245). For these reasons, STAT3 has been seriously considered as a silencing target in hepatocarcinoma, prostate cancer, T-cell lymphomas, melanoma, lung cancer and ovarian cancer (246-249). Yang and

co-workers have obtained consistent *in vitro* and *in vivo* results showing that STAT3 siRNA can effectively inhibit the growth of breast cancer cell and the development of human tumor xenografts in mice (250).

A promising strategy against cancer is to use RNAi as a tool to silence oncogenes, turning off major MDR mechanisms as increased drug efflux, decreased drug influx, activation of detoxifying systems, activation of DNA repair and blocked apoptosis (251). Overexpression of ATP-binding cassette (ABC) transporters, as MDR1 (ABCB1), MRP1 (ABCC1) and ABCG2, is one of those mechanisms and several attempts have been made to co-deliver siRNA targeting MDR1. Li et al. developed a MDR1 siRNA and Dox co-delivery system using drug resistant HeLa/Dox cells which culminated in reduced levels of MDR1 gene expression, enhanced intra-cellular Dox accumulation and an increased toxicity of Dox (252).

RNA interference has been very helpful as an adjuvant for chemotherapy and radiotherapy as it can increase cell sensitivity. Bcl-2 and nuclear factor erythoid-2-related factor 2 (Nrf2) siRNAs are two examples that illustrate such occurrence (253, 254). Cancer cell resistance to chemotherapy depends on two main components: nonpump resistance and pump resistance. Apoptosis regulator Bcl-2 plays a vital role in nonpump resistance by activating cellular anti-apoptotic defense and preventing cell death (255). Chen and collaborators deliver doxorubicin and Bcl-2-targeted siRNA simultaneously into multidrug resistant human ovarian cancer cells. Their results showed that Bcl-2 siRNA can effectively decrease the Bcl-2 mRNA by 80%, significantly suppress the nonpump resistance, and substantially enhance the anticancer action of doxorubicin (253).

One example of pump resistance is Nrf2, a transcription factor that play a physiological role in the regulation of oxidative stress and is involved in a cellular protective response that defends cells against toxic insults from a broad spectrum of chemicals (256). Nrf2 and its downstream genes are overexpressed in resistant cancer cells and human cancer tissues, which is thought to underlie acquired chemoresistance, providing cancer cells with an advantage for survival and growth (257). Activation of Nrf2 results in the induction of multidrug resistance-associated proteins (Mrps), membrane multidrug efflux transporters. Ma and collaborators used a cervical cancer mouse xenograft model transfected with plasmids containing Nrf2-shRNA and were able to decrease Nrf2 mediated-target genes expression levels (258). Nrf-2 siRNA in combination with cisplatin treatment had the ability to significantly inhibit tumor growth. Bcl-2 and Nrf-2 might therefore constitute promising therapeutic targets to enhance the efficacy of anticancer drugs. SiRNA and shRNA

therapeutics have been explored in numerous preclinical studies but only six RNAi-based drugs for cancer are currently being evaluated in clinical trials (Table 2).

Table 2: RNA interference based therapeutics in clinical trials [a]

Diseases	Target	Drug name	Phase	Sponsor/ Collaborators
Advanced or Metastatic Pancreatic Cancer	Protein Kinase N3	Atu027	1/2	Silence Therapeutics AG; Granzer Regulatory Consulting and Services; FGK Clinical Research GmbH
Pancreatic Cancer	KRASG12D	siG12D LODER	2	Silenseed Ltd
Solid Tumor Cancers	M2 subunit of ribonucleotide reductase	CALAA-01	1	Calando Pharmaceuticals
Advanced solid tumors	EphA2	siRNA-EphA2-DOPC	1	M.D. Anderson Cancer Center; Ovarian Cancer Research Fund
Solid Tumors; NSCLC; Renal Cell Carcinoma; Hepatocellular Carcinoma; Ewing's Sarcoma	furin	FANG™ Vaccine	1	Gradalis, Inc.
Advanced Cancer; Metastatic Cancer; Solid Tumors	STMN1	pbi-shRNA™STMN1	1	Gradalis, Inc.
Stage III Ovarian Cancer; Stage IV Ovarian Cancer	furin	FANG™ Vaccine	2	Gradalis, Inc.

[a] http://www.clinicaltrials.gov.

One of those is Atu027, which consists of a cationic lipoplex formulation with siRNAs targeting protein kinase N3 (PKN3) (259). Previous studies have shown that the depletion of this kinase resulted in the inhibition of lymph node metastasis in orthotopic prostate cancer mouse models (260). Aleku and co-workers evaluated the effect of siRNA molecules formulated into siRNA-lipoplexes that consisted of a mixture of cationic and fusogenic lipids complexed with the negatively charged siRNA. They were successful in the *in vivo* downregulation of the corresponding mRNA and protein levels, with significant inhibition of tumor growth and lymph node metastasis. Atu-027 is presently in Phase I clinical trials and has early exhibited signs of efficacy (259).

A transferrin receptor-targeted nanoparticle has been introduced by Calando Pharmaceuticals for siRNA delivery (261). This targeted siRNA nanoparticle formulation, denoted as CALAA-01, aims to inhibit the expression of M2 subunit of ribonucleotide reductase (RRM2), a gene involved in DNA replication, and to prevent the proliferation of tumor cells. RRM2 is a therapeutic target for DNA replication-dependent diseases such as

cancer and, when downregulated, exhibits significant antiproliferative activity (262). Taking into account that transferrin receptors are typically upregulated on cancer cells, human transferrin was used as a targeting ligand in the surface of the nanoparticle that consisted of a cyclodextrin-containing polymer and PEG as a steric stabilization agent. On phase I clinical trials, CALAA-01 was systemically administrated to patients with solid tumors and was able to silence the cancer-associated gene in specifically-targeted tumor cells (261).

The local microenvironment, or niche, plays important roles in tumor growth through central processes as angiogenesis and inflammation. The VEGF family of ligands and receptors are key regulators of these processes (263). Alnylam Pharmaceuticals has taken that in consideration and has developed ALN-VSP02, a lipid nanoparticle formulation encapsulating two modified siRNAs targeting either the VEGF or Eg5 kinesin. Eg5 is a member of the kinesin superfamily of microtubule-based motors and mediates centrosome separation and bipolar spindle assembly and maintenance (264). Its depletion in pre-clinical studies has led to cell cycle arrest at mitosis and ultimately, to cell death, while VEGF knockdown was associated with decreased tumor growth and microvessel density (265). ALN-VSP02 has shown the same effects in preliminary clinical data on phase I clinical trial, along with the potential to sensitize liver cancer to chemotherapy.

RNAi possesses high specificity and high efficiency in down regulating gene expression, it consists on a potential therapeutic strategy against many diseases. siRNA technology is therefore expected to be an invaluable treatment for number of diseases including cancer, although the future success of this approach will depend on the development of effective, specific and safe delivery systems.

6. CHALLENGES OF RNAI AS THERAPEUTIC PLATFORM

RNAi has shown immense potential in the treatment of cancer, viral, and genetic disorders. However, there are some disadvantages and limitations (266). RNAi can be more toxic than traditional drugs as they might affect the functions of undesired targets by non-specifically targeting other RNAs (the so-called off-target effects) (240). siRNAs may also activate components of the immune system in some cases, leading to non-specific consequences/phenotype. The most critical factor limiting the utility of siRNA as therapeutics is delivering siRNA to its intracellular target site (233). Delivery of these molecules into the desired organs, tissues and cell sites in the body is still minimally understood at this time and has known major obstacles as kidney filtration, degradation by endonucleases, aggregation with serum proteins, and uptake by phagocytes (Table 3) (240). Because of these reasons, the development of novel nano-sized carriers, viral and

non-viral, capable of delivering siRNA, will be critical for the systemic delivery of siRNA therapeutics.

Table 3: Major obstacles for therapeutic efficacy of siRNA without modifications

Stability
Specific targeting to diseased cells
Saturation of RNAi/miRNA machinery
Immune response stimulation
Off-target effects
Delivery:
• Renal filtration
• Serum protein aggregation
• Phagocytes uptake
• Vascular endothelium
• ECM
• Cellular uptake
• Endosome degradation
• RISC loading

First, the system should be preferably biocompatible, biodegradable and non-immunogenic; second, the system should be able to efficiently deliver siRNA to target cells without being attacked by serum nucleases; next, the delivery system should provide target specific distribution/ penetration, avoiding rapid hepatic or renal clearance; and finally, after delivery, the system should help the efficient endosome release of siRNA into cytoplasm allowing the interaction of siRNA with the endogenous RISC (224, 238). Although the viral vectors are very efficient delivery vehicles, due to the toxicity associated with this delivery, the non-viral/synthetic nanoparticle system has become an increasingly popular alternative for siRNA delivery. Some of the commonly used delivery systems include lipid based carriers, polymer systems, peptides/proteins and conjugates(240). These are known to passively accumulate in the tumor site due to their leaky vasculature and lack of the lymphatic drainage system.

7. CHITOSAN-BASED NANOSYSTEMS

In recent decades, gene delivery research has developed very quickly due to its vast potential as a therapeutic approach for clinical applications. However, as mentioned before, these naked therapeutic genes present major challenges and therefore, the improvement of safe and efficient delivery systems is essential for the success of gene therapy (267). In recent years, chitosan(CS)-based carriers have emerged as a powerful tool and gained increasing importance as a safe delivery system for nucleic acids (268). Due to its mucoadhesion, high positive charge density, low toxicity, low immunogenicity, biocompatibility, CS potential in the medical field is broadly promising (269). Reports indicate its application in very distinct areas such as microbiology, tissue engineering applications, dental implants, cosmetics, food industry, etc. (270, 271).

CS is a linear copolymer polysaccharide consisting of beta-(1-4)-linked 2-amino-2-deoxy-D-glucose (Dglucosamine) and 2-acetamido-2-deoxy-D-glucose (N-acetyl-D-glucosamine) units (Figure 10) (272).

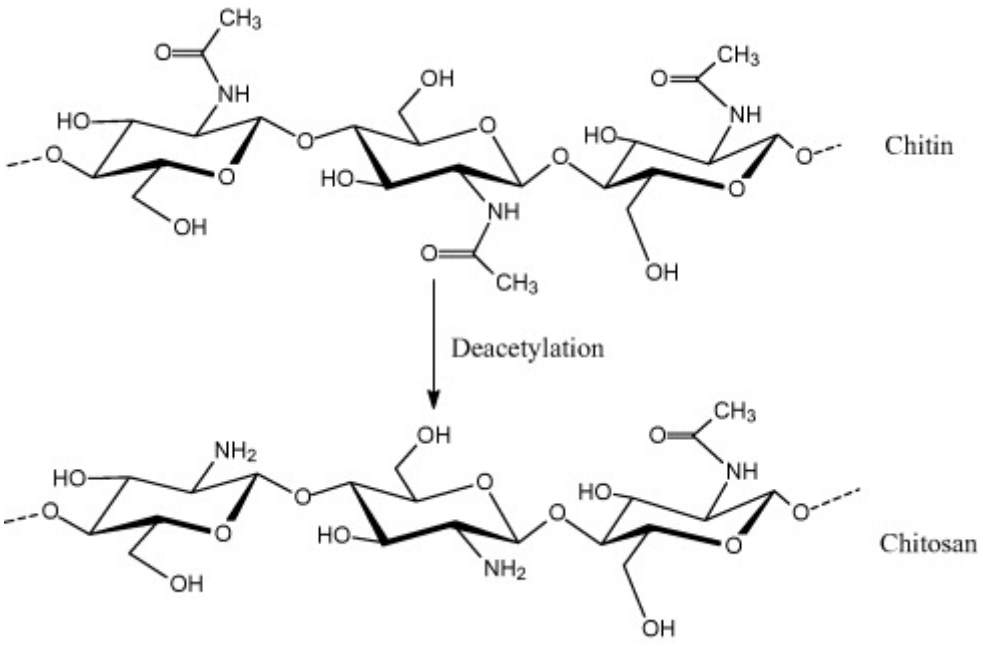

Figure 10: Chitin and Chitosan structure (272)

It is obtained by deacetylation of chitin, which is the structurally present in the exoskeleton of crustaceans and cell walls of fungi which makes it biodegradable and inexpensive (273). From the biopharmaceutical point of view, CS has very appealing characteristics such as pH sensitivity, biocompatibility, biodegradability, mucoadhesivity, very low toxicity (an LD50 in rats of 16 g/kg) and low immunogenicity (274).

CS is believed to be one of the most commonly exploited natural polymers for nanoparticles preparation because of its unique structural attributes. This polymer is poorly soluble in water and organic solvents, but soluble in most dilute aqueous acidic solution (pH < 6.5) (275). This property confers positive charges to CS that allow it to establish electrostatic interaction with the negative charges from the nucleic acids but also negatively charged molecules, such as phosphates, sulfates and citrates ions, to form hydrogels (276). The number of positive charges are directly related to the presence of the protonable amino group along D-glucosamine residues, which defines CS's deacetylation degree (DD). By definition, DD is calculated as the ratio of D-glucosamine to the sum of D-glucosamine and N-acetyl D-glucosamine. When chitin becomes deacetylated on its D-glucosamine residues above 60%, the polymer is now designated as CS (277). DD and molecular weight are the two parameters that usually characterize CS and directly dictate its properties. DD typically ranges between 60 and 100% while its molecular weight greatly varies from 5 to 1000 kDA, and together these two parameters can greatly influence properties such as biodegradability, drug release profile, cellular uptake, etc. (278). A high DD will imply a high density of positive charges enabling a greater loading capacity of nucleic acids. Also, the ratio between the charges in the final complex will be of extreme importance because it will ultimately determine the transport of siRNA across cellular membranes and endocytosis into the cells but also its release inside the cell(278). However, there are still some disagreement in which molecular weight is related to a higher transfection efficiency, the high or the low molecular weight. Some authors report that low molecular weight is not sufficient to create a stable interaction with siRNA, but in contrast, another paper showed that efficient silencing (279, 280). However, the molecular weight is an important factor that influences physicochemical properties (size, surface charge, morphology and complex stability) and gene silencing of chitosan/siRNA nanoparticles (270).

Meanwhile, CS is a versatile biomaterial with a relatively simple chemical structure that allows CS to be further modified to create a wide range of possible drug delivery carriers. Also, specific chemical modifications can be done to ideally achieve a sustained/controlled release of a drug into a specific environment creating an optimal response, with minimum side-effects and prolonged efficacy (281). An increasing number of studies are focusing on modification of CS that are characterized by pH sensitivity, thermosensitivity, targeting accuracy and hydrophobic modification (279, 282, 283). In this study CS functional blocks have been made to self-assemble and encapsulate a modified hydrophobic small molecule, and ultimately to deliver them to the target cells efficiently (282). One of the most common passive targeting modifications consists in adding a polyethylene glycol (PEG) chains (284, 285). PEG surface, in particular has the main advantage of providing a longer blood-

circulating half-life by blocking and delaying the opsonization process and so, protecting nanocarriers from the reticulo-endothelial system, thus minimizing their removal at the liver site (286). Active targeting can also be achieved by simple processes as chemical modification of nanoparticles surface or more complex processes such as particle conjugation with specific ligands or antibodies (287, 288). These systems allow the dosages frequency to be reduced which culminates in lesser side effects and fluctuation on drug levels and also a more stable effect of the drug.

In this context, CS *in vitro* and pre-clinical application have contribute with a large amount of knowledge supporting its large potential as tumor-targeted siRNA-delivery carrier for cancer therapy.

CHAPTER 2

Objective and Specific Aims

Objective and Specific Aims

The main goal of this dissertation project was to develop and evaluate a novel CS based nanoparticle system that efficiently encapsulates siRNA against the mitotic gene *mad2* to be used as a therapeutic strategy in lung cancer cells/ tumors.

The specific aims undertaken in the present thesis were:

i) Development, optimization and selection of EGFR-targeted and non-targeted CS nanoparticles for Mad2 siRNA delivery.

ii) *In vitro* evaluation of the biological activity and biocompatibility of the selected formulation.

iii) Investigation of the qualitative and quantitative biodistribution profile and assessment of pharmacokinetics parameters of the targeted and nontargeted nanoparticles in mice bearing subcutaneous, cisplatin sensitive or resistant, human lung adenocarcinoma xenograft tumors.

iv) Evaluation of the *in vivo* efficacy and safety of the different formulations as a single therapy and in combination with cisplatin in drug sensitive (A549-WT) and cisplatin-resistant (A549-DDP) subcutaneous tumor models of NSCLC.

v) Development of CS-based combinatorially designed nanoparticles platform technology that generates self-assembled nanoparticle constructs to encapsulate hydrophobic small molecules.

CHAPTER 3

In Vitro Mad2 Checkpoint Gene Silencing Using EGFR-Targeted Chitosan Nanoparticles in Non-Small Cell Lung Cancer Model

The information presented in this chapter was partially published in the following publications:

- Nascimento AV, Singh A, Bousbaa H, Ferreira D, Sarmento B, Amiji MM. Mad2 checkpoint gene silencing using epidermal growth factor receptor-targeted chitosan nanoparticles in non-small cell lung cancer model. Molecular Pharmaceutics. 2014 Sep 26;11(10):3515-27.

1. INTRODUCTION

Lung cancer is the most common cause of cancer related deaths worldwide, and NSCLC alone accounts for nearly 80% of the fatalities (289). One of the major causes of poor clinical outcomes in NSCLC is the development of multidrug resistance and metastatic dissemination to other parts of the body. Refractory disease is the major contributor to the failure of chemotherapy in NSCLC and it often develops due to poor drug availability, reduced residence time in tumor, ineffective intracellular penetration, dynamic tumor microenvironment, and other molecular mechanisms adapted by cancer cells (290, 291). Alternative approach to develop new targets to overcome multidrug resistance and augment the therapeutic effects of existing drugs has therefore gained central interest in scientific community. RNA interference (RNAi) has emerged as a powerful strategy for overcoming drug resistance in NSCLC, since it allows silencing of specific genes that could be associated with multidrug resistance (292). Small interfering ribonucleic acids (siRNAs) allows the possible targeting of vital genes in tumor cells, adapting it to specific tumor types and customizing it to personalized therapy for subtle genotypic and phenotypic variations. Molecular therapy using siRNA has shown therefore great potential in the treatment of diseases such as cancer, by silencing crucial genes (292-294).

The mitotic checkpoint thoroughly ensures that each new cell receives one copy of each chromosome from a dividing cell (131, 132). Many cancer cells have a weaker mitotic checkpoint which accelerates the rate of chromosome losses and gains, thereby acting as a driving force for carcinogenesis (131, 132). However, total suppression of the mitotic checkpoint activity is lethal, thus making it an attractive therapeutic target for siRNA mediated intervention (131). In fact, several small molecules targeting the mitotic checkpoint are already under clinical trials. Mad2 is one of the key mitotic checkpoint regulators that sequester Cdc20, thereby inactivating anaphase-promoting complex/cyclosome (APC/C), the complex responsible for trigging anaphase (132). Mad2 overexpression has been associated with aneuploidy and tumorigenesis and reported in various carcinomas such as such as liver cancer, breast cancer, soft-tissue sarcoma, B-cell lymphoma and NSCLC (218, 295-297). Decreased expression, but not complete obliteration of mitotic checkpoint genes has been associated with resistance to antimicrotubule drugs and DNA damaging agents (217, 298). In addition, low levels of Mad2 have been correlated with cisplatin resistance and high levels with sensitivity to the same drug (299, 300) Nonetheless, Mad2 knockdown has been shown to be catastrophic and incompatible with cell viability (191, 221). RNAi-mediated knockdown of Mad2 causes massive chromosome mis-segregation during mitosis and its null mutation in mice embryo causes early death during

embryogenesis (133). The selectivity and the catastrophic impact of *Mad2* gene silencing on cancer cells, therefore, would be a highly attractive alternative therapy for cancer.

The most challenging obstacle in siRNA therapeutics is their efficient delivery to the target cells. Some of the major difficulties includes poor pharmacokinetic property, enzymatic degradation, cellular permeability restrictions, endosomal trapping, off-target effects, and systemic interferon responses (267). Careful choice of a suitable delivery vector, however, can aid in circumventing many of these challenges and imparting significant benefit to RNAi as a clinically viable therapeutic option (301) An ideal delivery vector should fulfill certain criteria before it can be used for therapeutic applications. Biocompatibility, biodegradability and non-immunogenicity are some of the key consideration while designing a delivery system. We have recently demonstrated hyaluronic acid (HA) derivative-based self-assembling vectors for delivery of siRNA targeting anti-apoptotic genes, survivin and Bcl2, in NSCLC (302). HA is a natural polymer with backbone that imparts CD44 receptor targeting ability to the nanoparticles and could also be used for synthesis of different derivatives by easy chemical coupling reactions. A detailed *in vitro* study demonstrated efficient delivery of the payload to the A549 human NSCLC cells and subsequent knockdown of the target gene. *In vivo* studies in subcutaneous A549 (wild-type, drug sensitive) and A549-DDP (cisplatin-resistant) NSCLC tumor-bearing mice further demonstrated that this delivery approach could be used in combination with cisplatin to get synergy of antitumor activity and overcome multidrug resistance (303, 304).

CS is a similar natural polymer that has been extensively studied for nucleic acids delivery *in vitro* and *in vivo* (273, 305, 306) CS presents several advantages such as mucoadhesivity, biocompatibility, biodegradability and low cost of production. Most importantly, chitosan can bind with polyanionic molecules such as DNA or siRNA by electrostatic interaction due to the presence of protonated amine groups in the backbone, leading to the formation of nano-sized particles (268). Besides, the amine backbone of CS allows for chemical modifications such as attachment of PEG to impart stealth property or functionalization with ligands to target specific cancer cell type. Although there are no chitosan-based vectors for *in vivo* administration of nucleic acids at clinical level, there are numerous publications that report their use as a vaccine adjuvant for oral and intranasal peptide/vaccine delivery (269, 307, 308). Similarly, chitosan has been extensively used as a delivery vector for anticancer therapeutic small molecules and nucleic acid and therefore it serves as a promising candidate for siRNA administration *in vitro* and *in vivo* (309, 310).

In the present study, we have designed EGFR-targeted CS vector for delivery of siRNA to selectively silence *Mad2* gene, thereby depleting the corresponding protein expression and

study its impact in A549 cells. PEG and EGFR binding peptide derivatives of CS were synthesized, characterized and used for assembling CS-siMad2 complexes of the size below 250 nm and a net positive surface charge (Figure 11). *In vitro* transfection efficiency was evaluated as a function of dose and time and subsequent silencing activity of the siRNA was confirmed by qRT-PCR at gene level and flow cytometry at the protein level. Time-dependent cytotoxicity and apoptosis assessments were also carried out to confirm the impact of *Mad2* gene silencing on the cells.

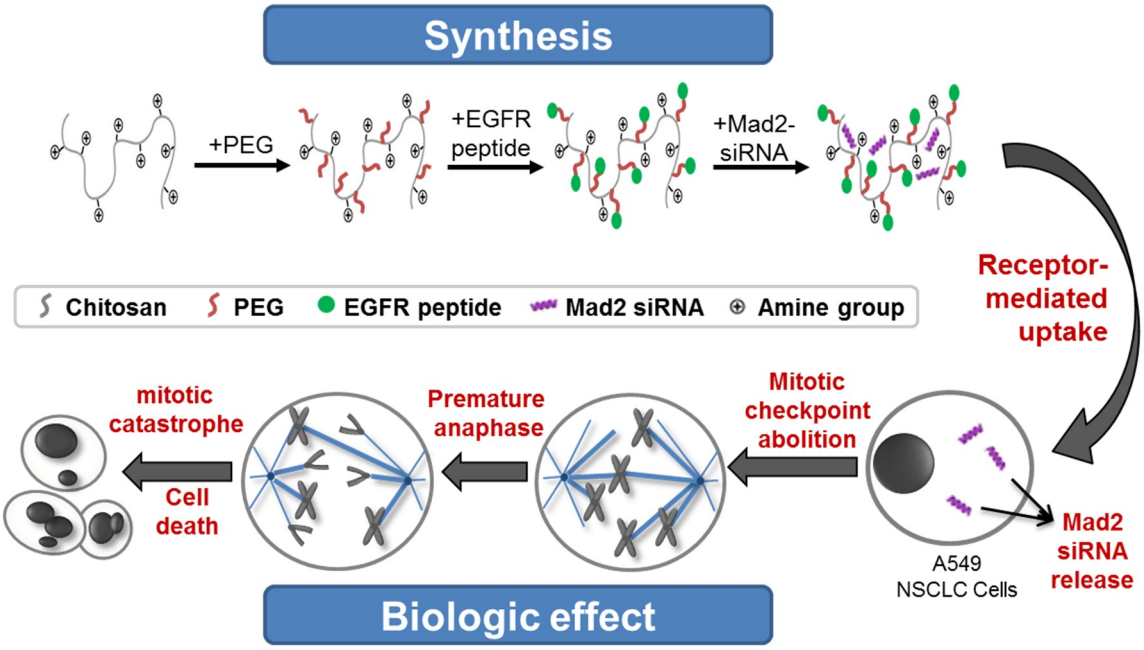

Figure 11: Schematic diagram

2. EXPERIMENTAL METHODS

2.1 Materials

Two types of chitosan were used in this study. The low molecular weight chitosan (LMW CS) had a viscosity-average molecular weight of 50 kDa and the degree of deacetylation was 75-85% and a higher molecular weight chitosan (HMW CS) had a viscosity-average molecular weight of 60-120 kDa and the degree of deacetylation was 80%. LMW CS and acetic acid glacial were purchase from Sigma-Aldrich Inc. (St. Louis, MO) while HMW CS was a kindly provided by KitoZyme S.A. (Belgium). Fluorescent dye DyLight-488 NHS ester as well as succinimidyl-([N-maleimidopropionamido]-ethyleneglycol) ester (NHS-PEG-MAL) were purchased from Thermo Scientific (Rockford, IL, USA). Double-stranded siRNAs against Mad2 and non-targeting (NT) siRNA sequence was purchased from Santa Cruz Biotechnology Inc. Amine-reactive Alexa Fluor 488 was purchased from Invitrogen/Life Technologies (Carlsbad, CA) and Label IT siRNA Tracker Kit was procured from Mirus

Corporation (Madison, WI). Pico-Green fluorescence reagent for quantification of double stranded nucleic acid constructs was purchased from Invitrogen/Life Technologies (Carlsbad, CA). For Mad2 protein quantification by flow cytometer, the antibody monoclonal anti-Mad2 clone 17D10 was obtained from Sigma (Sigma-Aldrich, St. Louis, MO and the secondary antibody goat anti-mouse conjugated with Alexa Fluor® 568 from Abcam (Abcam, Cambridge, UK).

2.2 Synthesis of Chitosan Derivatives

Both types of chitosan were dissolved in a 2% acetic acid solution, at 2mg/ml and reacted overnight with 10% molar equivalent of maleimide-p(ethylene glycol)-N-hydroxysuccinimide (Mal-PEG_{2000}-NHS) to achieve CS-PEG-Mal. Next day, the solution was purified by dialysis (molecular weight cutoff - 10 kDa) in water and half the amount of chitosan-PEG-Mal was used for EGFR-binding peptide modification. This peptide with the following sequence, YHWYGYTPQWVI-GGGG-C, was originally synthesized by Zonghai Li and coworkers, and has been demonstrated to be most efficient in targeting the EGFR receptor (311). We have extensively used this peptide previously to successfully demonstrate its targeting capability *in vitro* as well as *in vivo* in various EGFR over-expressing tumor cells (312-318). The peptide was obtained from Tufts University. A 2-fold molar excess of 17-amino acid EGFR binding peptide was added to the nanoparticle solution at 4°C in nitrogen atmosphere overnight to allow cysteine group of peptide to react with maleimide group. The solution was purified by dialysis (molecular weight cutoff - 10 kDa) in water. Glacial acetic acid was added to the dialyzed nanoparticle solution in order to achieve a 5% concentration and then freeze-dried and stored at -20 °C until further use. Non-targeted chitosan derivative was similarly prepared by reaction with mPEG_{2000}-NHS followed by acetic acid addition, dialysis and freeze drying. The degree of substitution value of PEG on chitosan was estimated by NMR analysis. For each sample, 4 mg of the lyophilized product were dissolved in 0.7 ml D_2O and characterized by 400 MHz ^1H NMR spectroscopy (Varian, Inc. CA)

2.3. Preparation and Characterization of siRNA-Encapsulated Chitosan Nanoparticles

Mad-2 and scrambled siRNA duplexes were encapsulated in CS-PEG derivatives in a molar ratio between nitrogen residues from chitosan per nucleic acid phosphate (N/P ratio) of 25/1, 50/1, 75/1 and 100/1 CS-PEG was dissolved in water (1 mg/ml) and siRNA dissolved in nuclease-free water was slowly added to it under magnetic stirring. The solution was incubated for 30 min at room temperature to facilitate CS-PEG and siRNA complexation and nanoparticle self-assembly prior to use. EGFR targeted CS-siRNA nanoparticles were

prepared using 1:1 ratio of CS-PEG_{2000}-peptide and $mPEG_{2000}$-CS by the same procedure as described above.

The formed self-assembled nanoparticles were characterized for size, surface charge, morphology, encapsulation efficiency, and stability of the siRNA payload. Particle size, surface charge and polydispersity index (PDI) of freshly prepared siRNA loaded chitosan (CS-siRNA) nanoparticles were measured using a ZetaSizer Nano ZS (Malvern Instruments, Worcestershire, UK). Each sample was analyzed in triplicate at 25°C and the size and zeta potential was reported as mean ± SD. The encapsulation efficiency was determined using Quant-iT™ Pico-Green reagent (Life Technologies, Carlsbad, CA, USA) using a microplate reader (Bio-Tek Instruments, Winooski, VT). A standard curve based on fluorescence emission generated from the binding of Pico-Green to known concentration of double-stranded siRNA was created and the loading in nanoparticles was determined by subtracting the calculated amount of free siRNA from initial amount added. Encapsulation efficiency was defined as the ratio percent of siRNA encapsulated in nanoparticles to the total siRNA added.

The morphological characterization of CS-siRNA nanoparticles was carried out under transmission electron microscopy (TEM) using JEOL JEM-1000 transmission electron microscope (JEOL, Tokyo, Japan). 10μL of nanoparticle was dropped on formvar-coated copper grid and allowed to stand for 1 min, excess fluid was drained using a Whatman filter paper and the sample was negatively stained with 1.5% uranyl acetate (1 min) prior to its visualization. The dark staining of siRNA by uranyl acetate offers a high contrast compared to chitosan that can help ascertain loading of genes in polymeric nanosystems.

2.4 Stability of Chitosan-siRNA Nanoparticles

Stability of Chitosan-siRNA nanoparticles against RNase digestion was investigated. Chitosan-siRNA nanoparticles in an amount equivalent to 2 μg of siRNA we tested. The nanoparticles were prepared as previously described, and in a N/P ratio of 50/1. Each set of particles was in phosphate buffer at pH 7.4 and was submitted into 4 different conditions: no treatment; incubated for 10 min with 5μl heparin (1000 U/ml) for displacing the siRNA from the chitosan nanoparticles; incubated with 4 uL of RNAse A (20ug/ml) for 30 min at 37°C; and incubation with incubation 4 uL of RNAse A (20ug/ml) for 30 min at 37°C followed by heat inactivation of the enzyme and incubation for 10 min with 5μl heparin (1000 U/ml). Resulting mixtures were applied to a 4% E-Gel (Invitrogen, Carlsbad, CA), and electrophoresis was carried for 15min using E-Gel iBase system. In each gel, free siRNA was applied as a reference. The experiments were performed in triplicate. The resulting gel

was imaged on ChemiDoc System (Bio Rad, Waltham, MA) using the software Quantity One.

2.5 Cell Culture and Transfection

A549 human lung carcinoma cell line from the American Type Culture Collection (ATCC, Rockville, MD) were cultured at 37°C in 5% CO2 environment in DMEM/F12 medium from Life Technologies (Carlsbad, CA). NIH-3T3 mouse embryo fibroblast cell line were also purchased from ATCC and cultured in DMEM (Life Technologies, Carlsbad, CA). Both cell culture media were supplemented with 10% fetal bovine serum and 1% penicillin/streptomycin (100 U/ml) (Thermo Fisher Scientific, Waltham, MA, USA). Human Pulmonary Alveolar Epithelial Cells (HPAEpiC) were purchased from ScienCell Research Laboratories and cultured in alveolar epithelial cell medium as recommended by the supplier.

Approximately 80,000 cells per well were seeded in a 6-well plate culture for 24h prior to experiments to achieve approximately 75% confluence for transfection and the transfection conditions was followed according to the description in Malmo *et al* (319). Briefly, fresh nanoparticles were assembled in water as described above and diluted with an equal volume of Opti-MEM Life Technologies (Carlsbad, CA), supplemented with 270 mM mannitol (Sigma-Aldrich, St. Louis, MO) and 20 mM HEPES (Sigma-Aldrich, St. Louis, MO). Preceding the addition of the nanoparticles, the cells were washed and briefly incubated with Hank's balanced salt solution, HBSS (Life Technologies, Carlsbad, CA), at 37°C and 5% CO_2. Next, the HBSS solution was removed and the nanoparticles were added to each well. The transfection solution was removed after 6h of incubation at 37°C and 5% CO_2 and replaced by regular growth media supplemented with 10% FBS and penicillin/streptomycin (100 U/ml).

2.6 Qualitative Analysis of Cellular Trafficking By Confocal Microscopy

Fluorescence confocal microscopy studies were performed in order to assess the qualitative cellular internalization of the nanoparticles. Cells (200,000 cells/well) were seeded on coverslips in 6-well plates and were allowed to attach for 24h. After incubation for specific periods of time, cells were washed with cold phosphate-buffered saline (PBS, pH 7.4), fixed with 4% paraformaldehyde for 20 min, washed with cold PBS and stained with the fluorescent DNA-binding dye Hoechst 33342 (Invitrogen, Carlsbad, CA) (1 µg/ml) for 5 min. The cells were finally washed with cold PBS and the coverslip was inverted on a glass slide in mounting medium. Microscopy images were acquired using LSM 700 confocal microscope (Carl Zeiss, Gottingen, Germany) equipped with a 40× and a 63× objectives. For each image, representative focus planes were shown. The images were obtained using

a 405 nm (5 mW) laser for Hoechst 33258 (417-477 nm emission), 488 nm (10 mW) laser for Alexa 488nm-labeled chitosan (500-550 nm emission) and 639 nm (5 mW) laser for Cy5-siMad2, (600-650 nm). Digital images were analyzed using the NIH Image-J software. All setting parameters for fluorescence detection and image analyses were held constant to allow consistency in imaging of the sample for comparison.

2.7 Quantitative Cellular Uptake Studies by Flow Cytometry

CS was conjugated with amine-reactive dye Alexa Fluor 488 (Life Technologies, Carlsbad, CA). In order to achieve this modification, the amine-reactive dye Alexa Fluor 488 was dissolved in DMSO (1mg/ml) and added to an aqueous solution of chitosan (1mg/ml) and incubated overnight. In the following day, the conjugate was purified by dialysis (molecular weight cutoff - 10 kDa) in PBS pH 7.4 and put to freeze-dry. Simultaneously, siRNA against Mad2 (siMad2) was labeled with Cy5 dye using the kit Label IT siRNA Tracker Kit (Mirus Corporation, Madison, WI) according to the manufacturer's specifications. For flow cytometry, 200,000 cells/well cells were seeded in 6-well plates and left to attach for 24h. Cells were then transfected with fluorescently labeled siRNA (Cy5-siMad2) encapsulated in Alexa Fluor 488 labeled chitosan. After specific times the transfection solution was removed, the cells were washed with PBS and prepared for analysis by flow cytometry.

Time dependent cellular uptake and EGFR targeting of CS-siRNA nanoparticles was quantitatively analyzed using a Becton Dickinson FACS-Calibur® 4 Color Flow Cytometer (BD Biosciences, Franklin Lakes, NJ). The obtained data were analyzed and visualized using the Cell Quest software (BD Biosciences, Franklin Lakes, NJ). After incubating with nanoparticles for specific time periods, the cells were washed with PBS (Life Technologies, Carlsbad, CA), trypsinized, re-suspended in ice-cold PBS supplemented with 5% FBS and kept on ice until the time of analysis. The relative amounts of intracellular siMad2, was evaluated in the FL-2 channel. The percentage of cellular uptake was calculated on the basis of the geometric mean (Gm) using the following formula:

$$Percent\ uptake\ = \frac{(Gm_{Exp})}{(Gm_{Ctrl})} \times 100$$

where Gm_{Exp} is the Gm of cells in the different experimental conditions and Gm_{Ctrl} is the Gm of cells in the control condition, without treatment. The data presented are the mean fluorescent signals from 10,000 events.

2.8 Assessment of EGFR-Specific Cellular Internalization

In order to confirm that entry of peptide modified CS-siRNA nanoparticles into cells is mediated by EGF receptor targeting, competitive inhibition study was performed in A549

cells. The cells were pre-treated for 1h with EGFR binding peptide (50 μg/ml) prior to exposure with nanoparticle treatment. Simultaneously, uptake study was also using an EGFR non-overexpressing cell line, NIH-3T3. Fluorescently labeled siRNA, purchased from Qiagen (Venlo, Neatherlands) was loaded into chitosan nanoparticles and was incubated with cells for 15 mins. Cells were washed with 1x PBS and harvested as described previously for flow cytometric analysis of cellular uptake. The amount of EGFR on A549 and NIH-3T3 was determined by direct immunofluorescence assay via 488nm-labeled EGFR antibody. Briefly, cells from both cell lines were harvested and washed with ice cold PBS, 10% FBS, 1% sodium azide and resuspended in 3% BSA/PBS solution. 488nm-labeled EGFR antibody was added to a final concentration of 20 μg/ml. After a 2h incubation, cells were washed with ice cold PBS, 10% FBS, 1% sodium azide and resuspended in the same solution followed by flow cytometric analysis.

2.9 In Vitro Gene Silencing Efficiency

In vitro gene silencing was assessed by qRT-PCR. Cells were transfected with different siMad2 concentrations and incubation periods as described above. At the time of analysis, cells were collected and total RNA was extracted using GeneJET RNA purification kit (Thermo Scientific, Tewksbury, MA) according to the manufacture's recommendations. RNA concentration was determined by spectrophotometry using NanoDrop 2000c (Thermo Scientific, Tewksbury, MA). For each sample, 0.5 μg of total RNA was used for cDNA synthesis and the reverse transcription reaction was performed with Verso cDNA Synthesis kit (Thermo Scientific, Tewksbury, MA) according to the manufacturer's instructions.

Real time polymerase chain reaction (qPCR) was performed with the LightCycler 480 SYBR Green I Master kit (Roche, Basel, Switzerland) and housekeeping gene glyceraldehyde 3-phosphate dehydrogenase (GAPDH) was used as endogenous control. The sequences of the primers used in this work were: Mad2 Forward (GTGGAACAACTGAAAGATTGGT), Mad2 Reverse (GTCACACTCAATATCAAACTGC), GAPDH Forward (ACAGTCAGCCGCATCTTC) and GAPDH Reverse (GCCCAATACGACCAAATCC). 2 μL of the cDNA was used to evaluate Mad2 expression levels. qPCR steps included a pre-incubation step for 5 min at 95°C, followed by 40 cycles of three steps: 10 sec at 95°C, 20 sec at 60°C and 30 sec at 72°C. The threshold cycle (Ct) values were generated automatically by the LightCycler® 480 Software, Version 1.5 and the comparative method for mRNA level quantification was calculated according to the following formulas:

$$\Delta Ct\ (Treated) = Ct(Target\ gene\ in\ Treated) - Ct(Reference\ gene\ in\ Treated)$$

$$\Delta Ct\ (Control) = Ct(Target\ gene\ in\ Control) - Ct(Reference\ gene\ in\ Control)$$

$$\Delta\Delta Ct = \Delta Ct(Treated) - \Delta Ct(Control)$$

Normalized target gene expression level = $2^{(-\Delta\Delta Ct)}$ where Ct is the threshold cycle

2.10 Determination of Mad2 Protein Expression Levels by Flow Cytometry

Cells suspensions from different treatments were collected and fixed with 4% formaldehyde for 10 min. at RT. After pelleting them, cells were permeabilized with a 0.3% Triton-X solution for 7min at RT. After blocking non-specific antigens with a PBS solution containing 10% FBS, cells were incubated for 2h in the primary antibody solution, mouse anti-Mad2 4 μg/ml in PBS. After three washing steps with PBS, cells were stained with secondary antibody, anti-mouse conjugated with Alexa 568, in a concentration of 2 μg/ml in PBS for 30 min. After two washing steps, cells were resuspended in 500 μL of PBS and analyzed by flow cytometry.

2.11 Cell Viability Analysis

The toxicity of the siRNA loaded and blank nanoparticles was assessed using the MTT (3-(4,5-Dimethylthiazol-2-yl)-2,5-diphenyltetrazoliumbromide) assay. Cells were seeded in 96-well-plates at a density of 2500 cells/well and were allowed to attach overnight. Then, cells were washed and 100μL of the nanoparticles solution were added to each well (n=8), incubated at 37 °C for 6h following which, the solution was replaced with complete growth media. At the specific time points, the media was renewed by fresh complete media containing 100 μL of 0.5 mg/ml MTT (Sigma-Aldrich, St. Louis, MO). Two hours after incubation, the medium was replaced by dimethyl sulfoxide (DMSO) to stop the reaction and lyse the cells. Untreated A549 served as a negative control. Absorbance of the solution was measured at 560 nm and the IC_{50} was calculated using GraphPad Prism Software.

2.12 Data Analysis

All data are presented as mean ± SD and are calculated from minimum of three independent experiments. Comparisons between two groups were made using Student's T-test and with more than two groups, the ANOVA test was used. A value of $p < 0.05$ was considered to be statistically significant.

3. RESULTS

3.1 Characterization of siRNA Encapsulated CS Nanoparticles

The grafting of Mal-PEG_{2000}-NHS onto chitosan was confirmed by ^{1}H-NMR spectroscopy and the degree of PEG modification was found to be approximately 10% for both LMW and HMW derivatives (Figure 12). NMR spectra of Mal-PEG_{2000}-NHS shows characteristic peaks for methylene protons between 3.5 and 3.7 ppm and a distinct peak at 6.9 for the protons corresponding to the ring protons of maleimide functional group. The peaks related

to the protons on carbon at α position to carboxylic group and NHS group are present between 2.5 and 3.0 ppm (Figure 12A). The peaks corresponding to protons on chitosan polymer backbone spans between 1.8 and 5.0 ppm and thus several peaks between PEG and CS overlap in that region (Figure 12C). Chitosan derivatives were characterized by a new signal at δ = 2.40 ppm, which was attributed to the oxyethylene group present in the copolymer.

The unique peak for maleimide group at 6.9 from Mal-PEG-NHS and for CS at 2 ppm was used to calculate the total PEG modification on the CS backbone (Figure 12D), which was found to be 10%. Further reaction of the PEG-CS derivatives with the EGFR-binding peptide leads to disappearance of the maleimide peak at 6.9 and the peaks in the range of 6.8-7.3 ppm corresponding to the protons from peptide appears (Figure 12B), confirming the successful formation of EGFR-binding peptide modified PEG-CS for both low (Figure 12E) and high (Figure 12F) molecular weight CS. NMR analysis could not be used for calculating the exact concentration for EGFR modification on Mal-PEG-CS. However, since the PEG modification was found to be 10% and the concentration of EGFR binding peptide used for the grafting to maleimide group was two-fold higher, we assume that 100% of maleimide groups were modified. The mPEG and peptide-PEG derivatives of LMW and HMW CS were complexed with Mad2 siRNA to form the non-targeted (NT-LMW and NT-HMW) and EGFR-targeted (T-LMW and T-HMW) nanoparticles respectively. We first optimized the siRNA loading efficiency of CS-derivatives as a function of N/P ratio.

However, the subsequent size and charge analysis of these formulations demonstrated that CS-siRNA complexes at a N/P ratio of 50/1 not only give optimum loading but also adequate size (< 300 nm) for gene delivery application (Figure 13B,C) and were therefore used for all further experiments. The size of the four chitosan/siRNA nanoparticles were measured by dynamic light scattering and were found to be in the range of 100-250 nm (Table 4).

The nanoparticles formed with LMW-CS were characteristically smaller in size compared to those formed using corresponding HMW-CS polymer, suggesting that the polymer chain length plays a role in the size of the nanoparticle assembly. Most importantly, addition of EGFR binding peptide to the polymer leads to a significant increase in the nanoparticles size. This could be due to the change in the net positive charge of the chitosan leading to a decrease in the particle packing density, although the ability to bind and encapsulate siRNA remains the same. That indeed appears to be true since the zeta potential measurement for NT-LMW nanoparticle was 33.6 ± 3.5 mV, which decreased to 28.3 ± 2 mV for the T-LMW nanoparticles suggesting a net decrease in positive charge.

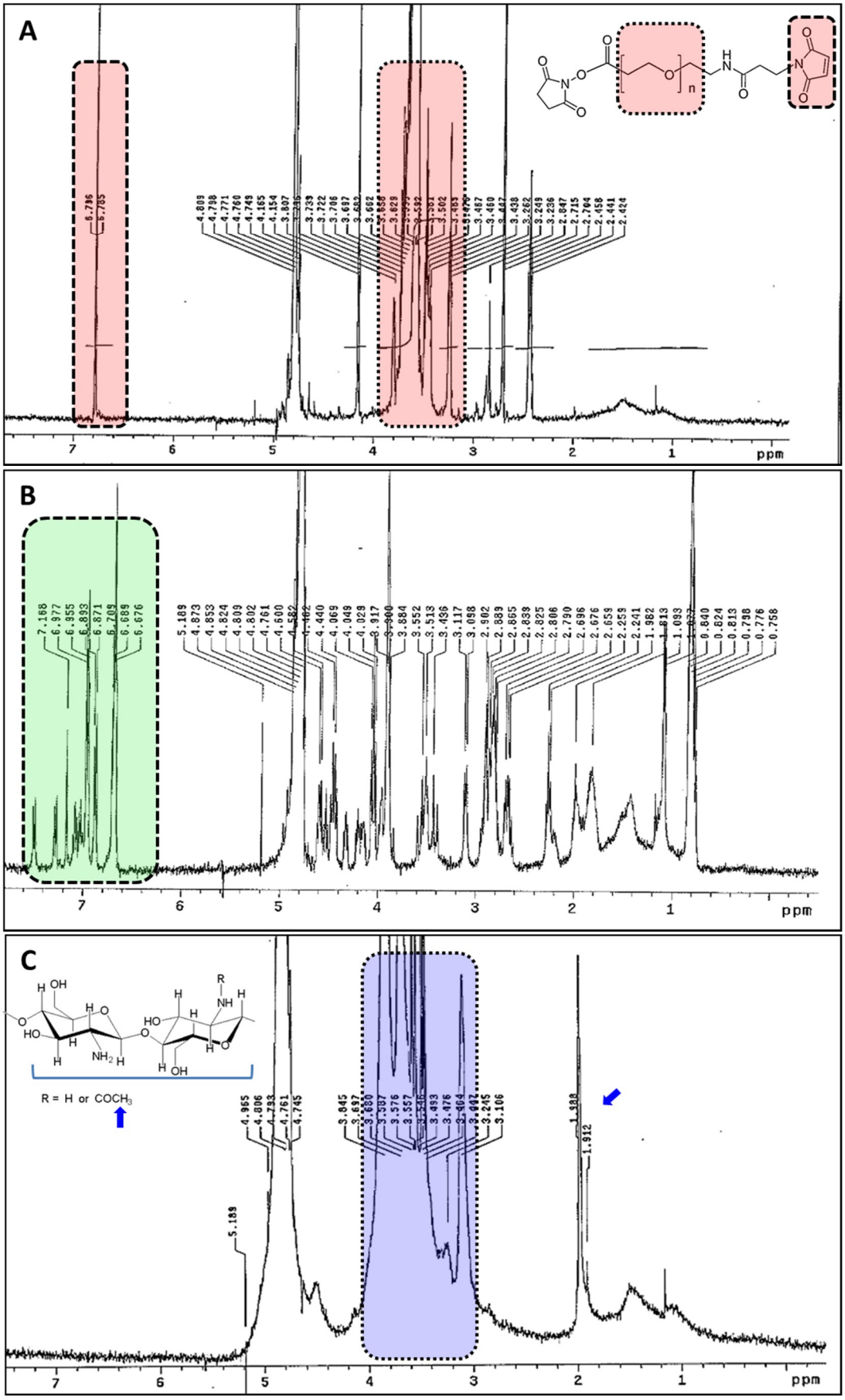
A
B
C
ppm
R = H or COCH3

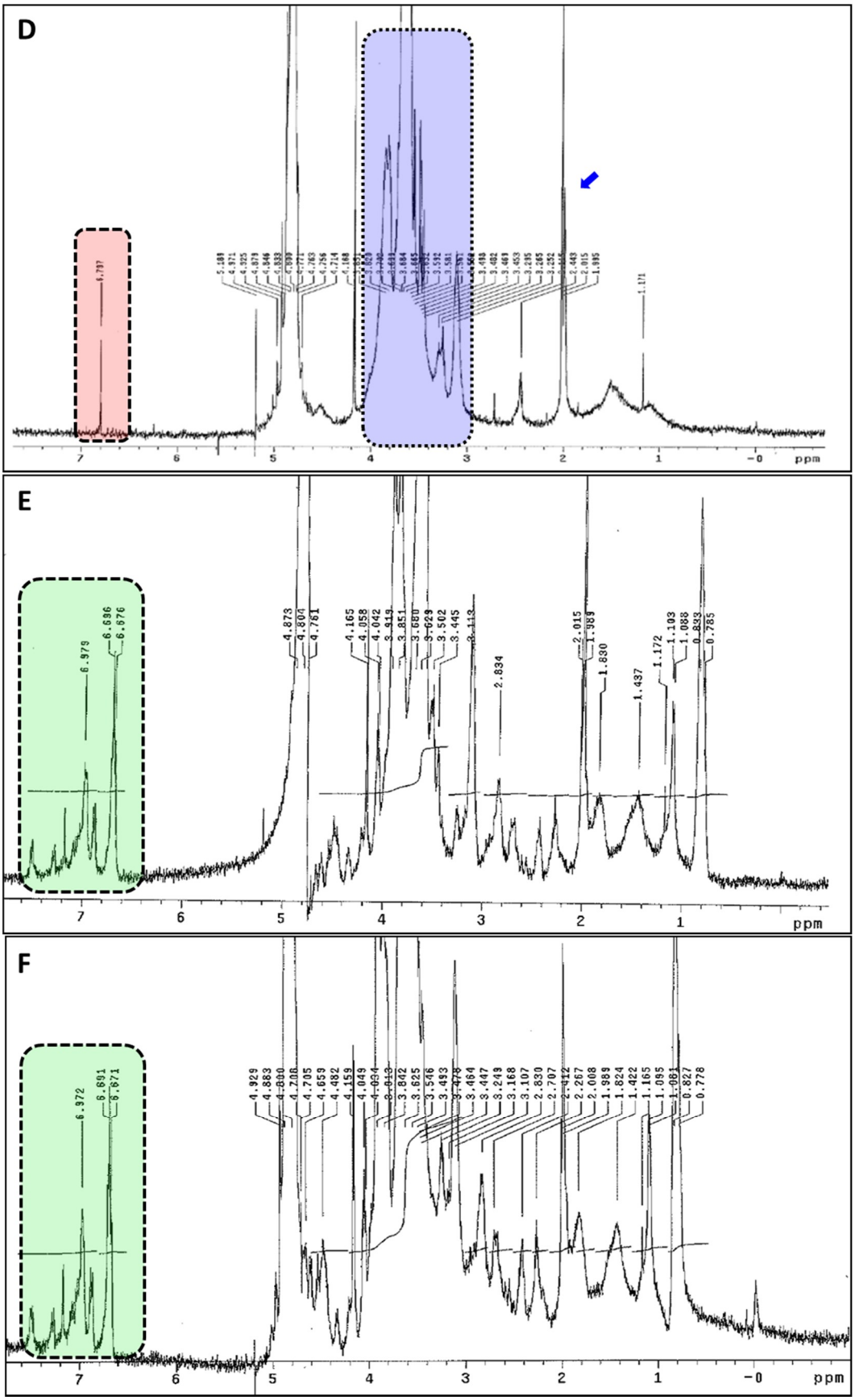

Figure 12: [1]H-NMR spectrums of (A) NHS-PEG-MAL, (B) EGFR binding peptide, (C) Chitosan, (D) Mal-PEG-CS, (E) T-LMW and (F) T-HMW.

The siRNA loading was found to be nearly 100% for the formulations with N/P ratio of 50/1, 75/1 and 100/1 (Figure 13).

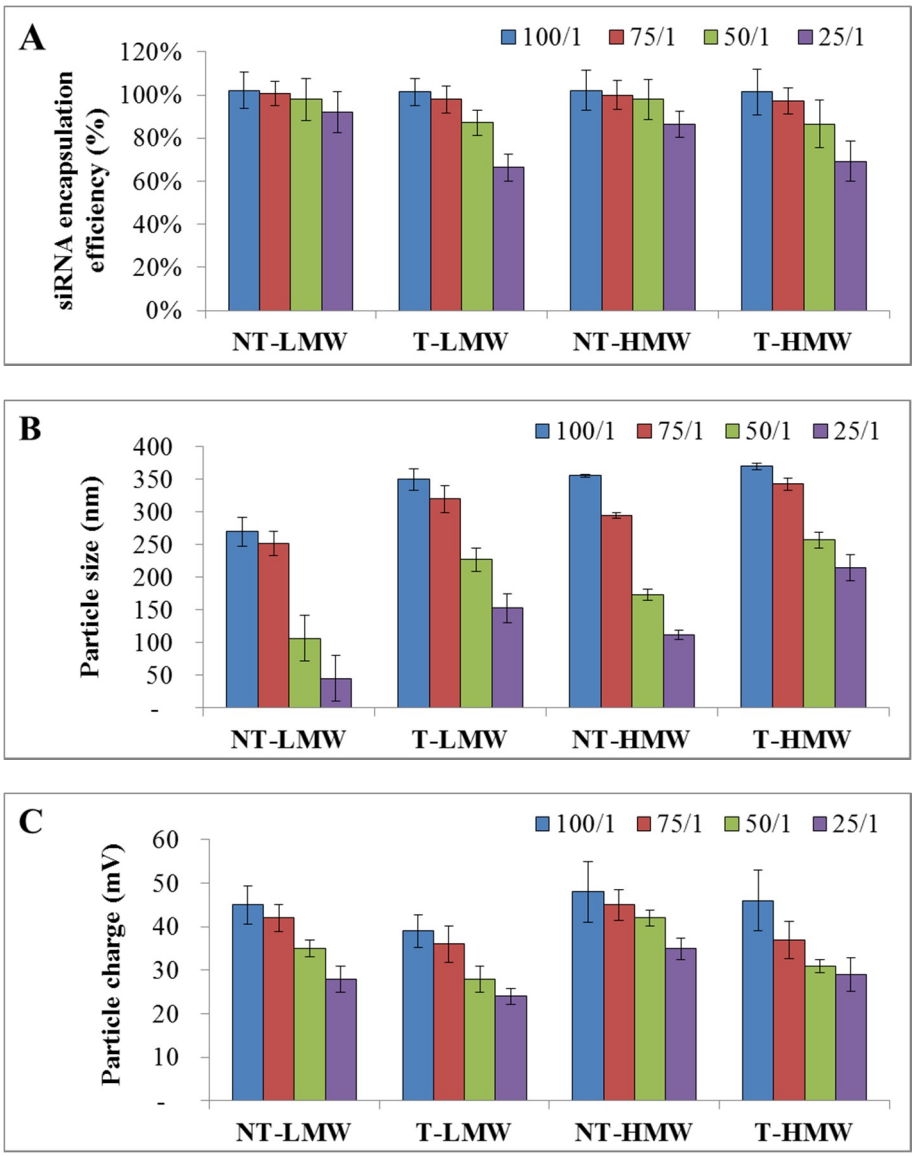

Figure 13: Effect of N/P ratio on the siRNA encapsulation efficiency (A), size (B) and charge (C) of nanoparticles formulated with targeted and non-targeted LMW and HMW chitosan. A concentration of 50 nM of siMad2 was used in a N/P ratio of 50/1. Data are shown as mean ± SD (n = 3).

The zeta potential of the HMW CS-siRNA nanoparticles also showed a similar trend confirming that peptide modification reduces the net positive charge of CS, thereby affecting its interaction with negatively charged siRNA and rendering a larger size for targeted nanoparticles. The polydispersity index (PDI) values for the chitosan nanoparticles decreased with the addition of EGFR peptide for both chitosan molecular weights. In order to analyze if the change in the net charge of CS leads to a change in siRNA loading efficiency of the targeted formulations, siRNA encapsulation efficiency of all the formulations were assessed. The siRNA loading efficiencies of all the nanoparticle systems were found

to be 100% irrespective of the difference in CS composition or molecular weight. This observation confirmed that even though presence of the peptide affects the assembly of the nanoparticle, it does not have any impact on the loading efficiency and that peptide modified PEG-CS could still encapsulate siRNA efficiently despite the charge compensation.

Table 4: Particle size, polydispersity index (PDI), zeta potential and siRNA encapsulation efficiency of chitosan/siRNA nanoparticles at a N/P ratio of 50/1.

Chitosan	Chitosan deacetylation degree (%)	Size (nm) ±SD	PDI ±SD	Zeta potential (mV) ±SD	Encapsulation Efficiency (%)
NT-LMW	75-85	106.8 ± 2.1	0.551 ±0.10	+35.6 ± 3.5	105.1 ± 4
T-LMW	75-85	227.3 ± 1.8	0.362 ±0.02	+28.3 ± 2.0	99.5 ± 2.4
NT-HMW	78	173.1 ± 1.3	0.672 ±0.03	+42.8 ± 2.4	101.6 ± 2.3
T-HMW	78	257.1 ± 3.1	0.421 ±0.01	+13.9 ± 2.9	97.5 ± 3.3

Transmission electronic microscopy (TEM) was used to examine the morphologies of the different CS-siRNA nanoparticles formulations (Figure 14).

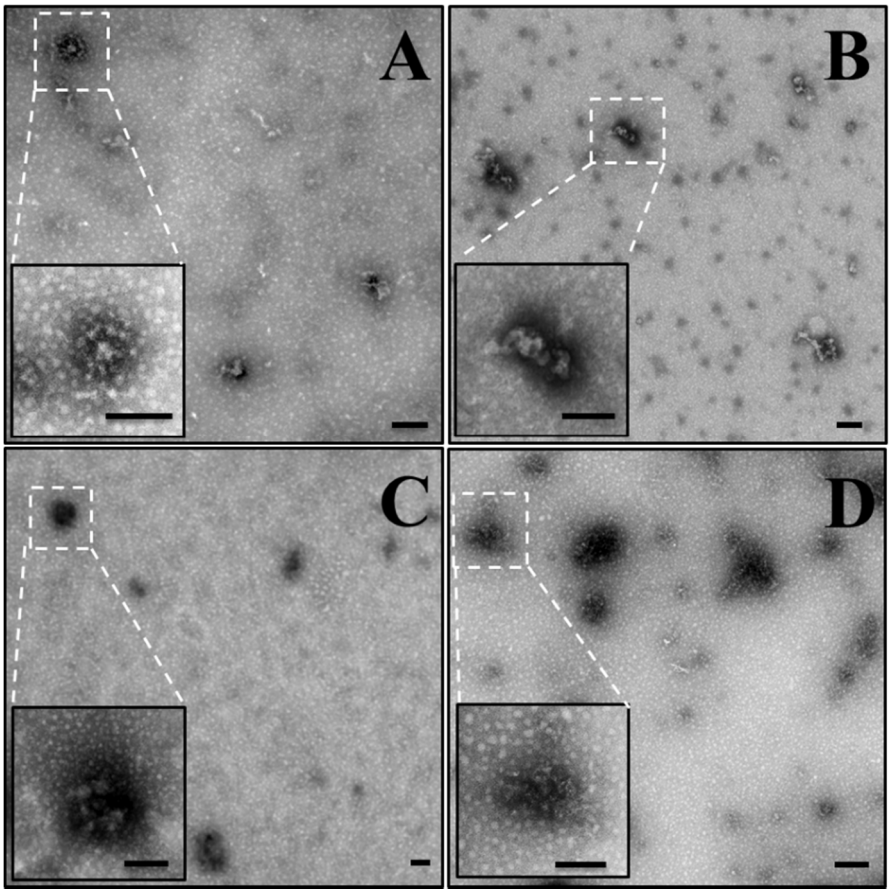

Figure 14: TEM image of chitosan/siRNA nanoparticles at a N/P ratio of 50/1 (A) NT-LMW, (B) T-LMW, (C) NT-HMW and (D) T-HMW. Scale bar in all the images corresponds to 100 nm.

The images of non-targeted CS-siRNA nanoparticles demonstrate a more linear, pendant like structures showing a compact packing of CS around the siRNA. The negative stain used for visualization of the particles seems to intercalate in the siRNA to give a dark contrast. On the contrary, the targeted nanoparticles with both type of CS complexed to siRNA show larger particle size confirming the observation made from the DLS measurement. The particle size from the TEM images corresponded well with the size obtained from the DLS measurement for different nanoparticle formulations.

3.2 Stability against Rnase digestion

siRNA degradation is one of the most important barriers for siRNA delivery. Considering that it is associated with loss of activity and therapeutic effect, we have evaluated the protection effect of different siRNA/chitosan derivative complexes against RNase digestion (Figure 15). As expected free siRNA was degraded completely in the presence of RNAse A while the presence of heparin had no effect on its stability. On the other hand, siRNA, which was incorporated in chitosan particles, remained intact. This result clearly showed the ability of CS-derivatives to protect siRNA from enzymatic degradation.

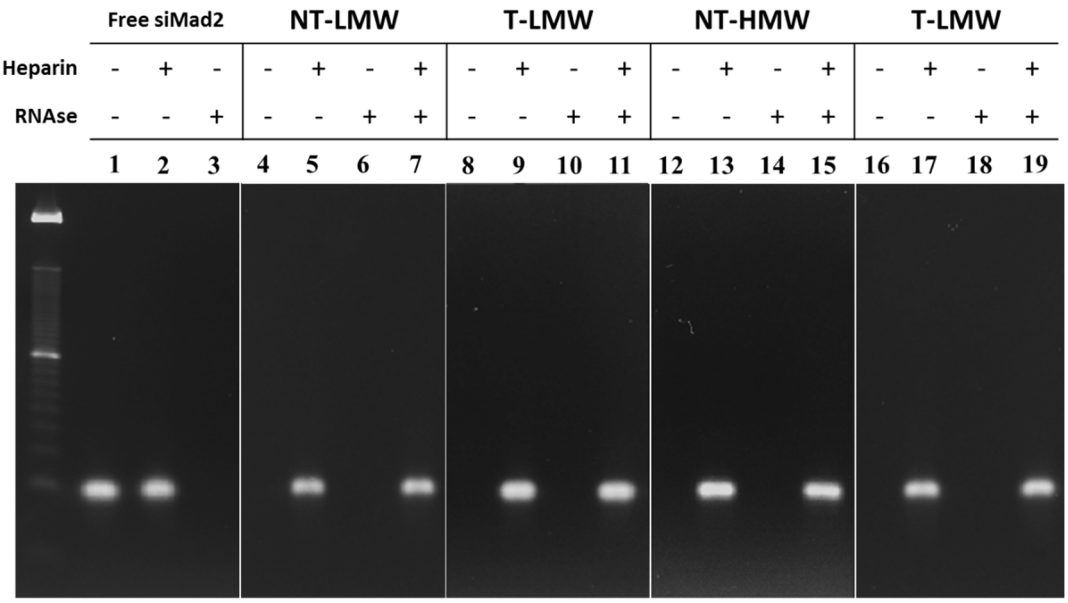

Figure 15: RNase stability of siRNA in the CS/PLA/siRNA complexes. Free siMad2 was a negative control. The complexes were incubated with RNase A (5 mIU/µg siRNA) at 37°C for 2h. The reaction was inactivated at 70°C and was the siRNA released after incubation for 10 min with 5µl heparin (1000 U/ml). Resulting mixtures were analyzed by 4% agarose gel electrophoresis.

3.3 Qualitative analysis of nanoparticle uptake and cellular trafficking

Fluorescence confocal microscopy was employed to visualize the qualitative intracellular uptake of non-targeted and EGFR-targeted CS-siRNA nanoparticles in A549 as a function of time. Intracellular uptake was analyzed at 15, 30 and 60 min for the non-targeted and targeted CS-siRNA nanoparticles at a siRNA concentration of 50 nM. CS was labeled with

green fluorescent Alexa Fluor 488 while siMad2 was labeled with red fluorescent Cy5 dye prior to nanoparticle formation. Figure 16 shows the confocal images for uptake of non-targeted and targeted LMW-CS nanoparticles in A549 cells.

The images taken after 15 min incubation with the non-targeted and targeted nanoparticles clearly show that while targeted nanoparticles show internalization, no evident uptake is shown by the non-targeted system. Non-targeted nanoparticles show internalization at 30 min, which confirms that the EGFR targeting peptide modification of the PEG-CS nanoparticles, facilitates an early uptake by receptor-mediated endocytosis. Most importantly, in both the cases green and red fluorescence co-localized on some of the nanoparticles attached to the cellular membrane and inside the cytoplasm, but the majority of red fluorescence (siRNA tag) was rapidly detected in the nucleus. Similar results were also obtained for the non-targeted and targeted HMW-CS nanoparticles (data not shown). The untreated control cells as well as cell labeled with unlabeled nanoparticle did not show any background auto-fluorescence (data not shown).

3.4 Quantitative cellular uptake by flow cytometry

In order to ascertain the trend of nanoparticle uptake shown by confocal images and get a quantitative estimate of intracellular uptake, A549 cells treated with fluorescently labeled non-targeted and targeted nanoparticles in a time dependent manner were also analyzed by flow cytometry. The fluorescence intensity for all the samples were normalized to the untreated control A549 NSCLC cells. Figure 17 shows the quantitative relative uptake of Cy5 labeled siRNA as a function of time for the different samples where the T-LMW and T-HMW nanoparticles show significantly higher uptake compared to the respective non-targeted nanoparticles, confirming the trend observed by confocal imaging.

Besides, cells show nearly 5-fold increase in fluorescence intensity after 15 min of incubation with NT-LMW and T-LMW nanoparticles indicating that targeted nanoparticles indeed are rapidly internalized by the cells by receptor mediated endocytosis and confirmed the much higher uptake show by confocal imaging. We also analyzed uptake after 5 min of incubation of nanoparticles to see the targeting efficiency of the EGFR binding peptide and the results obtained clearly show that T-LMW nanoparticles give better fluorescence intensity after 5 min than NT-LMW nanoparticles after 1h of incubation. Flow cytometry data also confirmed that LMW-CS nanoparticles are more readily internalized by the cells in comparison to the HMW-CS nanoparticles. T-LMW nanoparticles show a 312% increase in the relative fluorescence after 60 min on incubation while the T-HMW nanoparticles show 176% increase in the fluorescent intensity under similar experiment condition.

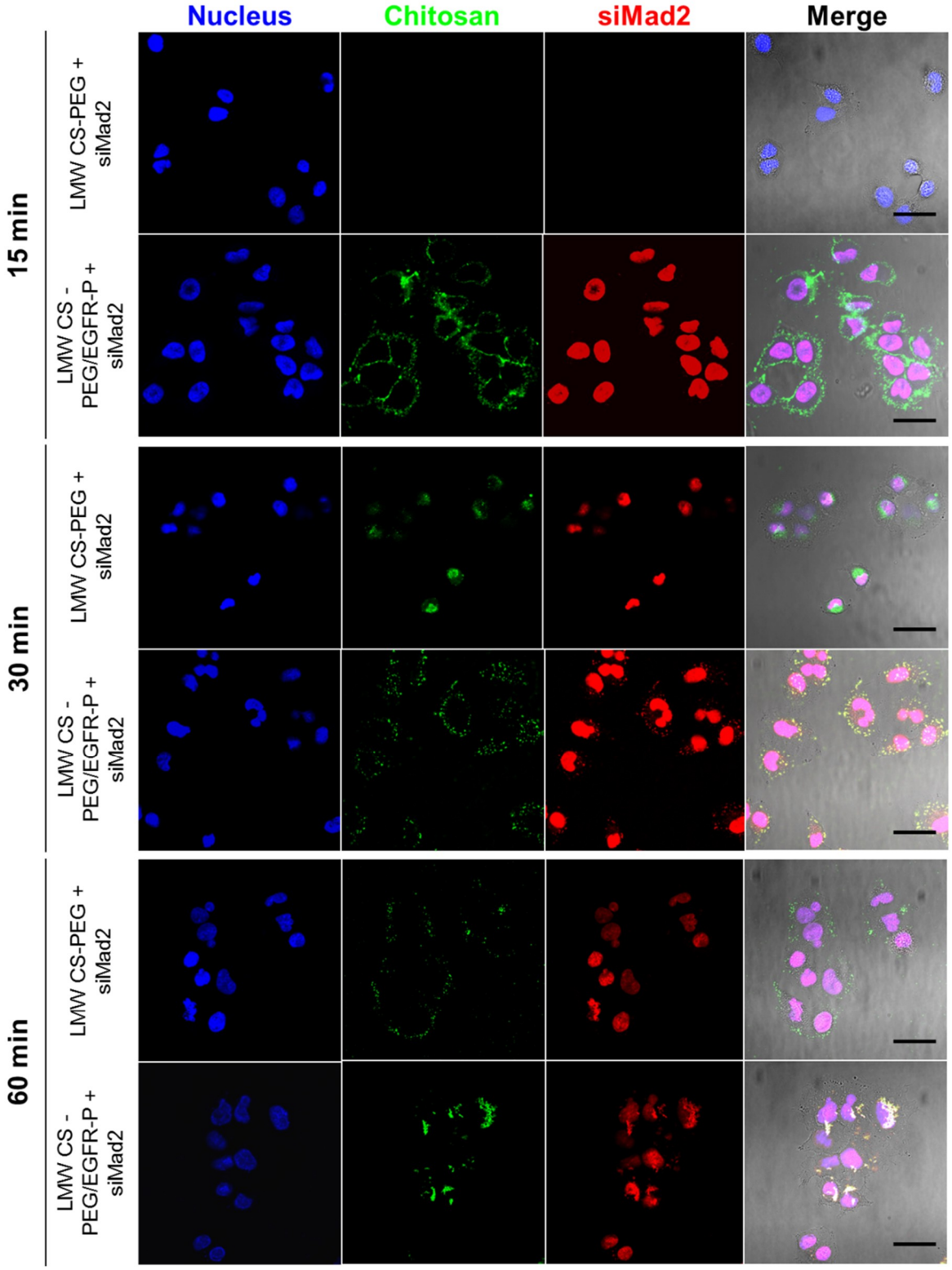

Figure 16: Cell uptake and intracellular trafficking of siMad2-Cy5 encapsulated in chitosan nanoparticles modified with Alexa 488nm. Similar results were obtained for 90kDa chitosan. The concentration of siMad2-Cy5 was 50 nm. Cell nuclei were counterstained with Hoechst 33258 (blue). The column on the right consists on the merge of the fluorescence images and the phase images. Scale bar = 10 µm

3.5 Evaluation of targeted receptor internalization

EGF is internalized by ligand-induced receptor-mediated uptake. (320) In order to confirm that higher uptake, better cytotoxicity and enhanced siRNA efficacy of EGFR-targeted chitosan nanoparticles is due to receptor-mediated endocytosis, the uptake of fluorescently labeled-siRNA-containing nanoparticles was evaluated in a series of experiments. One of the strategies adapted was to block the EGFR receptors on the surface of A549 cells by exposing to excess of EGFR binding peptide. Cells were pre-incubated with free EGFR binding peptide for 1h prior to exposing them to the targeted system and the nanoparticle uptake was quantitatively determined by FACS (Figure 18). The uptake of the targeted systems significantly decreased when cells were pre-incubation with free EGFR binding peptide, suggesting that the targeted nanoparticle indeed show better uptake dues to receptor-mediated endocytosis. After 15min of incubation with nanoparticles, A549 showed a decreased on the uptake from 47% to 13% for T-LMW and 36% to 11% for T-HMW. Concomitantly, we also studied the uptake of targeted siRNA loaded nanoparticles in NIH-3T3 fibroblast cells, a low-expressing EGFR expressing cell line.(321) To determine the expression level of EGFR by A549 and NIH-3T3 cells, the binding of anti-EGFR antibody to the cells was quantified using flow cytometry (Figure 19). The variation in the fluorescence intensity of A549 after incubation with anti-EGFR antibody was considerably higher than the variation in NIH-3T3 cells proving a much higher expression of EGFR on A549 than NIH-3T3 cells. The nanoparticle uptake by NIH-3T3 cells were found to be roughly the same irrespective of the presence or absence of targeting ligand, further cementing that the enhanced uptake of targeted particles in A549 cells is due to the receptor-mediated endocytosis.

Receptor-mediated endocytosis is an energy-dependent process and so we also performed a nanoparticle uptake study at 4 ˚C where receptor-mediated uptake will be minimum. Indeed, the uptake of targeted systems is dramatically low at 4 ˚C compared to that when the cells were maintained at 37 ˚C. Nanoparticle uptake was lower for all the treatments at 4 ˚C, the decrease was however statistically significant only in case of the targeted LMW and HMW nanoparticles. It is also noteworthy that the net uptake upon blocking the EGFR, using an EGFR non-expressing cell line or performing the study at 4 ˚C is the same indicating conclusively that presence of EGFR binding peptide on the nanoparticles indeed facilitates receptor-mediated endocytosis. It is important to understand that this data cannot be compare to the results represented in Figure 4 since the percent labeling of the siRNA was different for that experiment.

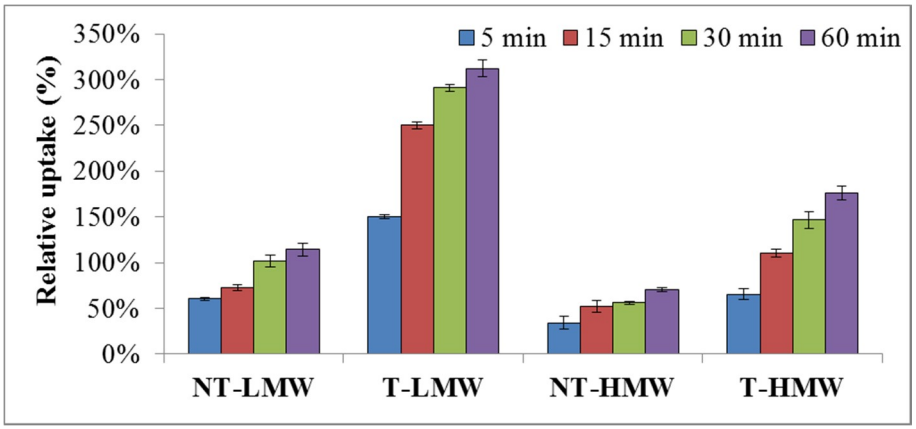

Figure 17: Quantitative relative intracellular uptake study of non-targeted and targeted siRNA loaded CS nanoparticles by flow cytometry in A549 cell line. Data are shown as mean ± SD (n=3).

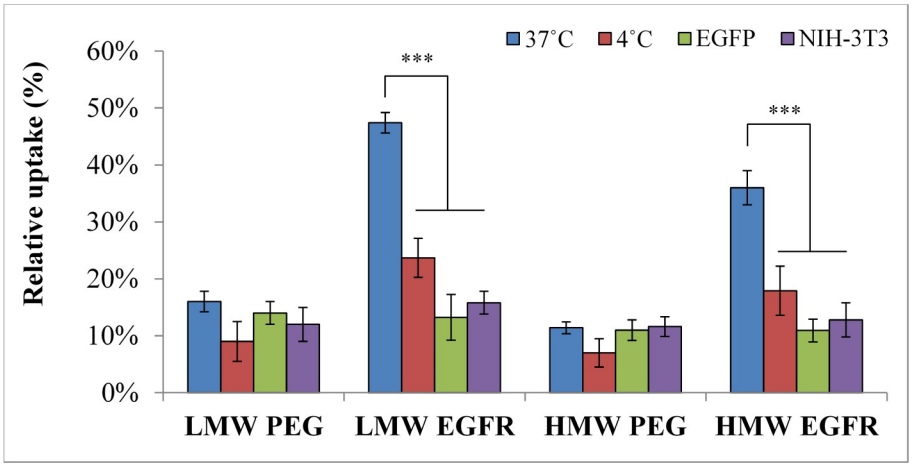

*Figure 18: Quantitative relative intracellular uptake study collected by flow cytometry of non-targeted and targeted siRNA loaded CS nanoparticles in A549 and NIH-3T3 cell line, at 37˚C and 4˚C. and a 50nM siRNA concentration. Data collected refers to a 15min incubation period. Data are shown as mean ± SD (n=3). ***P<0.001*

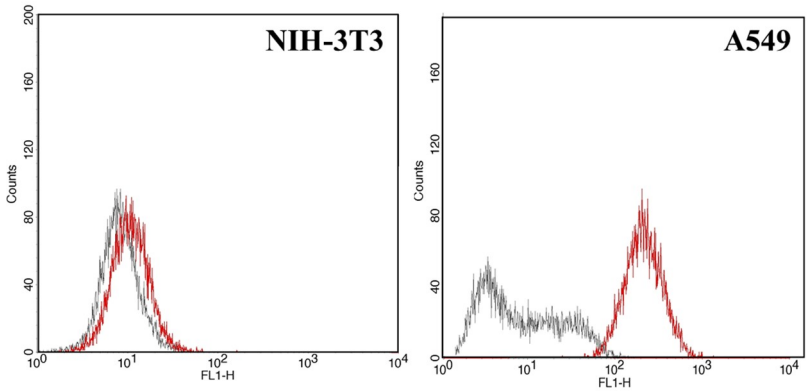

Figure 19: EGFR expression levels in NIH-3T3 and A549. EGFR expression was evaluated by flow cytometry in NIH3T3 (A) and A549 (B) cells using 488nm-labeled EGFR antibody. The grey line corresponds to the histograms for untreated cell lines and the red line to cells incubated with anti-EGFR antibody.

3.6 Optimization of EGFR peptide density on nanoparticles for specific cellular uptake

The density of EGFR binding peptide on the surface could be a key parameter to impact the net uptake of the nanoparticles by the cells. Peptide modified PEG-CS (10% modification) was blended at 0, 25, 50, 75 and 100 % (w/w) to the mPEG modified CS to vary total peptide content of the nanoparticles and was subsequently tested for uptake in A549 cells as a function of incubation time (Figure 20). The cellular uptake profile of nanoparticles with EGFR targeting at 50% or higher concentrations showed almost identical uptake behavior at all-time points up to 60 min of incubation. A 50-50 blend of peptide modified PEG-CS and mPEG modified CS was, therefore, chosen for all subsequent experiments with targeted nanoparticles.

3.7 In vitro Mad2 gene silencing in A459 NSCLC cells

qRT-PCR was used to evaluate the ability of different formulations to silence the expression of *Mad2* gene in A549 cells. *Mad2* specific mRNA expression was quantified in a dose and time-dependent manner after treatment with non-targeted and EGFR targeted CS nanoparticles. A N/P ratio of 50/1 was used for all the experiments and lipofectamine, a cationic lipid transfection reagent-complexed siRNA, was used as a positive control. The dose dependent gene silencing with varying siRNA concentrations ranging from 5 to 50 nM were tested after 48 hours of incubation with cells as shown in Figure 21A. Concentrations below 20 nM did not show a significant change in the *Mad2* expression levels in any of the treatment groups. The gene silencing effect was significantly improved at 30 nM dose of siRNA where non-targeted LMW and HMW nanoparticles show 73 ± 2% and 74 ± 7% decreases in the gene expression. However, the silencing effect was more dramatic with EGFR targeted nanoparticles that show 39 ± 6% and 53 ± 4% gene silencing for T-LMW and T-HMW nanoparticles respectively. *Mad2* expression shows a substantial decrease when the A549 cells were treated with 50 nM of siRNA loaded in CS nanoparticles with 4 ± 2% for NT-LMW, 1 ± 3% for T-LMW, 9 ± 3% for NT-HMW and 1 ± 2% for T-HMW nanoparticles.

Dose dependent study showed an efficient gene silencing at 50 nM concentration of siMad2 loaded in all the formulations and therefore the same concentration was chosen to evaluate a time dependent gene silencing profile of the formulation with lipofectamine as positive control (Figure 21B). Lipofectamine loaded siMad2 effectively decreases *Mad2* expression level to 10 ± 1% within 12h of dosing with a significant and sustained silencing efficiency till 96h. However, *Mad2* expression level starts to revive at later time points of 120 and 144h which could be due to the continued growth and proliferation of non-transfected cells leading to higher expression level of the gene. On the contrary, treatment with non-targeted and

targeted siRNA loaded CS nanoparticles not only showed an efficient silencing effect at early time points but also show a sustained silencing effect at the later time periods unlike lipofectamine. *Mad2* expression levels 144 hours post-transfection were 5 ± 3%, 3 ± 8%, 8 ± 5% and 5 ± 6% for NT-LMW, T-LMW, NT-HMW and T-HMW respectively. In contrast, lipofectamine mediated siRNA delivery led to 26 ± 1% and 27 ± 5% expression of the *Mad2* at 120 and 144h respectively, indicating that CS nanoparticles serve as a more potent delivery with an efficient and sustained gene silencing effect.

3.8 Determination of Mad2 protein levels in A549 NSCLC cells

Flow cytometry was used to further investigate the effect of *Mad2* gene silencing on the Mad2 protein level in A549 cells after treatment with CS-siMad2 nanoparticles (Figure 22).

A549 cells were exposed to 50 nM of siMad2 loaded in CS nanoparticles are the protein levels were evaluated up to 72h post-transfection. Level of Mad2 protein does not show any significant difference after 24h post-transfection and the relative protein content was found equivalent to untreated control. Mad2 protein content 48 hours post-transfection however shows a dramatic decrease in all the cells treated with CS-siMad2 nanoparticles as well as showing 19 ± 4%, 17 ± 5%, 6 ± 2%, 35 ± 1% and 23 ± 4% for Lipofectamine, NT-LMW, T-LMW, NT-HMW and T-HMW respectively. Incubation for 72h in different formulation further led to a decrease in the Mad2 protein level, which is consistent with the *Mad2* mRNA expression levels observed by qRT-PCR (Figure 21B).

3.9 cell viability analysis with siRNA-encapsulated CS nanoparticles

We further conducted cytotoxicity assessment of CS-derivatives alone and loaded with siMad2 to study the biocompatibility of the delivery material itself in A549. MTT assay with different CS-derivatives revealed that these derivatives by themselves did not show any apparent toxicity to both the cell lines even after long periods of incubation at the same concentration used for all the *in vitro* studies (Figure 23).

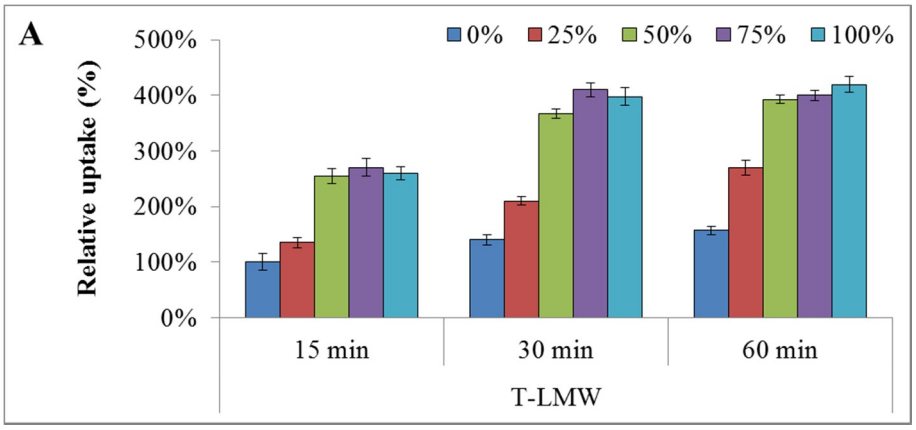

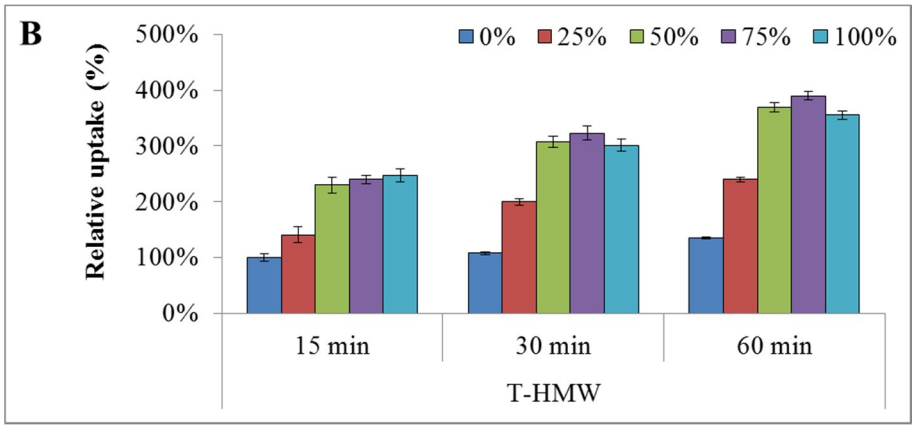

Figure 20: Effect of different percentages of EGFR-P modified chitosan in the targeted formulation, on the relative uptake. Uptake values were normalized against the value obtained for the non-targeted system, which consists on the 0% of EGFR-P modified chitosan, at 15 min post-transfection. A concentration of 50 nM of siMad2 was used in a N/P ratio of 50/1. Data are shown as mean ± SD (n = 3).

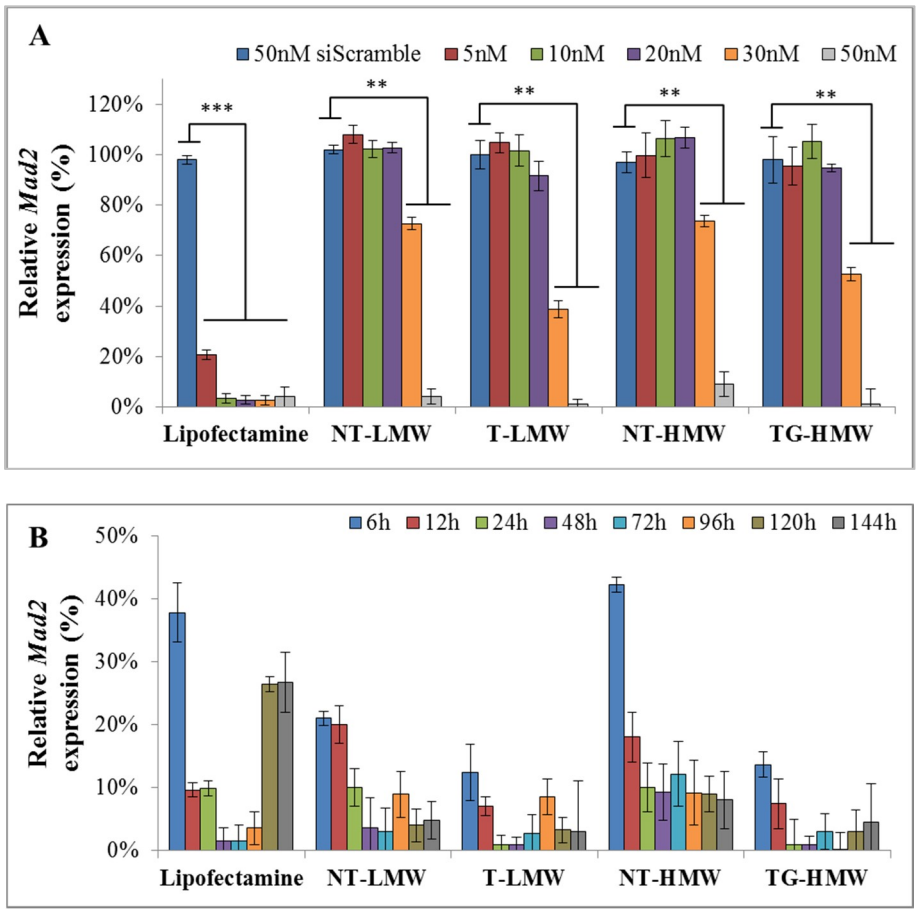

*Figure 21: Down-regulation of Mad2 expression by siMad2 loaded non-targeted and targeted CS nanoparticles in A549 cell line (A) dose-dependent gene silencing 48 h post-dosing and (B) time-dependent gene silencing with 50 nM siMad2 administration. The N/P ratio for all formulations were 50/1. Data are shown as mean ± SD (n=3). **P<0.01; ***P<0.001*

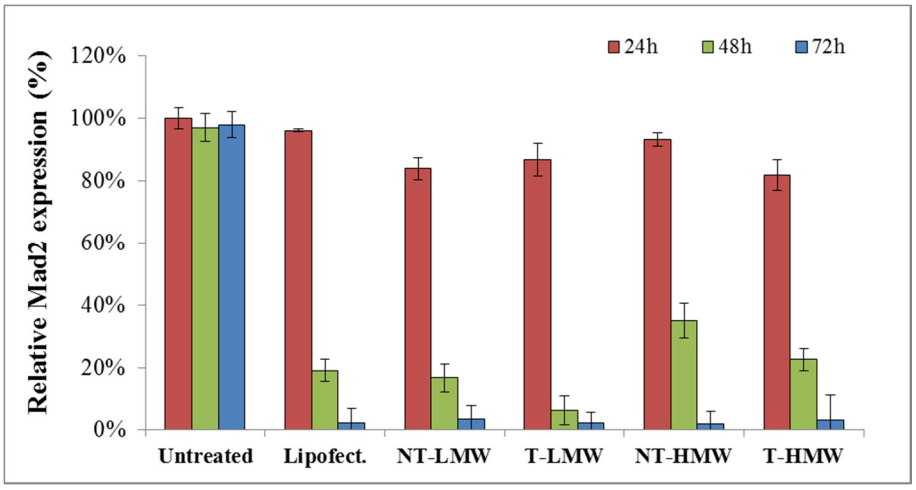

Figure 22: Mad2 protein levels in A549 cells. A549 cells were incubated with 50nM of siMad2 encapsulated in PEG-modified chitosan nanoparticles and EGFR targeting peptide-modified chitosan nanoparticles, using a N/P ratio in all of the cases of 50/1. Data are shown as mean ± SD (n=3).

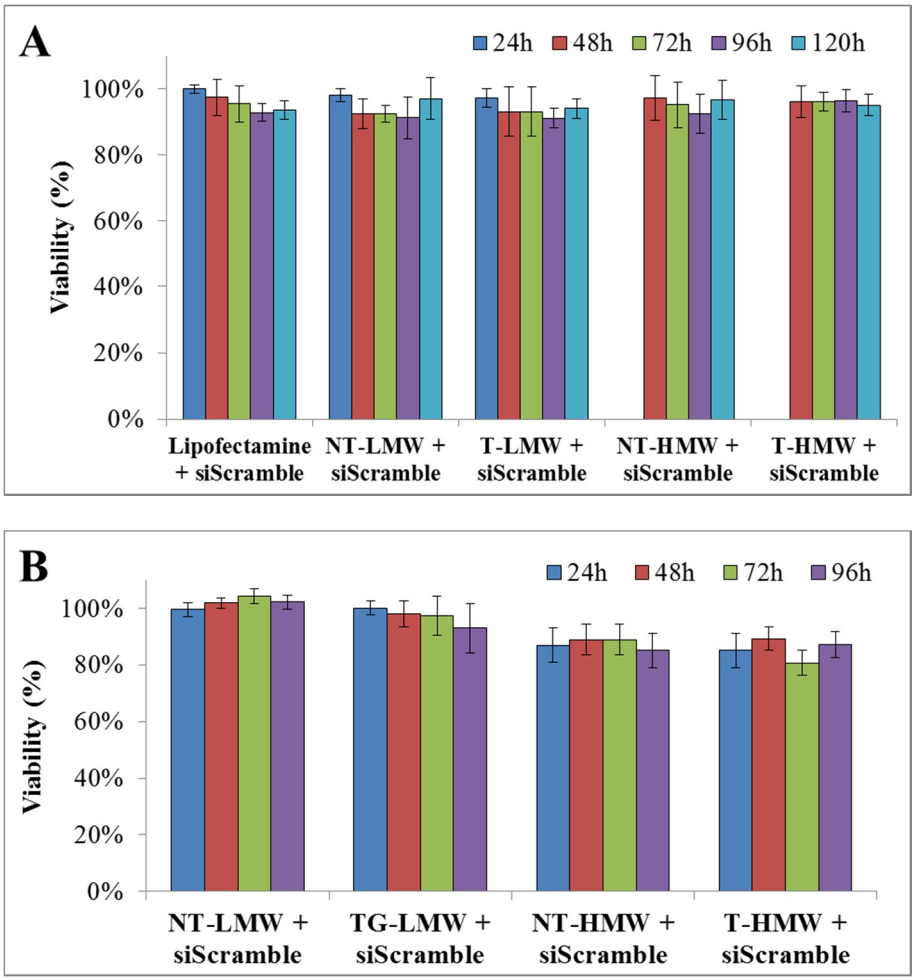

Figure 23: Time-dependent cytotoxicity for A549 cells (A) and HPAEpiC (B) upon incubation with 50nM of siScramble loaded in CS-derivatives in a N/P ratio of 50/1. Data are shown as mean ± SD (n = 3).

Previous studies have showed that chitosan is an attractive polymer for gene delivery due to several characteristics including its excellent biocompatibility, low toxicity, and low

immunogenicity (322). It has been demonstrated that chitosan only exhibited significant cytotoxicity at concentrations higher than 0.741 mg/ml, which is 7 times higher than the concentration used in this study. (323) SiMad2 loaded CS nanoparticles on the other hand showed severe cytotoxicity in A549 after 48h of incubation and kept this trend throughout till 120h of the study, where the cell viability for all the nanoparticles was around 25% (Figure 24A). These results clearly indicate that any cytotoxicity effect elicited by the CS nanoparticles is due to the contribution of the siMad2 and that CS-derivatives themselves are highly biocompatible and non-toxic. In order to evaluate the cytotoxicity of CS-siMad2 nanoparticles in EGFR non-expressing, non-cancerous cells, a human lung primary cell line, HPAEpiC was used (Figure 24B).

All the different nanoparticles formulations showed a delayed cytotoxic effect in HPAEpiC when compared to A549 cells. Only after 72h post treatment did the chitosan nanoparticles triggered a significant change in HPAEpiC cell viability, while in A549 the effect was visible after 48h. Interestingly, the cytotoxic effect of the non-targeted and targeted nanoparticles is similar in the primary cells indicating a similar uptake level, which would be expected since these cells do not over-express EGFR. Besides, the effect of the treatments was much milder in the primary cells compared to the tumor cells at the corresponding incubation periods.

3.10 cellular apoptosis studies with siRNA-encapsulated CS nanoparticles

In order to evaluate the mechanism of siMad2 induced cell toxicity in A549 cells and confirm that the observed cell death is through apoptotic pathway, we performed Annexin V-propidium iodide assay using flow cytometry (Figure 25). Annexin V conjugated to FITC specifically stains phosphatidylserine that translocate from the inner side to the outer surface of the plasma membrane in apoptotic cells. After 48 hours post-transfection, T-LMW nanoparticles loaded with siMad2, 58 ± 5% cells exhibit positive Annexin V staining, indicating apoptotic cell population. Treatment with other formulations including lipofectamine shows only 35% apoptotic cell population under similar conditions, which corroborates well with cytotoxicity results (Figure 24). The apoptotic cell population increased further after 72h post-transfection where T-LMW show nearly 87 ± 7% Annexin V positive cells while treatment with other formulations showed a lower increase in population. This study ascertains that cytotoxicity mediated by siMad2 administration is due to induction of apoptotic pathway in the cells.

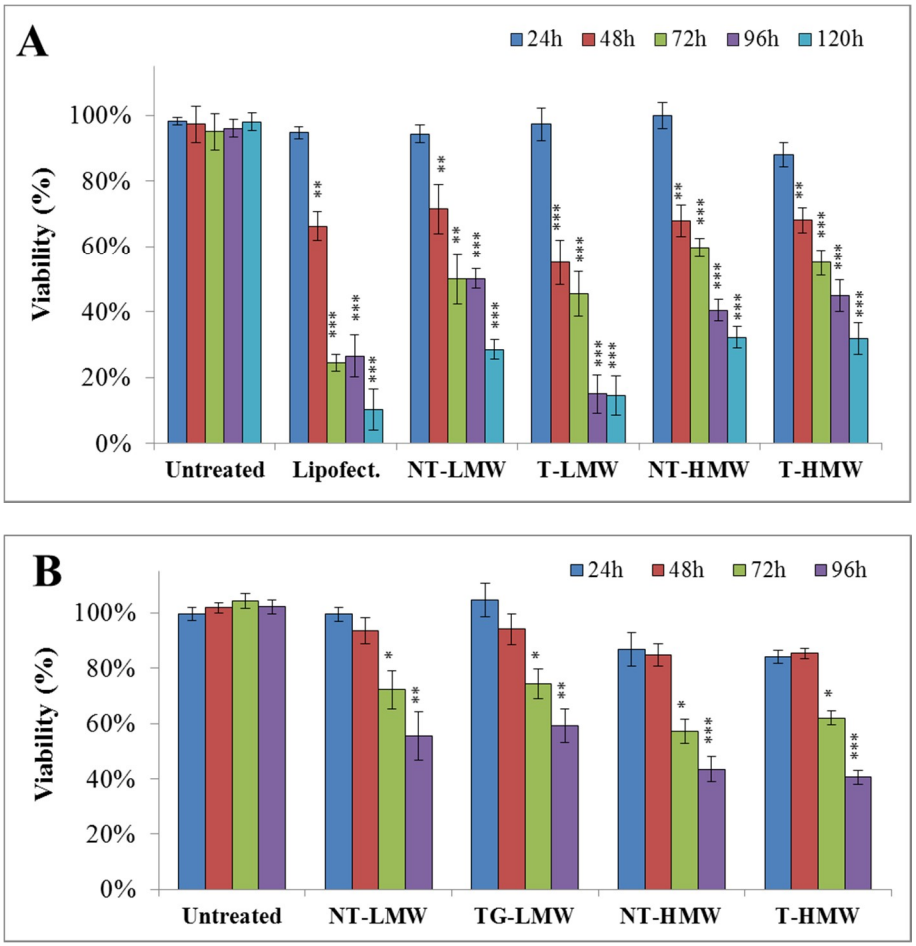

*Figure 24: Time-dependent cytotoxicity studies in (A) A549 cells and (B) HPAEpiC upon incubation with 50nM of siMad2 loaded in CS-derivatives. Data are shown as mean ± SD (n=3). **P<0.05; **P<0.01; ***P<0.001*

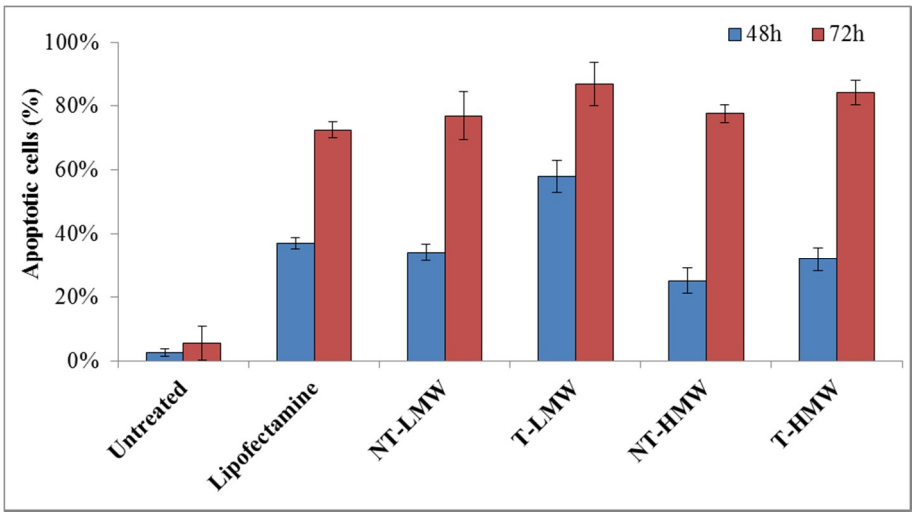

Figure 25: Apoptosis assay using Annexin V-PI staining after exposure of A549 cells to 50nM siMad2 loaded in CS nanoparticles and lipofectamine as positive control. Data are shown as mean ± SD (n=3).

4. DISCUSSION

Mad2 protein is a key component of the mitotic checkpoint and a tumor suppressor gene. Its knockdown leads to extensive cell death as a consequence of mitosis failure mainly due to premature mitotic exit (131, 191, 221). Therefore, modulating the expression of *Mad2* gene and subsequently reducing the Mad2 protein translation specifically in cancerous cells could be a promising anticancer strategy. siRNA therapy particularly has shown tremendous promise in selectively down-regulating the activity of a gene of interest.

In order to enhance siRNA delivery specifically for efficient *Mad-2* gene silencing in A549 NSCLC cells, we have developed EGFR-targeted and non-targeted chitosan nanoparticle complex for delivery of siMad2 for application in lung cancer therapy. Cancer cells overexpress several receptors on their surface to increase the uptake of nutrients and growth factors to meet their incessant demand. EGFR is one such surface receptor that has been long known to overexpress on the surface of majority of cancer tumors and has been intensively studied and characterized in lung cancer (290, 324, 325). Human lung adenocarcinoma A549 cells in particular have been reported to overexpress EGFR receptor on their surface and have shown sensitivity to anti-EGFR therapies (326). Targeting EGFR therefore serves as a logical approach and to this end, we derivatized the CS backbone with heterobifunctional PEG to subsequently bind the EGFR-binding peptide, while the non-targeted nanoparticles system was developed using methoxy-PEG modification. The use of EGFR antibody was avoided due to its larger size compared to EGFR binding peptide, which often contributes to steric resistance in conjugating to the nanoparticles surface and also due to its limited diffusion in tissues (327). Particle size measurement reveals that m-PEG modified non-targeted CS-siMad2 nanocomplexes were in the size range of 100-175 nm depending on the molecular weight of the CS where lower molecular weight CS gives smaller average particle size compared to high molecular weight CS (The zeta potential of the HMW CS-siRNA nanoparticles also showed a similar trend confirming that peptide modification reduces the net positive charge of CS, thereby affecting its interaction with negatively charged siRNA and rendering a larger size for targeted nanoparticles. The polydispersity index (PDI) values for the chitosan nanoparticles decreased with the addition of EGFR peptide for both chitosan molecular weights. In order to analyze if the change in the net charge of CS leads to a change in siRNA loading efficiency of the targeted formulations, siRNA encapsulation efficiency of all the formulations were assessed. The siRNA loading efficiencies of all the nanoparticle systems were found to be 100% irrespective of the difference in CS composition or molecular weight. This observation confirmed that even though presence of the peptide affects the assembly of the

nanoparticle, it does not have any impact on the loading efficiency and that peptide modified PEG-CS could still encapsulate siRNA efficiently despite the charge compensation.

Table 4). Subsequent EGFR binding peptide modification of CS prior to complexation with siMad2 leads to an increase in the net average particle size from 106.8 nm to 227.3 nm for LMW-CS and 173.1 nm to 257.1 nm for HMW-CS samples. This increase in the particle size could be attributed to the peptide modification of CS, which leads to decrease in the net positive charge on the polymer thereby affecting the complexation with the negatively charged siMad2. Zeta potential measurement indeed confirms that peptide-modified nanoparticles show a decrease in the net surface charge for both LMW and HMW formulations (The zeta potential of the HMW CS-siRNA nanoparticles also showed a similar trend confirming that peptide modification reduces the net positive charge of CS, thereby affecting its interaction with negatively charged siRNA and rendering a larger size for targeted nanoparticles. The polydispersity index (PDI) values for the chitosan nanoparticles decreased with the addition of EGFR peptide for both chitosan molecular weights. In order to analyze if the change in the net charge of CS leads to a change in siRNA loading efficiency of the targeted formulations, siRNA encapsulation efficiency of all the formulations were assessed. The siRNA loading efficiencies of all the nanoparticle systems were found to be 100% irrespective of the difference in CS composition or molecular weight. This observation confirmed that even though presence of the peptide affects the assembly of the nanoparticle, it does not have any impact on the loading efficiency and that peptide modified PEG-CS could still encapsulate siRNA efficiently despite the charge compensation.

Table 4), which would affect the nanoparticle packing in the presence of siRNA even though the encapsulation efficiency remains unaltered as demonstrated by similar siRNA loading profile. CS nanoparticle size upon condensation with siRNA has been studied as a function of the molecular weight of the polymer and the particle size observed by us is well in agreement with previously reported literature (268).

A difference in the nanoparticle size could result in differential uptake characteristics and siRNA release profile; especially since the size difference between non-targeted and targeted LMW-CS nanoparticles is dramatically large. In this regard, one would expect a lower intracellular uptake of large-sized particles due to limited diffusion capability (328) . However, on the contrary, all our experiments suggest that targeted nanoparticles, which are significantly larger, show greater intracellular uptake suggesting that any size dependent limitation in uptake is efficiently overcome by targeting EGFR receptor. Besides, the siRNA efficacy of targeted nanoparticles show marked improvement over respective

non-targeted nanoparticles at all studied time points indicating that change in nanoparticle size does not affect the siRNA release or activity in any manner.

The siRNA mediated silencing at gene and protein level clearly indicated that the EGFR targeted nanoparticles outperformed their corresponding non-targeted systems and that the LMW-CS nanoparticles had better activity than the corresponding HMW-CS nanoparticles. As with studying any cell-specific targeted system, it is pertinent to establish that the better activity of targeted nanoparticles is associated with increased intracellular accumulation due to receptor-mediated endocytosis. A series of experiments to study uptake of EGFR-targeted system in EGFR non-expressing cells, selective blocking of the receptor by target peptide and mitigating receptor-mediated endocytosis by performing the study at 4 °C conclusively proved that the enhanced intracellular uptake and subsequent great siRNA activity shown by targeted system indeed is a result of EGFR targeting.

Qualitative intracellular uptake studies of all the nanoparticle systems revealed another interesting phenomenon that is usually uncommon with siRNA delivery. Confocal images indicate that the delivery siRNA localizes in the nucleus of the cells especially at later time points while chitosan remains in the cytoplasm throughout the course of our chosen experimental time points (Figure 16). Such an observation is unusual especially since RNAi mechanism is known to occur in the cytoplasm where mRNA are mostly found; however it is not entirely surprising because several other previous studies have reported the same behavior of siRNA (329, 330) It has also been shown that by diffusion into the nucleus and subsequent export out of the nucleus by Exportin-5, siRNAs can shift between the cytoplasm and the nucleus in a sequence-dependent way (329-332). The exact mechanism that leads to the localization of siRNA in the nucleus is not well understood but it was important to understand whether this property is imparted by the delivery system or is governed by the siRNA itself. To discern this rather intriguing observation further, we repeated the same study with scrambled siRNA keeping the delivery system unaltered (data not shown) and we did not detect localization of the scrambled siRNA in the nucleus. It is therefore safe to assume that the nuclear localization of siMad2 is not related to the chitosan-based delivery system but is possibly due to the sequence-specific siRNA property.

Several siRNA loaded delivery vectors are efficiently internalized into the tumor cells but do not show any activity since they fail to escape endosomes and successfully deliver the payload into the cytoplasm. Chitosan as a positively charged biodegradable polymer has been extensively studied specifically for nucleic acid delivery since it can complex with these negatively charged biomolecules (268). However, several key characteristics of the polymer

can influence its *in vitro* and *in vivo* performance. Molecular weight of the polymer for example can have an impact on the nucleic acid complexation efficiency and subsequent protection. Low molecular weight CS (< 10kDa) show poor siRNA condensation while intermediate MW CS (<80 kDa) have shown a complete and efficient encapsulation (279, 333). Thus, MW of CS can greatly impact the size of the nanoparticles (The zeta potential of the HMW CS-siRNA nanoparticles also showed a similar trend confirming that peptide modification reduces the net positive charge of CS, thereby affecting its interaction with negatively charged siRNA and rendering a larger size for targeted nanoparticles. The polydispersity index (PDI) values for the chitosan nanoparticles decreased with the addition of EGFR peptide for both chitosan molecular weights. In order to analyze if the change in the net charge of CS leads to a change in siRNA loading efficiency of the targeted formulations, siRNA encapsulation efficiency of all the formulations were assessed. The siRNA loading efficiencies of all the nanoparticle systems were found to be 100% irrespective of the difference in CS composition or molecular weight. This observation confirmed that even though presence of the peptide affects the assembly of the nanoparticle, it does not have any impact on the loading efficiency and that peptide modified PEG-CS could still encapsulate siRNA efficiently despite the charge compensation.

Table 4) as well as the stability of the encapsulated siRNA(268). We therefore checked the ability of our nanoparticle system to protect the siRNA payload in the presence of RNAse and the studies clearly indicate that the 50 kDa and 90 kDa CS polymers could effectively shield the siRNA from enzymatic activity (Figure 15).

Activity of the siRNA can also be influenced by the choice of CS where delivery using higher molecular weight polymer tend to show better efficacy of the payload (279). High silencing activity of siMad2 at gene and protein level affirmed that CS delivery vector not only protect the payload from degradation but are also able to release them timely to show activity *in vitro*. However, molecular weight of the polymer alone cannot entirely govern the nanoparticle performance since our results clearly indicate that 50 kDa polymer formulation shows better activity compared to 90 kDa polymer formulation. Lipofectamine, a commonly used cationic lipid transfection agent, was used as a positive control which generated a boost effect on gene silencing but this but failed to provide a sustained silencing effect over time (334) CS nanoparticle mediated delivery, on the other hand, serves as a sustained source of siMad2 in the cells to achieve effective silencing activity for a significantly longer period compared to positive control (Figure 21). Biological activity of any siRNA is directly related to its release from the carrier, which in turn can be influenced by nanoparticle carrier size, interaction with the payload, stability etc. Kong et al. demonstrated that CS molecular

weight can impact the biological activity where changing the polymer from 20 to 40 or 80 kDa changed the net activity from 60 to 70% (279).

Reduction in the level of Mad2 protein results in premature mitotic exit, multi-nucleation and apoptosis-induced cell death (131, 191, 221). It was therefore relevant to assess if silencing of Mad2 gene and subsequent protein expression inflicts any cytotoxic effect on the cells. A time-dependent study with 50 nM dose of siMad2 loaded CS-derivatives in A549 cells demonstrated higher cytotoxicity as a function of increased incubation time post transfection (Figure 23). All formulation loaded with siMad2 start to show cytotoxic effects around 48h post transfection, which correlates extremely well with the Mad2 protein levels in A549 cells with identical dose of siRNA (Figure 22). Most importantly, blank CS derivatives did not cause any toxicity to the cells, thus confirming that the observed cytotoxicity from siMad2 loaded CS nanoparticles is due to siMad2 activity. It has been well documented that depletion of Mad2 protein level leads to apoptosis-mediated cell death (Figure 25) (191, 221).

The human lung primary cell line, HPAEpiC was used as an example of non-tumor human lung primary cell line to evaluate the toxicity profile of the formulation and assess a therapeutic window. The primary alveolar cell line was used to emphasize the two major differences between non-tumor cells and the tumor cells: i) non-tumor cells have a much lower proliferation rate. Since the mitotic checkpoint proteins such as Mad2 are only needed during cell division, its abolition would selectively affect proliferating tissues; therefore cancer cells with high cell proliferation rate would be much more prone to anti-Mad2 therapy compared to their normal counterpart (131) ii) EGFR is frequently overexpressed in NSCLC which would increase the uptake of the EGFR-targeted chitosan nanoparticles when compared with non-tumor cells (335). Due to the absence of EGFR overexpression in the primary cell line, the targeted and non-targeted particles seem to behave in a similar way while in A549 cells the effect of the targeted particles was more pronounced. This further confirms that the enhanced toxicity demonstrated by the EGFR targeted nanoparticles is indeed due to their targeting effect, which would augment the therapeutic efficacy more effectively in the *in vivo* setting.

5. CONCLUSIONS

We have developed an EGFR-targeted chitosan system for silencing *Mad2* mitotic checkpoint gene in treatment of NSCLC. We showed that this system exhibited higher and selective uptake, and efficiently knocked down Mad2, resulting in massive cell death by apoptosis. Collectively, our results indicate that the described system can be used as

potential therapeutic strategy for cancer treatment. Further studies are needed to validate these results *in vivo.*

CHAPTER 4

Biodistribution and Pharmacokinetics Analysis in Drug Sensitive and Resistant Non-Small Cell Lung Cancer Models

The information presented in this chapter was partially published in the following publications:

- Nascimento AV, Gattacceca F, Singh A, Bousbaa H, Ferreira D, Sarmento B, Amiji MM. Biodistribution and pharmacokinetics of Mad2 siRNA-loaded EGFR-targeted chitosan nanoparticles in cisplatin sensitive and resistant lung cancer models. Nanomedicine. *(in press)*

1. INTRODUCTION

Lung cancer is one of the deadliest type of malignancy worldwide, accounting for more than one quarter of all cancer related deaths with 85% of the cases being NSCLC (336). Most cases of lung cancer are diagnosed in their advanced stages, compromising long-term survival (1-year survival rate of approximately 10%) (337). Platinum-based therapy is the recommended first-line treatment for advanced NSCLC. However, systemic toxicity of platinates and development of acquired drug resistance have become an increasing problem in clinic, leading to high rate of mortality in NSCLC (338). As such, there is an urgent need for development of novel treatment approaches against NSCLC, especially in improving clinical outcomes in refractory disease. Some current therapies, such as the use of taxanes and vinca alkaloids, take advantage of those neoplastic cells with high proliferation rate to inhibit their division through targeting microtubules (339). The disadvantage on this strategy is the non-specific toxicity, such as nerve damage, associated with these drugs (340, 341). A promising alternative is the use of molecular targeted strategies to disrupt mitosis without interfering with microtubule dynamics. As the targeted proteins only intervene in actively dividing cells, these strategies would not affect non-dividing cells thereby decreasing the treatment-related adverse effects (342).

Mitotic arrest deficient-2 (*Mad2*) gene is an essential component of the mitotic checkpoint, a surveillance mechanism that inhibits the metaphase-to-anaphase transition whenever chromosomes are not properly attached to the mitotic spindle (131, 343). Overexpression of *Mad2* has been observed in several types of cancer including human NSCLC, oral cancer, cervical carcinogenesis and urothelial bladder cancer (218, 344-346). Mad2 depletion disrupts mitotic checkpoint function leading to premature mitotic exit, increased chromosome fragmentation and extensive cell death, and also sensitizes cancer cells to anticancer drugs. (347-349). We recently used RNA interference (RNAi) approach to highlight the potential of *Mad2* gene knockdown as antitumor therapeutic strategy (347). A major challenge in applying this technology is to effectively deliver the small interfering RNAs (siRNAs) to the tumor *in vivo*. Enzymatic degradation, removal from circulation by renal excretion or mononuclear phagocyte system (MPS), poor cellular uptake and endosomal release are examples of physiological barriers that siRNAs need to overcome (350, 351). Several viral and non-viral delivery vectors, such as adenovirus, polyplexes, liposomes, and micelles, amongst others, have been developed to overcome these obstacles and improve RNAi therapeutic efficacy *in vivo* (352-358).

CS, has gained increasing interest as a safer and more cost-effective vehicle for delivery of gene materials. The deacetylated derivative of chitin, is one of the most abundant

carbohydrate polymers with several essential features that make it a useful natural material for medical and pharmaceutical applications (359). As a random copolymer of poly(D-glucosamine) and poly(acetyl-D-glucosamine), CS is characterized by the degree of deacetylation and primary amine groups which, at low pH, are protonated and afford water solubility and cationic properties (271). The presence of positive charges on CS backbone is related to its improved mucoadhesive properties and hemostatic activity (360). The polymer interacts with membrane negative charges leading to a translocation of tight junction proteins from the membrane to the cytoskeleton, resulting in tight junction disruption and enhanced permeability (361-363). Many reports have shown that CS can be enzymatically degraded *in vivo* due to the cleavable glycosidic bonds, and has minimal toxicity upon systemic administration (359). CS has been widely used as a non-viral gene carrier since it can form complexes with nucleic acids by electrostatic interactions (364). This way, nucleic acids are protected from nucleases and there is an increased efficiency of gene delivery to the cells where these complexes can be released from endosomes to enter the nucleus (347, 364).

Chitosan may be delivered to the tumor tissues by taking advantage of 'leaky' and heterogeneous vascularization, which allows the migration of particles with diameter around 200 nm into the surrounding tumor region. Modifications such as anchoring PEG to the nanoparticle surface can be utilized to prolong *in vivo* circulation and improve tumor infiltration. This process refers to the *enhanced permeability and retention* (EPR) effect that allows for passive delivery of long circulating nanoparticle systems to the solid tumor (365, 366). Other surface alterations, such as the incorporation of targeting moieties (e.g., antibodies, proteins, polysaccharides, and small molecules) provide enhanced efficacy and selectivity to tumor tissue and cells, thereby enhancing specificity and reducing off-target effects. The active targeting approach takes advantage of the overexpression of certain ligands and receptors on the tumor cell surfaces that permits a molecular recognition and a more efficient uptake of functionalized nanoparticles (367).

Overexpression and activation of epidermal growth factor receptors (EGFRs) have been strongly indicated in tumorigenesis, tumor growth, progression, invasiveness and metastasis (324, 368). Due to their high overexpression, they have been extensively used as cancer cell selective targeting receptor. We have previously used a synthetic 12 amino acids peptide that has demonstrated efficient targeting of EGFR receptor and its targeting capability has been successfully validated *in vitro* as well as *in vivo* in various EGFR-overexpressing tumor cells such as A549 (311, 316, 317, 369-371). Most importantly, this peptide is capable of inducing nanoparticles cellular uptake without activating EGFR

signaling pathway and therefore was included as targeting ligand in our formulation approach (318).

We recently demonstrated efficient *in vitro* delivery and *Mad2* gene silencing by siRNA encapsulated in non-targeted (NTG) and EGFR-targeted (TG) CS-based self-assembling nanoparticles system, in cisplatin sensitive A549-WT and resistant A549-DDP NSCLC cells (347). Here, we have investigated the biodistribution profile of these Mad2 siRNA (siMad2)-loaded TG and NTG nanoparticles, in mice bearing subcutaneous, cisplatin sensitive or resistant, human lung adenocarcinoma xenograft tumors. The differences in the biodistribution and pharmacokinetics parameters between TG and NTG nanoparticles has been studied qualitatively and quantitatively.

2. MATERIALS AND METHODS

2.1 Materials

CS with a viscosity-average molecular weight of 55 kDa and a degree of deacetylation of 75-85% was purchased from Sigma-Aldrich Inc. (St. Louis, MO). Fluorescent dye DyLight 680 NHS-Ester and Pico-Green fluorescence reagent were obtained from Life Technologies (Carlsbad, CA, USA). Succinimidyl-([N-maleimidopropionamido]-ethyleneglycol) ester (MAL-PEG_{2000}-NHS, MW 2,000 Da) was purchased from JenKem (Allen, TX). EGFR specific peptide was synthesized at Tufts University's Peptide Synthesis Core Facility (Boston, MA). SiMad2 and its corresponding scrambled siRNA were obtained from Santa Cruz Biotechnology Inc. (Dallas, TX). All primers were ordered from Eurofins Scientific (Luxembourg City, Luxembourg). AgPath-ID One step RT-PCR kit was purchased from Thermo Scientific (Rockford, IL) to perform RT-PCR. All other reagents were obtained at high purity (>99%) from Sigma-Aldrich Inc. (St. Louis, MO) or Thermo Scientific (Rockford, IL).

2.2 Cisplatin sensitive and resistant cell lines and tumor models

Cisplatin sensitive (parenteral) NSCLC cell line (A549-WT) was obtained from American Type Culture Collections (ATCC, Manassas, VA). Cisplatin resistant NSCLC cell line (A549-DDP) was obtained from our collaborator, Massachusetts General Hospital (Boston, MA). Both cell lines were cultured at 37°C in 5% CO2 environment in DMEM/F12 medium from Life Technologies (Carlsbad, CA) supplemented with 10% fetal bovine serum and penicillin/streptomycin (100 U/mL) (Thermo Fisher Scientific, Waltham, MA, USA). A549-DDP were cultured in the presence of 2 μg/mL cisplatin to maintain the drug resistance phenotype. Three days before use, A549-DDP media was changed to a medium without cisplatin.

Six weeks old female *nu/nu* (athymic) mice, strain CrTac:NCr-Foxn1nu from Taconic Biosciences, Inc. (Hudson, NY), weighing approximately 20 g, were group-housed upon arrival in the Division of Laboratory Animal. The animals were allowed to acclimate for at least 72 h prior to any experimentation, raised under specific pathogen-free conditions, kept in individually ventilated cage racks and supplied with sterile rodent pellets and water *ad libitum*. Mice were housed under a 12 h light/dark cycle. For A549-WT and A549-DDP tumor model development, mice were injected subcutaneously with $3x10^6$ cells in a mixture of 50 µL DMEM/F12 medium and 50µL Matrigel on the right flank, under mild anesthesia. Tumor volume was measured with caliper every 3 days and calculated by the modified ellipsoid formula: Tumor volume = ½ (length × $width^2$)

Each study commenced when the tumors reached an average size of 200 mm^3 and the animals were randomly assigning to a specific group. The animals were monitored daily for food/water intake, body weight and any physical signs of discomfort. In all the experiments performed in this study, sample size was determined by power analysis using the software G*Power.

2.3 Synthesis of chitosan derivatives

For NTG and TG nanoparticles encapsulating Mad2 siRNA, CS derivatives were synthesized as previously described (347). Briefly, to a 2mg/mL CS solution in 2% acetic acid, a 10% molar equivalent of Mal-PEG_{2000}-NHS was added and left to react overnight at room temperature. Dialysis (molecular weight cutoff - 10 kDa) in water was performed in order to purify the conjugate. Cysteine was reacted in excess under N2 environment, to inactivate the maleimide group to obtain the NTG CS derivative. The synthesis of TG CS derivative was achieved by using a 17-amino acid peptide consisting of 12-amino acid EGFR recognition peptide, four glycine residues spacer and a terminal cysteine for conjugation via the thiol group (i.e., YHWYGYTPQWVI-*GGGG*-*C*). The peptide was added in a 2-fold molar excess to the CS derivative with a reactive maleimide group and left to react overnight at 4°C in nitrogen atmosphere to allow the cysteine group from the peptide to react with the maleimide group. NTG and TG derivatives were purified by dialysis (molecular weight cutoff - 10 kDa) against water, freeze-dried and stored at -20 °C until their use. Degree of PEG substitution on the CS backbone was estimated by NMR analysis in D_2O using 400 MHz ^1H nuclear magnetic resonance (NMR) spectroscopy (Varian Inc., CA).

2.4 Chitosan labeling with NIR dye for in vivo imaging

Near-infrared (NIR) labeled CS was obtained by mixing NTG CS derivative with the amine-reactive dye DyLight 680 NHS-Ester (DL680) in an aqueous solutions at an equivalent amount to achieve 5% substitution of the CS amine groups. DL680 is a near-infrared

imaging dye with 684/707 nm as Excitation/Emission maxima. After reacting overnight in the dark, the NIR derivative was dialyzed overnight using 10 kDa MW cut-off membrane (Spectrapore, Spectrum Labs, San Diego, CA) and freeze-dried. The degree of modification of the CS backbone with the dye was estimated against a standard curve obtained from the absorbance of the known concentrations of the dye measured at 680 nm.

2.5 siMad2-loaded chitosan nanoparticles

Both NTG and TG CS nanoparticles were obtained by self-assembly in aqueous solution maintaining a N/P ratio (ratio of CS bearing cationic amines to siRNA bearing anionic phosphates) of 50. Independent of the desired type of nanoparticles (NTG, TG or NIR-labeled), CS derivative was dissolved in water (1 mg/mL). SiMad2 was slowly added to this solution under magnetic stirring and incubated for 30 min at room temperature. This procedure allowed CS and siMad2 complexation and nanoparticles self-assembly prior to use. If we intended to produce TG CS nanoparticles, the initial mixture would be a 50 % (w/w) mixture of CS-PEG and CS-EGFR (1 mg/mL). In case of NIR-labeled nanoparticles, CS-PEG would be substituted by NIR-labeled CS-PEG. For every study, nanoparticles were freshly prepared and dissolved in PBS in order to obtain a desired concentration and also achieve an osmolarity of 300 mOsm/kg and a pH of 7.2.

Hydrodynamic diameter (particle size), surface charge and polydispersity index (PDI) of freshly prepared siMad2 loaded CS (CS-Mad2) nanoparticles were measured using a ZetaSizer Nano ZS (Malvern Instruments, Worcestershire, UK). Each sample was obtained from four independent batches in different days. They were diluted in PBS, analyzed in triplicate at 25°C and the different parameters reported as mean ± SD. The encapsulation efficiency (ratio of encapsulated siRNA over total siRNA added) was determined using Quant-iT Pico-Green kit (Life Technologies, Carlsbad, CA, USA).

2.6 Whole body and ex vivo NIR imaging

A549-WT and A549-DDP tumor bearing mice were intravenously injected into the lateral tail veins with a dose of 3 mg/kg of siMad2 encapsulated in NIR labeled TG and NTG CS nanoparticles, (n = 4/group). Intravenous injection was the route of nanoparticles administration in all of the experiments in order to avoid an absorption phase which would compromise an accurate estimation of distribution and elimination parameters (372). Mice were imaged every 24 h until 96 h after the injection, to monitor the distribution of the nanoparticles using Xenogen IVIS® Imaging System (Xenogen Corporation, Alameda, CA) (Ex: 685 nm, Em: 720 nm). Along with these formulations, free NIR dye in PBS at identical concentration was also injected into tumor bearing mice. For ex vivo imaging, the same

procedure was adapted but animals were sacrificed at different time points. Tumor and major organs (liver, spleen, kidneys, heart and lungs) were collected for imaging purposes.

2.7 Quantitative analysis of siMad2 in blood and tissues

siMad2 was encapsulated in NTG and TG CS nanoparticles as described above and injected once at time zero into A549-WT and A549-DDP tumor bearing mice at 3 mg/kg (n = 5/group). At different time points (12, 24, 48, 72, 96 and 120 h), animals were sacrificed and blood samples, the major organs (liver, spleen, lung, heart, kidney), and tumors were collected. Blood samples from the facial vein were also collected 6 h after injection. Plasma was isolated from the blood samples by centrifugation at 1,200g for 15 min at 4 °C, followed by siMad2 quantification.

Tumor and organs were homogenized in RNALater solution in order to preserve RNA integrity and the tissue lysates were diluted at 1:1000 dilution. Mad2 siRNA was then quantified in the samples based on an anti-primer quenching PCR method (373). The diluted samples were used for subsequent annealing step followed by qRT-PCR. The primers used were: *Reverse:* 5' GGA AGC CGA TGG CAG T; *Forward:* /56-FAM/ - 5' ACT CCC TCC CTC GAT TTT CAA TAT CAA AC; and anti-primer: 5' AAA TCG AGG GAG GGA GT /3BHQ_1/.

The procedure was performed according to the previously optimized protocol published by our group (374). Briefly, 6µL of diluted tissue sample was mixed with 18 µl of 100 nM reverse primer, and put through a cycle of denaturation by incubating at 95 °C for 5 min and another cycle of annealing for 2 min at each temperature of 80, 70, 60 and 45 °C. From this mixture, 3.5 µl were used and mixed with 8.5 µl from a AgPath-ID One step RT-PCR master mix constituted by the following components: RT-PCR buffer (6.25 mL), forward primer (10 mmol/L, 0.12 mL), reverse primer (10 mmol/L, 0.12 mL), anti-primer (100 mmol/L, 0.12 mL), 25 U RT-PCR enzyme (0.5 mL), and water (1.5 mL). The PCR conditions were as follows: 50 °C (10 min), 9 °C (10 min), 40 cycles, 95°C (15 sec), 45 °C (60 sec). Using lysate from untreated mouse tissue and spiked with known siRNA concentrations, we were able to do a standard curve and quantify. The quantitated siRNA in each tissue was then normalized towards the percentage of input dose per volume of plasma or per mass of tissue.

2.8 Quantitative pharmacokinetic analysis

SiMad2 plasma pharmacokinetic parameters and organs exposure were determined by non-compartmental analysis using Phoenix® WinNonLin® version 1.3 software (Certara, St. Louis, MO). Plasma half-life (HL) was calculated by log-linearly fitting the three last time points. The maximum observed concentration (C_{max}) and the last observed concentration (C_{last}) were calculated as the mean of observed concentrations at the time when the mean

concentration was the highest, and at the last time point respectively. Exposure, quantified as area under concentrations versus time curve from time zero to the last collection time (i.e., AUC_{last}), was calculated using the linear trapezoidal method. AUC extrapolated to infinity (AUC∞) was the sum of AUC_{last} and C_{last}/(ln2/HL). The associated standard error of the mean was estimated using equations provided by Nedelman and Jia, and later corrected by Holder (375, 376). The mean residence time (MRT) was calculated as the ratio of AUMC∞ (Area under the first moment (time * concentration) versus time curve) and AUC∞. Clearance (CL) was calculated as the ratio of dose (100%ID) and AUC. The volume of distribution at the steady-state (Vss), i.e. at the time when equilibrium is reached for exchanges between distribution compartments, was calculated using the formula: Vss = CL * MRT. Non-compartmental analysis for sparse data being a naive pooled method, no variability could be estimated for pharmacokinetic parameters. Tumor targeting efficiency was evaluated by comparing tumor exposure to plasma exposure, and to the sum of other organs' exposure. For each time-point and each condition, five animals were used.

2.9 Data analysis

With the exception of the quantitative pharmacokinetic analysis, statistical analyses were performed using GraphPad Prism software (San Diego, CA). Paired comparisons were performed by Student's t-test. A *p* value of 0.05 was considered to be statistically significant. Data presented are means ± standard deviation.

3. RESULTS AND DISCUSSION

In our previous *in vitro* studies, we designed and prepared EGFR targeted chitosan nanoparticles as a delivery system for Mad2 siRNA in lung adenocarcinoma cells (347). This nanoparticles were modified with PEG in order to provide a hydrophilic shielding and attain passive targeting to tumor site. NTG and TG nanoparticles loaded with siMad2 were able to efficiently silence *Mad2* gene, leading to increased cytotoxicity by induction of apoptosis (347). In the current study, our goal was to evaluate the biodistribution pattern of these two types of CS nanoparticles in a subcutaneous xenograft model of human drug sensitive A549-WT and platinum resistant A549-DDP tumors. A 3 mg/kg dose of siMad2 was used for all the experiments to ascertain accurate and consistent quantitative detection of the siRNA from various tissues samples.

3.1 Whole body and ex vivo qualitative biodistribution studies

Qualitative nanoparticles biodistribution studies were evaluated using an NIR dye, DL680, covalently bound to the CS skeleton. Due to the dye's strong signal, CS was modified in a very low percentage (4%) which did not significantly impact the nanoparticles characteristics

(Table 5). Both TG and NTG particles were prepared and used to encapsulate siMad2 using the same method, independently of the presence or absence of conjugated dye. NIR labeled CS/siRNA nanoparticles were intravenously injected via tail vein in A549-WT and A549-DDP tumor bearing mice at a single dose of 3 mg/kg of siMad2. Mice were imaged at different time points and the NIR signal was measured to capture the whole-body distribution pattern. Using the same conditions, a different set of animals were sacrificed and their major organs collected and imaged. Although studies were performed in A549-WT and A549-DDP tumor bearing mice, the results were identical in both models and even though we will refer to the results from the A549-WT model, the conclusions apply to both tumor models.

Table 5: NIR dye-loaded CS nanoparticles characterization

	Size (nm) ±SD	PDI ±SD	Zeta potential (mV) ±SD	siMad2 Encapsulation Efficiency (%)
NTG	106.8 ± 2.1	0.551 ± 0.10	+35.6 ± 3.5	105.1 ± 4
NTG-DL680	113.1 ± 5.3	0.472 ± 0.53	+32.8 ± 2.4	101.6 ± 2.3
TG	227.3 ± 1.8	0.362 ± 0.02	+28.3 ± 2.0	99.5 ± 2.4
TG-DL680	230.1 ± 4.1	0.341 ± 0.21	+29.9 ± 2.9	97.5 ± 3.3

NTG: Non-targeted; PDI: polydispersity index; SD: standard deviation; TG: Targeted; WT: wild type.

Within the first 12 h post-injection, a very strong NIR signal was observed throughout the whole body of animals injected with both systems, and only after 24 h the signal started to accumulate in certain areas (Figure 26). The whole body images (Figure 26A) show a strong signal at 24h for both TG and NTG nanoparticles in the liver and kidneys, which are the significant sites of CS nanoparticles accumulation and metabolism, mainly when using CS of low molecular weight (377). Tumors show nanoparticle accumulation, and the signal appeared to be stronger for TG nanoparticles compared to the NTG nanoparticles, particularly in posterior view images. Due to the limited depth penetration of the optical source through the tissue in the whole body imaging, mice were sacrificed and the organs were excised for *ex vivo* imaging. Previous annotations were confirmed by *ex vivo* fluorescent imaging where liver showed a strong signal until 48 h, while kidneys demonstrate higher accumulation throughout but mainly within the first 48 h (Figure 26C). These results are supported by the fact that CS has been described to have relatively long circulation time (377, 378).

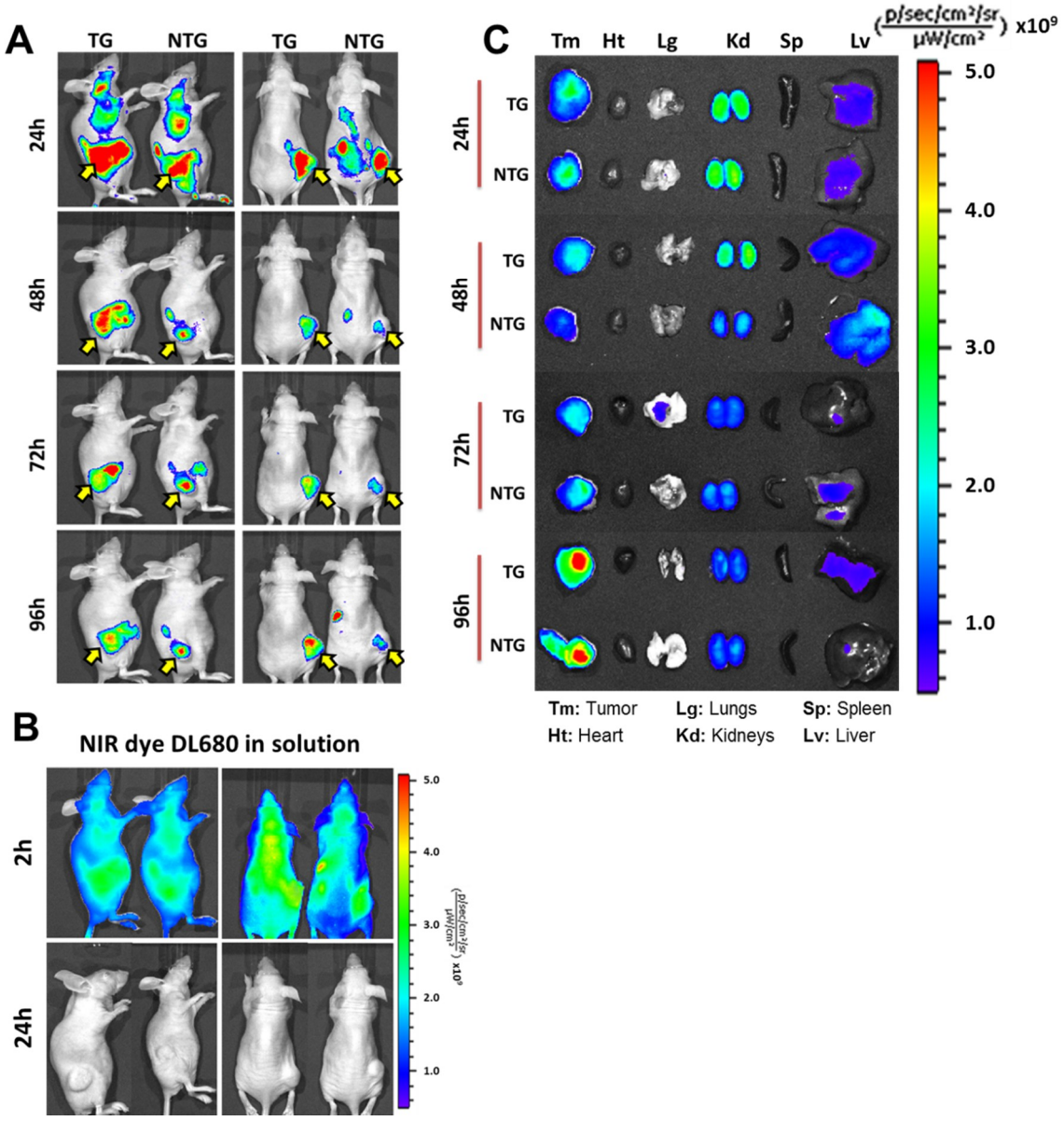

Figure 26: Whole body and ex vivo optical imaging of near-IR labeled chitosan/siMad2 nanoparticles in mice A549-WT tumor bearing mice for up to 96 h. Pre-labeled chitosan with a near-infrared Cy 5.5 dye was used to encapsulate siMad2 using a N/P ratio of 50/1. A549 tumor bearing mice were injected once in a concentration of 3 mg/kg of siMad2 encapsulated in non-targeted (NTG) or targeted (TG) CS nanoparticles. (A-B) Mice were imaged at different time points up to 96h, on their posterior and lateral view using IVIS live imaging system. In this images we have two representative animals although a total of four animals per tumor model were used. A solution of free dye was also administered at equivalent concentration but it was only detected until 2h after injection. Yellow arrow indicates tumor localization. (C) Ex-vivo NIR images of major tissues excised from A549 tumor bearing mice at different time points post injection. NTG: Non-targeted; TG: Targeted; WT: wild type.

Contrarily, heart, lungs and spleen did not show any nanoparticles accumulation with the only exception being lungs that show low signal with TG nanoparticles at 72h which could be due to some contamination during tissue collection, but a very low signal is detected. The excised tumors showed a strong signal after 24 h post-injection for both nanoparticles, although TG nanoparticles seemed to show a stronger signal at 48h. For the following time points, both systems seemed to have similar signal intensity and they reach their maximum at 96 h. Although both NTG and TG nanoparticles have shown a high level of signal in the

tumor site, the imaging technique is not sensitive enough to discern an improvement in tumor accumulation due to the presence of EGFR targeting peptide. In spite of this, both nanoparticle systems presented better delivery efficiency compared with free dye, which was not detected within the tumor. The body distribution of free NIR dye was monitored in order to ensure that the signal seen for NTG and TG nanoparticles was due to intact nanoparticles and not due to free dye released from nanoparticles. At 24 h, there was no detectable fluorescence signal in any of the mice injected with free dye and therefore mice had to be imaged at 1 and 2 h post-injection (Figure 26B). The rapid *in vivo* signal decrease of free NIR imaging dye could be attributed to fluorescence quenching in physiological environments and also indicative of a rapid hepatic clearance from the systemic circulation (379-381). Nanoparticles allow a long circulation of the dye, providing it with an effective shielding and preserving its fluorescence (382). An increased circulation associated with small sizes is beneficial since the nanoparticles will be able to extravasate across the fenestrated endothelium of the cancer vasculature and accumulate in tumor tissue through the EPR effect (366).

3.2 Plasma pharmacokinetic analysis

SiMad2 encapsulated in NTG or TG CS nanoparticles were administered by intravenous injection at a single dose of 3 mg/kg in mice bearing A549-WT and A549-DDP tumors. Later Mad2 siRNA was quantified in different organs, tumor, and plasma, using the anti-primer quenching based RT-PCR method (373). Data was processed and expressed as percentage of the injected dose per ml of plasma or mg of tissue (% ID/ml or % ID/mg). For all conditions, siMad2 was detected in plasma up to 48h after administration. This long circulation could be related to the presence of positive charges on CS structure. These charges can interact with negative charges on red blood cell membranes and allow the nanoparticles to circulate in the bloodstream for long periods of time (383, 384). SiMad2 concentrations were below the limit of quantification at 72 h post-injection. Regarding siRNA concentration in plasma in A549-WT tumor model (Figure 27A), both NTG and TG nanoparticles produced similar concentrations after 6 h, but then concentrations decreased faster for TG nanoparticles than for NTG nanoparticles, with concentrations at 12 and 24 h being significantly lower for TG nanoparticles. A similar trend was obtained in A549-DDP tumor model (Figure 27B) where siMad2 being at a similar concentration at 6 h for both type of particles and significantly lower for TG nanoparticles at 12 and 48 h.

AUC_{last} is an important pharmacokinetic parameter that expresses the concentration of the siRNA in the interstitium as a function of time (385). This parameter reflects the tissue degree of exposure to siRNA and also its clearance from the body. AUC_{last} was significantly

higher in NTG nanoparticles than in TG nanoparticles, independent of the tumor models (Figure 28).

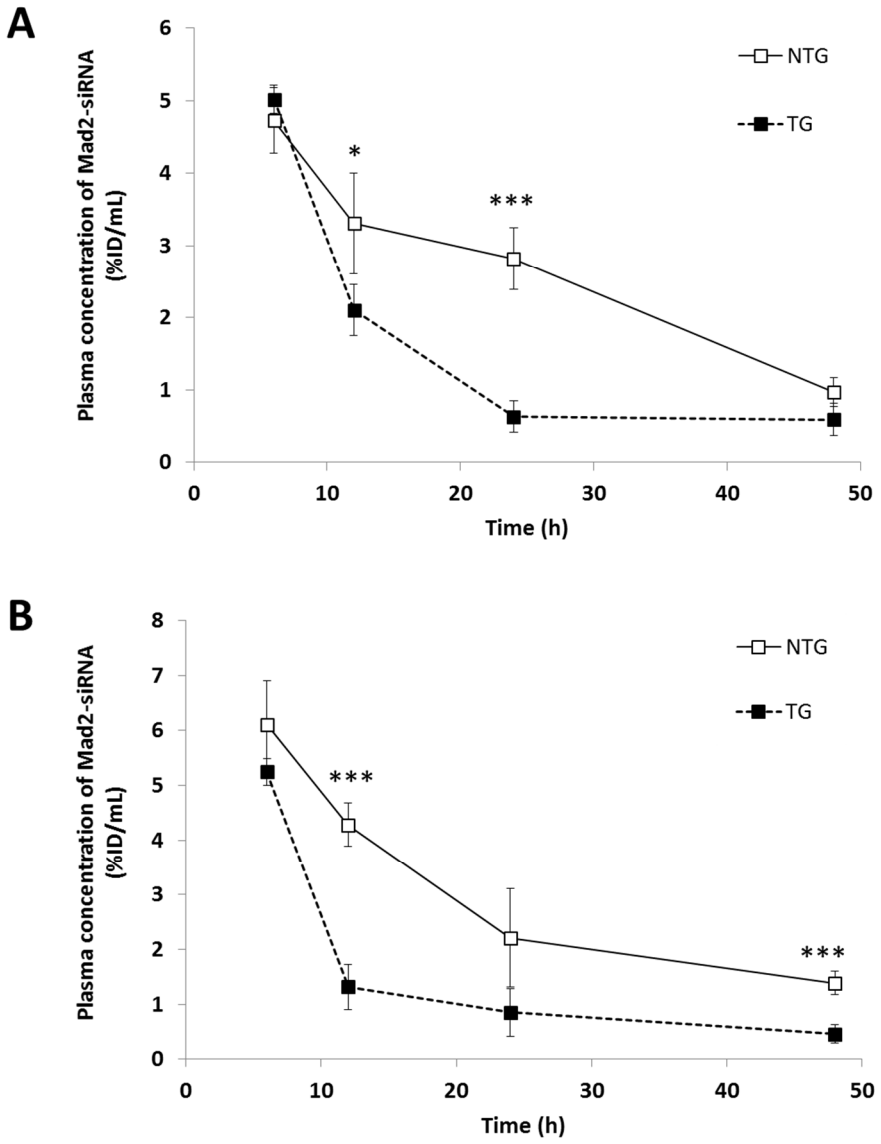

Figure 27: Plasma concentrations of siMad2 (%ID/mL) ± SD versus time (h) in A549-WT (A) and A549-DDP (B) tumor models, after IV injection of NTG and TG nanoparticles at 3 mg/kg equivalent siRNA. n = 5 mice. * p<0.05, ** p<0.01, *** p<0.001 (t-test TG vs NTG). DDP: Cisplatin; NTG: Non-targeted; SD: standard deviation; TG: Targeted; WT: wild type

This observation was consistent with the observed kinetics and exposures. The clearance of TG nanoparticles was higher than the clearance of NTG nanoparticles for both models studied, leading to a shorter mean residence time in the body (Table 6). Accordingly, Clast value was lower for TG nanoparticles than for NTG nanoparticles, while Cmax values were similar. The volume of distribution appeared reduced by the targeting peptide in the A549-DDP model only. Surprisingly, half-life calculated from the last three time-points showed no clear difference between nanoparticles. This might be ascribed to the small number of time-

points, which would not enable the characterization of a biphasic kinetics and a relevant elimination half-life. Overall, the addition of EGFR targeting peptide induced a significantly higher exposure to tumor tissue, which is in line with most published results (317, 386, 387).

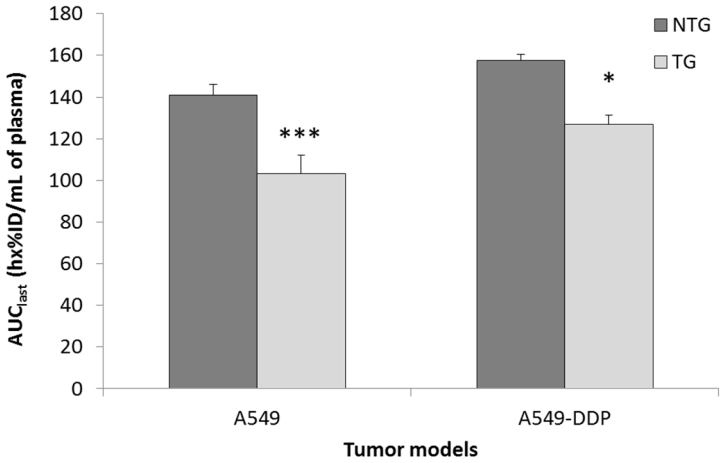

Figure 28: Plasma exposure to siMad2 over the duration of the study. AUClast +SE (in h%ID/mL of plasma) for A549-WT and A549-DDP tumor models, after IV injection of NTG and TG nanoparticles at 3 mg/kg equivalent siRNA. n = 5 mice. * p<0.05, ** p<0.01, *** p<0.001 (t-test TG vs NTG). AUClast = Area under the concentration versus time curve until the last time point; DDP: Cisplatin; NTG: Non-targeted; SE: standard error; TG: Targeted; WT: wild type.*

Table 6: Plasma PK parameters calculated by non-compartmental analysis using Phoenix® WinNonLin® software.

	A549-NTG	A549-TG	A549 DDP-NTG	A549 DDP-TG
HL (h)	19.5	22.6	23.4	24.1
Cmax (SE) (%ID/mL)	4.73 (0.23)	5.02 (0.10)	6.10 (0.40)	5.25 (0.12)
Clast (%ID/mL)	0.970	0.588	1.388	0.459
AUC∞ (h x %ID/mL)	168	122	205	143
MRT (h)	26.1	20.9	30.7	16.0
CL (mL/h)	0.595	0.817	0.489	0.700
Vss (mL)	15.5	17.1	15.0	11.2

AUC∞: Area under the time-concentration curve from time zero to infinity; CL: Total body clearance; C_{last}: concentration at the last time-point; C_{max}: maximum observed concentration; DDP: Cisplatin; HL: Half-life of the log-linear terminal part of the curve; MRT: Mean residence time; NTG: Non-targeted; SE: standard error of the mean; TG: Targeted; Vss: Volume of distribution at the steady-state;.

3.3 Tumor and other tissue pharmacokinetic analysis

Whole body images were informative regarding the nanoparticles biodistribution and *ex vivo* imaging allowed to identify the most exposed organs, but results needed to be confirmed

by quantitative measurements. In A549-WT model treated with NTG nanoparticles, the concentrations at 12 h were the highest in kidneys, followed by liver, tumor, heart, spleen and lungs (Figure 29A).

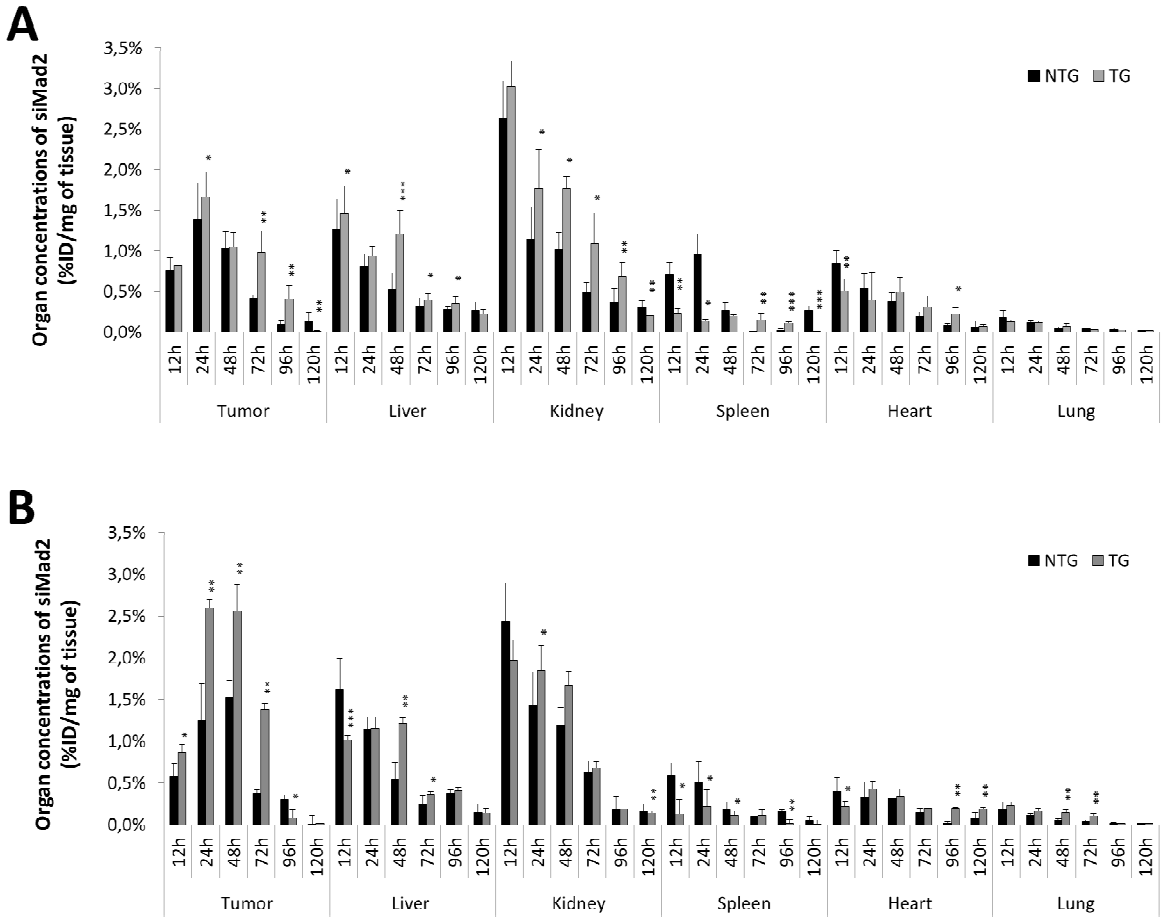

Figure 29: ***Biodistribution in tumor and major organs****. Organ concentrations of siMad2 (%ID/mg of tissue) ± SD at various times after injection (from 12 to 120 hours) in A549-WT (A) and A549-DDP (B) tumor models, after IV injection of NTG and TG nanoparticles at 3 mg/kg equivalent siRNA. n = 5 mice. * p<0.05, ** p<0.01, *** p<0.001 (t-test TG vs NTG). ID: Injected dose; DDP: Cisplatin; NTG: Non-targeted; TG: Targeted.*

At 24 h, the order was slightly different, with tumor displaying the highest concentration, followed by kidneys, spleen, liver, heart, and lungs. The addition of the targeting peptide increased siMad2 concentration in tumor (significantly at 24, 72 and 96h), but also in liver and kidneys. A significant decrease was seen in spleen and heart at early time points with TG nanoparticles, but not maintained later. No significant changes were observed in lungs. Interestingly, the quantitative approach allowed to observe differences, for which imaging was not sensitive enough. The quantitative approach also showed that tumor concentrations were peaking at 24 h and then decreasing, while *ex vivo* images suggested an increase of concentrations until 96 h. It is important to take into account that in one study we are quantifying siMad2 while in the imaging studies, we have labeled CS nanoparticles. Also, siMad2 is rapidly used by the cellular silencing mechanism once in the cytoplasm

while the fate of CS molecule is unsatisfactorily understood (350). In the A549-DDP tumor model (Figure 29B), the trends were very similar to the A549-WT model. However, a few differences could be observed. First, with NTG nanoparticles, concentration in spleen was not lower than in tumor at 12 h, and was higher than in heart. At 24 h, concentration in kidney was still higher than in tumor, and spleen was also less exposed than, in A549-WT model. When comparing TG to NTG particles, the most striking differences were a much higher increase of tumor concentrations, while liver and kidney concentrations were lower at 12 h by the addition of the targeted peptide. These results enhance the influence of active targeting on increasing target-site accumulation.

For some of the organs, it was not possible to properly estimate a log-linear terminal phase half-life and a mean residence time, due to an unclear decrease slope. For example, due to concentrations measurements variability, the spleen concentration at 120 h in the A549-WT model after NTG nanoparticles administration was higher than earlier concentrations in the same conditions. In order to compare the residence times for the different conditions, we chose to use an indirect parameter for residence time, which was available for all conditions, i.e. the C_{last}/C_{max} ratio (Table 7).

Table 7: Ratio of the last time-point concentration (C_{last}) versus the maximum concentration reached over the duration of the study (C_{max}), expressed in % (SD). n = 5 mice. * p<0.05, ** p<0.01, *** p<0.001 (t-test TG vs NTG).

	C_{last}/C_{max} (%) (SD)			
	A549-WT NTG	**A549-WT TG**	**A549-DDP NTG**	**A549-DDP TG**
Plasma	21.1 (6.4)	11.9 (4.7)	22.7 (0.6)	8.71 (3.11) ***
Tumor	8.62 (6.73)	0.619 (0.195)	0.452 (0.269)	0.544 (0.346)
Liver	20.8 (5.4)	15.1 (0.7)	9.07 (3.05)	11.8 (1.1)
Kidney	11.8 (2.8)	6.92 (1.15) *	7.19 (1.32)	7.11 (0.98)
Spleen	33.3 (13.5)	1.50 (0.12) **	11.0 (12.0)	1.84 (0.66)
Heart	6.89 (6.06)	16.5 (5.5)	19.8 (6.9)	50.3 (16.0) *
Lung	13.1 (6.7)	15.6 (6.7)	11.4 (5.8)	6.77 (1.73)

C_{last} : last time-point concentration; C_{max} : maximum concentration reached over the duration of the study; DDP: Cisplatin; NTG: Non-targeted; SD: standard deviation; TG: Targeted WT: wild type.

In plasma, the ratio was lower for TG particles, suggesting a faster elimination and a shorter residence time, which is in line with the PK parameters (Table 7). In tumor, the ratio was

particularly low compared to other tissues, suggesting a rapid clearance of siMad2 from the tumor. This might be due to consumption of the siRNA by its target, leading to a "target-mediated drug disposition". The differences were rarely significant between TG and NTG particles, except for kidney and spleen in A549 model where the ratio was significantly lower for TG particles, and for plasma and heart in A549-DDP model where the ratio was significantly lower and higher respectively. The clearest difference between nanoparticle types, confirmed in both models, was a decrease of the C_{last}/C_{max} ratio in spleen for TG vs NTG nanoparticles, suggesting that the targeting peptide might increase the clearance of the siRNA from the spleen.

Regarding the global exposure of the various tissues to siRNA over the study course (estimated as AUC_{last}), it appeared in both tumor models that kidneys were the most exposed to siRNA, followed by tumor, liver, spleen, heart, and lungs, when NTG nanoparticles were used (Figure 30).

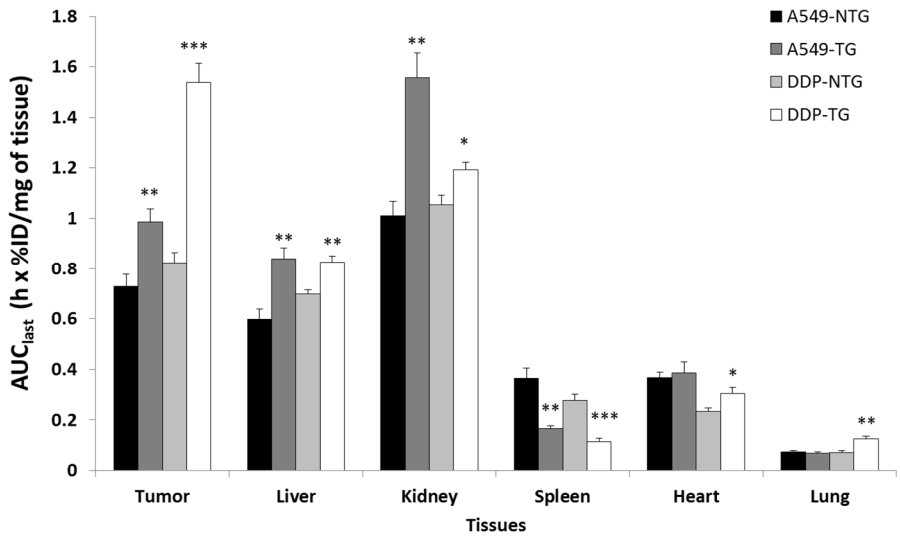

*Figure 30: Tissues exposure to siMad2 over the duration of the study. AUClast +SE (in h x %ID/mg of tissue) for A549-WT and A549-DDP tumor models, after IV injection of NTG and TG nanoparticles at 3 mg/kg equivalent siRNA. n = 5 mice. * p<0.05, ** p<0.01, *** p<0.001 (t-test TG vs NTG). AUClast: Area under the concentration versus time curve until the last time point; DDP: Cisplatin; NTG: Non-targeted; TG: Targeted.*

Introduction of the targeting peptide significantly increased exposure of tumor, liver, and kidneys for both models, of heart and lungs in A549-DDP model only, and significantly decreased spleen exposure in both models. In A549-DDP model, the enhancement of tumor exposure was far higher than in A549-WT model and this influence was felt not only in a higher tumor accumulation but also in a lower accumulation in other tissues. The difference between the tumor models can be ascribed to the slightly higher vascularization that had been detected in the A549-DDP model. Indeed, a higher permeability of the tumor allows nanoparticles to travel more deeply into the tumor tissues after extravasation (388). Another

reason that could contribute to such difference and probably more significantly, is the EGFR expression levels in these two models. We have used flow cytometry to measure EGFR) cell surface expression levels on A549-WT and A549-DDP and results showed that the cisplatin resistant cell line, A549-DDP has a significantly higher expression. This fact is of great influence on the amount of nanoparticles being taken up by tumor cells.

3.4 Evaluation Of The Tumor Targeting Efficiency

Since not only tumor exposure but also other main organs exposure was increased by the presence of targeting peptide, especially in A549-WT; we calculated a new parameter, the targeting efficiency (TE). With this parameter we wanted to check if the presence of the peptide in the TG nanoparticles was able to increase tumor exposure, i.e. the ability of the particle to deliver the siRNA preferably to the tumor than to other tissues. TE was calculated as the ratio of tumor exposure versus plasma exposure or non-target organs exposure. In all conditions, plasma was far more exposed than tumor, the ratio reaching a maximum of 3.16% (Figure 31A). However, TE was significantly increased by the targeting strategy in both models, a 3.4 fold increase in A549-WT and 5.5 in A549-DDP model. It is apparent that the presence of the peptide in the TG nanoparticles has assisted the process of concentrating them into the cancer tissue in comparison to the NTG nanoparticles. We should also keep in mind that both nanoparticles are PEGylated, which by itself promotes tumor accumulation based on the EPR effect (366). Many studies have associated PEG with greater tumor uptake and longer circulation time (389, 390). Besides, PEG contributes to increased particle hydrophilicity, stability, avoidance of plasma protein identification and escape from opsonization and clearance (391).

When comparing tumor exposure to the sum of other organs exposure (Figure 31B), we observed that TE was high, with tumor exposure ranging between 28.3 and 49.0% of the global organ exposure. TE was increased by the targeting strategy in both models, increasing from 28.3 to 31.0% in A549 model, and from 34.8 to 49.0% in A549-DDP model. However, the difference was statistically significant only in the A549-DDP model. These results confirm the influence of EGFR-peptide targeted nanoparticles to target the cancer cells, which is in agreement with previous studies from our group where the same peptide was successfully used (370, 392, 393).

Based only on the imaging data, the targeting effect could not be clearly detected from the whole body and ex-vivo images. These comes from the fact that near-IR images are not sensitive enough to allow for visualization of the difference that was later detected from the quantitative data. Based on the siMad2 quantification study, we could conclude that the presence of the targeting peptide leads to a significant decrease in plasma exposure of

targeted nanoparticles and a higher targeting efficiency, i.e. a higher tumor exposure to Mad2-siRNA associated to no or a moderate increase of off-target organs exposure. The advantage of the targeting strategy was particularly clear for the A549-DDP model, with a higher increase of tumor exposure and targeting efficiency, probably due in some part to its higher EGFR cell surface expression levels.

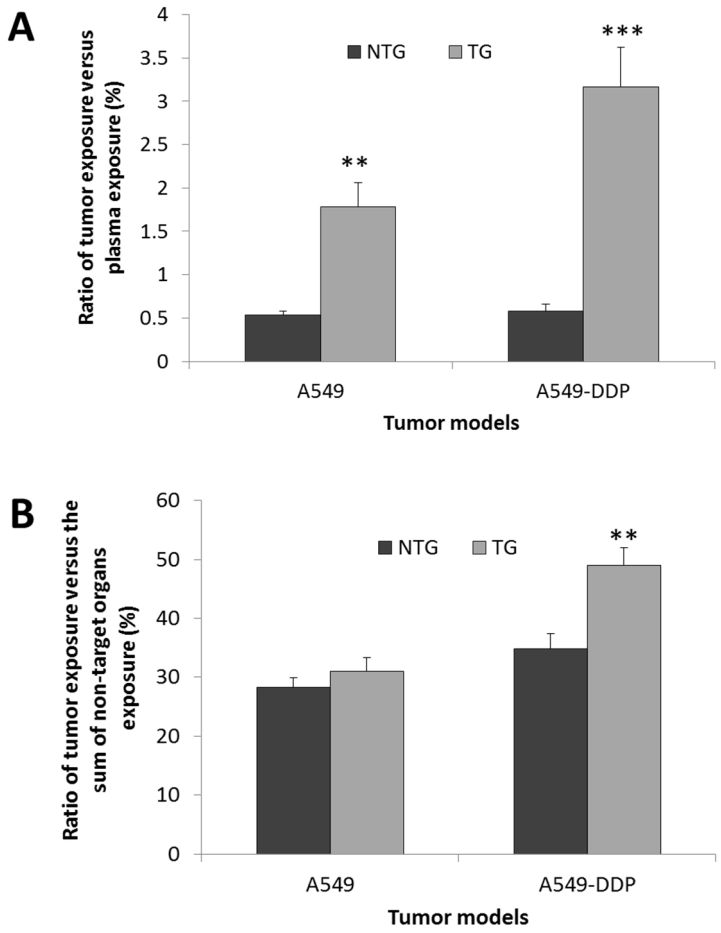

*Figure 31: Targeting efficiency. Ratio (expressed in %) + SE of tumor exposure versus plasma exposure (A) or versus the sum of non-target organs exposure (liver, kidney, spleen, heart, lung) for A549-WT and A549-DDP tumor models, after IV injection of NTG and TG nanoparticles at 3 mg/kg equivalent siRNA. n = 5 mice. * p< 0.05, ** p<0.01, ***p<0.001 (t-test TG vs NTG). DDP: Cisplatin; NTG: Non-targeted; SE: standard error; TG: Targeted.*

4. CONCLUSIONS

The imaging and distribution studies together with the pharmacokinetic parameters showed that the tested CS formulations were efficient in delivering siMad2 to the tumor tissue in both models. In both tumor models, the addition of the targeting peptide resulted in a higher clearance, reflecting a faster elimination from the organism, leading to decreased plasma concentrations. Since tumor exposure was simultaneously increased, the targeting strategy proved efficient in both models to favor the entry of the siRNA inside the tumor. However,

the entry of the siRNA was also increased in other tissues. Calculating the ratio of tumor exposure versus non-target organs exposure, we proved that the tumor targeting efficiency was enhanced by the EGFR peptide, giving a specific advantage for delivery to the tumor when compared to other tissues, particularly in A549-DDP model. With an increased tumor targeting efficiency demonstrated *in vivo* and an efficient induction of apoptosis shown *in vitro*, our targeted delivery strategy proved to be a promising approach for NSCLC therapy *in vivo* (347).

CHAPTER 5

Overcoming Cisplatin Resistance in Non-Small Cell Lung Cancer with Mad2 Silencing siRNA Delivered Systemically using EGFR-Targeted Chitosan Nanoparticles

The information presented in this chapter was partially published in the following publications:

- Nascimento AV, Singh A, Bousbaa H, Ferreira D, Sarmento B, Amiji MM. Overcoming Cisplatin Resistance in Non-Small Cell Lung Cancer with Mad2 Silencing siRNA Delivered Systemically using EGFR-Targeted Chitosan Nanoparticles. Cancer Research. *(submited)*

1. INTRODUCTION

Lung cancer is the leading cause of cancer related death in both men and women in the United States(394). Non-small cell lung cancer (NSCLC) represents 87% of the cases of lung cancer (395). Most of NSCLC patients are frequently diagnosed with advanced-stage disease and have a 5-year survival rate of only 17.4%, lower than many other cancer sites (394, 395).

Cisplatin (cis-diamminedichloroplatinum (II)) (DDP) is usually the first-line chemotherapy treatment in combination with another drug such as gemcitabine, vinorelbine, docetaxel, or paclitaxel (396, 397). In terms of molecular mechanism of action, cisplatin undergoes aquation in the cytoplasm and due to the positive charge it is incapable to cross the cell membrane (398).

Cisplatin cytotoxic activity is due to its ability to interact with DNA forming platinum-DNA adducts that inhibit DNA replication (398). Cell cycle checkpoints monitor the cell accurate order of events, including DNA damage and when an error is detected a delay occurs to provide time for the lesion to be repaired (131, 343). It has been reported that cisplatin effects causes arrest during the G2/M phase of the cell cycle in cells with an intact DNA damage checkpoint(399). In case cells are not able to repair DNA damage caused by cisplatin, two different modes of cell death are induced, necrosis and apoptosis (400). If G2/M phase checkpoint is defective, the DNA damage might pass unnoticed to the next cell cycle phase, the mitotic phase (M phase), where the spindle assembly checkpoint (SAC) can be induced and either arrest the cell cycle and initiate DNA repair, or initiate apoptosis (401).

Cisplatin therapy has two major complications, the augmentation of tumor resistance and its acute side effects (398). In terms of mechanisms responsible for the acquired resistance to cisplatin, several factors have been identified: decreased cytoplasmic accumulation; cytoplasmic sequestration; enhanced DNA repair (402, 403). Tumor resistance could be circumvented by the use of higher doses but that would aggravate the secondary effects (nephrotoxicity, emetogenesis and neurotoxicity), most due to its non- specificity(404). This limitations make new approaches urgently needed.

The demand of new strategies, the constant improved knowledge of cancer molecular biology and nanotechnology innovation in the last few decades has made gene therapy a novel and attractive treatment modality (405, 406). The addition of gene therapy could significantly augment cancer drugs efficacy and allow lower doses, alleviating their secondary effects. On the other hand, although gene therapy are more specific, they are

not as potent and widespread as chemotherapeutic agents. Gene therapy could also benefit and have its efficacy treatment significantly augmented when used together with chemotherapy (406). Chemotherapy and gene therapy is a promising combination strategy to be applied in the treatment of aggressive tumors such as lung cancer.

Strategies targeting mitosis in cancer has been an established clinical approach not only with classical microtubule-targeting drugs but also with newly proposed small molecules targeting Aurora kinases, kinesin spindle proteins, Polo-like kinases, etc. (407, 408). Mitotic arrest deficient-2 (Mad2) is an essential component of the mitotic checkpoint that has a crucial role in the correct segregation of chromosomes during mitosis (132). Mad2, together with other checkpoint proteins, delays anaphase until all chromosomes are attached to the mitotic spindle, assuring the fidelity of chromosome segregation in mitosis (131).

Mad2 is involved both in the SAC and in G2/M phase checkpoint although its role in the DNA damage response was only recently described and is still unclear (409). It is suggested that Mad2 is involved in the DNA damage response pathway leading to mitotic arrest and activation of apoptosis pathway (409, 410). The dual implication of Mad2 on both surveillance mechanisms, SAC and G2/M phase checkpoints can explain previous findings that showed that Mad2 overexpression conferred sensitivity to DNA-damaging agents, especially cisplatin, associated with induction of cell cycle arrest (300).

The opposite effect can also be used as a therapeutic strategy. Mad2 knockdown leads to an early mitosis exit, increased level of severe segregation errors and extensive cell death (221, 347, 411). This process is designated by mitotic catastrophe and although a small minority of daughter cells could survive, they are condemned to death due to the absence of genes coding for essential proteins (412).On the other hand, since Mad2 is a mitotic protein, it's gene silencing will mainly affect cells with increased cell division, one of the hallmarks of tumor cells (413). The selectivity and the severe impact of Mad2 silencing on cancer cells, makes this approach a very attractive alternative therapy.

Mad2 silencing is a compelling method that can be achieved by RNA interference (RNAi)-based therapeutics with small interfering RNAs (siRNAs). RNAi has the potential to become a powerful therapeutic approach in many illnesses such as cancer since it allows to sequence-specifically target genes involved in the mechanism of proliferation, apoptosis evasion, drug resistance, and metastasis (414). The major challenge in RNA-based therapeutics *in vivo* is to ensure siRNAs tumoral delivery (415). Unprotected siRNA present a short half-life due to serum nuclease degradation and renal clearance, and are not easily taken by the cells (415). These difficulties could be overcome by carefully choosing a suitable delivery vector with some particular characteristics such as biocompatible,

biodegradable and non-immunogenic (416). Chitosan (CS) is a nonviral vectors extensively used for nucleic acid delivery *in vitro* and *in vivo* because of its mucosa permeation properties, high biocompatibility, low toxicity and biodegradability (377). This natural polysaccharide is composed of glucosamine and *N*-acetylglucosamine residues resulting from partial deacetylation of chitin (333). CS is available with different degree of deacetylation, molecular weight and depending on the pH, the deacetylated amine groups along the CS chain will be protonated and available to interact with the negatively charged siRNA (333). CS is capable of protecting siRNA, increasing its stability in the blood stream but also, the innumerous chemical modification that can be done to its structure, make it capable of enhancing cell specificity and transfection efficiency (417). The addition of different groups to CS backbone allows to functional moieties to be added, like cell-targeted ligands, making CS an efficient and versatile drug delivery platforms (418, 419). One common modification is the anchoring of poly(ethylene glycol) (PEG) chains to the nanoparticle surface which is used to improve the circulatory half-lives of therapeutics and higher tumor accumulation (420). This effect is associated to the enhanced permeability and retention (EPR) effect that describes the preferential accumulation of nanoparticles at tumor sites due to leaky vasculature (420)

In our previous *in vitro* study, we successfully developed an epidermal growth factor receptor (EGFR)-targeted chitosan system capable of silencing *Mad2* gene and inducing cell death in EGFR overexpressing human A549 cell line (347). Here, we have investigated the effects of siRNA targeting Mad2 (siMad2) alone or in combination with cisplatin at sub-therapeutic dosage. This study was performed in mice bearing subcutaneous, cisplatin sensitive or resistant, human lung adenocarcinoma xenograft tumors, with the aim of examining its efficacy in the inhibition of tumor growth.

2. EXPERIMENTAL SECTION

2.1 Materials

The following products were purchased from Sigma-Aldrich Inc. (St. Louis, MO): ALT Activity Assay Kit (CAT. MAK052); AST Activity Assay Kit (CAT. MAK055); Blood Urea Nitrogen Assay Kit (CAT. MAK006); Creatinine Assay Kit (CAT. MAK080); CS (MW = 55kDa; degree of deacetylation of 75-85%); cisplatin (CAT. P4394). A pool of 3 sequences of siRNA duplexes targeted against Mad2 mRNA (CAT. sc-35837) and a non-targeting negative control duplexes (CAT. sc-37007) were purchased from Santa Cruz Biotechnology Inc. (Dallas, TX). All primers were customized and ordered from Eurofins Scientific (Luxembourg City, Luxembourg). EGFR-specific peptide was synthesized at Tufts University's Peptide Synthesis Core Facility (Boston, MA). Succinimidyl-([N-

maleimidopropionamido]-ethyleneglycol) ester (MAL-PEG_{2000}-NHS, MW 2,000 Da) was purchased from JenKem (Allen, TX). All cell culture material was purchased from Invitrogen/Life Technologies (Carlsbad, CA). The BMP LeukoChek Test Kit to count white blood cells (WBC) and platelets was acquired from Biomedical Polymers, Inc. (Gardner, MA).

2.2 Cell Lines

A549 human lung adenocarcinoma cells were obtained from American Type Culture Collections (Manassas, VA). A cisplatin-resistant version of this cell line (A549-DDP) was obtained from Massachusetts General Hospital (Boston, MA). Both cell lines were cultured in DMEM/F12 medium from Life Technologies (Carlsbad, CA) supplemented with 10% FBS and penicillin/streptomycin (100 U/mL) (Thermo Fisher Scientific, Waltham, MA, USA) and grown at 37°C, 5% CO_2. A549-DDP cells were cultured with 2 µg/mL (6.7 µM) cisplatin to maintain their drug-resistant phenotype. The resistant phenotype of these cells was regularly assessed by cytotoxicity analysis to ensure their IC_{50} (dose that kills 50% of cells) values.

2.3 Synthesis and characterization of pegylated chitosan and epidermal growth factor receptor-targeted chitosan derivatives

PEGylated CS and EGFR-targeted CS derivatives were synthesized according to our previously optimized and established protocol reported elsewhere (347, 418). Briefly, to obtain both CS derivatives, a 10% molar equivalent of Mal-PEG_{2000}-NHS was added to a 2mg/mL CS solution in 2% acetic acid and left to react overnight at room temperature. In order to purify the conjugate, dialysis was performed in water with a molecular weight cutoff of 10 kDa. At this step, to obtain the PEGylated CS, cysteine was added in excess under N2 environment to inactivate the maleimide group. The synthesis of EGFR-targeted CS derivative was achieved by using a 17-amino acid peptide consisting of 12-amino acid EGFR recognition peptide, four glycine residues spacer and a terminal cysteine for conjugation via the thiol group (i.e., YHWYGYTPQWVI-*GGGG*-*C*). The EGFR-peptide was added in a 2-fold molar excess to the PEGylated CS derivative. After reacting overnight at 4°C in nitrogen atmosphere, cysteine was added in excess. Both derivatives were purified by dialysis (molecular weight cutoff - 10 kDa) against water, freeze-dried and stored at -20 °C. Proton nuclear magnetic resonance (^{1}H-NMR) spectroscopy was employed to characterize both derivatives. All NMR samples were prepared by dissolving 2-4 mg of the lyophilized product in 0.7 mL of D_2O with 0.2% DCl and characterized by 400 MHz ^{1}H NMR spectroscopy (Varian, Inc. CA).

2.4 Nanoparticle formulation and characterization

CS nanoparticles encapsulating siRNA were prepared by self-assembly in aqueous solution maintaining a N/P ratio (ratio of CS bearing cationic amines to siRNA bearing anionic phosphates) of 50. A pool of 3 sequences of siRNA duplexes targeted against the Mad2 mRNA was used for best knockdown efficiency. This process conditions have been developed and optimized in our lab (347, 418). Succinctly, in the interested of getting the non-targeted (NTG) nanoparticles, the PEGylated CS is the only CS to be added and after dissolving it in water (1 mg/mL), siMad2 was slowly added to this solution under magnetic stirring and incubated for 30 min at room temperature. In order to obtain targeted (TG) nanoparticles, the initial mixture would be a 50 % (w/w) mixture of PEGylated CS and EGFR-targeted CS (1 mg/mL). This procedure allowed CS and siMad2 complexation and nanoparticles self-assembly prior to use. As done in the previous *in vitro* study, the average hydrodynamic diameter and the polydispersity index (PDI) of the nanoparticles were measured by dynamic light scattering at room temperature and a 90° fixed angle using Zetasizer ZS (Malvern, Worcestershire, UK) (347). Similarly, the zeta potential of the nanoparticles was measured using an electrophoretic cell. For every study, nanoparticles were freshly prepared and dissolved in PBS in order to obtain a desired concentration and also achieve an osmolarity of 300 mOsm/kg and a pH of 7.2.

2.5 In vitro cytotoxicity studies for cisplatin in combination with siRNA therapy

To measure the cytotoxicity of cisplatin together with siMad2-loaded CS nanoparticles, A549 WT and A549-DDP cells were cultured overnight at a cell density of 3000 cells/well in a 96-well plate in 200 µl of supplemented culture media. Then, the cells were washed, and 100 µL of the nanoparticle solution was added to each well (n= 8), incubated at 37°C for 6 h, and followed by replacement of the solution with complete growth medium. After a 48h period, incubation time necessary to produce a satisfactory Mad2 knockdown (ref), growth media was replaced with serum-supplemented media containing 0.01 µM-10 000 µM cisplatin as free drug. Cell toxicity was assessed 24h later by the MTT (3-(4,5-dimethylthiazol-2-yl)-2,5-diphenyltetrazolium bromide) assay. For that, medium was replaced with fresh complete medium containing 100 µL of 0.5 mg/mL MTT (Sigma-Aldrich, St. Louis, MO) for two hours Then, medium was replaced by dimethyl sulfoxide (DMSO) to stop the reaction and lyse the cells. Absorbance of the solution was measured at 560 nm, and the IC50 was calculated using GraphPad Prism software. Untreated cells served as a negative control and cells incubated with poly(ethyleneimine) (PEI, MW 10kDa), a known cytotoxic cationic polymer, were used as positive control for all cytotoxicity experiments.

2.6. Human Lung Adenocarcinoma Xenograft Tumors

Animal procedures were performed according to a protocol approved by Northeastern University, Institutional Animal Care and Use Committee (NUIACUC). Five to six weeks old female *nu/nu* (athymic) mice, strain CrTac:NCr-Foxn1nu, weighing approximately 20 g, were purchased from Taconic Biosciences, Inc. (Hudson, NY). The animals were allowed to acclimate for at least 72 h prior to any experimentation, raised under specific pathogen-free conditions, kept in individually ventilated cage racks and supplied with sterile rodent pellets and water *ad libitum*. Mice were housed under a 12 h light/dark cycle.

For A549-WT and A549-DDP tumor model development, mice were injected subcutaneously under mild anesthesia on the right flank, with $3x10^6$ cells in a mixture of 50 µL DMEM/F12 medium and 50 µL Matrigel. Tumor volume was calculated by the modified ellipsoid formula: tumor volume = 1/2(length × width^2). When tumors grew to approximately 200 ± 20 mm^3 in volume the animals were randomized into groups to yield even distribution of tumor sizes. Sample size was determined by power analysis using the software G*Power. Each animal was identified with an ear tag which allowed us to perform blind experiments in order to reduce bias in animal selection and outcome assessment. The animals were daily monitored for food/water intake, body weight and any physical signs of discomfort.

2.7 In vivo mad2 gene knockdown in A549 WT and A549-DDP tumor model

Animals with 200 ± 20 mm^3 tumors, A549-WT or A549-DDP, were randomized into groups (n = 5) and intravenously injected into the lateral tail veins with one of the treatments (PBS, NTG with a scramble sequence siRNA (SCR), TG with SCR, NTG with siMad2 and TG with siMad2). At time zero, and based on our recent biodistribution data, mice were given a single dose of 3 mg/kg of encapsulated siRNA (either Mad2 siRNA or SCR) and at 24, 48, 72 and 96 h the animals were euthanized and the tumors excised and Mad2 expression evaluated on them.

Tumors were divided in two sections, one for RNA extraction and another for protein extraction. Concerning RNA extraction, tumors were homogenized in RNALater solution in order to preserve RNA integrity. Tissue total RNA was extracted using GeneJET RNA Purification Kit from Thermo Fisher Scientific (Waltham, MA) and later 0.5 µg of total RNA from each sample was used for cDNA synthesis with Verso cDNA synthesis kit (Thermo Fisher Scientific, Waltham, MA) according to the manufacturer's instructions. Finally, Mad2 siRNA was then quantified by quantitative qPCR with the LightCycler 480 SYBR Green I Master kit (Roche, Basel, Switzerland) and primers for 28S ribosomal gene as endogenous control in analysis of gene transcription. The sequences of the primers used in this work

were as follows: Mad2 forward (GTGGAACAACTGAAAGATTGGT), Mad2 reverse (GTCACACTCAATATCAAACTGC), 28S forward (GGGTTTAGACCGTCGTGAGA), 28S reverse (TCCTCAGCCAAGCACATACA). All the kits were used accordingly to the manufacturer's instructions. Mad2 gene expression levels were normalized against 28S ribosomal expression levels which has shown to have a stable expression throughout the tissues. The comparative method for mRNA level quantification was calculated according to the following formulas:

$$\Delta Ct\ (Treated) = Ct(Target\ gene\ in\ Treated) - Ct(Reference\ gene\ in\ Treated)$$

$$\Delta Ct\ (Control) = Ct(Target\ gene\ in\ Control) - Ct(Reference\ gene\ in\ Control)$$

$$\Delta\Delta Ct = \Delta Ct(Treated) - \Delta Ct(Control)$$

Normalized target gene expression level = $2^{(-\Delta\Delta Ct)}$ where Ct is the threshold cycle.

Concerning Western blot analysis, tumors were homogenized in lysis buffer for protein extraction. The BCA Protein Assay Kit was utilized to measure the protein concentration. Protein were separated on 4-20% gradient SDS-PAGE gels and transferred onto a PVDF membrane. The membrane was blocked incubating it for 2 h on blocking buffer (Abcam). For antibody staining, the membrane was incubated with primary antibody overnight at 4˚ C, washed with TBST and later incubated with HRP secondary antibody for 2 h. The bands were visualized after incubation with chemiluminescence detection reagent (Pierce) as described in the manufacturer's instructions. The primary antibodies used were the rabbit anti-Mad2 (1:500; Abcam, #ab180579) and the mouse anti-tubulin (1:5000; Abcam, #ab80779); the secondary were goat anti-rabbit HRP (horseradish peroxidase) secondary antibody (1:5000; SantaCruz, #SC-2054) and goat anti-mouse HRP secondary antibody (1:5000; SantaCruz, #SC-2005). Tubulin was used as a protein loading control.

2.8 In vivo efficacy studies for the combination treatment of Mad2 siRNA/chitosan conjugates and cisplatin solution

Animals bearing A549 WT or A549-DDP tumors with a volume close to 200 ± 20 mm^3 were randomized into 8 groups (n=8). At day 1, siMad2 (3mg/kg) in NTG or TG nanoparticles was administered intravenously via tail vein and 48h later, day 3, cisplatin (1 mg/kg) in solution was administered (Figure 34A). This 5-day dosage regimen was repeated for 30 days. As a negative control, one group was administer with saline solution (Figure 34B). A group of animals was only injected with cisplatin (1 mg/kg) and another 2 set of groups were given NTG or TG nanoparticles with SCR. Tumor volume was measured daily for the first week and every 2 days for the rest of the study. At day 30, animals were sacrificed by isoflurane inhalation followed by cervical dislocation. Blood was collected from all groups in

order to assess several safety parameters. Liver, kidney, and spleen samples from mice were also collected for histopathological analysis.

2.9 Measuring Body Weight Changes, Liver and Kidney Enzyme Levels Quantification, White Blood Cells Count and Platelets

Mice of different experimental groups were weighed daily till the end of the first week and every two days until the end of the experiment. The body weight change was calculated and recorded as mean ± standard deviation (SD). Blood was collected in EDTA coated K2 tubes (Greiner Bio-one, Monroe, NC) from all groups at the end of the study and different parameters were measured. Alanine aminotransferase (ALT) and aspartate aminotransferase (AST) levels were assessed as indicator of liver damage and serum creatinine and blood urea nitrogen as indicators of kidney function. WBC and platelets were also counted. All these parameters were measured using the kits mentioned in the materials section and used accordingly to the manufacturer's instructions.

2.10 Histopathological Analysis

Liver, kidney, spleen and tumor samples from mice were collected for histopathological analysis at the end of the efficacy study. The tissue samples were processed for histological sectioning, H&E staining, and analysis at the Veterinary Clinical Laboratory INNO (Braga, Portugal).

2.11 Statistical analysis

Comparisons between two groups were made using Student's T-test and with more than two groups, the ANOVA test was used. A value of $p < 0.05$ was considered to be statistically significant. Data is presented as means ± standard deviation.

3. RESULTS AND DISCUSSION

Improvements in siRNA delivery methods must be made before RNAi can reach its maximum therapeutic potential. It is required the development of drug delivery systems that are clinically safe, efficient in encapsulating therapeutic siRNAs and can selectively deliver them(421).

3.1 Characterization of chitosan- siRNA nanoparticles

As previously described, siMad2-loaded NTG and TG nanoparticles were obtained by self-assembly and their key characteristics are shown on Table 8 (347). The mean particle diameters of different nanoparticles ranged between 100-230 nm which are suitable sizes for IV administration. Zeta potential were in the range of +28 to +35 and high encapsulation efficiencies were obtained for both systems. Earlier, we have extensively studied these

particles and validated that the EGFR-targeted CS nanoparticles out-perform the NTG nanoparticles by preferred receptor-mediated endocytosis (347). Also, we were able to induce apoptotic cell death by depleting Mad2 expression in non-small cell lung cancer cell line, A549.

Table 8: CS nanoparticles characterization (particle size, zeta-potential, and siMad2 encapsulation efficiency) of CS/siRNA nanoparticles at a N/P ratio of 50/1.

	Particle Size (nm) ±SD	Zeta potential (mV) ±SD	siMad2 Encapsulation Efficiency (%)
NTG	106.8 ± 2.1	+35.6 ± 3.5	105.1 ± 4
TG	227.3 ± 1.8	+28.3 ± 2.0	99.5 ± 2.4

3.2 Mad2 knockdown potentiates cisplatin effects and sensitizes Cisplatin-Resistant Lung Cancer Cells in vitro

Cancer drugs that includes platinum-based compounds such as cisplatin act against cancer cell proliferation by damaging their DNA. As a consequence of this DNA damage, DNA replication is prevented before cell division, which usually induces apoptosis. However, cancer cells can escape apoptosis through translesion synthesis (TLS), a type of DNA replication that is highly prone to errors and, thus, favors drug resistance and tumor aggressiveness (422, 423). DNA damage in mitosis activates the spindle assembly checkpoint (SAC) which causes cell death after a sustained mitotic arrest (424). However, because most cancer cells exhibit a weakly functional SAC, they escape mitosis and survive. Complete abrogation of SAC leads to premature cell division with massive chromosome segregation errors that are incompatible with life. We thus reasoned that the suppression of the SAC component Mad2 by specific siRNA-loaded nanoparticles would kill cancer cells that escape cisplatin effect and, consequently, sensitize cancer cells to chemotherapy.

Based on our previous works, we prepared and conducted nanoparticles-mediated gene silencing in vitro. Accordingly, down-regulation of Mad2 expression by siMad2-loaded NTG and TG CS nanoparticles was efficiently achieved in A549-WT and A549-DDP, with no silencing effect in untreated or blank nanoparticles-treated controls, and with TG nanoparticles leading to a stronger depletion (Figure 32) (347).

Before carrying out the Mad2 depletion and cisplatin combination experiments, we first assessed the resistance levels of cisplatin in sensitive A549-WT and resistant A549-DDP cell lines. The 50% inhibitory concentration (IC50) of cisplatin was more than tenfold higher in A549-DDP (IC50=140.73 μM) than in A549-WT (IC50=12.24 μM), confirming the drug-resistant phenotype of A549-DDP cells (Table 9).

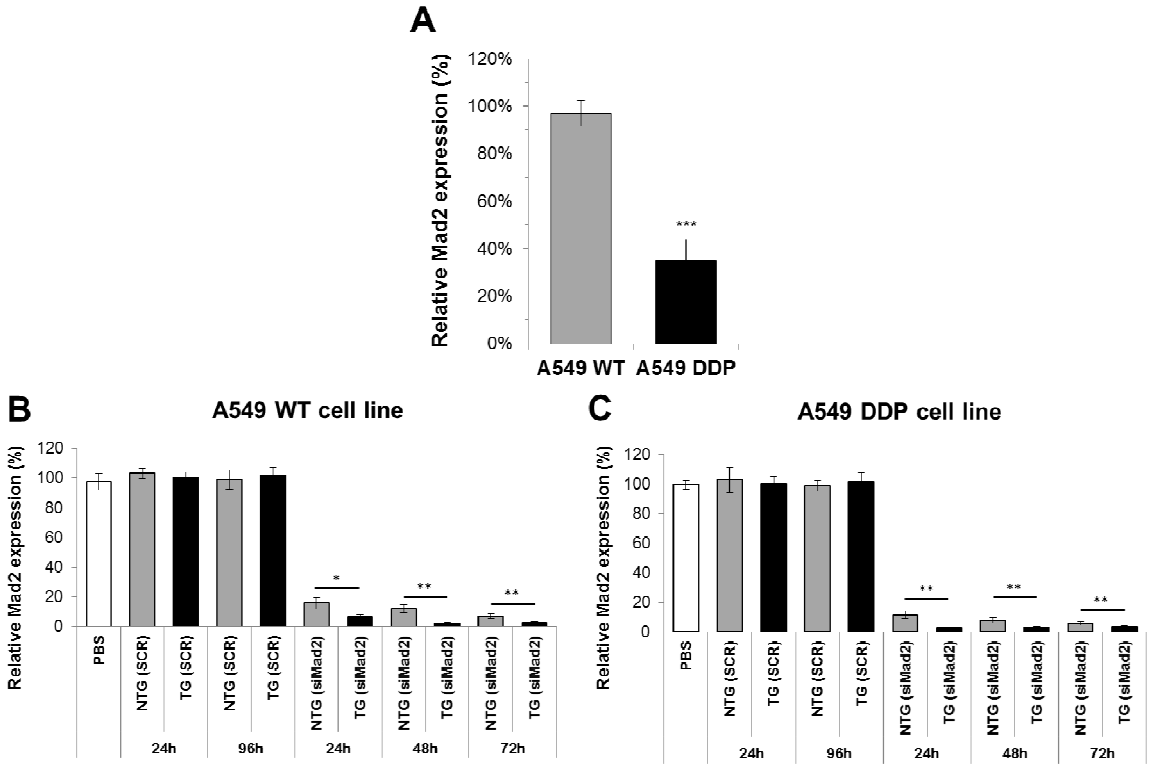

*Figure 32: In vitro Mad2 expression in the A549 WT and A549 DDP cell line. (A) Mad2 expression comparison between the two cell lines. The results are represented as a normalization towards A549 WT expression for an easier analysis of the expression differences. (B and C) In vitro down-regulation of Mad2 gene expression by siMad2-loaded NTG and TG CS nanoparticles in A549 WT and A549 DDP cell lines. A concentration of 50 nM of Mad2 siRNA and a N/P ratio of 50/1 was used in all the cases. Data are shown as mean ± SD (n = 3); *P < 0.05; **P < 0.01; ***P < 0.001.*

Table 9: IC50 values of free cisplatin treatment, 48h post-transfection with siMad2 encapsulated in TG or NTG nanoparticles in A549-WT (A) and A549-DDP (B) cells.

		Cisplatin IC50 (± SD)		Fold change
A549-WT	DDP	12.24	± 1.09	—
	Lipofectamine (siMad2 50 nM)	0.306	± 0.008	40x less
	NTG (siMad2 50 nM)	0.999	± 0.015	12x less
	TG (siMad2 50 nM)	0.132	± 0.012	95x less
A549-DDP	DDP	142.204	± 2.156	—
	Lipofectamine (siMad2 5nM)	0.325	± 0.017	437x less
	NTG (siMad2 1 nM)	0.178	± 0.021	799x less
	TG (siMad2 1 nM)	0.094	± 0.023	1513x less
	NTG (siMad2 5 nM)	0.086	± 0.033	1653x less
	TG (siMad2 5 nM)	0.057	± 0.031	2495x less

For the combination study, cells were incubated for 48h with siMad2-loaded CS nanoparticles containing 50 nM siRNA and later 24h with cisplatin at increasing concentrations to determining cisplatin $IC_{50.}$ Combination of Mad2 depletion and cisplatin treatment leads to a dramatic increase in cytotoxicity in both cell lines, compared to individual treatments, with an even stronger effect in the cisplatin-resistant line. Indeed, a significant decrease in cisplatin IC50, up to 95-fold in the sensitive cell line and to 2495-fold in the resistant cell line, was observed when combined with TG Mad2-siRNA-loaded nanoparticles (Table 9). Of note, in the resistant cell line, a strong reduction in cisplatin IC50 (up to 1513-fold) was still achieved even with reduced amount (50-fold lesser) of Mad2 siRNA. Interestingly, gene expression analysis by qPCR revealed that Mad2 mRNA levels was three times less abundant in A549-DDP compared to A549-WT (Figure 32), which may explain why in the resistant line much less siRNA is required to achieve efficient Mad2 depletion, thereby reducing the toxicity potential associated with high dosage.

Overall, these results suggest that siRNA-mediated Mad2 downregulation enhances the sensitivity of lung cancer cells to cisplatin with a high level of reversal of drug resistance. The improvement observed in the *in vitro* cytotoxicity profile of TG nanoparticles compared to the NTG nanoparticles seems mainly due to the EGFR peptide modification triggering receptor-mediated endocytosis and this phenomenon has been extensively study in our previous work (347).

Cisplatin, as a crosslinking agent, binds to DNA to form intrastrand and interstrand crosslinks and adducts which originates changes in DNA conformation and interferes with DNA replication (422, 423). This culminates in G2/M cell cycle arrest that can lead to DNA repair, promoting resistance to the drug, or resulting in apoptosis (423). If cells are able to escape G2/M arrest and progress to the mitotic phase, since Mad2 is absent, cell will failure to arrest and an aberrant chromosome segregation will take place, triggering cell death (221, 407). Due to these mechanisms, the combination of CS nanoparticle containing siMad2 with cisplatin treatment was found to be more effective when compared with cisplatin alone treatment.

3.3 Mad2 gene silencing in tumor bearing mice

Using xenograft model of cisplatin-sensitive A549-WT and cisplatin-resistant A549-DDP lung cancer, we examined whether nanoparticles formulations were able to silence Mad2 in tumors. Mad2 silencing was analyzed both at mRNA and protein levels in tumor extracts harvested from the mice at the designated time points. As shown in figure 1A, Mad2 mRNA levels decreased to 20% control levels (i.e. 48h post-treatment in both sensitive and resistant tumor models), being TG nanoparticles more efficient in gene silencing than NTG

nanoparticles. A similar decrease response was also achieved at protein levels, with a drop to 35% Mad2 protein levels relative to the control on A549-WT and 22% on A549-DDP (Figure 33). Interestingly, this Mad2 silencing effect upon a single dose of nanoparticles was still noticeable at 96h post-treatment, further demonstrating the effectiveness of the nanoparticles in inhibiting Mad2 expression in tumors.

3.4 In vivo efficacy assessment of siMad2/cisplatin combination treatment

The aim of this study was to determine whether Mad2-siRNA nanoparticles formulations would result in increased sensitivity and even reversal of resistance to cisplatin which would enhances antitumor activity effects. As could be depicted from Figure 34, this strategy resulted in a clear and enhanced antitumor activity. None of the controls had a significant effect on tumor growth (Figure 34). Either sensitive or resistant tumors treated with Mad2-siRNA nanoparticles displayed delayed tumor growth which was more accentuated with TG (A549-WT: 45 %; A549-DDP: 51.2 %) than with NTG nanoparticles (A549-WT: 26.2 %; A549-DDP: 43 %).

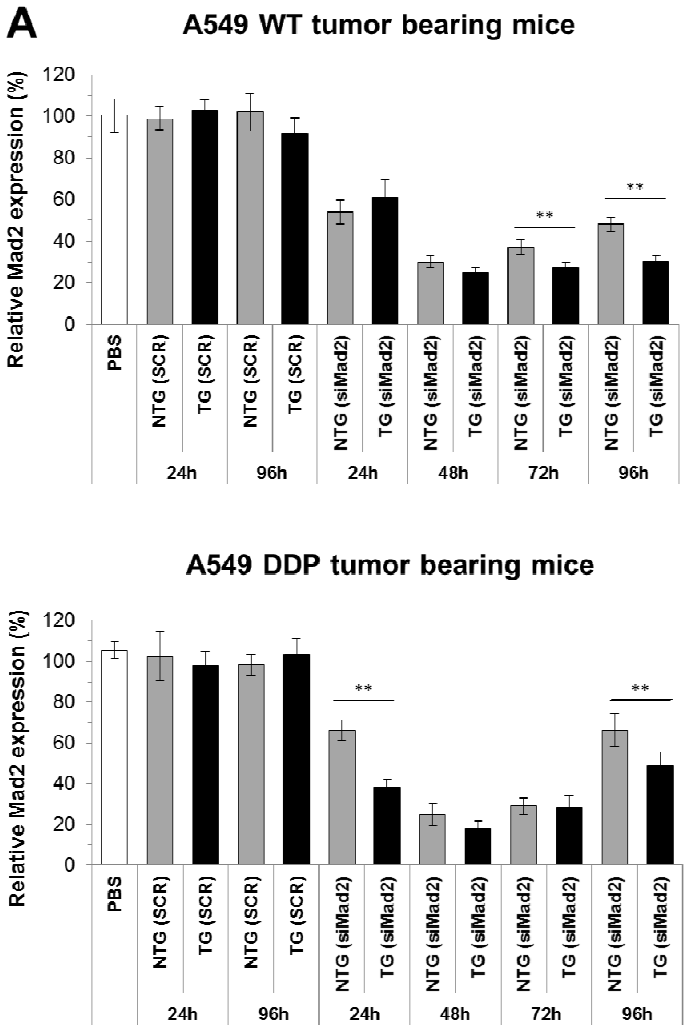

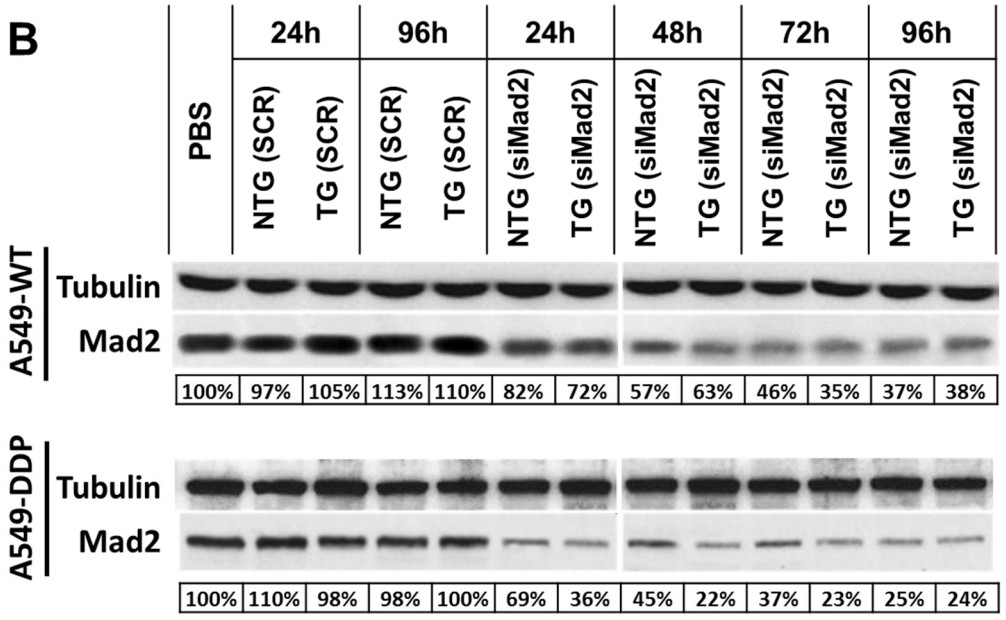

*Figure 33: Knockdown efficiency of siRNA targeting Mad2 in NSCLC tumor bearing mice. (A) qPCR and (B) western blot analysis of Mad2 knockdown efficiency in A549 WT and A549 DDP tumors. A 3 mg/kg single dose of siRNA, encapsulated either in TG or NTG NPS, was administered to tumor bearing mice. Tumors were collected at different time points for evaluation of the Mad2 gene silencing. (n = 5 animals/group). On qPCR data, bars represent the mean ± standard deviation from three independent experiments. *** = p< 0.01. Referring to the western data, tubulin protein was used as an internal control. Data represents one of the three independent experiments with similar results.*

In contrast, and as expected, cisplatin treatment was more effective in sensitive than in resistant tumors. TG siRNA nanoparticles, and to a lesser extent NTG siRNA nanoparticles, plus cisplatin resulted in the greatest efficacy in both lung tumor models (NTG (siM2) + DDP: 58.9 %; TG (siM2) + DDP: 70.6 %). These results strongly suggests that the combinational effects of Mad2-siRNA-loaded nanoparticles and an anticancer drug such as cisplatin can be a valuable therapeutic strategy to increase drug sensitivity and overcome resistance.

3.5 In vivo safety profiles

During this study, to monitor the safety of the formulations, the body weight of each group was monitored every two days and the percentage weight change is presented (Figure 34A). Initially all the groups went through a slight decrease in body weight which is quite common due to handling stress but the animals quickly recovered the initial weight.

A

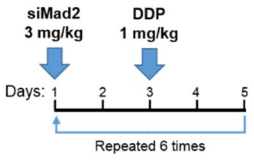

B

Abbreviation	Experimental Group	siRNA dose	DDP dose
PBS	Saline solution	—	—
NTG (SCR)	Non-targeted nanoparticle (scramble siRNA)	3 mg/kg	—
TG (SCR)	Targeted nanoparticle (scramble siRNA)	3 mg/kg	—
DDP	DDP	—	1 mg/kg
NTG (siM2)	Non-targeted nanoparticle (Mad2 siRNA)	3 mg/kg	—
NTG (siM2) + DDP	Non-targeted nanoparticle (Mad2 siRNA) + DDP	3 mg/kg	1 mg/kg
TG (siM2)	Targeted nanoparticle (Mad2 siRNA)	3 mg/kg	—
TG (siM2) + DDP	Targeted nanoparticle (Mad2 siRNA) + DDP	3 mg/kg	1 mg/kg

C

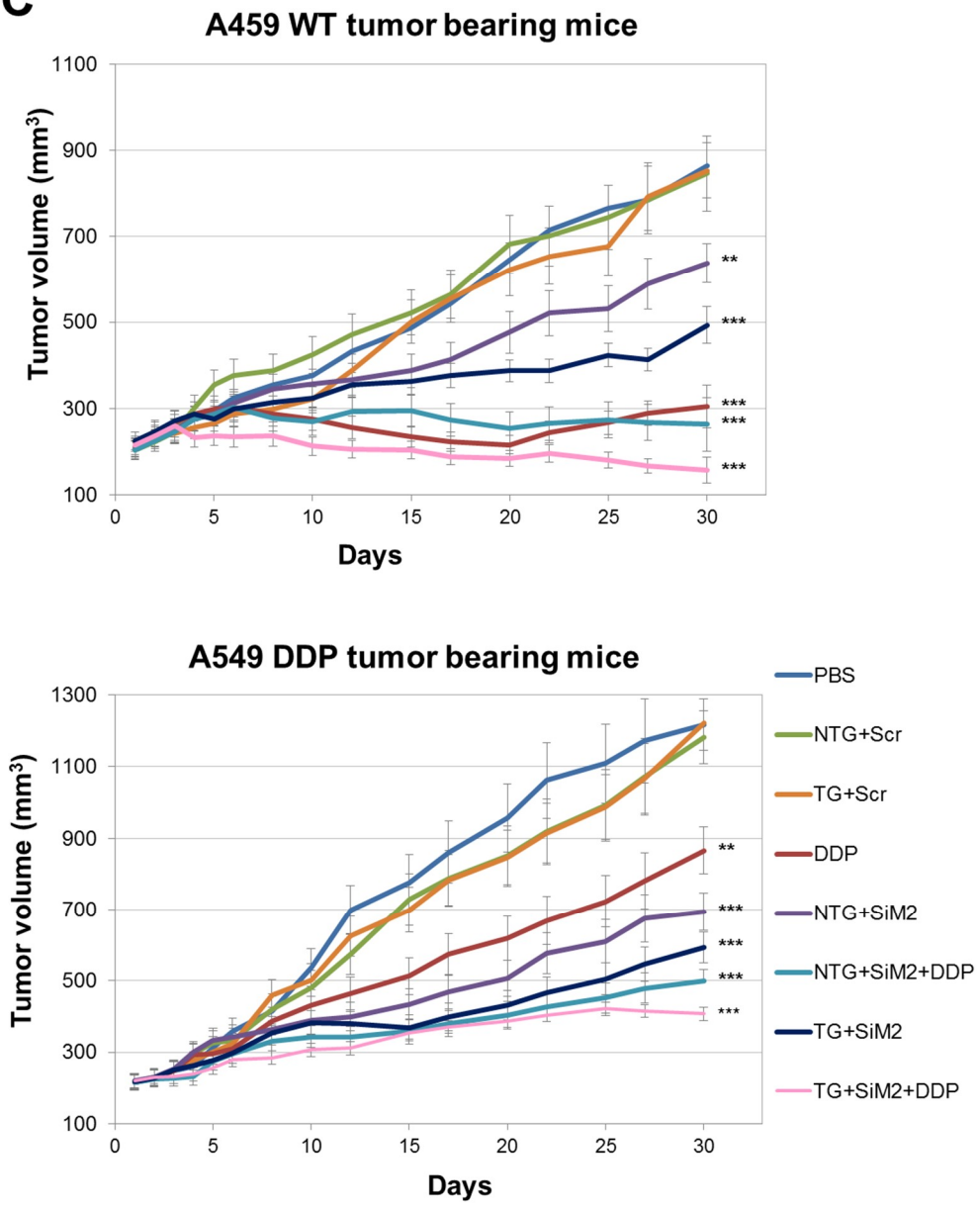

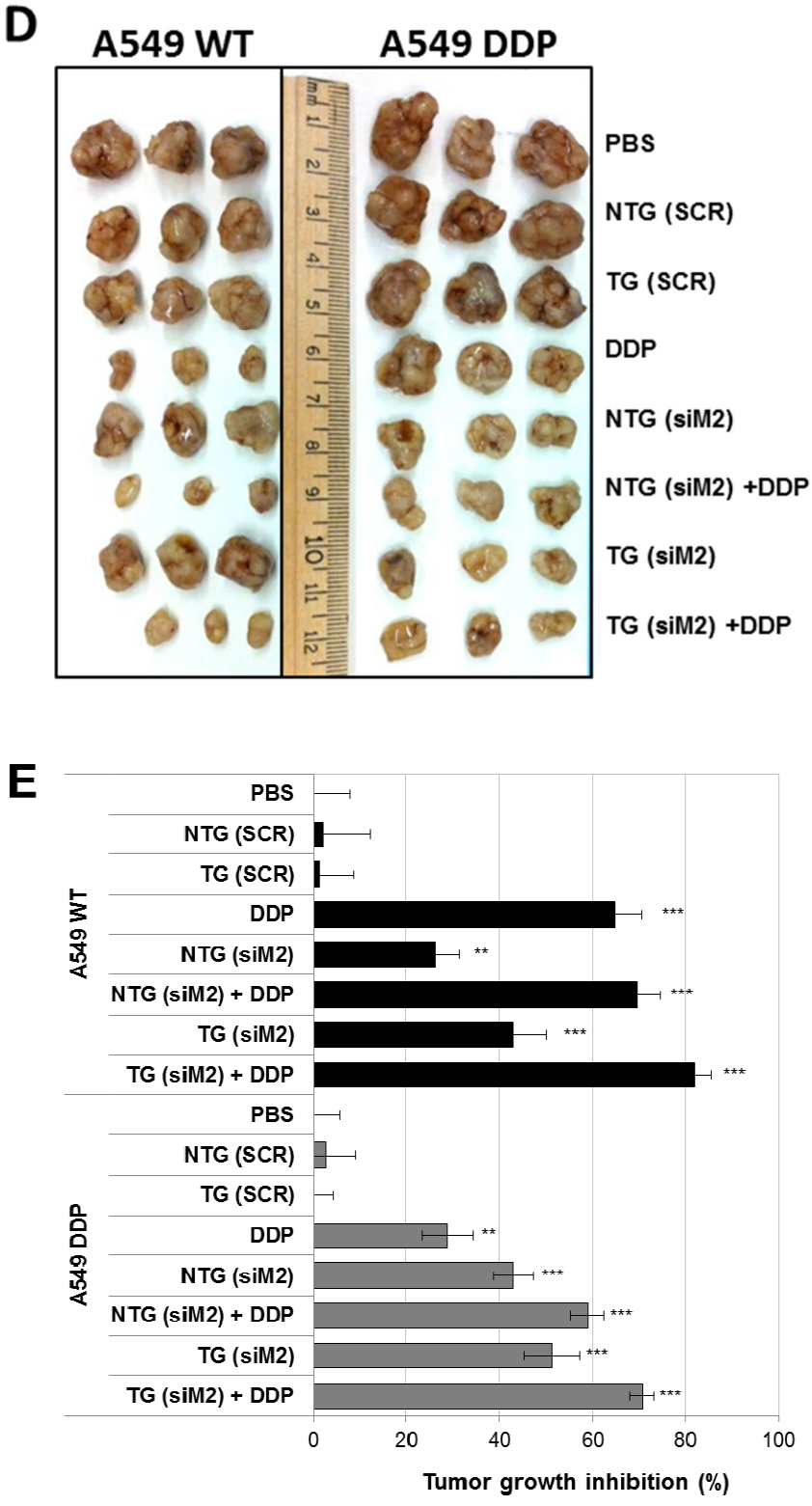

*Figure 34: Effect of the combination of cisplatin treatment and Mad2 silencing on growth of sensitive and resistant A549 tumor bearing mice. (A) The following dosage regimen was used in order to evaluate the in vivo tumor inhibitory effect of the combination therapy. (B) Experimental treatment groups. (C) Tumor volume variations for the different treatments intravenously injected in A549 WT (left) and A549 DDP (right) tumor bearing mice. (D) A549 WT and A549 DDP xenograft tumors representative of the samples from each treatment group. (B) Tumor growth inhibition rates for each treatment group in both tumor models. n = 8 mice. ** p<0.01, *** p<0.001 (t-test comparing to PBS treatment). PBS: Phosphate Buffered Saline; NTG: Non-Targeted; TG: Targeted; DDP: Cisplatin; SCR: Scramble Sequence siRNA, siM2: small interfering RNA Mad2.*

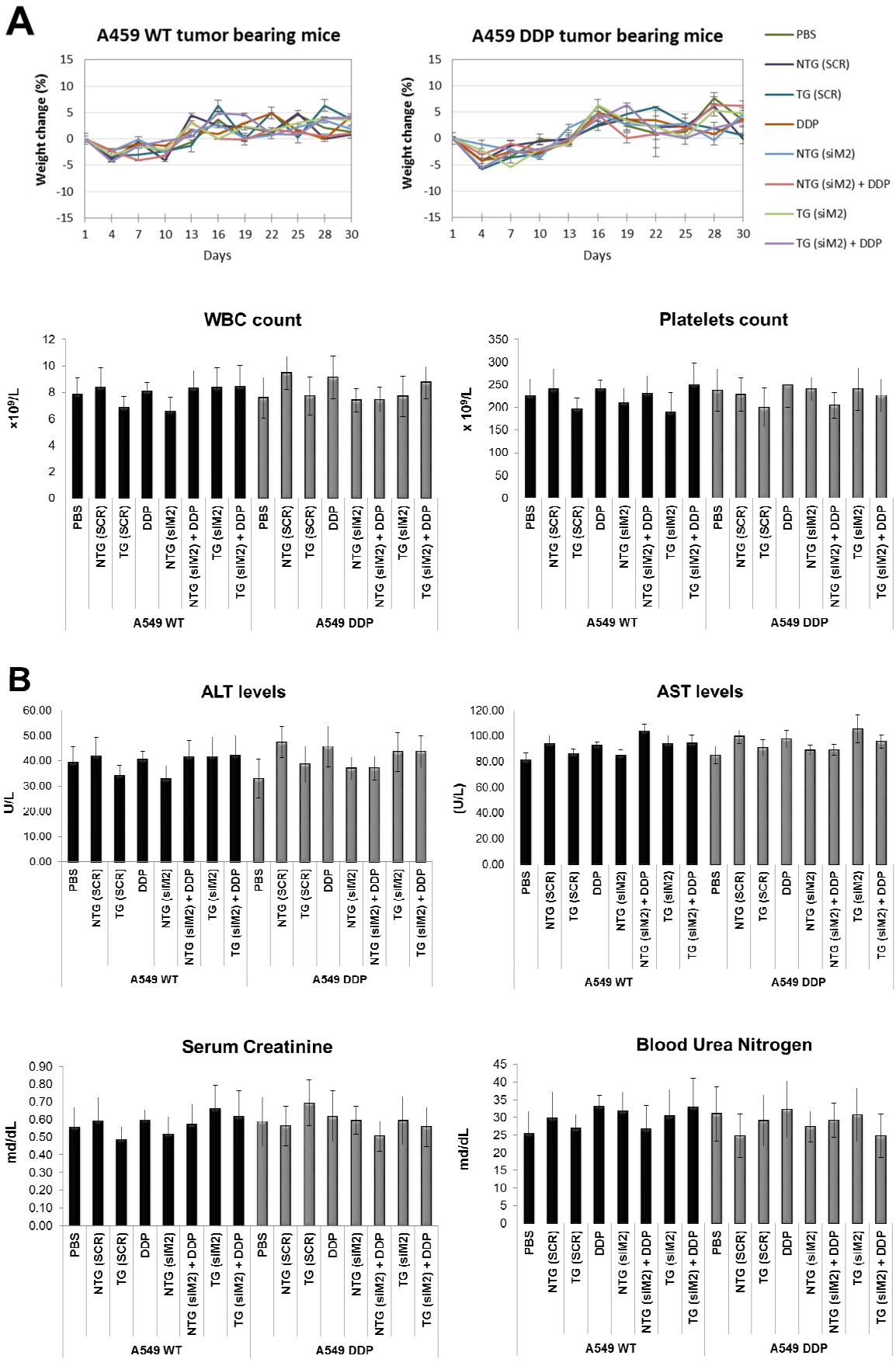

Figure 35: Safety profile. (A) Body weight variations mice from different treatment of A549 WT and A549 DDP tumor bearing mice. (B) Histograms that show the levels of several safety parameters in the different treatment

groups. The parameters tested were: the concentrations of the enzymes aspartate transaminase (AST) and alanine transaminase (ALT) that are reasonably sensitive indicators of liver damage; the number of white blood cells (WBC); the number of platelets; serum creatinine and blood urea nitrogen as indicators of kidney function.

In addition to the body weight, some serum safety markers were analyzed in order to evaluate the nanoparticles safety. As indicators of liver damage we measured the concentrations of the enzymes AST and ALT; serum creatinine and blood urea nitrogen were measured as indicators of kidney function; and the number of WBC number of platelets were also quantified. During the study period, there was no elevation in liver enzymes levels observed (Figure 35B). For both tumor models, AST and ALT levels on the treatment groups showed no significant differences from the control group (PBS-treated mice), indicating a lack of damage to the liver. Similar results were also obtained for the kidney function indicators. Serum creatinine and blood urea nitrogen were unchanged when compared to control group demonstrating kidney function did not seemed to be affected. Elevated WBC counts is often associated with tissue damage and a decrease in platelet counts are indicative of chemotherapy toxicity. WBC and platelets number were found to be consistent between the different experimental groups.

On end of the study, the liver, kidney and spleen of mice from each group, from both tumor models were collected and tissue sections were used for hematoxylin and eosin staining (Figure 36). For all the groups on both tumor models, the tissues did not show any pathological changes in the histology analysis which is in agreement with the serum safety markers previously analyzed. We were not expecting toxicity from cisplatin since the dose was very low compared to the clinical dose.

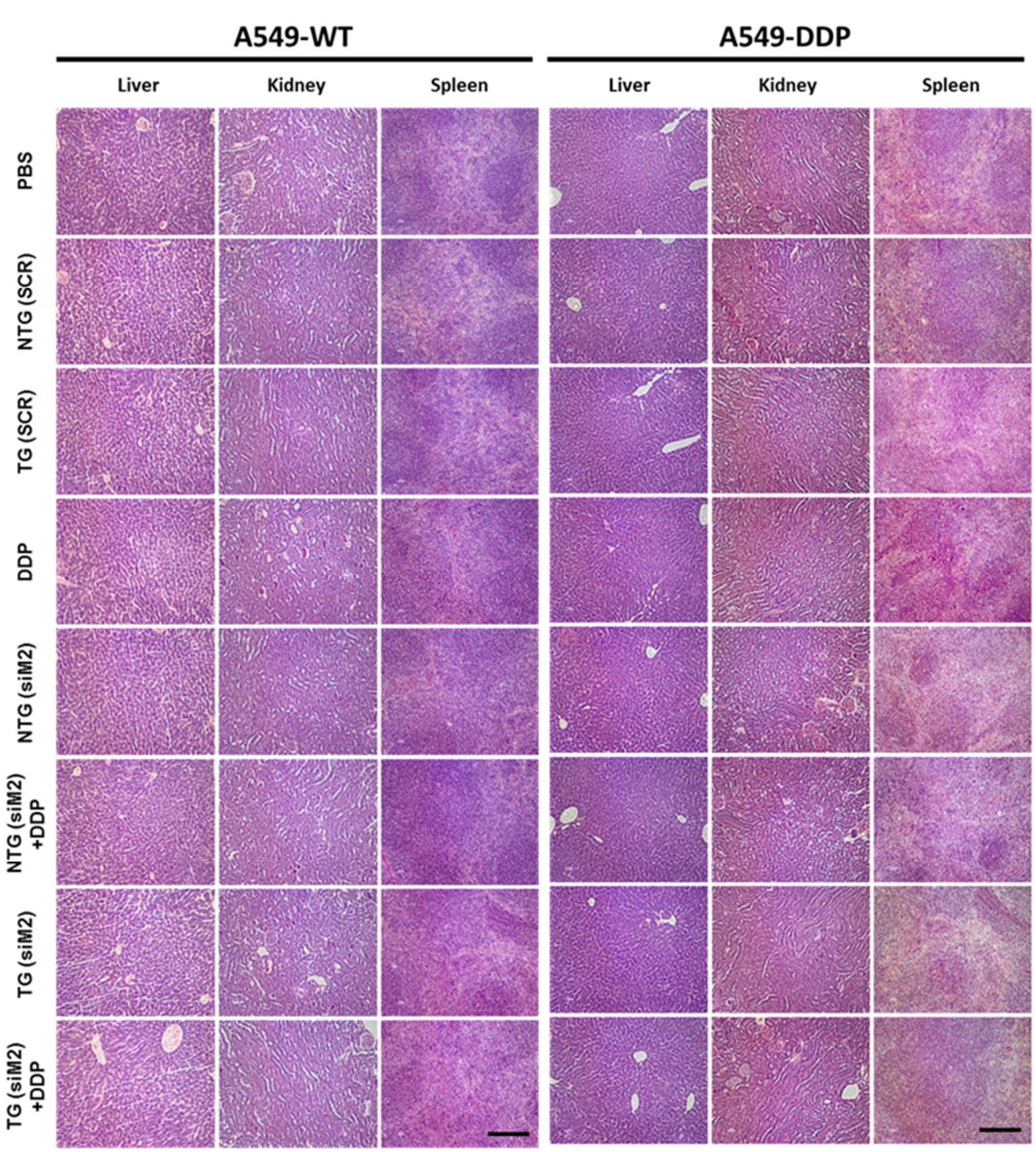

Figure 36: Histological sections after H&E staining of liver, kidney, and spleen from mice from different treatment of (A) A549 WT and (B) A549 DDP tumor bearing mice. Scale bar = 100 µm.

CONCLUSIONS

In summary, EGFR-targeted chitosan nanoparticles were employed as a new delivery carrier for Mad2 siRNA in combination with cisplatin to achieve maximal therapeutic efficacy by overcoming chemo-drug resistance in NCSLC. Both siRNA and cisplatin were used at low but effective doses minimizing adverse side effects. In this study, we evaluated two formulations that differ on the presence of a target moiety. The targeted delivery showed effective and improved tumor growth inhibition when compared to non-targeted and this effect was even more pronounced when used in combination with cisplatin. Also, Mad2

siRNA results in mitotic failure and extensive cell death but the advantage of such strategy is that it preferentially affects mitotic cells, so highly proliferative tumors will be the most affected. Collectively, our study validates an effective EGFR-targeted chitosan carrier for siRNA, together with a promising therapeutic target, Mad2 and also shows that siRNA can be an effective strategy in cancer therapy by itself or in combination with anticancer drugs to increase the therapeutic potential of these drugs.

We have previously reported the development of EGFR targeting CS-based nanoparticles for the delivery of Mad2 siRNA (347). Down-regulation of Mad2 expression by siMad2-loaded NTG and TG CS nanoparticles was observed in A549-WT and A549-DDP, with blank nanoparticles showing no toxicity **(**Figure 32**)**. Similar to our previous reports, TG nanoparticles lead to a stronger depletion attesting the advantage of the targeting strategy (347).

CHAPTER 6

Combinatorial-Designed EGFR-Targeted Chitosan Nanoparticles for Encapsulation and Delivery of Lipid-Modified Platinum Derivatives in Wild-Type and Resistant Non-Small-Cell Lung Cancer Cells

The information presented in this chapter was partially published in the following publications:

- Nascimento AV, Singh A, Bousbaa H, Ferreira D, Sarmento B, Amiji MM. Combinatorial-Designed Epidermal Growth Factor Receptor-Targeted Chitosan Nanoparticles for Encapsulation and Delivery of Lipid-Modified Platinum Derivatives in Wild-Type and Resistant Non-Small-Cell Lung Cancer Cells. Molecular pharmaceutics. 2015 Nov 17;12(12):4466-77.

1. INTRODUCTION

Cancer as a disease shows tremendous ability to adapt to the environment, evolve aggressively and metastasize to distant sites, making it a disease replete of complexity and heterogeneity (431). First-line therapies often fail, leading to the recurrence of drug resistant forms of the disease that are often unresponsive to conventional therapeutic approaches, thereby demanding a more ingenious and novel approach. Besides physical and molecular factors, complex cellular and extracellular matrix of the tumor microenvironment gravely impedes drug penetration to the cancer cells, affecting their activity. The abnormalities underlying the processes of oncogenesis, cell survival, apoptosis escape, metastasis and drug resistance are almost always multifactorial and rely on redundant mechanisms (432). Cancer therapy therefore has become a major challenge in modern medicine and development of novel therapeutic approaches to overcome these challenges is urgently required. An effective method to fight cancer resistance and improve treatment efficacy will be to inhibit multiple targets in a combination therapy regime. When compared to a single-agent therapy, this strategy will allow the chemotherapeutic drugs to be used in smaller doses, decrease their cytotoxic side effects and improve their therapeutic response (433). To this end, material science and nanoparticle based drug delivery approach has revolutionized the outlook and changed the whole paradigm of cancer therapeutics (433). Our improved understanding of materials property and ability to tailor them in order to impart them with desired chemical and physical characteristics has become a cornerstone for drug delivery.

The conventional nanoparticle based delivery approach has heavily relied on the properties of the host therapeutic molecules to choose the appropriate material to serve as the carrier system. The paradigm however severely limit the options available for vectors selection, and therefore, while there is a plethora of literature on application of polymeric, lipid and inorganic carriers for delivery of therapeutic molecules, more recent advances have focused on tailoring the properties of existing materials for such application. Combinatorial design, a concept classically and widely used in drug discovery, has been imported in to material design where the backbone of a material could be chemically modified to develop a library of novel derivatives that can be tailored to achieve the desired final delivery vector. The seminal contributions from Langer's lab introduced this concept to drug delivery and has been actively researched since to develop smart materials for cancer imaging, diagnostics and therapeutics (304, 314, 434). This approach is particularly powerful since it allows the use of simple chemistries and minimal use of organic solvent to generate new, biocompatible and biodegradable blocks with desired properties to develop delivery

systems capable of carrying combinations of therapeutic payloads such as the most conventional chemotherapeutic and molecular anti-cancer agents (e.g. DNA, siRNA and miRNA) (304, 314, 434). Each blocks in the delivery system confers a specific advantage such as improved circulation time, targeting mechanisms, enhance accumulation at the tumor site or versatility of payload (433, 435-437).

Among the various classes of polymers, polysaccharides stand out as an interesting choice of materials since they are natural polymers with high biocompatibility and biodegradability, low immunogenicity, widespread availability and low cost. CS, α(1-4)2-amino-2-deoxy-β-D glucan, has additional advantages such as pH sensitivity, mucoadhesiveness, relatively longer blood circulation times, successful evasion of reticuloendothelial system (RES) as well as a high positive charge density(278, 363, 438). Negatively charged nucleotides can therefore easily establish electrostatic interaction with positively charged CS and spontaneously form nano-size complexes (polyplexes). This feature has made chitosan a very attractive and safe alternative. As a gene delivery carrier, it can be controlled based on its properties such as degree of deacetylation, molecular weight, ionic strength of the solution and pH(268). Not surprisingly, CS has been widely used as nucleic acid carrier but it is less amenable for delivery of small chemotherapeutic agents. However, abundance of primary amine and hydroxyl groups on the CS backbone makes it an ideal candidate for developing combinatorially-designed library of derivatives through specific chemical modifications. There have been sporadic attempts to use CS as carrier of small molecules but a systematic approach for such delivery application is lacking (439-442).

In previous studies, CS modified with PEG and EGFR have proven to be an efficient delivery system for siRNA into lung cancer cells. In the present manuscript, we have developed a lipid chain derivative of CS as the third functional block that allows self-assembly of polymer to encapsulate hydrophobic small molecules (Figure 37). Different hydrophobic platinum derivatives, starting from cisplatin, have been used as a model system to develop a library of cytotoxic drugs that were mixed and matched and the resultant nanoparticles were investigated for their size, charge, drug encapsulating capability and subsequent cytotoxic effect on drug sensitive A549 and platinum resistant A549-DDP lung adenocarcinoma cells. Molecular characterizations of the cells reveal that the combinatorial-designed nanoparticles show efficient cell death by inducing apoptotic pathway. This body of work cements that application of a combinatorial approach to nanoparticle design can aid in developing a customizable small molecule delivery platform using CS, which is otherwise popularly used for nucleic acid therapeutics.

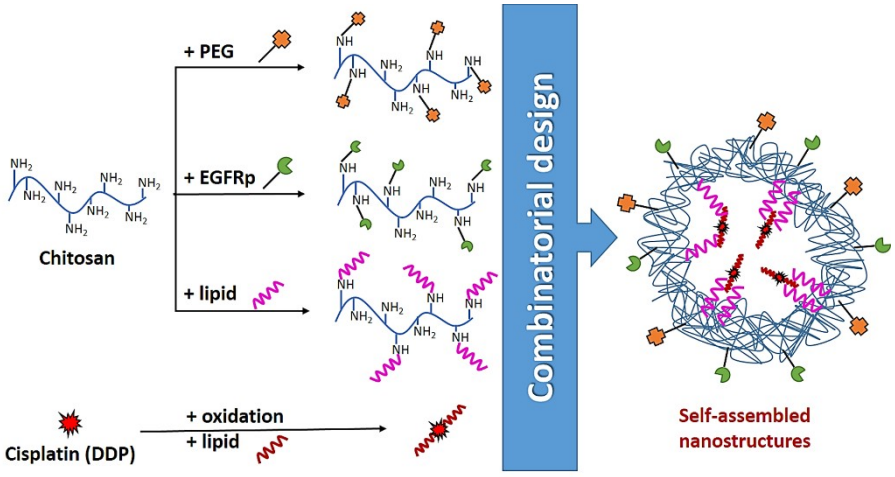

Figure 37: Schematic diagram

2. EXPERIMENTAL SECTION

2.1 Materials

CS was purchased from Sigma-Aldrich Inc. (St. Louis, MO), with average molecular weight of 50 kDa, and the degree of deacetylation between 75 and 85 %. Cis-Pt$(NH_3)_2Cl_2$ (cisplatin or DDP) was purchased from Sigma-Aldrich Inc. (St. Louis, MO). 1-Ethyl-3-[3-dimethylaminopropyl]carbodiimide hydrochloride (EDC), n-hydroxysuccinimide (NHS), succinimidyl-([N-maleimidopropionamido] ethylene glycol) ester (NHS-PEG2000-MAL), butanoic anhydride, hexanoic anhydride, octanoic anhydride, decanoic anhydride, tetradecanoic anhydride, octadecanoic anhydride, butanoic acid, hexanoic acid, octanoic acid and decanoic acid were purchased from Thermo Fisher Scientific (Waltham, MA). The EGFR-binding peptide used in this study was custom synthesized at peptide synthesis core facility of Tufts University (Boston, MA). This peptide (YHWYGYTPQWVI-), was originally synthesized by Li and co-workers and has been proven to be most efficient in targeting the EGFR receptor among several tested (311). Chitosanase (*Streptomyces*) and lysozyme were purchased from Sigma Aldrich (St. Louis, MO). 1H, 13C and 195 Pt NMR measurements were performed on a 400 MHz ^{1}H NMR spectroscopy (Varian, Inc. CA).

2.2 A549-WT and A549-DDP resistant NSCLC cell lines

Human NSCLC cell line A549 was obtained from ATCC (Manassas, VA) and the corresponding platinum resistant cell line A549-DDP, was obtained from Massachusetts General Hospital, Boston, MA. Both cell lines were subcultured at 37°C in 5% CO_2 environment in DMEM/F12 medium from Life Technologies (Carlsbad, CA) supplemented with 10% fetal bovine serum and 1% penicillin/streptomycin (100 U/mL) (Thermo Fisher Scientific, Waltham, MA). A549-DDP were cultured in medium supplemented with cisplatin

at a final concentration of 2 µg/mL, to maintain drug resistance. Three days before any experiment, A549-DDP media was changed to a media without cisplatin.

2.3 Synthesis and characterization of CS derivatives

CS was chemically modified with fatty acids by using a coupling agent, EDC, in the presence of NHS, to chemically conjugate the carboxylic group from the fatty acid to the CS free amine groups. Fatty acids with a general formula $CH_3(CH_2)_nCOOH$ were used to modified CS where *n* could be 2, 4, 6 and 8. Briefly, 0.62 µmol CS (MW: 50 kDa) was dissolved in 0.1 M MES, 0.9% sodium chloride, pH 4.7, and 0.18 mmol of fatty acid in 10 mL ethanol, respectively. Then, both solution were mixed and an aqueous solution of EDC was added into the mixture with continuous stirring. The 1:1 mole ratio of EDC to fatty acid was used in all synthesis procedures. After 24 h of reaction, the reaction mixture was dialyzed for another 24 h (molecular weight cutoff = 30 kDa) against a 10% ethanol solution with frequent exchange of fresh ethanol solution to remove side products. Finally, the reaction mixture was dialyzed against deionized water for 6 h to remove any residual solvent and the dialyzed product was lyophilized until further use. NMR analysis was performed to estimate the degree of substitution of lipids on the CS backbone.. IR spectra of the resulted products were measured to attest the chemical interaction between CS and the fatty acid chain using FTIR spectrophotometer ABB MB3000 (ABB, Switzerland).

CS-PEG derivative was independently synthesized as previously described (288). In summary, 15% molar equivalent of maleimide-poly (ethylene glycol)-N-hydroxysuccinimide (Mal-PEG_{2000}-NHS) was added to a 2 mg/mL solution of CS in 2% acetic acid and left to react overnight at room temperature under continuous stirring. Next day, excess of cysteine was added to block the reactive maleimide group and the solution was dialyzed (molecular weight cutoff= 10 kDa) against 5% acetic acid solution for 24 h. Finally, the dialyzed product was lyophilized and the CS-PEG derivative was obtained in powder form. The degree of substitution of PEG on chitosan was estimated by NMR analysis.

For synthesis of CS-PEG-EGFR peptide derivative, the CS-PEG-Mal derivative was reacted with EGFR-binding peptide to facilitate the conjugation of thiol group of terminal cysteine on the peptide with the maleimide group of PEG. A 2-molar excess of the EGFR-binding peptide was added to a 2mg/mL CS-PEG solution to saturate all the maleimide groups. The reaction was carried out at 4°C under nitrogen environment overnight. This peptide has been successfully used in our lab as a targeting moiety *in vitro* as well as *in vivo* (288, 314, 443). Upon completion of the reaction, excess of cysteine was added to react with any unreacted maleimide group and the solution was dialyzed (molecular weight cutoff= 10 kDa) against 5% acetic acid solution for 24h, followed by freeze-drying and stored at -20°C until

further use. NMR analysis was performed to evaluate the degree of substitution on chitosan. All NMR samples of CS were prepared by dissolving 2-4 mg of the lyophilized product in 0.7 mL of D_2O with 0.2% DCl and characterized by 400 MHz ^1H NMR spectroscopy (Varian, Inc. CA)

2.4 Synthesis and characterization of lipid-modified platinum derivatives

The synthesis of c,c,t-$Pt(NH_3)_2Cl_2(OH)_2$ was optimized from previous studies (444, 445). A mixture of cisplatin (6.67 mmol) and H_2O_2 (100.0 mmol) in 90 mL H_2O was heated to 80°C for 5 h in the dark with vigorous stirring following which, it was allowed to cool down to room temperature. The final product was concentrated to 10 mL with rotary evaporator and allowed to precipitate at 4°C overnight. The product was collected by vacuum filtration and washed with ice-cold water, ethanol, diethyl ether and vacuum dried until a bright yellow powder was obtained. An average yield of 83% was obtained.

Hydrophobic platinum (IV) derivatives have a general formula of c,c,t-$Pt(NH_3)_2Cl_2(OOC(CH_2)_nCH_3)_2$ and were obtained by covalently modifying c,c,t-$Pt(NH_3)_2Cl_2(OH)2$ with fatty acids anhydrides of varying carbon chain length (4, 6, 8, 10, 14 and 18). DMF was used to dissolve c,c,t-[$Pt(NH_3)_2Cl_2(OH)_2$] (2 mmol) and the solution was heated to 70 °C while stirring. The fatty acid anhydride (8 mmol) was added to the mixture and let to react while stirring at room temperature for 48 h. The above solution was concentrated to a volume of 20 mL and then poured into water. The light yellow precipitate was collected by centrifugation and dissolved in acetonitrile. The solvent was evaporated by rotary evaporation and the solid was washed several times with diethyl ether and dried. An average yield of 74% was usually obtained. LCMS measurements were performed on an LCMS-IT-TOF (Shimadzu Corporation, Columbia, MD) with quadrupole ion trap (QIT) and electrospray ionization (ESI). The lipid derivatives of DDP samples at a concentration of ~100 ppm/mL were prepared in methanol prior to injection onto the LC system coupled to IT-TOF and 50:50 methanol-water was used as the mobile phase. Nanoparticle tracking analysis was used to assess the self-assembled nanoparticle forming characteristics of the lipid modified DDP derivatives. The DDP derivatives were dispersed in water at a concentration of 10 mg/mL and were analyzed by NanoSight NS500 (Malvern Instruments, Westborough, MA). The samples were diluted to 30% by water during analysis.

2.5 Formulation and characterization of control and targeted nanoparticles

We assessed the ability of the CS derivatives (containing varying lipid content, PEG and EGFR) to form self-assembling nanosystems with hydrophobic platinum derivatives. In order to do so, the mass ratio between the platinum and the total amount of CS derivatives was kept as 1:3. The molar ratio between CS modified with fatty acids (CS-C_n), CS-PEG

and CS-EGFR was kept as 2:1:1. Before starting, all the derivatives were dissolved in a very small volume of DMF and finally, 20 times deionized water was added to allow self-assembly of the nanoparticles and cisplatin derivatives. The solution was mixed with a vortex mixer for 5 min and probe ultrasonicated for 15 minutes using Vibra-Cell VC 505 ultrasound instrument (Sonics and Materials, Inc., Newton). The nanoparticles were washed using Amicon ultracentrifugation filtration membranes with a molecular mass cutoff of 30 kDa, allowing any free cisplatin to be removed. Using a ZetaSizer Nano ZS (Malvern Instruments, Worcestershire, UK), we were able to obtain information related to particle size, surface charge and polydispersity index (PDI). Each sample was analyzed in triplicate at 25°C and the result reported as mean ± standard deviation.

The platinum content in the nanoparticles was measured using a high-performance liquid chromatography (HPLC) assay. Two independent methods were used for prodrug quantification; the indirect and the direct method and total calculated amount of drug was matched to theoretical amount by mass balance. In the indirect method the NANOPARTICLEs were centrifuged at 4000 rpm for 10 min and the free platinate were quantified in the supernatant by HPLC. In the direct method, CS went through an enzymatic digestion with chitosanase and lysozyme in order to disrupt the NANOPARTICLEs and release the prodrug. In order to do that, 100 µL of platinate loaded NANOPARTICLEs were incubated with 0.02 U chitosanase and 2 U lysozyme in 50 mM of NaAc-HOAc buffer (pH 5.5) for 4 h at 37°C. The solution was then centrifuged and the supernatant was used for cisplatin detection by an RP-HPLC method. The samples were diluted in a solution of 1:1 methanol/water containing 5% DMF prior to analysis. A Waters LC system (model 2487, Waters Corporation, Milford, MA) with a quaternary pump, an autosampler and a UV-detector was utilized on the analysis. A reverse phase C18 column (4.6 mm x 15 mm, 5mm, Hypersil Gold, US) with a C18 pre-column (4 mm x 20 mm, 5mm, Phenomenex, US) was used with a mobile phase consisting of 1:1 methanol/water at a flow rate of 0.5 mL/min and sample injection volume was 20 µL. A standard curve of each platinum derivative was generated with a linear range of detection between 10-250 µg/µl and the elution was monitored at 260 nm. Blank CS NANOPARTICLEs were also subjected to the same treatment and used as control. Encapsulation efficiency was calculated using the formula: Encapsulation efficiency (EE %) = (Wt-Wf)/Wt ×100 where Wt is the total amount of drug used during preparation and Wf is the amount of free drug.

Transmission electron microscopy (TEM) analysis was performed to visualize the morphology of the platinum loaded CS nanoparticles. 20 µl of the sample were drop-coated on to a Formvar-coated copper grids (Electron Microscopy Science, Hatfield, PA) and allowed to stand for 1 min. The excess fluid was gently removed using a Whatman filter

paper and the sample was negatively stained with 1.5% uranyl acetate for 1 min, excess stain was removed using a Whatman filter paper and the sample was allowed to air-dry prior to imaging. The nanoparticles were finally visualized under a JEOL 100-X transmission electron microscope (Peabody, MA) operating at an accelerating voltage of 80 kV.

2.6 Analysis of cell-kill in wild-type and resistant NSCLC cells

A549-WTand A549-DDP resistant NSCLC cells were seeded in 96-well plates at a concentration of 3,000 cells/well and allowed to adhere overnight. Next day, the media was removed from the wells and different nanoparticle formulation was added in 100 µl of fresh media. The cells were incubated for 6 h at 37 °C followed by replacement of the solution with complete growth medium. The cytotoxic activity of formulations was evaluated after 48 h by renewing the medium with fresh complete medium containing 100 µL of 0.5 mg/mL (3-(4, 5-dimethylthiazol-2-yl)-2,5-diphenyltetrazolium bromide) MTT (Sigma-Aldrich, St. Louis, MO). After 2 h of incubation at 37 °C, the medium was discarded and 200 µl of dimethyl sulfoxide (DMSO) was added to each well to dissolve the formazan crystals. The absorbance of the colored solution was measured at 560 nm the IC_{50} calculated using GraphPad Prism® software. All treatments were performed for n=8.

2.7 Cellular apoptotic response

A549-WTand A549-DDP resistant were seeded in 6-well plates at a density of 0.2 x 10^6 cells per well and incubated overnight at standard conditions (37°C in 5% CO_2 environment). Next day, different formulations were added to the media for 6h of incubation after which, the media was removed, the cells were washed twice with warm PBS and fresh media was added. After different time periods, total cellular RNA was isolated using the PureLink RNA Mini Kit (Ambion, Austin, TX). cDNA synthesis and the reverse transcription reaction was performed on 500 ng of total RNA from each sample with Verso cDNA Synthesis kit (Thermo Scientific, Tewksbury, MA) according to the manufacturer's instructions. The LightCycler 480 SYBR Green I Master kit (Roche, Basel, Switzerland) was used for Real time polymerase chain reaction (qPCR). Regarding the primer sequences, the housekeeping gene glyceraldehyde 3-phosphate dehydrogenase (GAPDH) was used as endogenous control and the sequences used were: forward (ACAGTCAGCCGCATCTTC) and reverse (GCCCAATACGACCAAATCC). Caspase 3 primer sequences were: forward (GTTTGTGTGCTTCTGAGCC) and reverse (CACTGTCTGTCTCAATGCC). qPCR steps included a pre-incubation step for 5 min at 95 °C, followed by 40 cycles of three steps: 10 sec at 95 °C, 20 sec at 60 °C and 30 sec at 72 °C. All samples were normalized to the relative levels of GAPDH, and results are expressed as the folds increase of levels of caspase-3 relative to non-treated cells.

Apoptosis detection using annexin V-FITC apoptosis detection kit I (BD Biosciences, San Jose, CA) was performed in order to evaluate the effect of the DDP derivatives, both in solution and encapsulated in nanoparticles, at their IC_{50} concentrations. A549-WTand A549-DDP resistant cells (0.2 x 10^6 cells per well) were seeded in 6-well plates and incubated overnight at 37 °C in 5% CO_2 environment. Different formulations were seeded into the respective wells and after 6 h of incubation, the media was removed, the cells washed twice with warmed PBS, and fresh media added. Blank CS nanoparticles served as negative control for the experiment. Cells were incubated for 24 h, trypsinized, centrifuged and washed twice with PBS and were stained with annexin V-FITC and propidium iodide as per manufacturer's protocol. The stained sample were analyzed by flow cytometry (BD Biosciences, San Jose, CA).

Apoptotic cell death induced after incubation with parent cisplatin and various lipid-modified platinum derivatives was examined by microscopic observation of inter-nucleosomal fragmentation. In order to do so, we used DeadEnd™ Fluorometric TUNEL (Promega Co., Madison, WI, USA). A549-WTand A549-DDP resistant NSCLC were seeded (10,000 cells/chamber) in a Falcon Lab-Tek 4-grid chamber and after 24 h, the media was removed and 0.6 mL of nanoparticle formulation at its corresponding IC_{50} was dissolved in media and added to the chamber. Following incubation at 37°C for 6 h, the solution was removed, the cells washed with PBS and new complete cell culture media added. After 24 h since nanoparticle treatment, the media was removed, cells were washed three times with 0.6 mL of cold PBS and fixed in 0.4 mL of a 3.7% formalin. Manufacturer instructions were followed for the remaining steps. Microscopy images were acquired using an LSM 700 confocal microscope (Carl Zeiss, Gottingen, Germany) equipped with 40X and 63X objectives. The 520 and 405 nm lasers were used for the observation of fluorescein and DAPI, respectively.

2.8 Data analysis

Statistical analyses were performed using GraphPad Prism software (San Diego, CA). Paired comparisons were performed by Student's ***t***-test. A p value of 0.05 was considered to be statistically significant. Data presented are means ± standard deviation.

3. RESULTS AND DISCUSSION

3.1 Characterization of the CS derivatives

Control (non-targeted) CS nanoparticles were self-assembled using lipid and PEG derivatives of CS (1:1 mole ratio) while the EGFR targeted CS nanoparticles were self-assembled using lipid, PEG and PEG-EGFR peptide derivatives of CS (1:1:1 mole ratio). Each derivative was characterized for its functional modification by ^{1}H-NMR. Fatty acids

saturated chains with different number of carbons were tested (n = 4, 6, 8 and 10) in order to evaluate its influence on self-assembly, nanoparticle size, charge and encapsulation efficiency. The two blocks, CS-PEG and CS-EGFR were used to impart a hydrophilic characteristic to the system simultaneously harvest their other impressive features (288). PEG is known to confer long-circulating properties and preferential tumor targeting by means of the EPR effect and the EGFR peptide has shown to enhance the targeting effect in EGFR-overexpressing cells such as NCSLC (288, 290, 446).

In order to improve the encapsulation of hydrophobic compounds, the third block of hydrophobized CS was introduced in to the nanoparticle system and different chain lengths tested. The library of lipid modified CS was characterized by ^{1}H-NMR spectroscopy to estimate the grafting of the different fatty acids onto the chitosan backbone (Figure 38).

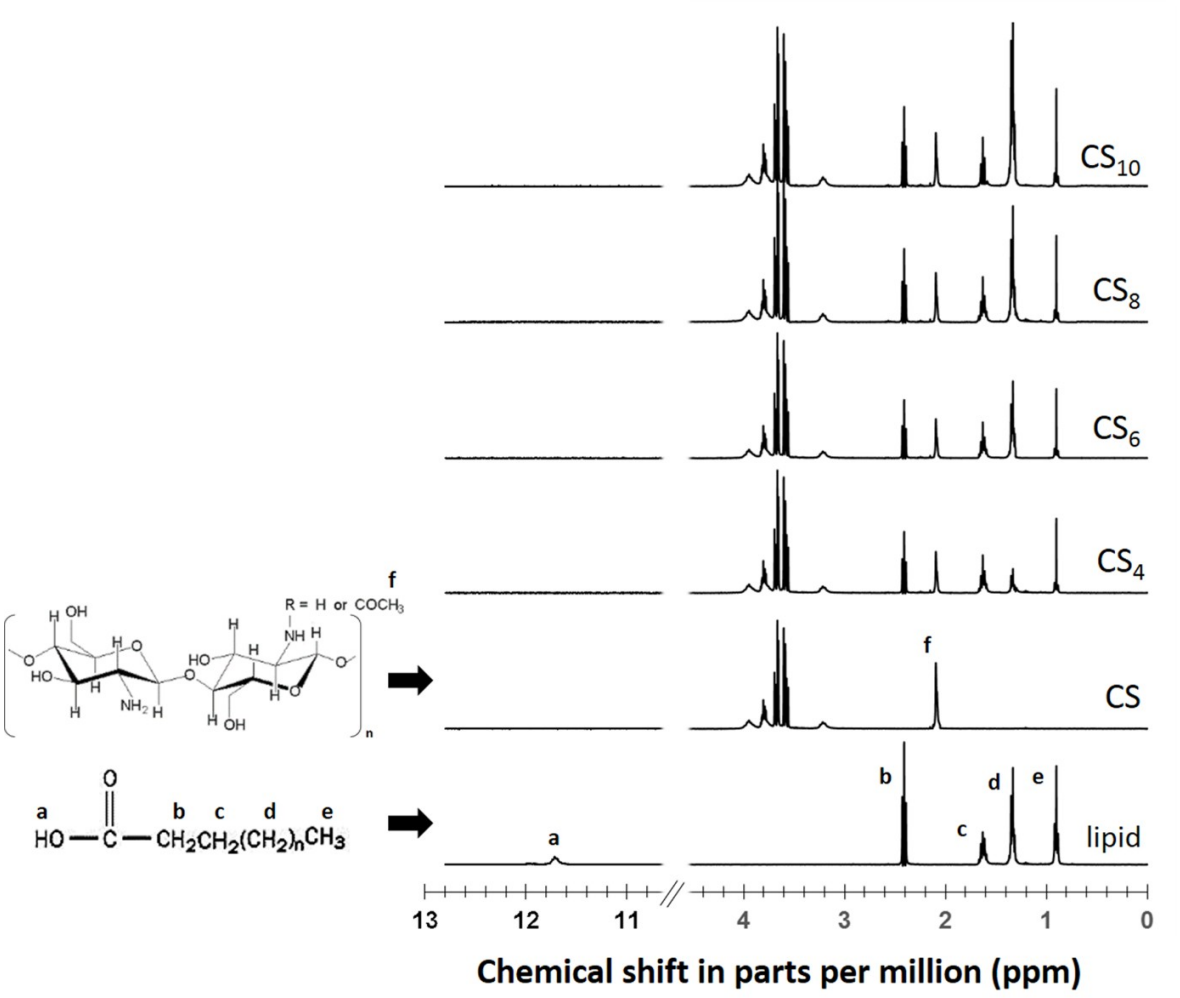

Figure 38: 1H-NMR spectrum for the CS derivatives (CS4, CS6, CS8, CS10) obtained by the modification of chitosan (CS) with lipids with different carbon chain lengths. All 1H spectra were obtained in D2O with 0.2% DCl, 400 MHz.

The proton peak corresponding to -CH_3 group of the fatty acids was present between 0.85-0.90 ppm and was used as the signature peak for lipid modification while the acetyl group

protons of CS with a peak around 2 ppm were considered the signature peak for all calculations. All the four lipid derivatives of CS had nearly similar modifications; CS modified with butanoic, hexanoic, octanoic and decanoic acids showed 56, 53, 48 and 45 % modification. The IR spectra from these CS derivatives also confirmed the signature vibrational stretches from the lipid molecules. The CS spectra showed the characteristic peaks for primary amine I and II bending at 1652 cm^{-1} and 1588 cm^{-1} respectively. The N-H stretching vibrational peak that usually appears between 3200-3600 cm^{-1} could not be discerned due to a strong O-H stretching peak in the region. However, the spectra of lipid modified CS derivatives showed a very strong signature peaks from amide I and II observed at 1652 cm^{-1} and 1560 cm^{-1}, suggesting formation of new amide peaks during lipid conjugation. More conclusively, the strong amide C=O stretching peak at 1714 cm^{-1} in the conjugate was completely absent in CS, confirming the lipid conjugation on the CS backbone by amide linkage. The detailed assignment of different peaks has been included in the supporting information (Figure 39).

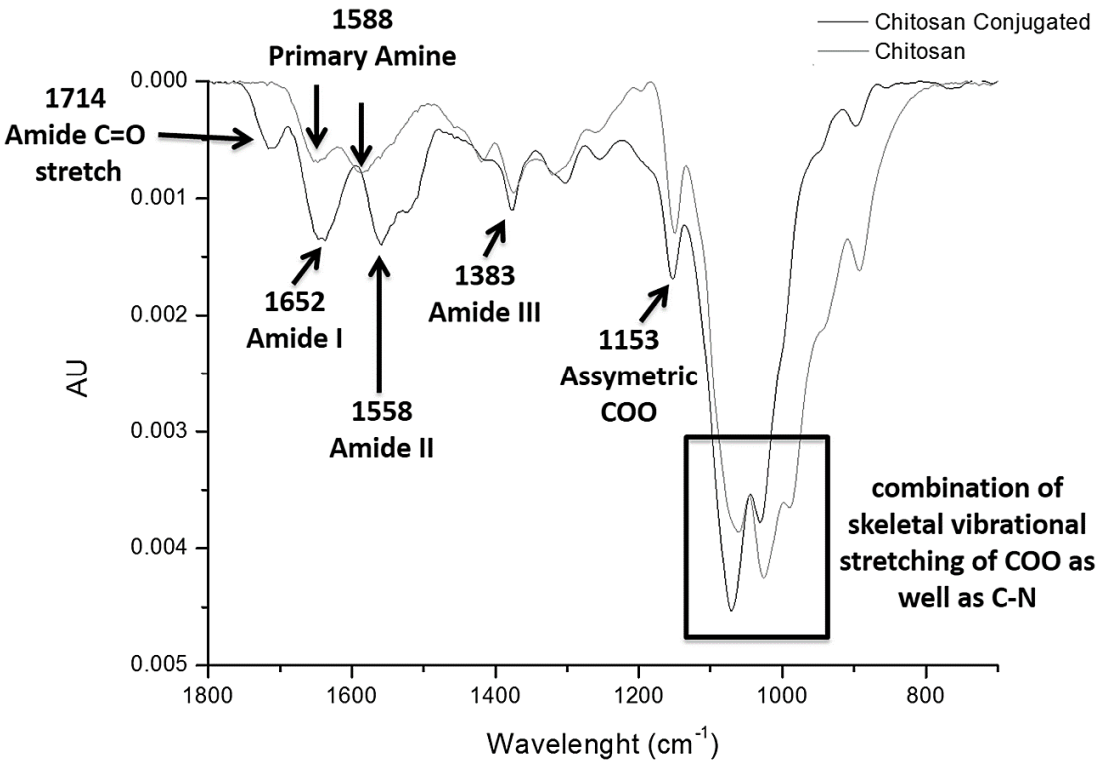

Figure 39: FTIR spectra of CS and CS6: The light (CS) and dark (conjugated CS) gray lines correspond to the FTIR spectra of CS before and after conjugation with C6 lipid chain through primary amine conjugation. The arrows correspond to the various bond stretches identified.

3.2 Characterization of the platinum derivatives

The parent drug cisplatin was also modified with lipid chain of lengths varying from 4 to 18 (4, 6, 8, 10, 14 and 18) to impart hydrophobicity and subsequently incorporate them in the lipid modified CS CS nanoparticles by virtue of hydrophobic interaction with lipid modified CS. All the six cisplatin prodrugs were characterized by 1H NMR, 13C NMR, 195PT NMR and LCMS-IT-TOF in order to verify the structural modifications. Similar results were obtained for all and the representative spectra are presented. All the ^{1}H NMR spectra (Figure 40) contained a broad singlet peak at approximately 6.57 ppm consistent with platinum amine proton.

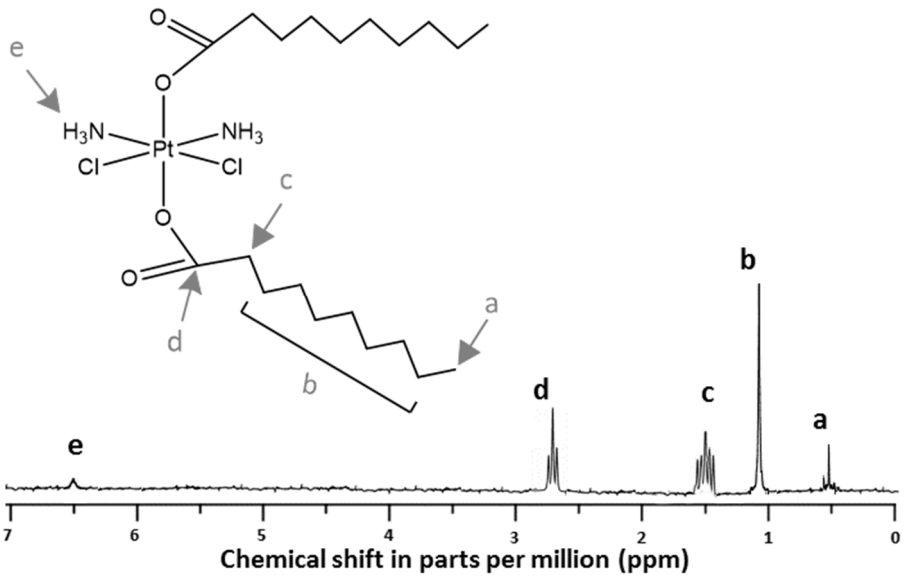

Figure 40: ^{1}H NMR spectrum (DMSO-d_6) for cisplatin derivative DDP_{10}.

The presence of characteristic peaks for methylene protons at 1.237 ppm substantiated the successful synthesis of cisplatin prodrug. The ratio between the integration values for the methylene protons and the amine protons indicated the presence of two lipidic ligands per platinum center. Despite nearly overlapping signals, the ^{13}C NMR spectra (Figure 41) displayed resolved peaks for the expected number of carbon atoms. The ^{195}Pt NMR resonance (Figure 42) exhibited a single peak at 1250.5 ppm consistent with other platinum (IV)(447, 448). The mass spectrum for individual DDP derivatives further confirms the presence of molecular weights corresponding to double substitution of the lipid ligand per platinum center. The DDP_{10} derivative shows a mass of 676.802 corresponding to the chlorine adduct [M-1+Cl] of the expected mass of the double lipid substituted DDP (Figure 43). Lipid modification of cisplatin was efficiently achieved by conjugation of fatty anhydrides with varying alkyl chains lengths into the coordination sphere of a cis,cis,trans-$[Pt(NH_3)_2Cl_2L_2]$, platinum(IV) complex, where L represents a hydrophobic axial ligands.

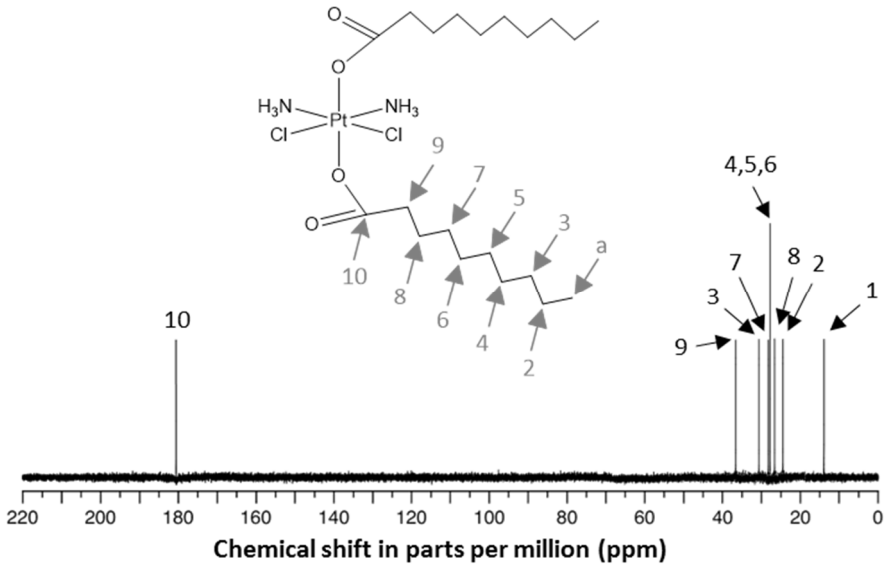

Figure 41: ^{13}C NMR spectrum (DMSO-d_6) for cisplatin derivative DDP_{10}.

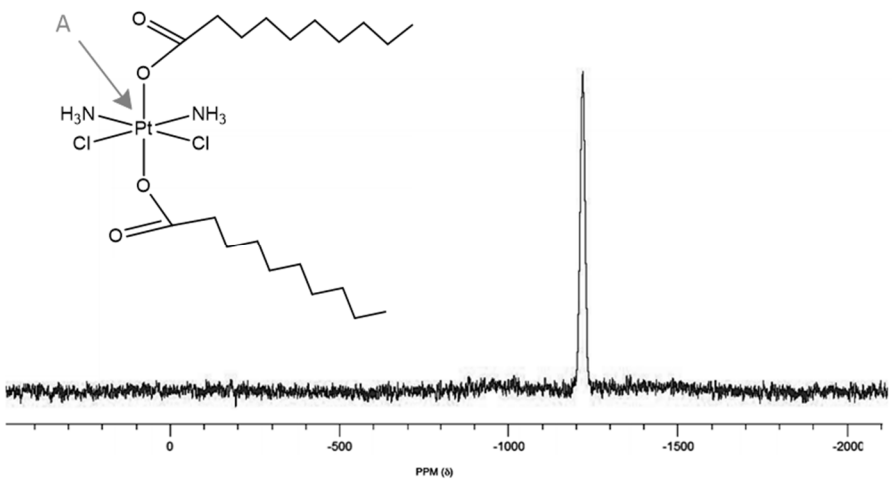

Figure 42: ^{195}Pt NMR spectrum (DMSO-d_6) for cisplatin derivative DDP_{10}.

3.3 Characterization of the platinum encapsulated chitosan nanoparticles

The graphical abstract shows the general scheme of synthesis of different lipid CS and platinum derivatives and their mix and match with PEG and PEG-EGFR derivative of CS to combinatorially design drug-encapsulated nanoparticles. In aqueous environment, the lipid-modified CS could easily self-assemble to form micelles and the micelle core can non-specifically entrap lipophilic drugs through hydrophobic interactions. To better evaluate the nanoparticle self-assembly and drug encapsulation characteristic, the 4 chitosan derivatives and six platinum derivatives were used to produce a library of twenty-four drug loaded nanoparticles along with 6 self-assembled nanoparticle formulations of lipid modified platinum derivatives.

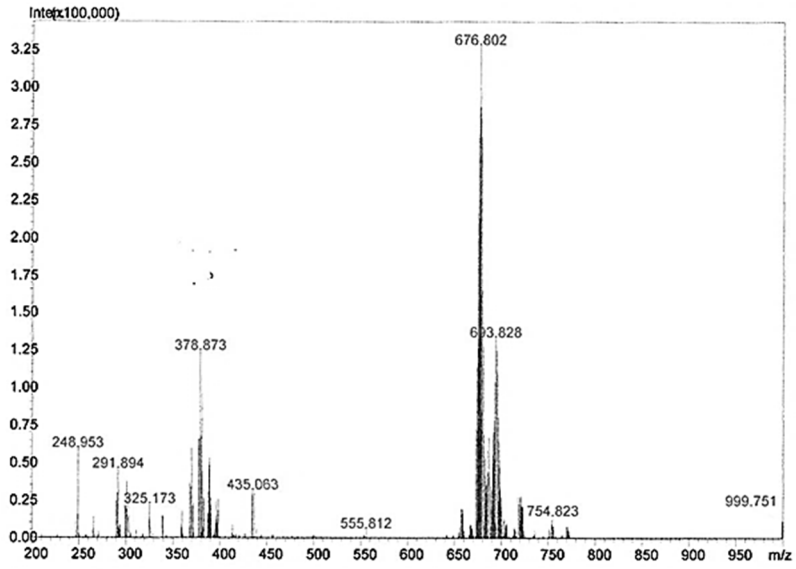

Figure 43: Mass spectrum of the DDP_{10} derivative. The LCMS-IT-TOF analysis of DDP_{10} derivative in negative mode shows the peak at 676.802 corresponding to the chlorine adduct [M-1+Cl] of the derivative with expected mass of a double C_{10} lipid substituted DDP.

Presence or absence of the EGFR-CS derivatives therefore gives a library of 24 non-targeted and 24 EGFR-targeted CS nanoparticles that could be evaluated for their anti-cancer properties. This combinatorial approach towards designing the drug candidate and the delivery platform to produce a "*mixed and matched library*" of nanoparticles, enabling us to perform rigorous study of the effect of hydrophobic interactions on the physical properties of the nanoparticles, their self-assembling behavior and their drug delivery efficacy. The effect of the lipid chain present both on the CS backbone and on encapsulation of platinum derivatives was initially studied for the hydrodynamic diameter and polydispersity index of the nanoparticles, their zeta potential and their drug encapsulation capability (Table 10).

Nanoparticle tracking analysis confirmed that the lipid-derived DDP could self-assemble to form nanoparticles in an aqueous environment (Figure 44). The average particle sizes of the different formulations varied from 220 to 365 nm, with the exception of nanoparticles obtained from two combinations: cisplatin modified with fourteen (DDP_{14}) and eighteen (DDP_{18}) carbon lipid chains encapsulated with CS modified with octanoic acid (CS_4), designated by CS_4-DDP_{14} and CS_4-DDP_{18}, respectively. These two formulations gave values much lower than the rest, and we believe that the drug could not be successfully encapsulated in these nanoparticles due to the weak hydrophobic interaction between the short lipid chain on the CS backbone and the long lipid chain on the DDP. These two formulations also show a very low drug encapsulation efficiency (CS_4-DDP_{14} = 36% and CS_4-DDP_{18} = 22%) compared to the other formulations (Table 10D), which corroborates with our theory.

Table 10: Physical Characterization of Combinatorial-Designed Control and Epidermal Growth Factor Receptor-Targeted Chitosan Nanoparticlesa

				Platinum Derivatives					
A	Size (nm) ± SD		No DDP	DDP_4	DDP_6	DDP_8	DDP_{10}	DDP_{14}	DDP_{18}
	No CS		-	125.5 ± 18.2	142.4 ± 15.1	117.5 ± 17.6	177.8 ± 14.9	132.3 ± 12.8	165.4 ± 15.4
CS NPS	Fatty acids chain length	CS_4	322.3 ± 28.3	364.0 ± 16.2	360.0 ± 14.2	365.0 ± 15.2	354.0 ± 13.5	100.9 ± 13.1	90.2 ± 16.4
		CS_6	531 ± 45.2	222.0 ± 17.9	327.0 ± 16.8	227.8 ± 15.7	252.0 ± 16.1	331.0 ± 16.1	335.0 ± 10.0
		CS_8	378.5 ± 28.2	336.0 ± 19.0	213.0 ± 14.3	229.0 ± 13.5	243.0 ± 12.0	261.0 ± 9.9	272.0 ± 11.7
		CS_{10}	364.7 ± 28.1	242.0 ± 17.5	282.0 ± 15.0	321.0 ± 13.6	347.0 ± 12.7	353.0 ± 7.9	365.0 ± 7.3
				Platinum Derivatives					
B	Polydispersity Index ± SD		No DDP	DDP_4	DDP_6	DDP_8	DDP_{10}	DDP_{14}	DDP_{18}
	No CS		-	0.267 ± 0.011	0.263 ± 0.012	0.269 ± 0.076	0.299 ± 0.029	0.240 ± 0.028	0.255 ± 0.025
CS NPS	Fatty acids chain length	CS_4	0.632 ± 0.073	0.582 ± 0.023	0.596 ± 0.052	0.587 ± 0.022	0.609 ± 0.015	0.761 ± 0.025	0.768 ± 0.026
		CS_6	0.530 ± 0.048	0.589 ± 0.079	0.565 ± 0.038	0.605 ± 0.027	0.627 ± 0.032	0.556 ± 0.021	0.468 ± 0.020
		CS_8	0.560 ± 0.047	0.564 ± 0.010	0.606 ± 0.023	0.657 ± 0.015	0.583 ± 0.010	0.573 ± 0.09	0.482 ± 0.027
		CS_{10}	0.622 ± 0.068	0.340 ± 0.012	0.354 ± 0.014	0.592 ± 0.030	0.514 ± 0.227	0.638 ± 0.079	0.565 ± 0.073
				Platinum Derivatives					
C	Zeta-potential (mV) ± SD		No DDP	DDP_4	DDP_6	DDP_8	DDP_{10}	DDP_{14}	DDP_{18}
	No CS		-	46.2 ± 1.3	38.2 ± 1.8	40.2 ± 5.4	43.5 ± 1.5	44.2 ± 5.3	43.3 ± 1.1
CS NPS	Fatty acids chain length	CS_4	32.1 ± 3.5	28.1 ± 3.3	30.2 ± 1.8	30.8 ± 1.4	32.8 ± 3.7	34.8 ± 1.6	35.6 ± 1.2
		CS_6	34.2 ± 2.5	28.9 ± 2.3	31.1 ± 1.3	32.7 ± 1.2	33.8 ± 2.3	35.8 ± 1.3	36.7 ± 2.3
		CS_8	33.7 ± 2.8	29.8 ± 1.2	32.0 ± 2.5	32.7 ± 1.4	34.8 ± 1.5	36.9 ± 2.4	37.8 ± 1.7
		CS_{10}	36.1 ± 2.3	30.6 ± 1.4	31.4 ± 2.3	32.8 ± 1.5	33.5 ± 2.3	35.0 ± 4.3	36.0 ± 1.4
				Platinum Derivatives					
D	Encapsulation Efficiency (%) ± SD		DDP_4	DDP_6	DDP_8	DDP_{10}	DDP_{14}	DDP_{18}	
CS NPS	Fatty acids chain length	CS_4	68.8 ± 3.4	72.9 ± 5.3	79.6 ± 3.2	84.2 ± 4.4	36.2 ± 4.1	22.1 ± 2.1	
		CS_6	75.7 ± 3.2	76.1 ± 6.2	86.2 ± 5.4	88.4 ± 2.3	89.4 ± 5.1	85.2 ± 3.8	
		CS_8	86.1 ± 7.3	90.2 ± 2.2	89.5 ± 2.7	89.4 ± 4.5	95.8 ± 3.2	64.4 ± 2.3	
		CS_{10}	58.9 ± 6.7	66.6 ± 0.9.3	65.4 ± 5.7	72.2 ± 4.2	83.2 ± 1.1	45.2 ± 2.2	

The library of 24 nanoparticles were characterized for the particle size (A), polydispersity Index (B), zeta-potential (C) and cisplatin encapsulation efficiency (D) variations. All particles had also chitosan-PEG and chitosan-PEG-EGFR conjugates in their constitution together with the CS modified with fatty acids. All nanoparticles were synthesized with 1:1:1 molar ratio of lipid, PEG and EGFR derivative of CS. Encapsulation efficiency was evaluated by HPLC by a direct method.

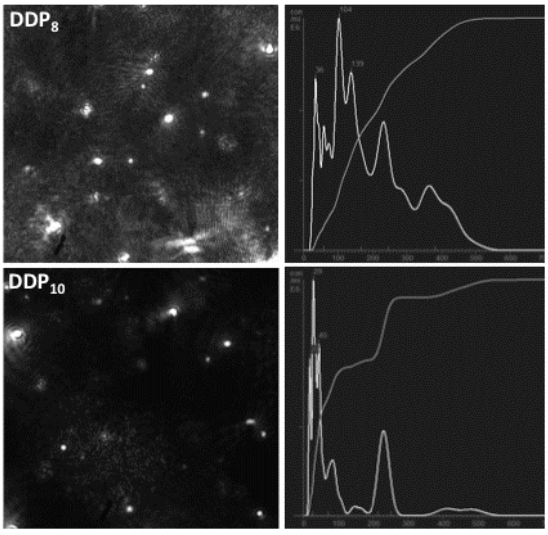

Figure 44: Nanosight DLS measurement of the DDP_8 and DDP_{10} nanoparticles. The DDP_8 (top panel) and DDP_{10} (bottom panel) derivatives were suspended in water to allow the self-assembly, forming nanoparticles. The measurement shows the morphology of the particles (left) and their size distribution (right). The average particle size for the DDP_8 and DDP_{10} nanoparticles was 130 and 185 nm, consistent with the previously measured values.

In the optimization step, the same results of encapsulation efficiency were obtained for several formulations by the indirect and direct methods. Since the direct method is known

to give a more realistic result, we decided to use the direct method for all of our samples for any further analysis. Table 11 gives the retention times of different lipid derivatives of cisplatin. An increase in the retention time of the derivatives as a function of the increasing chain length of the lipid was expected due to increased interaction of the platinum derivatives with the reverse phase C18 column. A standard curve was generated for each derivative to assess the drug encapsulation efficiency of the corresponding nanoparticle. HPLC chromatograms used to determine pro-drug encapsulation efficiency have been provided in the supporting information (Figure 45). Since the nanoparticles are disrupted and there is separation of the CS derivatives from the DDP palatinate derivatives, it makes us possible to use HPLC as technique to quantify the drug encapsulation efficiency at the 260 nm wavelength. The HPLC method is simple, direct, good linear, sensitive, accurate and robust for the quality analysis of cisplatin that is pertinent to this study.

Table 11: Retention Times of Cisplatin and Lipid-Modified Platinum Derivatives

Compound	Retention time (min)
DDP	5.70
DDP_4	7.82
DDP_6	8.11
DDP_8	8.64
DDP_{10}	9.70
DDP_{14}	15.72
DDP_{18}	28.76

Among the 24 formulations, the ones containing DDP_4 and DDP_6 showed lower encapsulation efficiency and larger hydrodynamic diameter sizes with greater variability in the physical properties. This could be probably due to weaker hydrophobic interaction between the smaller lipid chains of CS and cisplatin, therefore affecting the self-assembly of the lipid derivatives and forming less compact nanoparticles. These nanoparticle formulations were therefore eliminated from the further evaluations.

3.4. In vitro cell-kill efficacy in wild-type and resistant NSCLC cells

The remaining 16 self-assembled nanoparticles formulations were evaluated for the *in vitro* activity of the encapsulated drug in A549-WT and A549-DDP resistant cells (Table 12) and the results were compared with the derivatives in solution as well as unmodified cisplatin. The parent cisplatin showed an IC_{50} of 12.24 μM in A549-WTand 140.73 μM in A549-DDP resistant cells, confirming the drug resistant phenotype of A549-DDP cells. The DDP_8 and

DDP_{10} derivatives improved the potency of the encapsulated drug and decreased the IC_{50} in both the cell lines. However, the same effect was not observed with DDP_{14} and DDP_{18} where the IC_{50} value increased to 35.8 ± 5.2 μM and 198.3 ± 27.7 μM, respectively in A549-WTand 453.2 ± 65.4 μM and 954.0 ± 123.5 μM, respectively, in A549-DDP resistant cells.

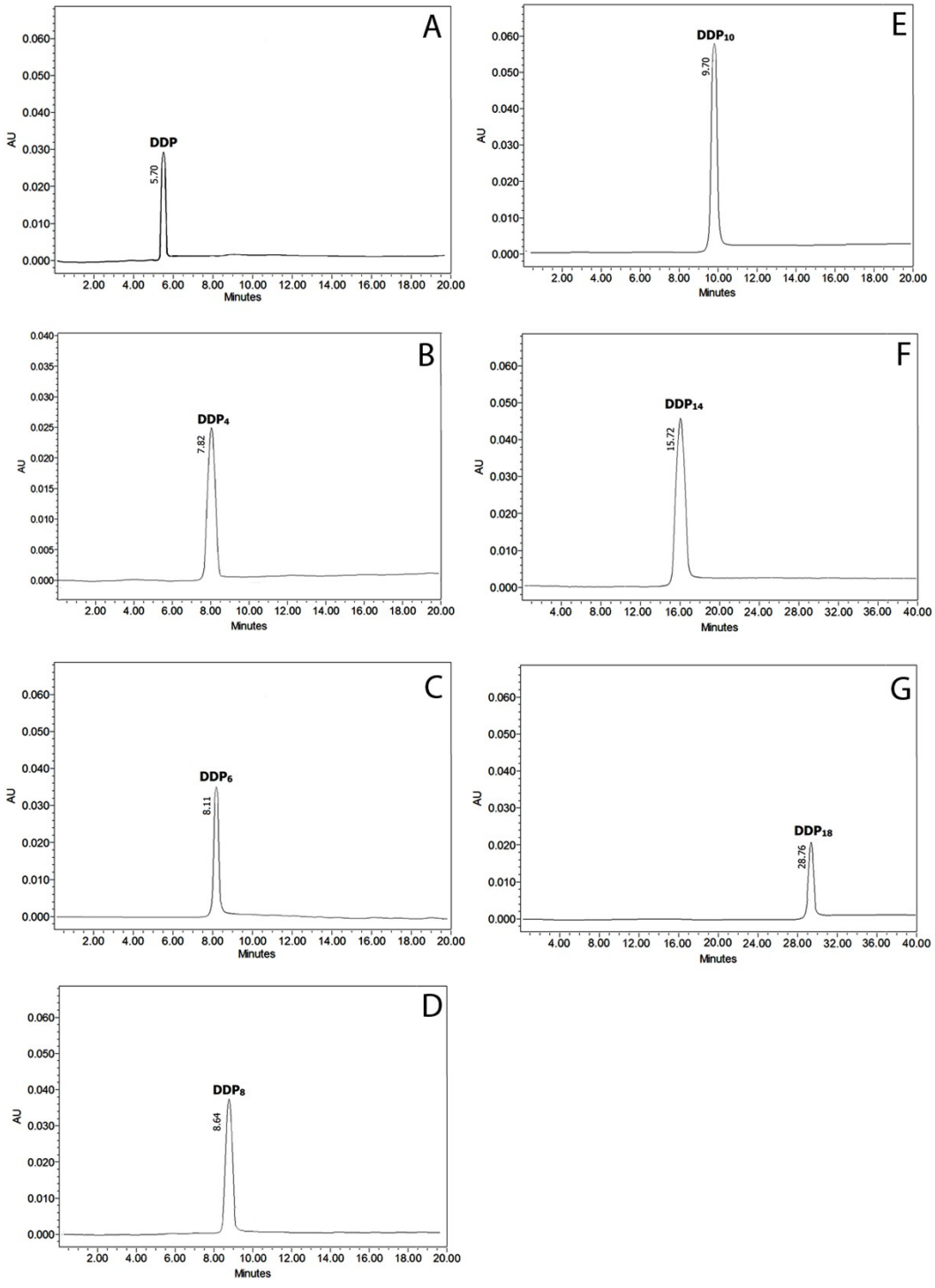

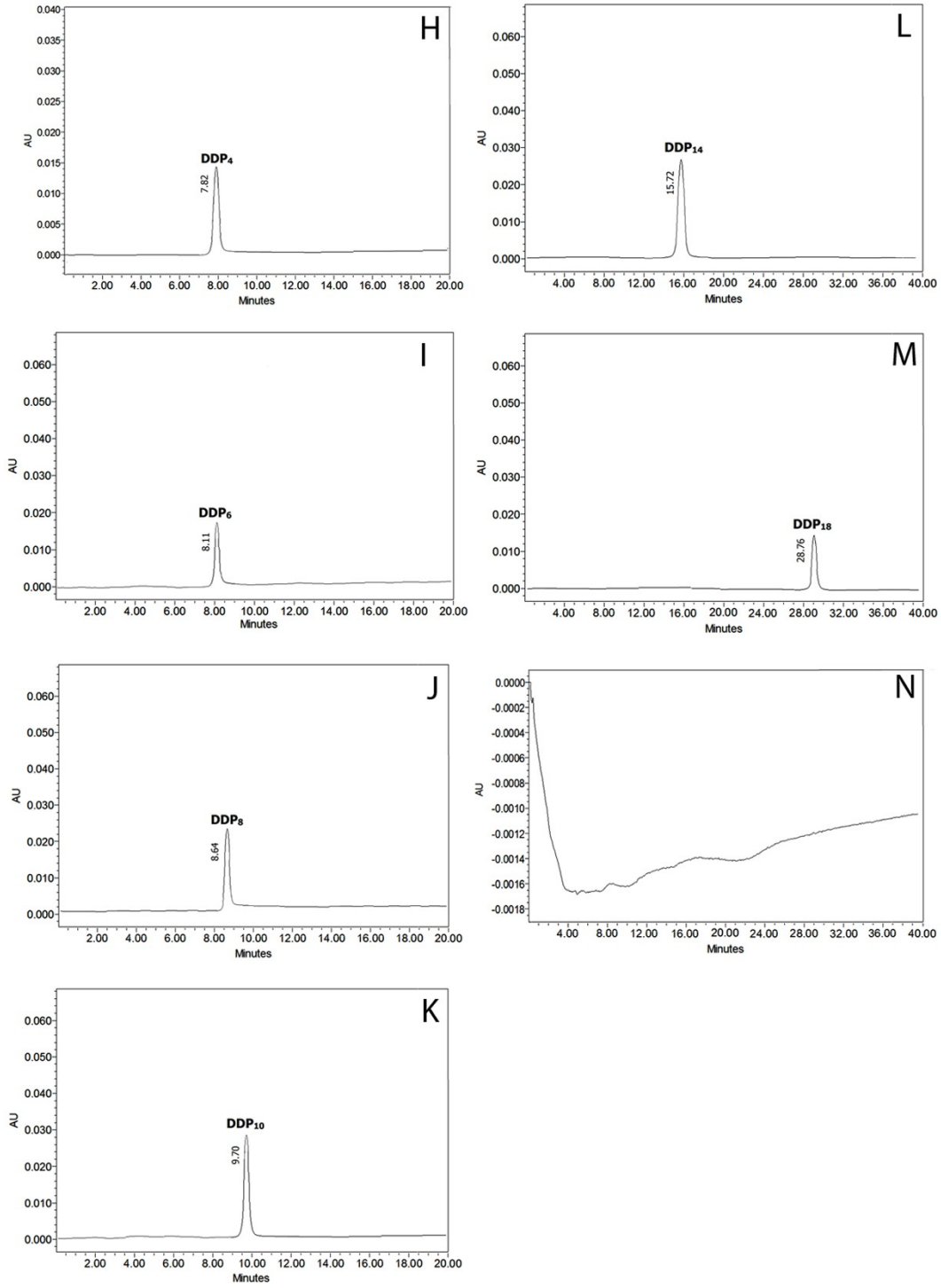

Figure 45: HPLC chromatograms used to determine pro-drug encapsulation efficiency. Spectra A-G refer to individual prodrugs while H-N refer to prodrugs extracted from CS nanoparticles. The direct method was used to assayed the encapsulation efficiency of palatinate pro-drugs encapsulated in CS nanoparticles. Nanoparticles spectra refer to formulations where CS_8 was used but similar ones were obtain for CS_4, CS_6 and CS_{10} formulations. Spectra were obtained from the following standard solutions or formulations: (A) DDP standard solution, (B) DDP_4 standard solution, (C) DDP_6 standard solution, (D) DDP_8 standard solution, (E) DDP_{10} standard solution, (F) DDP_{14} standard solution, (G) DDP_{18} standard solution, (H) CS_8-DDP_4 formulation, (I) CS_8-DDP_6 formulation, (J) CS_8-DDP_8 formulation, (K) CS_8-DDP_{10} formulation, (L) CS_8-DDP_{14} formulation, (M) CS_8-DDP_{18} formulation, (N) Blank nanoparticles. Chromatographic conditions: reverse phase C18 column with a C18 pre-column; mobile phase, 1:1 methanol/water (v/v) used at a rate of 0.5 mL/min; detection, 260 nm.

This dramatic loss of activity in longer lipid chain platinum derivatives might be related to the trapping for the drug in the exoplasmic leaflet bilayer, thereby losing access to the cytosolic leaflet (449). The prodrugs were dispersed at a high concentration in DMSO and subsequently diluted in culture media for dosing the cells in cytotoxicity studies and the effective final DMSO concentration (<0.1%) as control did not show any adverse effects on the viability of the cells.

Table 12: IC50 values of platinum derivatives in solution or encapsulated in EGFR-targeted chitosan nanoparticles.

A

IC_{50} (nM) ± SD			A549 Wild Type (IC_{50} free cisplatin = 12.24 µM)				
			No DDP	Platinum Derivatives			
				DDP_8	DDP_{10}	DDP_{14}	DDP_{18}
In solution			-	2.7 ± 1.2 ***	1.3± 0.1 ***	35.8± 5.2***	198.3± 27.7
CS nanoparticles	fatty acids chain length	CS_4	n.o.t	10.0 ±2.4	7.7±1.0 *	4.8±0.6 **	1.2±0.1 ***
		CS_6	n.o.t	1.6 ±0.2 ***	1.4±0.24 ***	6.1±0.8 *	3.0±0.4 **
		CS_8	n.o.t	0.9 ±0.3 ***	0.6±0.1 ***	0.8±0.1 ***	0.8±0.1 ***
		CS_{10}	n.o.t	2.4 ±0.4 ***	1.8 ±0.2 ***	1.6±0.2 ***	6.2±0.8 *

B

IC50 (nM) ± SD			A549-DDP (IC_{50} free cisplatin = 140.73 µM)				
			No DDP	Platinum Derivatives			
				DDP_8	DDP_{10}	DDP_{14}	DDP_{18}
In solution			n.o.t	70.7±9.8 ***	28.3±3.9 ***	453.2±65.4	954.0 ±123.5
CS nanoparticles	fatty acids chain length	CS_4	n.o.t	113.8±15.9 **	87.8±12.8 ***	54.4±7.6 ***	24.8±3.4 ***
		CS_6	n.o.t	28.1±3.9 ***	26.5±3.8 ***	69.7±9.7 ***	33.9±4.7 ***
		CS_8	n.o.t	20.4±2.8 ***	17.4±2.4 ***	19.1±2.6 ***	19.9±2.7***
		CS_{10}	n.o.t	27.2±3.8 ***	30.8±3.5 ***	29.2±4.0 ***	71.0±9.7 ***

*IC50 values were obtained by incubating human cancer cell lines A549 wild type (A) and A549-DDP resistant (B) with serial dilutions of the different derivatives in solution or encapsulated in CS nanoparticles followed by cell viability was assessment using the MTT assay. Values are shown as mean values ± standard deviation for three independent determinations. ***p< 0.01, **p< 0.05, *p< 0.1 when compared to IC_{50} for free cisplatin. n.o.t: No observed toxicity.*

The EGFR-targeted hydrophobic derivatives of CS themselves did not show any cytotoxic effect of the cells, demonstrating that the derivatized chitosan continues to be a non-toxic

material as described in earlier literature(269, 450). All the formulations except DDP_8 encapsulated in CS_4 showed a significantly higher cytotoxicity than the respective derivatives in solution or parent drug, confirming that the CS derivatives are able to efficiently deliver the platinum derivatives to the cancer cells. More importantly, the drug activity is improved in the A549-DDP resistant cells, suggesting that the drug encapsulated in hydrophobized CS helps overcoming drug resistant property of the A549-DDP cells. We also observed that the nanoparticles encapsulating DDP_{14} and DDP_{18} showed effective cell killing efficiency unlike the corresponding lipid-modified platinum derivatives when administered in solution, highlighting the merit of the delivery vector. Most importantly, we have demonstrated in our earlier work that these EGFR-targeted CS nanoparticles selectively target the overexpressed receptor on the surface of A549 sensitive and resistant cells and their improved cytotoxic activity is associated with receptor-mediated endocytosis(288).

The candidate selection from a library of such formulations is a vital parameter to consider in eliminating any influence of the physical characteristics of the nanoparticle on its *in vitro* and *in vivo* activity. All CS_8 formulations gave comparable sizes, surface charge, drug encapsulation efficiency as well as identical IC_{50} values for different platinum derivatives in both A549-WTand A549-DDP resistant cells and were, therefore, selected for further evaluation. Importantly, the preferred nanoparticle size limit to achieve tumor penetration by EPR effect has been documented as < 300 nm and all the CS_8 formulations show sizes between 230 - 270 nm (451). Therefore, they serve as ideal candidates for future animal studies and were explored further in this study.

Nanoparticles obtained by self-assembling CS_8 derivative in the presence of DDP_8, DDP_{10}, DDP_{14} and DDP_{18} were negatively stained with 1.5% uranyl acetate and were visualized under TEM to observe their morphology (Figure 46). All four nanoparticle systems showed a spherical morphology with an average size (obtained from measuring the size of 30 individual particles across different regions of interest) smaller than that obtained by DLS measurement (Table 10). This was expected since TEM images show the actual size of the particles unlike DLS measurement that gives the hydrodynamic diameter. The TEM images confirm that lipid-modified CS forms self-assembled, micelle like spherical particles in an aqueous environment.

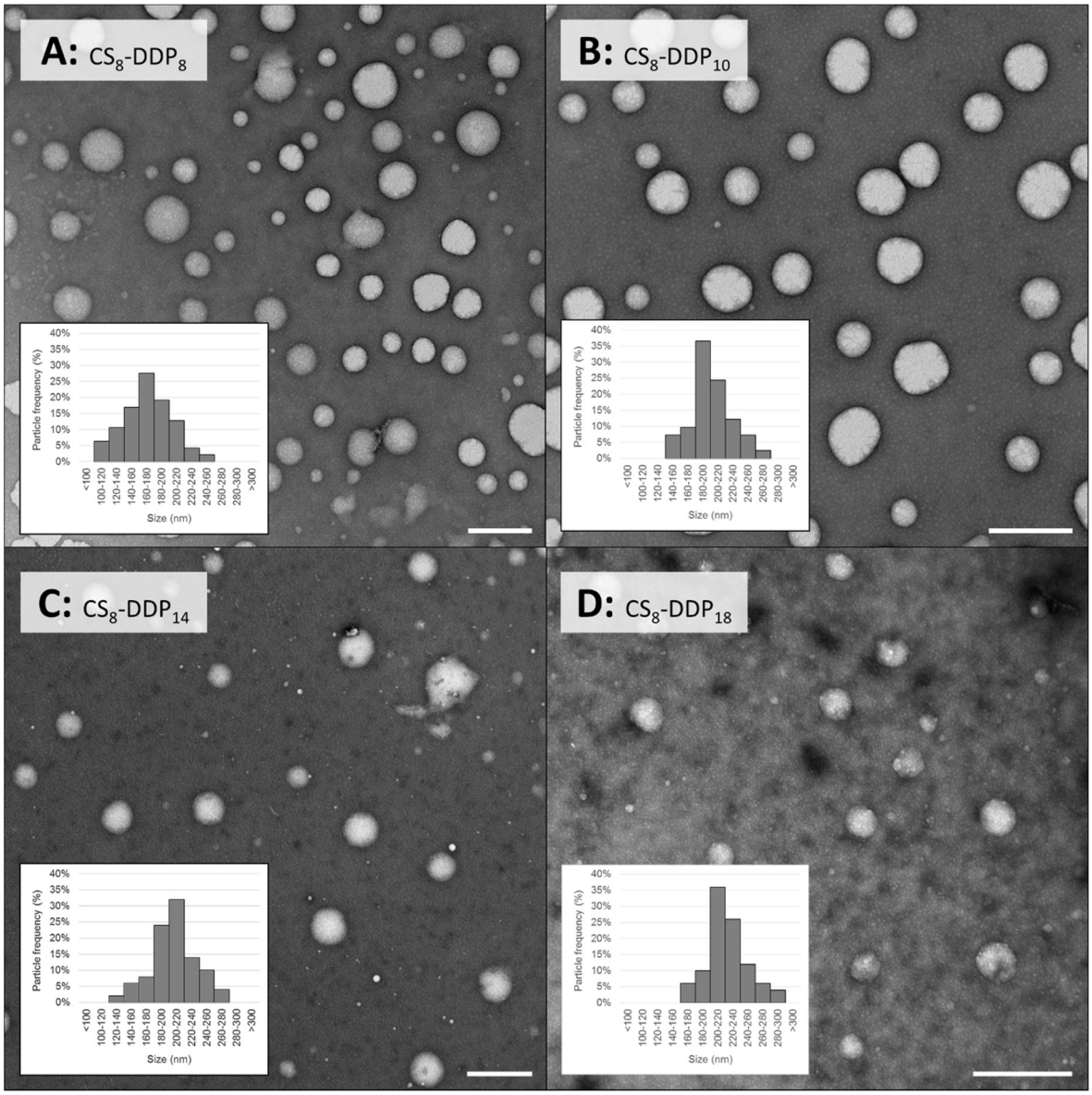

Figure 46: Transmission electron microscopy images of epidermal growth factor receptor-targeted chitosan nanoparticles. The lipid-modified platinum derivatives (C_8, C_{10}, C_{14} and C_{18}) were encapsulated in CS_8 nanoparticles and negatively stained with 1.5% uranyl acetate prior to imaging. The corresponding particle size distribution plot as inset in each image has been calculated from a minimum of 30 nanoparticles for the respective sample. Scale bar in all images corresponds to 100 nm.

3.5 Cellular apoptosis studies

In order to confirm that the cytotoxicity of the parent and the hydrophobic platinum derivatives is due to induction and upregulation of apoptotic pathways, quantitative and qualitative apoptotic analysis was performed in A549-WTand A549-DDP resistant cells. All the formulations were dosed at their corresponding IC50 value to confirm that their *in vitro* cytotoxic activity is mediated by apoptotic pathway and not through any alternate mechanism. Since the cytotoxic effect at the corresponding IC50 concentration would be uniform across all the samples, any difference in the route of the cytotoxic effect could be easily discerned.

Caspase-3 is an "effector" caspase associated with the initiation of the apoptotic-signaling pathway and thus is used as a marker of the cell's entry point into the "death cascade" (452). Since initiation of caspase-3 activity is an early event in the apoptotic pathway, expression levels of the enzyme was measured after 12, 18 and 24 h of incubation with the platinum derivatives encapsulated in CS_8 nanoparticles and was compared to the activity by the corresponding derivative in solution (Figure 47).

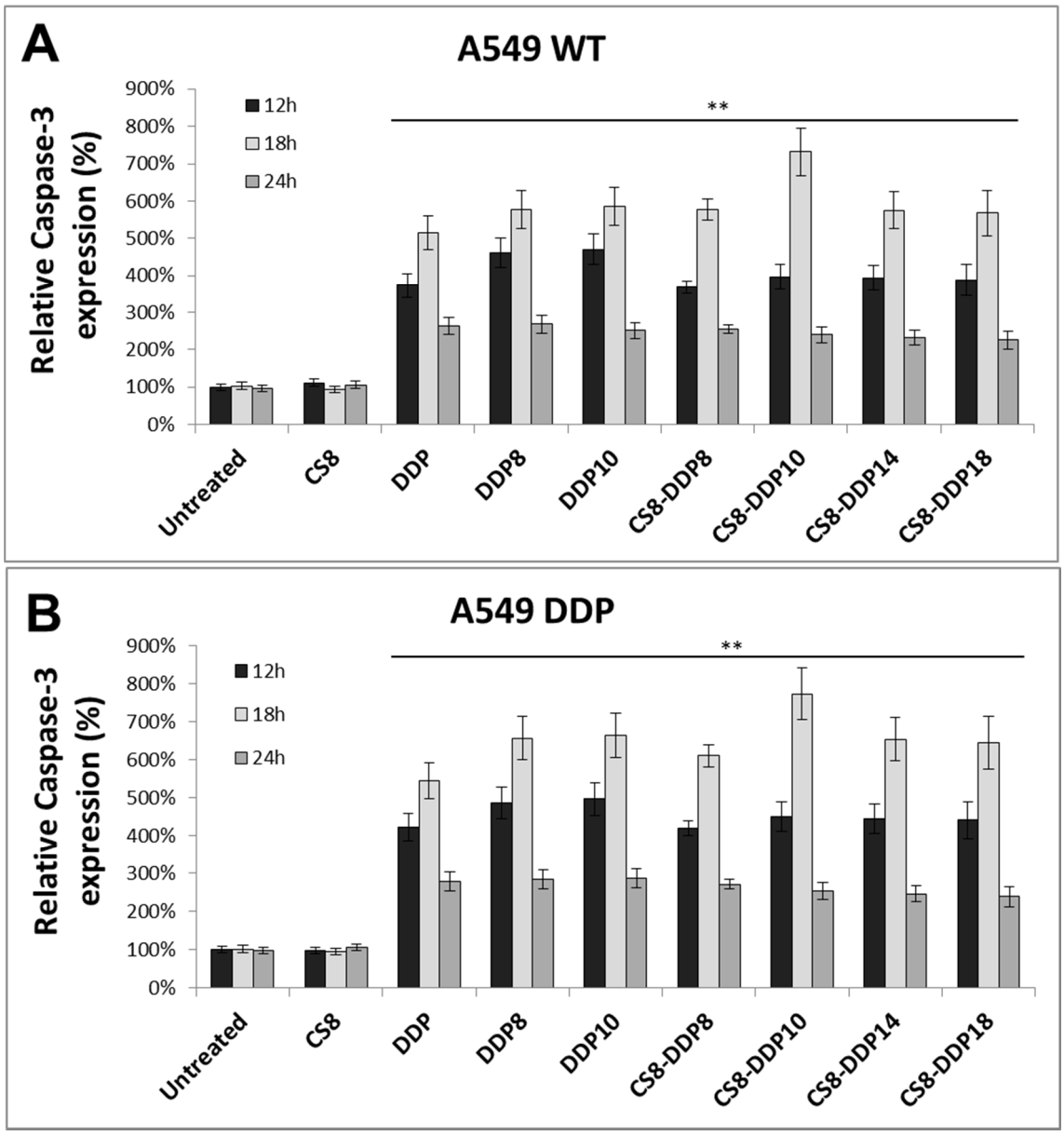

*Figure 47: Caspase-3 expression level in A549-WT(A) and A549-DDP resistant (B) non-small cell lung cancer cells after 24 hours treatment with platinum derivatives, both in solution and encapsulated in CS8 nanoparticles, at their IC50 concentrations. Caspase-3 mRNA expression was normalized to GAPDH expression and presented as a percentage of the level in untreated cellular controls. Bars represent the mean ± standard deviation from three independent experiments. ** = $p < 0.01$ compared to the untreated group at the correspondent time point.*

All the cells were dosed with formulations at their IC_{50} values to maintain uniformity in the drug activity (Table 13). Caspase-3 mRNA expression was normalized to GAPDH

expression and presented as a percentage of the level in untreated cellular controls. No significant change in the caspase-3 expression level was observed when cells were tested with CS_8 alone, which indicated its non-cytotoxic nature. The DDP_{14} and DDP_{18} in solution were omitted from these studies due to their poor *in vitro* cytotoxic activity. For the parent cisplatin in solution as well as for all the lipid-modified platinum derivatives, from 12h to 24h, caspase-3 expression levels were significantly higher than in the untreated cells or cells treated with CS_8 only. This is observed both in A549-WTand A549-DDP resistant cells, showing the induction of apoptosis. We confirmed that hydrophobic modifications of cisplatin and its encapsulation in hydrophobic CS was able to induce apoptosis even at much lower concentrations of the drug, in line with the *in vitro* cytotoxicity results.

Table 13: Cell-kill efficacy as measured by IC50 values of values of platinum derivatives encapsulated in solution or encapsulated in CS8 nanoparticles that were tested for cellular apoptosis studies.

	A549 Wild-Type		A549-DDP	
	IC_{50} value	Fold improvement	IC_{50} value	Fold improvement
DDP	12.24 ± 4.2	-	140.73 ± 6.5	-
DDP_8	2.7 ± 1.2	4.5	70.7 ± 9.8	2.0
DDP_{10}	1.3 ± 0.1	9.4	28.3 ± 3.9	5.0
DDP_{14}	35.8 ± 5.2	0.3	453.2 ± 65.4	0.3
DDP_{18}	198.3 ± 27.7	0.1	954 ± 123.5	0.1
CS_8-DDP_8	0.9 ± 0.3	13.6	20.4 ± 2.8	6.9
CS_8-DDP_{10}	0.6 ± 0.1	20.4	17.4 ± 2.4	8.1
CS_8-DDP_{14}	0.8 ± 0.1	15.3	19.1 ± 2.6	7.4
CS_8-DDP_{18}	0.8 ± 0.1	15.3	19.9 ± 2.7	7.1

Apoptotic activity was additionally monitored by flow cytometry using annexin V-FITC staining to detect translocation of phosphatidylserine to the outer leaflet of cell membrane, an event that occurs early in apoptosis (453). A549 and wild-type A549-DDP resistant were treated for 24 h with cisplatin in solution, different platinum derivatives in solution or encapsulated in CS_8 as well as CS_8 alone. Cisplatin and its lipid-modified derivatives were tested at their determined IC_{50} concentrations (Table 13). Once again, DDP_{14} and DDP_{18} derivatives in solution were not tested due to their poor *in vitro* cytotoxic activity. The results indicated that control cell samples and cells treated with CS_8 had a very low apoptotic index, indicating that the hydrophobic chitosan nanoparticles on their own do not show any cytotoxic effect (Figure 48 and Figure 49).

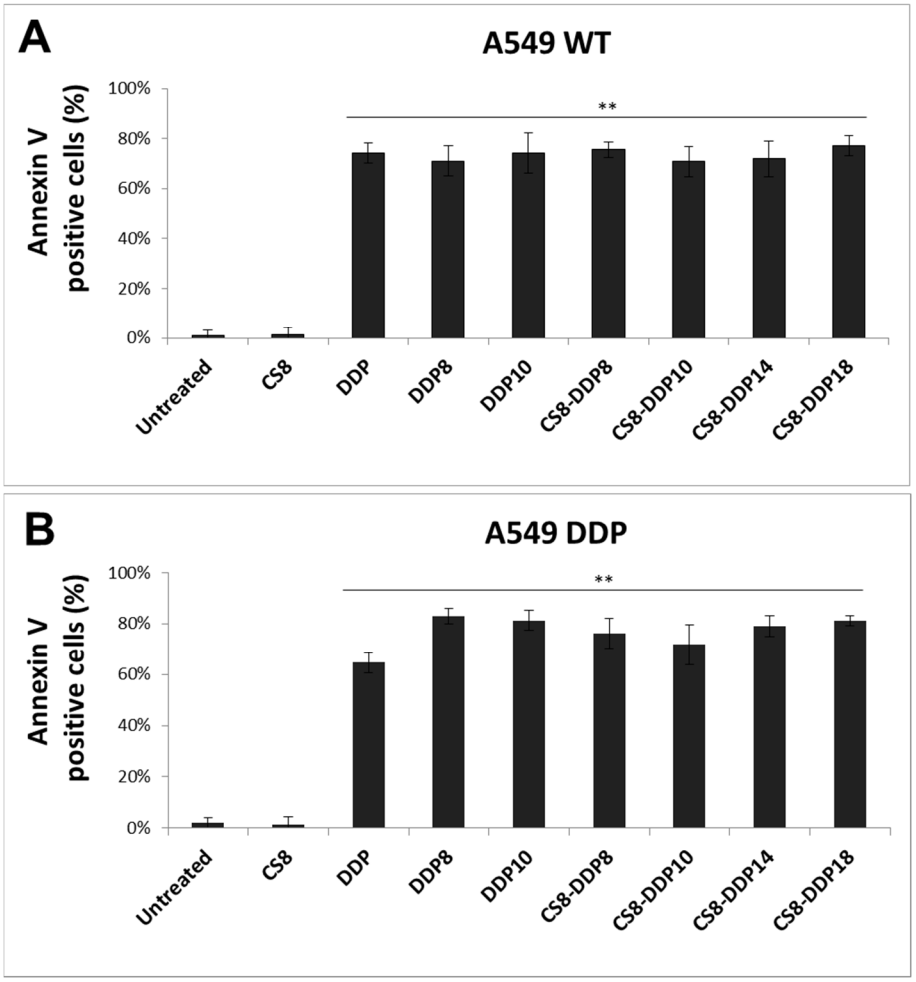

*Figure 48: Analysis of cell death effect of cisplatin and lipid-modified platinum (DDP) derivatives encapsulated in CS8 hydrophobic derivative at their IC50 concentration. Apoptosis was determined in A549-WT (A) and A549-DDP (B) by flow-cytometric detection of annexin V-FITC-positive cells after 24 h of incubation with DDP derivatives, both in solution and encapsulated in nanoparticles, at their IC50 concentrations. Cells were also incubated with CS8 to check for toxicity coming from the chitosan derivative. Bars represent the mean ± standard deviation from three independent experiments. ** = $p < 0.01$ compared to the untreated group.*

In all the drug treatment groups in both the cell lines, a significant increase in annexin V positive cells was observed compared to control cells, being this effect in apoptosis induction indistinguishable between the different treatments with cisplatin and lipid-modified platinum derivatives in solution or encapsulated in CS_8 nanoparticles. This observation suggests that the platinum derivatives (DDP_8 and DDP_{10}) were able to efficiently trigger cell apoptosis even at a lower concentration than the parent cisplatin. Overall, DDP derivatives in solution proved to be more potent than cisplatin in eliciting an apoptotic response, and when encapsulated in CS_8 nanoparticles they are efficient even at lower doses.

A qualitative assessment of cellular apoptosis using TUNEL assay was performed in order to visually detect DNA fragmentation in the apoptotic cells. DNA strand breaks during apoptosis, which generates free 3′-OH ends that can be detected by TUNEL assay.

Figure 50 shows TUNEL staining images of A549-WTand A549-DDP cells treated with cisplatin in solution, and the platinum derivatives in solution, DDP_n-CS_8 formulations and CS_8 alone after 24 h of incubation at their corresponding IC_{50} concentrations (Table 4). Apart from control and CS_8-treated cells, all other treatment groups exhibited consistent accumulation of TUNEL-positive apoptotic population of cells.

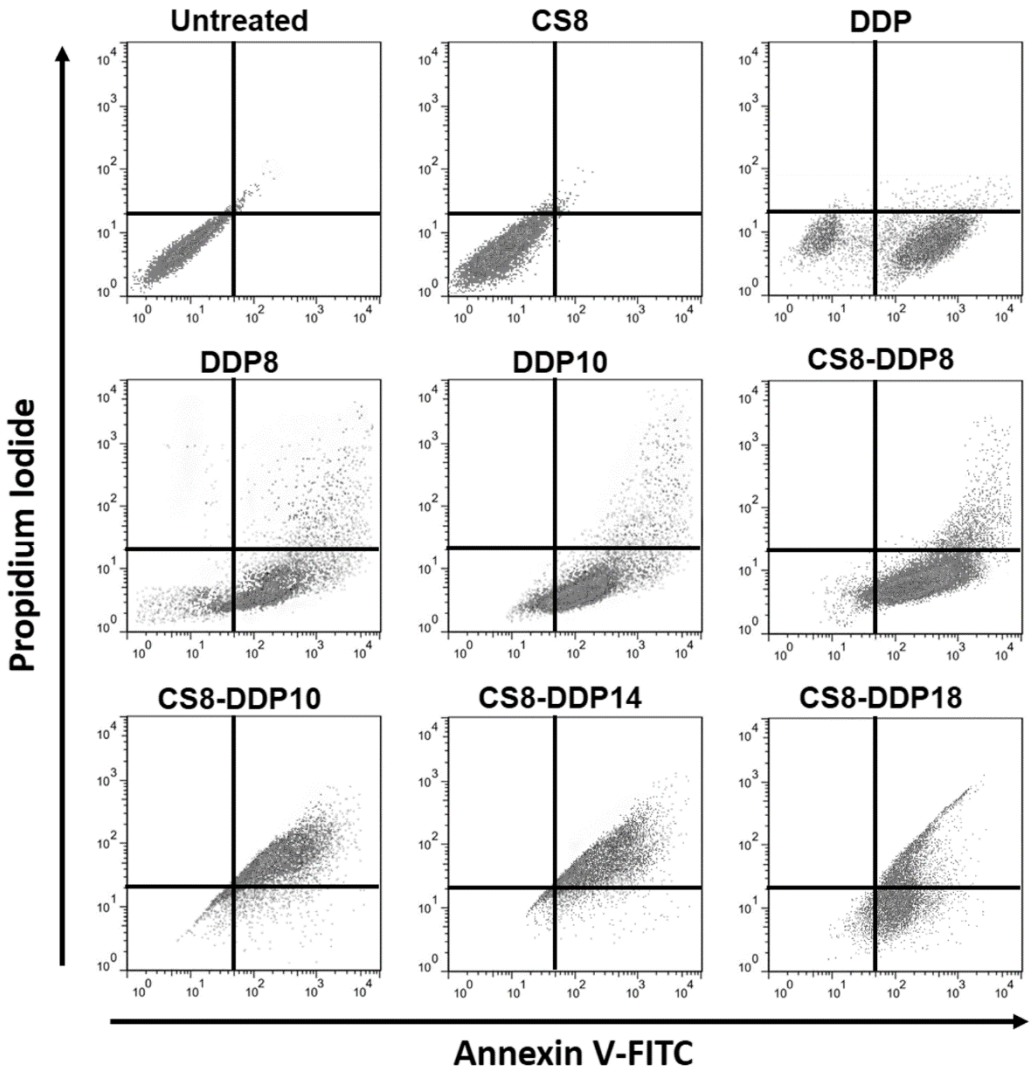

Figure 49: Annexin V-PI analysis for Apoptotic population of A549-DDP cells. The two-dimensional plot for apoptosis assay using Annexin V−PI staining in A549-DDP cells after treatment with DDP and lipid-modified DDP derivatives encapsulated in CS_8 derivative at their IC50 concentration. Apoptosis was determined by flow cytometry after 24 h of drug treatment. Cells incubated with CS_8 empty nanoparticles served as positive control to evaluate the toxicity of blank nanoparticles. Total number of events: 10,000.

Collectively, the data from our cytotoxic assays and evaluation of apoptotic events showed that while CS_8 alone had no significant toxic effect, a strong apoptotic response was achieved by the DDP_8 and DDP_{10} derivatives at very lower concentrations as compared to parent cisplatin. Furthermore, a significant improvement in their activity was achieved when encapsulated with hydrophobic CS_8, as judged by the significant decrease in their IC_{50}, yet

maintaining the same effects in terms of apoptosis induction. Introduction of a lipid chain improved the cisplatin apoptotic efficiency in the case of membrane-permeable DDP_8 and DDP_{10}, but the same did not apply to DDP_{14} and DDP_{18}. In case of these last two derivatives, the introduction of a long hydrophobic chain has probably produced a compound likely to be entrapped in the lipid bilayer membranes, resulting in poor drug transport to the intracellular compartment for enhanced efficacy.

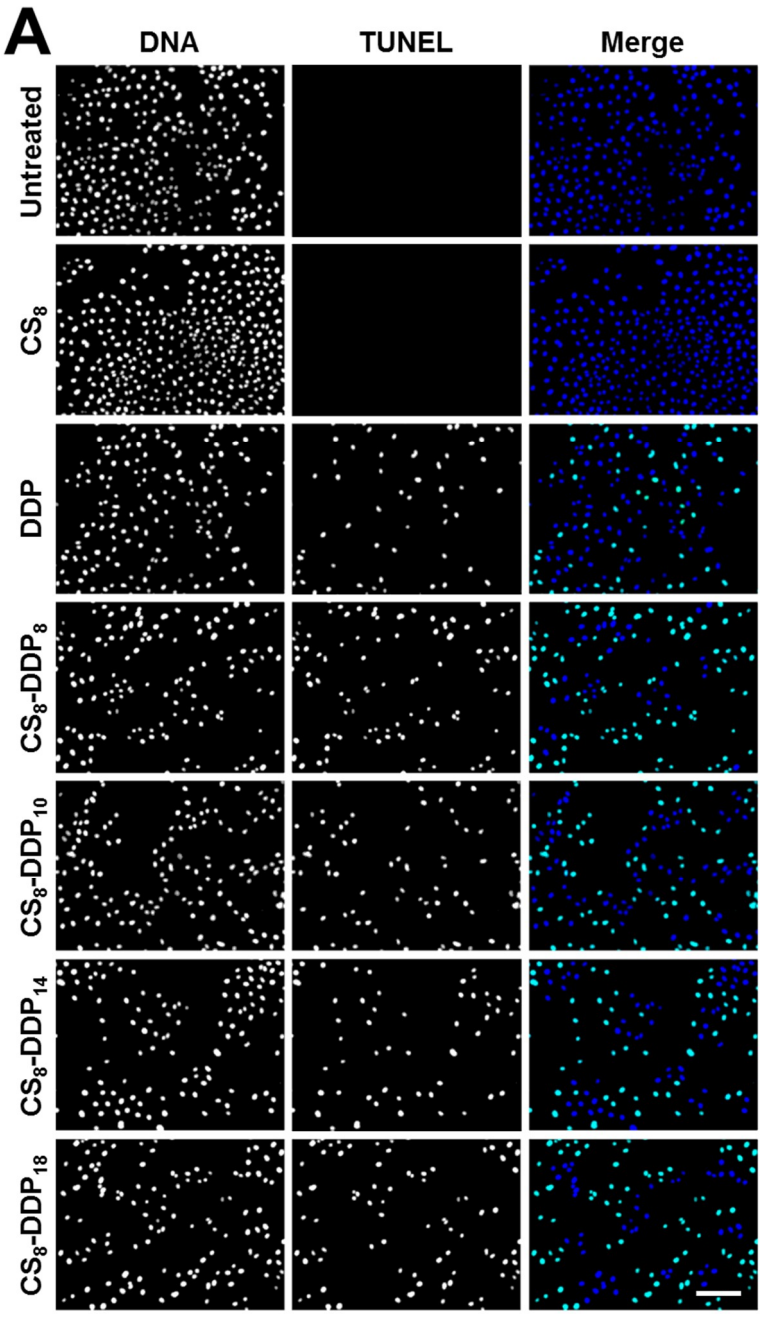

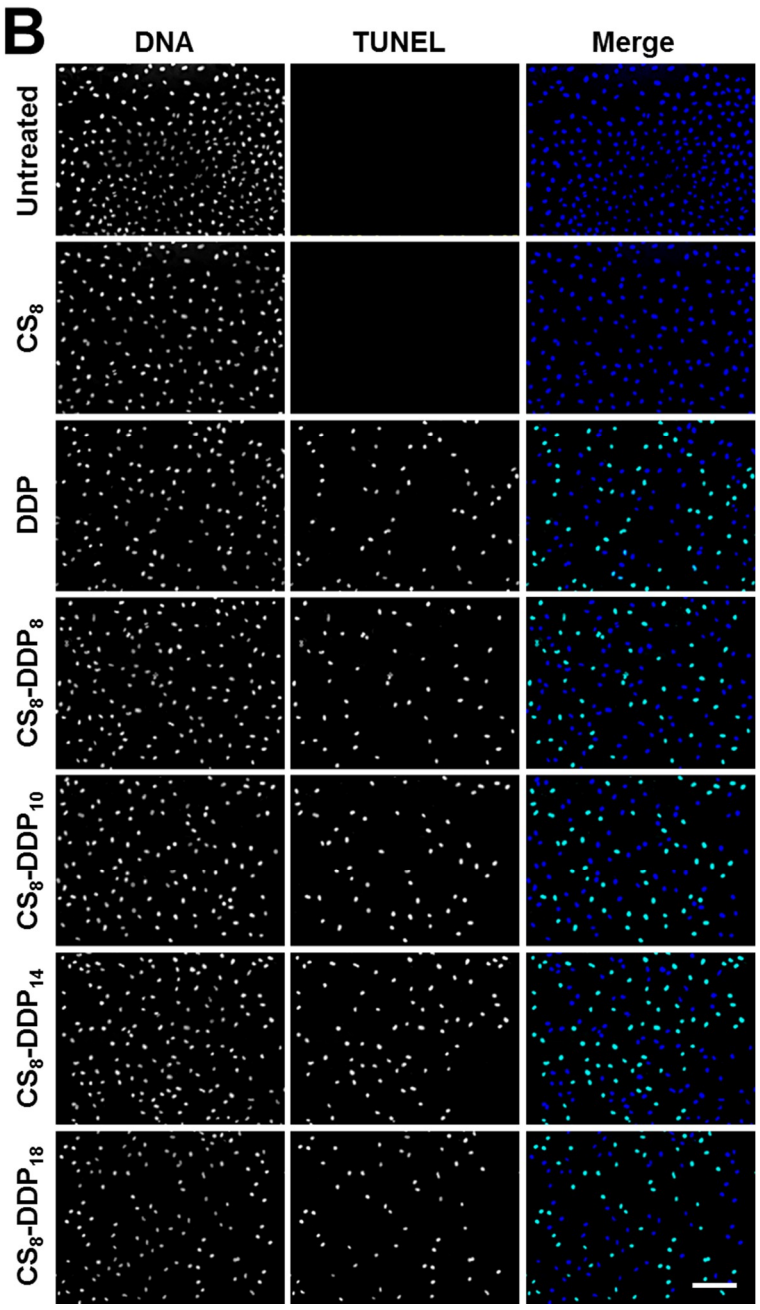

Figure 50. TUNEL staining images of (A) A549-WTand (B) A549^{DDP} cells treated with lipid-modified platinum derivatives CS formulations. *Cell's nucleus was stained with DAPI. In the merge images DAPI is shown in blue and the TUNEL staining in green. Images obtained at 10× magnification. Scale bar = 100 µm*

Encapsulation of the four platinum derivatives with CS_8 to form nanoparticles improved the cellular uptake, which may be due the specific receptor-mediated endocytosis in both A549-WT and A549-DDP resistant cells while the parent cisplatin and the derivatives when in solution enter the cells via passive permeation (454).

These results are in agreement with our previous reports as to the potential advantage of using EGFR as an active targeting moiety for lung tumor specific drug delivery (288, 290). It is noteworthy that CS_8 nanoparticles have three blocks in their constitution that can

contribute for an enhanced efficacy: an hydrophobic modified block, responsible for interacting with hydrophobic modified platinum; a PEG-modified block, highly soluble in aqueous solutions; and an EGFR-peptide modified block, as a the targeting modality since it is overexpressed in both A549-WT and A549-DDP resistant cell lines (288).

In this study, we have successfully synthesized CS modified with lipid, PEG and EGFR. Together they were able to self-assemble into nanoparticles in water and be utilized to deliver a hydrophobic derivative of the antitumor drug cisplatin. Based on a combinatorial approach, we evaluated the effect of different lipid chain lengths on nanoparticles physicochemical characteristics but also encapsulation efficiency and in vitro cytotoxicity studies. These studies indicated that the CS therapeutic platinum nanoformulations were more effective for suppressing cellular growth in both sensitive and resistant lung cancer cells than the drug solution. The remarkable increase in potency with this combination of platinum hydrophobic derivatives in a 3-block CS system can be a benefit to therapy and also limit toxic side effects. An especially interesting feature of this nanomedicine design is the versatility and customizable method that can be specifically designed to be able to load different therapeutic cargos with different hydrophobicities. The multifunctionality of this novel CS-targeted platinum loaded formulations holds promising results as it not only empowers co-delivery of combinatorial drugs but also has the potential to reduce the toxicity associated with these drug by reducing the therapeutic dose

.

CHAPTER 7

General conclusions

General conclusions

The dismal 15% of 5-year survival rate makes lung cancer as the leading cause of cancer-related deaths. NSCLC is the leading cause of cancer-related deaths worldwide and accounts for 85% of all cases of lung cancer (455). Cancer being a disease of rapidly dividing cells, targeting molecular components that act during mitosis has emerged as an attractive therapeutic opportunity for new cancer therapies. This approach represents an appealing strategy to kill cancer cells, especially those with high rate of proliferation (407).

In this study, we have developed an EGFR-targeted chitosan nanoparticles for silencing the *mad2* gene as a strategy to efficiently induce cell death in EGFR overexpressing human lung cancer cells. We have chosen the mitotic checkpoint component, Mad2, as the molecular target since it is a key cell cycle component that ensures an accurate segregation of chromosomes during mitosis by delaying the onset of anaphase until all chromosomes are properly attached to a bipolar mitotic spindle. Failure in the mitotic checkpoint leads to severe chromosome missegregation and cell death. While a weakened mitotic checkpoint is frequently seen in cancer cells and may contribute to tumorigenesis, a severe loss in checkpoint signalling is a possible anticancer strategy (189). In order to suppress *mad2* gene, siRNA-mediated knockdown was implemented. Intracellular delivery of highly labile biomolecules such as siRNA is a challenging task. CS was explored as siRNA vector due to its cationic polyelectrolyte nature, low toxicity, mucoadhesion, biodegradability and biocompatibility(456). Furthermore, a EGFR-binding peptide was used as targeting moiety that has previously demonstrated efficient targeting of EGFR receptor and its targeting capability has been successfully validated *in vitro* as well as *in vivo* in various EGFR-overexpressing tumor cells such as A549 (311, 316, 317, 369-371).

Initially, CS of two molecular weights (50 and 90 kDa) were tested in the optimization process but the one with an average molecular weight of 50 kDa showed better *in vitro* results overall. In order to increase its solubility and achieve longer blood-circulating half-life, CS was modified with PEG chains prior to the modification with EGFR-binding peptide.

SiMad2-loaded CS nanoparticles were formed by self-assembly when positively charged CS couls electrostatically bind and encapsulate the negatively charged nucleic acids. These nanoparticles were characterized for their size, surface charge, morphology, encapsulation efficiency and stability. *In vitro* studies were performed to demonstrate efficient gene silencing by both TG and NTG nanoparticles in EGFR overexpressing human A549 NSCLC cells. Nevertheless, the EGFR-targeted CS system exhibited higher and selective uptake,

indicating that TG nanoparticles are rapidly internalized within the cells by receptor-mediated endocytosis, culminating into an enhanced apoptotic cell death.

The *in vitro* studies also verified that Mad2 knockdown results in massive cell death by apoptosis of A549 cells while the cytotoxic impact was significantly less in the non-cancerous human lung primary cell line; and this helped us assess a therapeutic window. Since the mitotic checkpoint protein, Mad2 is only needed during cell division, its depletion would selectively affect proliferating tissues; therefore, cancer cells with high cell proliferation rate would be much more prone to anti-Mad2 therapy compared to their normal counterpart.

The next step was to assess the pharmacokinetics and biodistribution profile of siMad2 encapsulated in NTG or TG CS nanoparticles in A549-WT and cisplatin resistant A549-DDP tumor-bearing mice via intravenous administration at a dose of 3 mg/kg. The differences in the biodistribution were studied qualitatively and quantitatively. Qualitative biodistribution profile based on near-IR labeled CS nanoparticles showed a long-lasting exposure of the tumor (up to 96 h) to the nanoparticles, independent of the tumor model or targeting property. A quantitative pharmacokinetic study was performed based on siMad2 quantification. Non-compartmental analysis for both tumor models showed that the presence of targeting peptide lead to a significant decrease in plasma exposure of targeted nanoparticles. The targeting strategy led to a higher targeting efficiency, i.e. a higher tumor exposure to Mad2-siRNA. The advantage of the targeting strategy was particularly clear for the A549-DDP model, with a higher increase of tumor exposure and targeting efficiency.

After verifying Mad2 knockdown in the tumors by both NTG and TG formulations, we tested their effect on tumor growth inhibition. The antitumor efficacy of TG and NTG nanoparticles was tested as a single therapy and in combination with cisplatin in A549-WT and cisplatin-resistant, A549-DDP subcutaneous tumor models of NSCLC. SiMad2-loaded NTG and TG nanoparticles were injected intravenously at a dose of 3 mg/kg of siMad2 and cisplatin was used at a dose 1 mg/kg. For both tumor models, the administration of cisplatin in combination with Mad2 siRNA-loaded nanoparticles exhibited higher tumor inhibition than cisplatin in solution. This fact was even more pronounced in the cisplatin-resistant tumor models indicating that Mad2 may be promising in mitigating the molecular mechanisms of cisplatin resistance and enhancing therapeutic efficacy.

Finally, an endeavor was made to develop CS-based platform technology for delivery of small molecule along with nucleic acid for such combination therapies. We developed a strategy to deliver cisplatin encapsulated in CS nanoparticle in an attempt to improve its bioavailability and reduce the associated toxicity by reducing its therapeutic dose and off-

target effects. In order to achieve this, we synthesized CS modified with lipid chains and used it as a 3-block CS system along with CS modified with PEG and EGFR to self-assemble into nanoparticles. Simultaneously, cisplatin was derivatized with lipid chains to impart it a hydrophobic characteristics and allow its encapsulation within the hydrophobic pockets of the 3-block nanoparticle system. In the *in vitro* studies, this system proved to be more effective in suppressing cellular growth in both sensitive and resistant lung cancer cells compared to the drug solution. This novel EGFR-targeted platinum-loaded CS formulation presents with promising opportunity to perform *in vivo* studies using it as a single therapy or in combination with Mad2 siRNA-loaded nanoparticles.

Collectively, our results indicate that Mad2 has a huge potential as a therapeutic molecular target for cancer treatment and that RNAi therapeutics could effective in curbing cancer as a disease when delivered through a suitable delivery vector such as CS nanoparticles.

CHAPTER 8

References

References

1. Ferlay J, Shin HR, Bray F, Forman D, Mathers C, Parkin DM. Estimates of worldwide burden of cancer in 2008: GLOBOCAN 2008. Int J Cancer. 2010;127(12):2893-917.
2. McErlean A, Ginsberg MS. Epidemiology of lung cancer. Semin Roentgenol. 2011;46(3):173-7.
3. Proctor RN. The history of the discovery of the cigarette-lung cancer link: evidentiary traditions, corporate denial, global toll. Tob Control. 2012;21(2):87-91.
4. Brambilla E, Travis WD, Colby TV, Corrin B, Shimosato Y. The new World Health Organization classification of lung tumours. Eur Respir J. 2001;18(6):1059-68.
5. Wahbah M, Boroumand N, Castro C, El-Zeky F, Eltorky M. Changing trends in the distribution of the histologic types of lung cancer: a review of 4,439 cases. Ann Diagn Pathol. 2007;11(2):89-96.
6. Kumar S, Mohan A, Guleria R. Prognostic implications of circulating anti-p53 antibodies in lung cancer--a review. Eur J Cancer Care (Engl). 2009;18(3):248-54.
7. Wajed SA, Laird PW, DeMeester TR. DNA methylation: an alternative pathway to cancer. Ann Surg. 2001;234(1):10-20.
8. Miller YE. Pathogenesis of lung cancer: 100 year report. Am J Respir Cell Mol Biol. 2005;33(3):216-23.
9. Crino L, Weder W, van Meerbeeck J, Felip E. Early stage and locally advanced (non-metastatic) non-small-cell lung cancer: ESMO Clinical Practice Guidelines for diagnosis, treatment and follow-up. Annals of oncology : official journal of the European Society for Medical Oncology / ESMO. 2010;21 Suppl 5:v103-15.
10. d'Amato TA, Landreneau RJ, Ricketts W, Huang W, Parker R, Mechetner E, et al. Chemotherapy resistance and oncogene expression in non-small cell lung cancer. J Thorac Cardiovasc Surg. 2007;133(2):352-63.
11. Ou SH. Second-generation irreversible epidermal growth factor receptor (EGFR) tyrosine kinase inhibitors (TKIs): A better mousetrap? A review of the clinical evidence. Crit Rev Oncol Hematol. 2012.
12. National Cancer Institute. NCI Dictionary of Cancer Terms 2012 [cited 2012 June 17]. Available from: http://www.cancer.gov/cancertopics/factsheet/Therapy/targeted.
13. Custodio A, Mendez M, Provencio M. Targeted therapies for advanced non-small-cell lung cancer: current status and future implications. Cancer Treat Rev. 2012;38(1):36-53.
14. Zhang H, Berezov A, Wang Q, Zhang G, Drebin J, Murali R, et al. ErbB receptors: from oncogenes to targeted cancer therapies. J Clin Invest. 2007;117(8):2051-8.
15. Charpidou A, Blatza D, Anagnostou V, Syrigos KN. Review. EGFR mutations in non-small cell lung cancer--clinical implications. In Vivo. 2008;22(4):529-36.
16. Gazdar AF. Personalized medicine and inhibition of EGFR signaling in lung cancer. N Engl J Med. 2009;361(10):1018-20.
17. Stella GM, Luisetti M, Inghilleri S, Cemmi F, Scabini R, Zorzetto M, et al. Targeting EGFR in non-small-cell lung cancer: lessons, experiences, strategies. Respir Med. 2012;106(2):173-83.
18. Zhang X, Chang A. Molecular predictors of EGFR-TKI sensitivity in advanced non-small cell lung cancer. Int J Med Sci. 2008;5(4):209-17.
19. Cataldo VD, Gibbons DL, Perez-Soler R, Quintas-Cardama A. Treatment of non-small-cell lung cancer with erlotinib or gefitinib. N Engl J Med. 2011;364(10):947-55.
20. Wu JY, Wu SG, Yang CH, Chang YL, Chang YC, Hsu YC, et al. Comparison of gefitinib and erlotinib in advanced NSCLC and the effect of EGFR mutations. Lung Cancer. 2011;72(2):205-12.
21. Felip E, Rosell R. Clinical experience with erlotinib in non-small-cell lung cancer. Drugs Today (Barc). 2006;42(3):147-56.
22. Bareschino MA, Schettino C, Rossi A, Maione P, Sacco PC, Zeppa R, et al. Treatment of advanced non small cell lung cancer. J Thorac Dis. 2011;3(2):122-33.
23. Gao G, Ren S, Li A, Xu J, Xu Q, Su C, et al. Epidermal growth factor receptor-tyrosine kinase inhibitor therapy is effective as first-line treatment of advanced non-small-cell lung cancer with mutated EGFR: A meta-analysis from six phase III randomized controlled trials. Int J Cancer. 2011.
24. Azzoli CG, Baker S, Jr., Temin S, Pao W, Aliff T, Brahmer J, et al. American Society of Clinical Oncology Clinical Practice Guideline update on chemotherapy for stage IV non-small-cell lung cancer. J Clin Oncol. 2009;27(36):6251-66.
25. Ogino A, Kitao H, Hirano S, Uchida A, Ishiai M, Kozuki T, et al. Emergence of epidermal growth factor receptor T790M mutation during chronic exposure to gefitinib in a non small cell lung cancer cell line. Cancer Res. 2007;67(16):7807-14.
26. Hirsh V. Afatinib (BIBW 2992) development in non-small-cell lung cancer. Future Oncol. 2011;7(7):817-25.

27. Yang JC, Shih JY, Su WC, Hsia TC, Tsai CM, Ou SH, et al. Afatinib for patients with lung adenocarcinoma and epidermal growth factor receptor mutations (LUX-Lung 2): a phase 2 trial. Lancet Oncol. 2012;13(5):539-48.

28. Kelly RJ, Carter C, Giaccone G. Personalizing therapy in an epidermal growth factor receptor-tyrosine kinase inhibitor-resistant non-small-cell lung cancer using PF-00299804 and trastuzumab. J Clin Oncol. 2010;28(28):e507-10.

29. Gossage L, Eisen T. Targeting multiple kinase pathways: a change in paradigm. Clin Cancer Res. 2010;16(7):1973-8.

30. Bou-Assaly W, Mukherji S. Cetuximab (erbitux). AJNR Am J Neuroradiol. 2010;31(4):626-7.

31. Herbst RS. EGFR inhibition in NSCLC: the emerging role of cetuximab. J Natl Compr Canc Netw. 2004;2 Suppl 2:S41-51.

32. Ettinger DS. Emerging profile of cetuximab in non-small cell lung cancer. Lung Cancer. 2010;68(3):332-7.

33. Ray MR, Jablons D, He B. Lung cancer therapeutics that target signaling pathways: an update. Expert Rev Respir Med. 2010;4(5):631-45.

34. Tsiambas E, Stamatelopoulos A, Karameris A, Panagiotou I, Rigopoulos D, Chatzimichalis A, et al. Simultaneous EGFR and VEGF alterations in non-small cell lung carcinoma based on tissue microarrays. Cancer Inform. 2007;3:275-84.

35. Ferrara N, Hillan KJ, Gerber HP, Novotny W. Discovery and development of bevacizumab, an anti-VEGF antibody for treating cancer. Nat Rev Drug Discov. 2004;3(5):391-400.

36. Soria JC, Mauguen A, Reck M, Sandler AB, Saijo N, Johnson DH, et al. Systematic review and meta-analysis of randomised, phase II/III trials adding bevacizumab to platinum-based chemotherapy as first-line treatment in patients with advanced non-small-cell lung cancer. Annals of oncology : official journal of the European Society for Medical Oncology / ESMO. 2013;24(1):20-30.

37. Gridelli C, Maione P, Del Gaizo F, Colantuoni G, Guerriero C, Ferrara C, et al. Sorafenib and sunitinib in the treatment of advanced non-small cell lung cancer. Oncologist. 2007;12(2):191-200.

38. Socinski MA, Novello S, Brahmer JR, Rosell R, Sanchez JM, Belani CP, et al. Multicenter, phase II trial of sunitinib in previously treated, advanced non-small-cell lung cancer. J Clin Oncol. 2008;26(4):650-6.

39. Scagliotti GV, Krzakowski M, Szczesna A, Strausz J, Makhson A, Reck M, et al. Sunitinib Plus Erlotinib Versus Placebo Plus Erlotinib in Patients With Previously Treated Advanced Non-Small-Cell Lung Cancer: A Phase III Trial. J Clin Oncol. 2012;30(17):2070-8.

40. Scagliotti G, Novello S, von Pawel J, Reck M, Pereira JR, Thomas M, et al. Phase III study of carboplatin and paclitaxel alone or with sorafenib in advanced non-small-cell lung cancer. J Clin Oncol. 2010;28(11):1835-42.

41. Abdollahi A, Folkman J. Evading tumor evasion: current concepts and perspectives of anti-angiogenic cancer therapy. Drug Resist Updat. 2010;13(1-2):16-28.

42. Reck M. BIBF 1120 for the treatment of non-small cell lung cancer. Expert Opin Investig Drugs. 2010;19(6):789-94.

43. Schiller JH, Larson T, Ou SH, Limentani S, Sandler A, Vokes E, et al. Efficacy and safety of axitinib in patients with advanced non-small-cell lung cancer: results from a phase II study. J Clin Oncol. 2009;27(23):3836-41.

44. Hilberg F, Roth GJ, Krssak M, Kautschitsch S, Sommergruber W, Tontsch-Grunt U, et al. BIBF 1120: triple angiokinase inhibitor with sustained receptor blockade and good antitumor efficacy. Cancer Res. 2008;68(12):4774-82.

45. Doebele RC, Conkling P, Traynor AM, Otterson GA, Zhao Y, Wind S, et al. A phase I, open-label dose-escalation study of continuous treatment with BIBF 1120 in combination with paclitaxel and carboplatin as first-line treatment in patients with advanced non-small-cell lung cancer. Annals of oncology : official journal of the European Society for Medical Oncology / ESMO. 2012.

46. Pennell NA, Lynch TJ, Jr. Combined inhibition of the VEGFR and EGFR signaling pathways in the treatment of NSCLC. Oncologist. 2009;14(4):399-411.

47. Gridelli C, Rossi A, Bareschino MA, Schettino C, Sacco PC, Maione P. The potential role of insulin-like growth factor receptor inhibitors in the treatment of advanced non-small cell lung cancer. Expert Opin Investig Drugs. 2010;19(5):631-9.

48. Bruchim I, Attias Z, Werner H. Targeting the IGF1 axis in cancer proliferation. Expert Opin Ther Targets. 2009;13(10):1179-92.

49. Pandini G, Frasca F, Mineo R, Sciacca L, Vigneri R, Belfiore A. Insulin/insulin-like growth factor I hybrid receptors have different biological characteristics depending on the insulin receptor isoform involved. J Biol Chem. 2002;277(42):39684-95.

50. Malaguarnera R, Belfiore A. The insulin receptor: a new target for cancer therapy. Front Endocrinol (Lausanne). 2011;2:93.

51. Reungwetwattana T, Weroha SJ, Molina JR. Oncogenic Pathways, Molecularly Targeted Therapies, and Highlighted Clinical Trials in Non-Small-Cell Lung Cancer (NSCLC). Clin Lung Cancer. 2012;13(4):252-66.

52. ClinicalTrials.gov. 2015 [cited 2015 June 15]. Available from: http://clinicaltrials.gov/.

53. Scagliotti GV, Novello S. The role of the insulin-like growth factor signaling pathway in non-small cell lung cancer and other solid tumors. Cancer Treat Rev. 2012;38(4):292-302.

54. Kim ES, Salgia R. MET pathway as a therapeutic target. J Thorac Oncol. 2009;4(4):444-7.

55. Dempke WC, Suto T, Reck M. Targeted therapies for non-small cell lung cancer. Lung Cancer. 2010;67(3):257-74.

56. Cappuzzo F, Janne PA, Skokan M, Finocchiaro G, Rossi E, Ligorio C, et al. MET increased gene copy number and primary resistance to gefitinib therapy in non-small-cell lung cancer patients. Annals of oncology : official journal of the European Society for Medical Oncology / ESMO. 2009;20(2):298-304.

57. Yakes FM, Chen J, Tan J, Yamaguchi K, Shi Y, Yu P, et al. Cabozantinib (XL184), a novel MET and VEGFR2 inhibitor, simultaneously suppresses metastasis, angiogenesis, and tumor growth. Mol Cancer Ther. 2011;10(12):2298-308.

58. Yee D. Receptor kinase inhibitors target NSCLC: two antibodies and a small-molecule MET inhibitor. BioDrugs. 2011;25(4):271-3.

59. Dai Y, Bae K, Pampo C, Siemann DW. Impact of the small molecule Met inhibitor BMS-777607 on the metastatic process in a rodent tumor model with constitutive c-Met activation. Clin Exp Metastasis. 2012;29(3):253-61.

60. Pal SK, Figlin RA, Reckamp K. Targeted therapies for non-small cell lung cancer: an evolving landscape. Mol Cancer Ther. 2010;9(7):1931-44.

61. Santarpia L, Lippman SM, El-Naggar AK. Targeting the MAPK-RAS-RAF signaling pathway in cancer therapy. Expert Opin Ther Targets. 2012;16(1):103-19.

62. Mascaux C, Iannino N, Martin B, Paesmans M, Berghmans T, Dusart M, et al. The role of RAS oncogene in survival of patients with lung cancer: a systematic review of the literature with meta-analysis. Br J Cancer. 2005;92(1):131-9.

63. Ahearn IM, Haigis K, Bar-Sagi D, Philips MR. Regulating the regulator: post-translational modification of RAS. Nat Rev Mol Cell Biol. 2012;13(1):39-51.

64. Aviel-Ronen S, Blackhall FH, Shepherd FA, Tsao MS. K-ras mutations in non-small-cell lung carcinoma: a review. Clin Lung Cancer. 2006;8(1):30-8.

65. Linardou H, Dahabreh IJ, Kanaloupiti D, Siannis F, Bafaloukos D, Kosmidis P, et al. Assessment of somatic k-RAS mutations as a mechanism associated with resistance to EGFR-targeted agents: a systematic review and meta-analysis of studies in advanced non-small-cell lung cancer and metastatic colorectal cancer. Lancet Oncol. 2008;9(10):962-72.

66. Yamaguchi T, Kakefuda R, Tajima N, Sowa Y, Sakai T. Antitumor activities of JTP-74057 (GSK1120212), a novel MEK1/2 inhibitor, on colorectal cancer cell lines in vitro and in vivo. Int J Oncol. 2011;39(1):23-31.

67. Jing J, Greshock J, Holbrook JD, Gilmartin A, Zhang X, McNeil E, et al. Comprehensive predictive biomarker analysis for MEK inhibitor GSK1120212. Mol Cancer Ther. 2012;11(3):720-9.

68. Yoon J, Koo KH, Choi KY. MEK1/2 inhibitors AS703026 and AZD6244 may be potential therapies for KRAS mutated colorectal cancer that is resistant to EGFR monoclonal antibody therapy. Cancer Res. 2011;71(2):445-53.

69. Hong DS, Cabanillas ME, Wheler J, Naing A, Tsimberidou AM, Ye L, et al. Inhibition of the Ras/Raf/MEK/ERK and RET kinase pathways with the combination of the multikinase inhibitor sorafenib and the farnesyltransferase inhibitor tipifarnib in medullary and differentiated thyroid malignancies. J Clin Endocrinol Metab. 2011;96(4):997-1005.

70. Sato S, Trackman PC, Maki JM, Myllyharju J, Kirsch KH, Sonenshein GE. The Ras signaling inhibitor LOX-PP interacts with Hsp70 and c-Raf to reduce Erk activation and transformed phenotype of breast cancer cells. Mol Cell Biol. 2011;31(13):2683-95.

71. Sharma V, Shaheen SS, Dixit D, Sen E. Farnesyltransferase inhibitor manumycin targets IL1beta-Ras-HIF-1alpha axis in tumor cells of diverse origin. Inflammation. 2012;35(2):516-9.

72. Mason WP, Belanger K, Nicholas G, Vallieres I, Mathieu D, Kavan P, et al. A phase II study of the Ras-MAPK signaling pathway inhibitor TLN-4601 in patients with glioblastoma at first progression. J Neurooncol. 2012;107(2):343-9.

73. Li H, Schmid-Bindert G, Wang D, Zhao Y, Yang X, Su B, et al. Blocking the PI3K/AKT and MEK/ERK signaling pathways can overcome gefitinib-resistance in non-small cell lung cancer cell lines. Adv Med Sci. 2011;56(2):275-84.

74. Manning BD, Cantley LC. AKT/PKB signaling: navigating downstream. Cell. 2007;129(7):1261-74.

75. Xu CX, Jin H, Shin JY, Kim JE, Cho MH. Roles of protein kinase B/Akt in lung cancer. Front Biosci (Elite Ed). 2010;2:1472-84.

76. Papadimitrakopoulou V. Development of PI3K/AKT/mTOR Pathway Inhibitors and Their Application in Personalized Therapy for Non-Small-Cell Lung Cancer. J Thorac Oncol. 2012.

77. Bryce AH, Rao R, Sarkaria J, Reid JM, Qi Y, Qin R, et al. Phase I study of temsirolimus in combination with EKB-569 in patients with advanced solid tumors. Invest New Drugs. 2011.

78. Price KA, Azzoli CG, Krug LM, Pietanza MC, Rizvi NA, Pao W, et al. Phase II trial of gefitinib and everolimus in advanced non-small cell lung cancer. J Thorac Oncol. 2010;5(10):1623-9.

79. Matsubara H, Sakakibara K, Kunimitsu T, Matsuoka H, Kato K, Oyachi N, et al. Non-small cell lung carcinoma therapy using mTOR-siRNA. Int J Clin Exp Pathol. 2012;5(2):119-25.

80. Willems L, Tamburini J, Chapuis N, Lacombe C, Mayeux P, Bouscary D. PI3K and mTOR signaling

pathways in cancer: new data on targeted therapies. Curr Oncol Rep. 2012;14(2):129-38.

81. Takahashi T, Sonobe M, Kobayashi M, Yoshizawa A, Menju T, Nakayama E, et al. Clinicopathologic features of non-small-cell lung cancer with EML4-ALK fusion gene. Ann Surg Oncol. 2010;17(3):889-97.

82. Mano H, Takeuchi K. EML4-ALK fusion in lung. Am J Pathol. 2010;176(3):1552-3; author reply 3-4.

83. Li Y, Ye X, Liu J, Zha J, Pei L. Evaluation of EML4-ALK fusion proteins in non-small cell lung cancer using small molecule inhibitors. Neoplasia. 2011;13(1):1-11.

84. Gandhi L, Janne PA. Crizotinib for ALK-rearranged Non-Small Cell Lung Cancer: A new targeted therapy for a new target. Clin Cancer Res. 2012.

85. Wong RS. Apoptosis in cancer: from pathogenesis to treatment. J Exp Clin Cancer Res. 2011;30:87.

86. Huang N, Zhu J, Liu D, Li YL, Chen BJ, He YQ, et al. Overexpression of Bcl-2-associated death inhibits A549 cell growth in vitro and in vivo. Cancer Biother Radiopharm. 2012;27(2):164-8.

87. Speirs CK, Hwang M, Kim S, Li W, Chang S, Varki V, et al. Harnessing the cell death pathway for targeted cancer treatment. Am J Cancer Res. 2011;1(1):43-61.

88. Moretti L, Li B, Kim KW, Chen H, Lu B. AT-101, a pan-Bcl-2 inhibitor, leads to radiosensitization of non-small cell lung cancer. J Thorac Oncol. 2010;5(5):680-7.

89. Ready N, Karaseva NA, Orlov SV, Luft AV, Popovych O, Holmlund JT, et al. Double-blind, placebo-controlled, randomized phase 2 study of the proapoptotic agent AT-101 plus docetaxel, in second-line non-small cell lung cancer. J Thorac Oncol. 2011;6(4):781-5.

90. Shinohara ET, Gonzalez A, Massion PP, Chen H, Li M, Freyer AS, et al. Nuclear survivin predicts recurrence and poor survival in patients with resected nonsmall cell lung carcinoma. Cancer. 2005;103(8):1685-92.

91. Zhang LQ, Wang J, Jiang F, Xu L, Liu FY, Yin R. Prognostic value of survivin in patients with non-small cell lung carcinoma: a systematic review with meta-analysis. PLoS One. 2012;7(3):e34100.

92. Giaccone G, Zatloukal P, Roubec J, Floor K, Musil J, Kuta M, et al. Multicenter phase II trial of YM155, a small-molecule suppressor of survivin, in patients with advanced, refractory, non-small-cell lung cancer. J Clin Oncol. 2009;27(27):4481-6.

93. Liu GF, Zhao QG, Si L, Cao YG, Li GY, Wang LX. Effects of survivin interference RNA on non-small cell lung carcinoma. Clin Invest Med. 2009;32(6):E225.

94. Shinohara ET, Hallahan DE, Lu B. The Use of Antisense Oligonucleotides in Evaluating Survivin as a Therapeutic Target for Radiation Sensitization in Lung Cancer. Biol Proced Online. 2004;6:250-6.

95. Khan O, La Thangue NB. HDAC inhibitors in cancer biology: emerging mechanisms and clinical applications. Immunology and cell biology. 2012;90(1):85-94.

96. Tan J, Cang S, Ma Y, Petrillo RL, Liu D. Novel histone deacetylase inhibitors in clinical trials as anti-cancer agents. J Hematol Oncol. 2010;3:5.

97. Fulda S. Histone deacetylase (HDAC) inhibitors and regulation of TRAIL-induced apoptosis. Exp Cell Res. 2012;318(11):1208-12.

98. Dos Santos Ferreira AC, Fernandes RA, Kwee JK, Klumb CE. Histone deacetylase inhibitor potentiates chemotherapy-induced apoptosis through Bim upregulation in Burkitt's lymphoma cells. J Cancer Res Clin Oncol. 2012;138(2):317-25.

99. Kawano T, Akiyama M, Agawa-Ohta M, Mikami-Terao Y, Iwase S, Yanagisawa T, et al. Histone deacetylase inhibitors valproic acid and depsipeptide sensitize retinoblastoma cells to radiotherapy by increasing H2AX phosphorylation and p53 acetylation-phosphorylation. Int J Oncol. 2010;37(4):787-95.

100. Seo S-K, Jin H-O, Woo S-H, Kim Y-S, An S, Lee J-H, et al. Histone Deacetylase Inhibitors Sensitize Human Non-small Cell Lung Cancer Cells to Ionizing Radiation Through Acetyl p53-Mediated c-myc Down-Regulation. Journal of Thoracic Oncology. 2011;6(8):1313-9 10.097/JTO.0b013e318220caff.

101. Millward M, Price T, Townsend A, Sweeney C, Spencer A, Sukumaran S, et al. Phase 1 clinical trial of the novel proteasome inhibitor marizomib with the histone deacetylase inhibitor vorinostat in patients with melanoma, pancreatic and lung cancer based on in vitro assessments of the combination. Invest New Drugs. 2011.

102. Nahleh Z, Tfayli A, Najm A, El Sayed A, Nahle Z. Heat shock proteins in cancer: targeting the 'chaperones'. Future medicinal chemistry. 2012;4(7):927-35.

103. Whitesell L, Lin NU. HSP90 as a platform for the assembly of more effective cancer chemotherapy. Biochim Biophys Acta. 2012;1823(3):756-66.

104. Nowakowski GS, McCollum AK, Ames MM, Mandrekar SJ, Reid JM, Adjei AA, et al. A phase I trial of twice-weekly 17-allylamino-demethoxy-geldanamycin in patients with advanced cancer. Clin Cancer Res. 2006;12(20 Pt 1):6087-93.

105. Goetz MP, Toft DO, Ames MM, Erlichman C. The Hsp90 chaperone complex as a novel target for cancer therapy. Annals of oncology : official journal of the European Society for Medical Oncology / ESMO. 2003;14(8):1169-76.

106. Gorska M, Popowska U, Sielicka-Dudzin A, Kuban-Jankowska A, Sawczuk W, Knap N, et al.

Geldanamycin and its derivatives as Hsp90 inhibitors. Front Biosci. 2012;17:2269-77.

107. Zhou J, Giannakakou P. Targeting microtubules for cancer chemotherapy. Curr Med Chem Anticancer Agents. 2005;5(1):65-71.

108. Perez EA. Microtubule inhibitors: Differentiating tubulin-inhibiting agents based on mechanisms of action, clinical activity, and resistance. Mol Cancer Ther. 2009;8(8):2086-95.

109. Galan-Malo P, Vela L, Gonzalo O, Calvo-Sanjuan R, Gracia-Fleta L, Naval J, et al. Cell fate after mitotic arrest in different tumor cells is determined by the balance between slippage and apoptotic threshold. Toxicol Appl Pharmacol. 2012;258(3):384-93.

110. Brito DA, Rieder CL. Mitotic checkpoint slippage in humans occurs via cyclin B destruction in the presence of an active checkpoint. Curr Biol. 2006;16(12):1194-200.

111. Lee J, Kim JA, Margolis RL, Fotedar R. Substrate degradation by the anaphase promoting complex occurs during mitotic slippage. Cell Cycle. 2010;9(9):1792-801.

112. Schvartzman JM, Sotillo R, Benezra R. Mitotic chromosomal instability and cancer: mouse modelling of the human disease. Nat Rev Cancer. 2010;10(2):102-15.

113. Sak A, Stuschke M, Groneberg M, Kubler D, Pottgen C, Eberhardt WE. Inhibiting the Aurora B Kinase Potently Suppresses Repopulation During Fractionated Irradiation of Human Lung Cancer Cell Lines. Int J Radiat Oncol Biol Phys. 2012.

114. Huszar D, Theoclitou ME, Skolnik J, Herbst R. Kinesin motor proteins as targets for cancer therapy. Cancer Metastasis Rev. 2009;28(1-2):197-208.

115. Li JJ, Li SA. Mitotic kinases: the key to duplication, segregation, and cytokinesis errors, chromosomal instability, and oncogenesis. Pharmacol Ther. 2006;111(3):974-84.

116. Kollareddy M, Zheleva D, Dzubak P, Brahmkshatriya PS, Lepsik M, Hajduch M. Aurora kinase inhibitors: Progress towards the clinic. Invest New Drugs. 2012.

117. Murugan RN, Park JE, Kim EH, Shin SY, Cheong C, Lee KS, et al. Plk1-targeted small molecule inhibitors: molecular basis for their potency and specificity. Mol Cells. 2011;32(3):209-20.

118. Medema RH, Lin CC, Yang JC. Polo-like kinase 1 inhibitors and their potential role in anticancer therapy, with a focus on NSCLC. Clin Cancer Res. 2011;17(20):6459-66.

119. Kawata E, Ashihara E, Maekawa T. RNA interference against polo-like kinase-1 in advanced non-small cell lung cancers. J Clin Bioinforma. 2011;1(1):6.

120. Perpelescu M, Fukagawa T. The ABCs of CENPs. Chromosoma. 2011;120(5):425-46.

121. Putkey FR, Cramer T, Morphew MK, Silk AD, Johnson RS, McIntosh JR, et al. Unstable kinetochore-microtubule capture and chromosomal instability following deletion of CENP-E. Dev Cell. 2002;3(3):351-65.

122. Chung V, Heath EI, Schelman WR, Johnson BM, Kirby LC, Lynch KM, et al. First-time-in-human study of GSK923295, a novel antimitotic inhibitor of centromere-associated protein E (CENP-E), in patients with refractory cancer. Cancer Chemother Pharmacol. 2012;69(3):733-41.

123. Lock RB, Carol H, Morton CL, Keir ST, Reynolds CP, Kang MH, et al. Initial testing of the CENP-E inhibitor GSK923295A by the pediatric preclinical testing program. Pediatric blood & cancer. 2012;58(6):916-23.

124. Jackson JR, Patrick DR, Dar MM, Huang PS. Targeted anti-mitotic therapies: can we improve on tubulin agents? Nat Rev Cancer. 2007;7(2):107-17.

125. Saijo T, Ishii G, Ochiai A, Yoh K, Goto K, Nagai K, et al. Eg5 expression is closely correlated with the response of advanced non-small cell lung cancer to antimitotic agents combined with platinum chemotherapy. Lung Cancer. 2006;54(2):217-25.

126. Marra E, Palombo F, Ciliberto G, Aurisicchio L. Kinesin spindle protein SiRNA slows tumor progression. Journal of cellular physiology. 2013;228(1):58-64.

127. Sarli V, Giannis A. Targeting the kinesin spindle protein: basic principles and clinical implications. Clin Cancer Res. 2008;14(23):7583-7.

128. Jones R, Vuky J, Elliott T, Mead G, Arranz JA, Chester J, et al. Phase II study to assess the efficacy, safety and tolerability of the mitotic spindle kinesin inhibitor AZD4877 in patients with recurrent advanced urothelial cancer. Invest New Drugs. 2013.

129. Escobar M, Velez M, Belalcazar A, Santos ES, Raez LE. The role of proteasome inhibition in nonsmall cell lung cancer. Journal of biomedicine & biotechnology. 2011;2011:806506.

130. Frankland-Searby S, Bhaumik SR. The 26S proteasome complex: an attractive target for cancer therapy. Biochim Biophys Acta. 2012;1825(1):64-76.

131. Barbosa J, Nascimento AV, Faria J, Silva P, Bousbaa H. The spindle assembly checkpoint: perspectives in tumorigenesis and cancer therapy. Frontiers in Biology. 2011;6(2):147-55.

132. Silva P, Barbosa J, Nascimento AV, Faria J, Reis R, Bousbaa H. Monitoring the fidelity of mitotic chromosome segregation by the spindle assembly checkpoint. Cell proliferation. 2011;44(5):391-400.

133. Manchado E, Guillamot M, Malumbres M. Killing cells by targeting mitosis. Cell Death Differ. 2012;19(3):369-77.

134. Thompson SL, Bakhoum SF, Compton DA. Mechanisms of chromosomal instability. Curr Biol. 2010;20(6):R285-95.

135. Kaestner P, Aigner A, Bastians H. Therapeutic targeting of the mitotic spindle checkpoint through nanoparticle-mediated siRNA delivery inhibits tumor growth in vivo. Cancer Lett. 2011;304(2):128-36.

136. Colombo R, Caldarelli M, Mennecozzi M, Giorgini ML, Sola F, Cappella P, et al. Targeting the mitotic checkpoint for cancer therapy with NMS-P715, an inhibitor of MPS1 kinase. Cancer Res. 2010;70(24):10255-64.

137. Vermeulen K, Van Bockstaele DR, Berneman ZN. The cell cycle: a review of regulation, deregulation and therapeutic targets in cancer. Cell proliferation. 2003;36(3):131-49.

138. Sherr CJ, Roberts JM. Living with or without cyclins and cyclin-dependent kinases. Genes Dev. 2004;18(22):2699-711.

139. Deves M, Bourrat F. Transcriptional mechanisms of developmental cell cycle arrest: problems and models. Semin Cell Dev Biol. 2012;23(3):290-7.

140. Dorn JF, Maddox PS. Kinetochore dynamics: how protein dynamics affect chromosome segregation. Curr Opin Cell Biol. 2012;24(1):57-63.

141. Dong Y, Vanden Beldt KJ, Meng X, Khodjakov A, McEwen BF. The outer plate in vertebrate kinetochores is a flexible network with multiple microtubule interactions. Nat Cell Biol. 2007;9(5):516-22.

142. McIntosh JR, Grishchuk EL, Morphew MK, Efremov AK, Zhudenkov K, Volkov VA, et al. Fibrils connect microtubule tips with kinetochores: a mechanism to couple tubulin dynamics to chromosome motion. Cell. 2008;135(2):322-33.

143. Nigg EA. Mitotic kinases as regulators of cell division and its checkpoints. Nat Rev Mol Cell Biol. 2001;2(1):21-32.

144. McGowan CH. Regulation of the eukaryotic cell cycle. Prog Cell Cycle Res. 2003;5:1-4.

145. Rahal R, Amon A. Mitotic CDKs control the metaphase-anaphase transition and trigger spindle elongation. Genes Dev. 2008;22(11):1534-48.

146. de Medina-Redondo M, Meraldi P. The spindle assembly checkpoint: clock or domino? Results Probl Cell Differ. 2011;53:75-91.

147. Nezi L, Musacchio A. Sister chromatid tension and the spindle assembly checkpoint. Curr Opin Cell Biol. 2009;21(6):785-95.

148. Khodjakov A, Pines J. Centromere tension: a divisive issue. Nat Cell Biol. 2010;12(10):919-23.

149. Vader G, Maia AF, Lens SM. The chromosomal passenger complex and the spindle assembly checkpoint: kinetochore-microtubule error correction and beyond. Cell Div. 2008;3:10.

150. Musacchio A, Salmon ED. The spindle-assembly checkpoint in space and time. Nat Rev Mol Cell Biol. 2007;8(5):379-93.

151. Logarinho E, Bousbaa H. Kinetochore-microtubule interactions "in check" by Bub1, Bub3 and BubR1: The dual task of attaching and signalling. Cell Cycle. 2008;7(12):1763-8.

152. Liu ST, Chan GK, Hittle JC, Fujii G, Lees E, Yen TJ. Human MPS1 kinase is required for mitotic arrest induced by the loss of CENP-E from kinetochores. Mol Biol Cell. 2003;14(4):1638-51.

153. Fisk HA, Mattison CP, Winey M. A field guide to the Mps1 family of protein kinases. Cell Cycle. 2004;3(4):439-42.

154. Hewitt L, Tighe A, Santaguida S, White AM, Jones CD, Musacchio A, et al. Sustained Mps1 activity is required in mitosis to recruit O-Mad2 to the Mad1-C-Mad2 core complex. J Cell Biol. 2010;190(1):25-34.

155. Santaguida S, Tighe A, D'Alise AM, Taylor SS, Musacchio A. Dissecting the role of MPS1 in chromosome biorientation and the spindle checkpoint through the small molecule inhibitor reversine. J Cell Biol. 2010;190(1):73-87.

156. Lan W, Cleveland DW. A chemical tool box defines mitotic and interphase roles for Mps1 kinase. J Cell Biol. 2010;190(1):21-4.

157. Mapelli M, Massimiliano L, Santaguida S, Musacchio A. The Mad2 conformational dimer: structure and implications for the spindle assembly checkpoint. Cell. 2007;131(4):730-43.

158. Luo X, Yu H. Protein metamorphosis: the two-state behavior of Mad2. Structure. 2008;16(11):1616-25.

159. Tipton AR, Tipton M, Yen T, Liu ST. Closed MAD2 (C-MAD2) is selectively incorporated into the mitotic checkpoint complex (MCC). Cell Cycle. 2011;10(21):3740-50.

160. Campbell MS, Chan GK, Yen TJ. Mitotic checkpoint proteins HsMAD1 and HsMAD2 are associated with nuclear pore complexes in interphase. J Cell Sci. 2001;114(Pt 5):953-63.

161. De Antoni A, Pearson CG, Cimini D, Canman JC, Sala V, Nezi L, et al. The Mad1/Mad2 complex as a template for Mad2 activation in the spindle assembly checkpoint. Curr Biol. 2005;15(3):214-25.

162. Simonetta M, Manzoni R, Mosca R, Mapelli M, Massimiliano L, Vink M, et al. The influence of catalysis on mad2 activation dynamics. PLoS Biol. 2009;7(1):e10.

163. Fang G. Checkpoint protein BubR1 acts synergistically with Mad2 to inhibit anaphase-promoting complex. Mol Biol Cell. 2002;13(3):755-66.

164. Sudakin V. Purification of the mitotic checkpoint complex (MCC) and the anaphase promoting complex/cyclosome (APC/C) from HeLa cells. Cold Spring Harb Protoc. 2010;2010(6):pdb prot5449.

165. Bolanos-Garcia VM, Blundell TL. BUB1 and BUBR1: multifaceted kinases of the cell cycle. Trends Biochem Sci. 2011;36(3):141-50.

166. Elowe S. Bub1 and BubR1: at the interface between chromosome attachment and the spindle checkpoint. Mol Cell Biol. 2011;31(15):3085-93.

167. Williams GL, Roberts TM, Gjoerup OV. Bub1: escapades in a cellular world. Cell Cycle. 2007;6(14):1699-704.

168. Chan GK, Jablonski SA, Sudakin V, Hittle JC, Yen TJ. Human BUBR1 is a mitotic checkpoint kinase that monitors CENP-E functions at kinetochores and binds the cyclosome/APC. J Cell Biol. 1999;146(5):941-54.

169. Martinez-Exposito MJ, Kaplan KB, Copeland J, Sorger PK. Retention of the BUB3 checkpoint protein on lagging chromosomes. Proc Natl Acad Sci U S A. 1999;96(15):8493-8.

170. Logarinho E, Resende T, Torres C, Bousbaa H. The human spindle assembly checkpoint protein Bub3 is required for the establishment of efficient kinetochore-microtubule attachments. Mol Biol Cell. 2008;19(4):1798-813.

171. Emre D, Terracol R, Poncet A, Rahmani Z, Karess RE. A mitotic role for Mad1 beyond the spindle checkpoint. J Cell Sci. 2011;124(Pt 10):1664-71.

172. Marchetti F, Venkatachalam S. The multiple roles of Bub1 in chromosome segregation during mitosis and meiosis. Cell Cycle. 2010;9(1):58-63.

173. Westhorpe FG, Tighe A, Lara-Gonzalez P, Taylor SS. p31comet-mediated extraction of Mad2 from the MCC promotes efficient mitotic exit. J Cell Sci. 2011;124(Pt 22):3905-16.

174. Bader JR, Vaughan KT. Dynein at the kinetochore: Timing, Interactions and Functions. Semin Cell Dev Biol. 2010;21(3):269-75.

175. Mapelli M, Filipp FV, Rancati G, Massimiliano L, Nezi L, Stier G, et al. Determinants of conformational dimerization of Mad2 and its inhibition by p31comet. EMBO J. 2006;25(6):1273-84.

176. Reddy SK, Rape M, Margansky WA, Kirschner MW. Ubiquitination by the anaphase-promoting complex drives spindle checkpoint inactivation. Nature. 2007;446(7138):921-5.

177. Ma HT, Poon RY. Orderly inactivation of the key checkpoint protein mitotic arrest deficient 2 (MAD2) during mitotic progression. J Biol Chem. 2011;286(15):13052-9.

178. Stegmeier F, Rape M, Draviam VM, Nalepa G, Sowa ME, Ang XL, et al. Anaphase initiation is regulated by antagonistic ubiquitination and deubiquitination activities. Nature. 2007;446(7138):876-81.

179. Jia L, Li B, Warrington RT, Hao X, Wang S, Yu H. Defining pathways of spindle checkpoint silencing: functional redundancy between Cdc20 ubiquitination and p31(comet). Mol Biol Cell. 2011;22(22):4227-35.

180. Meadows JC, Shepperd LA, Vanoosthuyse V, Lancaster TC, Sochaj AM, Buttrick GJ, et al. Spindle checkpoint silencing requires association of PP1 to both Spc7 and kinesin-8 motors. Dev Cell. 2011;20(6):739-50.

181. Rosenberg JS, Cross FR, Funabiki H. KNL1/Spc105 recruits PP1 to silence the spindle assembly checkpoint. Curr Biol. 2011;21(11):942-7.

182. Chao WC, Kulkarni K, Zhang Z, Kong EH, Barford D. Structure of the mitotic checkpoint complex. Nature. 2012.

183. Lee AJ, Endesfelder D, Rowan AJ, Walther A, Birkbak NJ, Futreal PA, et al. Chromosomal instability confers intrinsic multidrug resistance. Cancer Res. 2011;71(5):1858-70.

184. Ozery-Flato M, Linhart C, Trakhtenbrot L, Izraeli S, Shamir R. Large-scale analysis of chromosomal aberrations in cancer karyotypes reveals two distinct paths to aneuploidy. Genome Biol. 2011;12(6):R61.

185. Mitelman F JBaMFE. Mitelman Database of Chromosome Aberrations and Gene Fusions in Cancer (2012) 2012. Available from: http://cgap.nci.nih.gov/Chromosomes/Mitelman.

186. Barbero JL. Sister chromatid cohesion control and aneuploidy. Cytogenet Genome Res. 2011;133(2-4):223-33.

187. Nicholson JM, Cimini D. How mitotic errors contribute to karyotypic diversity in cancer. Adv Cancer Res. 2011;112:43-75.

188. Kops GJ, Foltz DR, Cleveland DW. Lethality to human cancer cells through massive chromosome loss by inhibition of the mitotic checkpoint. Proc Natl Acad Sci U S A. 2004;101(23):8699-704.

189. Kops GJ, Weaver BA, Cleveland DW. On the road to cancer: aneuploidy and the mitotic checkpoint. Nat Rev Cancer. 2005;5(10):773-85.

190. Weaver BA, Cleveland DW. Does aneuploidy cause cancer? Curr Opin Cell Biol. 2006;18(6):658-67.

191. Michel LS, Liberal V, Chatterjee A, Kirchwegger R, Pasche B, Gerald W, et al. MAD2 haplo-insufficiency causes premature anaphase and chromosome instability in mammalian cells. Nature. 2001;409(6818):355-9.

192. Wang Q, Liu T, Fang Y, Xie S, Huang X, Mahmood R, et al. BUBR1 deficiency results in abnormal megakaryopoiesis. Blood. 2004;103(4):1278-85.

193. Iwanaga Y, Chi YH, Miyazato A, Sheleg S, Haller K, Peloponese JM, Jr., et al. Heterozygous deletion of mitotic arrest-deficient protein 1 (MAD1) increases the incidence of tumors in mice. Cancer Res. 2007;67(1):160-6.

194. Babu JR, Jeganathan KB, Baker DJ, Wu X, Kang-Decker N, van Deursen JM. Rae1 is an essential mitotic checkpoint regulator that cooperates with Bub3 to prevent chromosome missegregation. J Cell Biol. 2003;160(3):341-53.

195. Dai W, Wang Q, Liu T, Swamy M, Fang Y, Xie S, et al. Slippage of mitotic arrest and enhanced tumor development in mice with BubR1 haploinsufficiency. Cancer Res. 2004;64(2):440-5.

196. Schliekelman M, Cowley DO, O'Quinn R, Oliver TG, Lu L, Salmon ED, et al. Impaired Bub1 function in vivo compromises tension-dependent checkpoint function leading to aneuploidy and tumorigenesis. Cancer Res. 2009;69(1):45-54.

197. Matsuura S, Matsumoto Y, Morishima K, Izumi H, Matsumoto H, Ito E, et al. Monoallelic BUB1B mutations and defective mitotic-spindle checkpoint in seven families with premature chromatid separation (PCS) syndrome. Am J Med Genet A. 2006;140(4):358-67.

198. Yuan B, Xu Y, Woo JH, Wang Y, Bae YK, Yoon DS, et al. Increased expression of mitotic checkpoint genes in breast cancer cells with chromosomal instability. Clin Cancer Res. 2006;12(2):405-10.

199. Shin HJ, Baek KH, Jeon AH, Park MT, Lee SJ, Kang CM, et al. Dual roles of human BubR1, a mitotic checkpoint kinase, in the monitoring of chromosomal instability. Cancer Cell. 2003;4(6):483-97.

200. Wei JH, Chou YF, Ou YH, Yeh YH, Tyan SW, Sun TP, et al. TTK/hMps1 participates in the regulation of DNA damage checkpoint response by phosphorylating CHK2 on threonine 68. J Biol Chem. 2005;280(9):7748-57.

201. Gordon DJ, Resio B, Pellman D. Causes and consequences of aneuploidy in cancer. Nat Rev Genet. 2012;13(3):189-203.

202. Thompson SL, Compton DA. Examining the link between chromosomal instability and aneuploidy in human cells. J Cell Biol. 2008;180(4):665-72.

203. Janssen A, Kops GJ, Medema RH. Elevating the frequency of chromosome mis-segregation as a strategy to kill tumor cells. Proc Natl Acad Sci U S A. 2009;106(45):19108-13.

204. Mao Y, Desai A, Cleveland DW. Microtubule capture by CENP-E silences BubR1-dependent mitotic checkpoint signaling. J Cell Biol. 2005;170(6):873-80.

205. Schafer-Hales K, Iaconelli J, Snyder JP, Prussia A, Nettles JH, El-Naggar A, et al. Farnesyl transferase inhibitors impair chromosomal maintenance in cell lines and human tumors by compromising CENP-E and CENP-F function. Mol Cancer Ther. 2007;6(4):1317-28.

206. Maiato H, Logarinho E. Motor-dependent and -independent roles of CENP-E at kinetochores: the cautionary tale of UA62784. Chem Biol. 2011;18(6):679-80.

207. Ferenz NP, Gable A, Wadsworth P. Mitotic functions of kinesin-5. Semin Cell Dev Biol. 2010;21(3):255-9.

208. Infante JR, Kurzrock R, Spratlin J, Burris HA, Eckhardt SG, Li J, et al. A Phase I study to assess the safety, tolerability, and pharmacokinetics of AZD4877, an intravenous Eg5 inhibitor in patients with advanced solid tumors. Cancer Chemother Pharmacol. 2012;69(1):165-72.

209. Maresca TJ. Cell division: aurora B illuminates a checkpoint pathway. Curr Biol. 2011;21(14):R557-9.

210. Katayama H, Sen S. Aurora kinase inhibitors as anticancer molecules. Biochim Biophys Acta. 2010;1799(10-12):829-39.

211. Kwiatkowski N, Jelluma N, Filippakopoulos P, Soundararajan M, Manak MS, Kwon M, et al. Small-molecule kinase inhibitors provide insight into Mps1 cell cycle function. Nat Chem Biol. 2010;6(5):359-68.

212. Huang J, Sheung J, Dong G, Coquilla C, Daniel-Issakani S, Payan DG. High-throughput screening for inhibitors of the e3 ubiquitin ligase APC. Methods Enzymol. 2005;399:740-54.

213. Zeng X, Sigoillot F, Gaur S, Choi S, Pfaff KL, Oh DC, et al. Pharmacologic inhibition of the anaphase-promoting complex induces a spindle checkpoint-dependent mitotic arrest in the absence of spindle damage. Cancer Cell. 2010;18(4):382-95.

214. Huang HC, Shi J, Orth JD, Mitchison TJ. Evidence that mitotic exit is a better cancer therapeutic target than spindle assembly. Cancer Cell. 2009;16(4):347-58.

215. Manchado E, Guillamot M, de Carcer G, Eguren M, Trickey M, Garcia-Higuera I, et al. Targeting mitotic exit leads to tumor regression in vivo: Modulation by Cdk1, Mastl, and the PP2A/B55alpha,delta phosphatase. Cancer Cell. 2010;18(6):641-54.

216. Yamamoto Y, Matsuyama H, Chochi Y, Okuda M, Kawauchi S, Inoue R, et al. Overexpression of BUBR1 is associated with chromosomal instability in bladder cancer. Cancer Genet Cytogenet. 2007;174(1):42-7.

217. Furlong F, Fitzpatrick P, O'Toole S, Phelan S, McGrogan B, Maguire A, et al. Low MAD2 expression levels associate with reduced progression-free survival in patients with high-grade serous epithelial ovarian cancer. J Pathol. 2012;226(5):746-55.

218. Kato T, Daigo Y, Aragaki M, Ishikawa K, Sato M, Kondo S, et al. Overexpression of MAD2

predicts clinical outcome in primary lung cancer patients. Lung Cancer. 2011;74(1):124-31.

219. Hao X, Zhou Z, Ye S, Zhou T, Lu Y, Ma D, et al. Effect of Mad2 on paclitaxel-induced cell death in ovarian cancer cells. J Huazhong Univ Sci Technolog Med Sci. 2010;30(5):620-5.

220. Xu HZ, Huang Y, Wu YL, Zhao Y, Xiao WL, Lin QS, et al. Pharicin A, a novel natural ent-kaurene diterpenoid, induces mitotic arrest and mitotic catastrophe of cancer cells by interfering with BubR1 function. Cell Cycle. 2010;9(14):2897-907.

221. Michel L, Diaz-Rodriguez E, Narayan G, Hernando E, Murty VV, Benezra R. Complete loss of the tumor suppressor MAD2 causes premature cyclin B degradation and mitotic failure in human somatic cells. Proc Natl Acad Sci U S A. 2004;101(13):4459-64.

222. Park SY, Kim S, Cho H, Kwon SH, Chae S, Kang D, et al. Depletion of BubR1 promotes premature centrosomal localization of cyclin B1 and accelerates mitotic entry. Cell Cycle. 2009;8(11):1754-64.

223. Obbard DJ, Gordon KH, Buck AH, Jiggins FM. The evolution of RNAi as a defence against viruses and transposable elements. Philos Trans R Soc Lond B Biol Sci. 2009;364(1513):99-115.

224. Seyhan AA. RNAi: a potential new class of therapeutic for human genetic disease. Hum Genet. 2011;130(5):583-605.

225. Ghildiyal M, Zamore PD. Small silencing RNAs: an expanding universe. Nat Rev Genet. 2009;10(2):94-108.

226. Kim DH, Behlke MA, Rose SD, Chang MS, Choi S, Rossi JJ. Synthetic dsRNA Dicer substrates enhance RNAi potency and efficacy. Nat Biotechnol. 2005;23(2):222-6.

227. Hammond SM. Dicing and slicing: the core machinery of the RNA interference pathway. FEBS Lett. 2005;579(26):5822-9.

228. Pratt AJ, MacRae IJ. The RNA-induced silencing complex: a versatile gene-silencing machine. J Biol Chem. 2009;284(27):17897-901.

229. Jinek M, Doudna JA. A three-dimensional view of the molecular machinery of RNA interference. Nature. 2009;457(7228):405-12.

230. Kole R, Krainer AR, Altman S. RNA therapeutics: beyond RNA interference and antisense oligonucleotides. Nat Rev Drug Discov. 2012;11(2):125-40.

231. Watts JK, Deleavey GF, Damha MJ. Chemically modified siRNA: tools and applications. Drug discovery today. 2008;13(19-20):842-55.

232. Laskin JJ, Nicholas G, Lee C, Gitlitz B, Vincent M, Cormier Y, et al. Phase I/II trial of custirsen (OGX-011), an inhibitor of clusterin, in combination with a gemcitabine and platinum regimen in patients with previously untreated advanced non-small cell lung cancer. J Thorac Oncol. 2012;7(3):579-86.

233. Wang J, Lu Z, Wientjes MG, Au JL. Delivery of siRNA therapeutics: barriers and carriers. AAPS J. 2010;12(4):492-503.

234. Rossi JJ. Expression strategies for short hairpin RNA interference triggers. Hum Gene Ther. 2008;19(4):313-7.

235. Sliva K, Schnierle BS. Selective gene silencing by viral delivery of short hairpin RNA. Virol J. 2010;7:248.

236. Jackson AL, Linsley PS. Recognizing and avoiding siRNA off-target effects for target identification and therapeutic application. Nat Rev Drug Discov. 2010;9(1):57-67.

237. Cullen LM, Arndt GM. Genome-wide screening for gene function using RNAi in mammalian cells. Immunology and cell biology. 2005;83(3):217-23.

238. Lares MR, Rossi JJ, Ouellet DL. RNAi and small interfering RNAs in human disease therapeutic applications. Trends Biotechnol. 2010;28(11):570-9.

239. Bora RS, Gupta D, Mukkur TK, Saini KS. RNA interference therapeutics for cancer: Challenges and opportunities (Review). Mol Med Report. 2012;6(1):9-15.

240. Chen SH, Zhaori G. Potential clinical applications of siRNA technique: benefits and limitations. Eur J Clin Invest. 2011;41(2):221-32.

241. Petrocca F, Lieberman J. Promise and challenge of RNA interference-based therapy for cancer. J Clin Oncol. 2011;29(6):747-54.

242. Roschke V, Sosnovtseva S, Ward CD, Hong JS, Smith R, Albert V, et al. BLyS and APRIL form biologically active heterotrimers that are expressed in patients with systemic immune-based rheumatic diseases. J Immunol. 2002;169(8):4314-21.

243. Wang J, Ding W, Sun B, Jing R, Huang H, Shi G, et al. Targeting of colorectal cancer growth, metastasis, and anti-apoptosis in BALB/c nude mice via APRIL siRNA. Mol Cell Biochem. 2012;363(1-2):1-10.

244. Garcia R, Jove R. Activation of STAT transcription factors in oncogenic tyrosine kinase signaling. J Biomed Sci. 1998;5(2):79-85.

245. Corcoran RB, Contino G, Deshpande V, Tzatsos A, Conrad C, Benes CH, et al. STAT3 plays a critical role in KRAS-induced pancreatic tumorigenesis. Cancer Res. 2011;71(14):5020-9.

246. Alshamsan A, Hamdy S, Samuel J, El-Kadi AO, Lavasanifar A, Uludag H. The induction of tumor apoptosis in B16 melanoma following STAT3 siRNA delivery with a lipid-substituted polyethylenimine. Biomaterials. 2010;31(6):1420-8.

247. Zhang Q, Wang HY, Woetmann A, Raghunath PN, Odum N, Wasik MA. STAT3 induces transcription of the DNA methyltransferase 1 gene (DNMT1) in malignant T lymphocytes. Blood. 2006;108(3):1058-64.

248. Yang CL, Liu YY, Ma YG, Xue YX, Liu DG, Ren Y, et al. Curcumin Blocks Small Cell Lung Cancer Cells Migration, Invasion, Angiogenesis, Cell Cycle and Neoplasia through Janus Kinase-STAT3 Signalling Pathway. PLoS One. 2012;7(5):e37960.

249. Seo JM, Park S, Kim JH. Leukotriene B4 receptor-2 promotes invasiveness and metastasis of ovarian cancer cells through signal transducer and activator of transcription 3 (STAT3)-dependent up-regulation of matrix metalloproteinase 2. J Biol Chem. 2012;287(17):13840-9.

250. Yang Z, Cai JH, Xie SJ, Li GX, Song WQ, Yan QH, et al. Therapeutic effects of signal transducer and activator of transcription 3 siRNA on human breast cancer in xenograft mice. Chin Med J (Engl). 2011;124(12):1854-61.

251. Wu Q, Yang Z, Nie Y, Shi Y, Fan D. Multi-drug resistance in cancer chemotherapeutics: Mechanisms and lab approaches. Cancer Lett. 2014.

252. Li JM, Wang YY, Zhao MX, Tan CP, Li YQ, Le XY, et al. Multifunctional QD-based co-delivery of siRNA and doxorubicin to HeLa cells for reversal of multidrug resistance and real-time tracking. Biomaterials. 2012;33(9):2780-90.

253. Chen AM, Zhang M, Wei D, Stueber D, Taratula O, Minko T, et al. Co-delivery of doxorubicin and Bcl-2 siRNA by mesoporous silica nanoparticles enhances the efficacy of chemotherapy in multidrug-resistant cancer cells. Small. 2009;5(23):2673-7.

254. Wang H, Fan L, Xia X, Rao Y, Ma Q, Yang J, et al. Silencing Wnt2B by siRNA Interference Inhibits Metastasis and Enhances Chemotherapy Sensitivity in Ovarian Cancer. Int J Gynecol Cancer. 2012;22(5):755-61.

255. Adams JM, Cory S. Bcl-2-regulated apoptosis: mechanism and therapeutic potential. Curr Opin Immunol. 2007;19(5):488-96.

256. Schafer M, Farwanah H, Willrodt AH, Huebner AJ, Sandhoff K, Roop D, et al. Nrf2 links epidermal barrier function with antioxidant defense. EMBO Mol Med. 2012;4(5):364-79.

257. Kensler TW, Wakabayashi N. Nrf2: friend or foe for chemoprevention? Carcinogenesis. 2010;31(1):90-9.

258. Ma X, Zhang J, Liu S, Huang Y, Chen B, Wang D. Nrf2 knockdown by shRNA inhibits tumor growth and increases efficacy of chemotherapy in cervical cancer. Cancer Chemother Pharmacol. 2012;69(2):485-94.

259. Strumberg D, Schultheis B, Traugott U, Vank C, Santel A, Keil O, et al. Phase I clinical development of Atu027, a siRNA formulation targeting PKN3 in patients with advanced solid tumors. Int J Clin Pharmacol Ther. 2012;50(1):76-8.

260. Santel A, Aleku M, Roder N, Mopert K, Durieux B, Janke O, et al. Atu027 prevents pulmonary metastasis in experimental and spontaneous mouse metastasis models. Clin Cancer Res. 2010;16(22):5469-80.

261. Davis ME, Zuckerman JE, Choi CH, Seligson D, Tolcher A, Alabi CA, et al. Evidence of RNAi in humans from systemically administered siRNA via targeted nanoparticles. Nature. 2010;464(7291):1067-70.

262. Heidel JD, Liu JY, Yen Y, Zhou B, Heale BS, Rossi JJ, et al. Potent siRNA inhibitors of ribonucleotide reductase subunit RRM2 reduce cell proliferation in vitro and in vivo. Clin Cancer Res. 2007;13(7):2207-15.

263. Giacca M, Zacchigna S. VEGF gene therapy: therapeutic angiogenesis in the clinic and beyond. Gene Ther. 2012;19(6):622-9.

264. Sarli V, Giannis A. Targeting the Kinesin Spindle Protein: Basic Principles and Clinical Implications. Clinical Cancer Research. 2008;14(23):7583-7.

265. Raskopf E, Vogt A, Sauerbruch T, Schmitz V. siRNA targeting VEGF inhibits hepatocellular carcinoma growth and tumor angiogenesis in vivo. J Hepatol. 2008;49(6):977-84.

266. Pai SI, Lin YY, Macaes B, Meneshian A, Hung CF, Wu TC. Prospects of RNA interference therapy for cancer. Gene Ther. 2006;13(6):464-77.

267. Burnett JC, Rossi JJ. RNA-based therapeutics: current progress and future prospects. Chem Biol. 2012;19(1):60-71.

268. Ragelle H, Vandermeulen G, Preat V. Chitosan-based siRNA delivery systems. Journal of controlled release : official journal of the Controlled Release Society. 2013;172(1):207-18.

269. Andrade F, Antunes F, Nascimento AV, da Silva SB, das Neves J, Ferreira D, et al. Chitosan formulations as carriers for therapeutic proteins. Current drug discovery technologies. 2011;8(3):157-72.

270. Rinaudo M. Chitin and chitosan: properties and applications. Progress in polymer science. 2006;31(7):603-32.

271. Sarmento B, das Neves J. Chitosan-based systems for biopharmaceuticals: delivery, targeting and polymer therapeutics: John Wiley & Sons; 2012.

272. Wang JJ, Zeng ZW, Xiao RZ, Xie T, Zhou GL, Zhan XR, et al. Recent advances of chitosan nanoparticles as drug carriers. Int J Nanomedicine. 2011;6:765-74.

273. Lai WF, Lin MC. Nucleic acid delivery with chitosan and its derivatives. Journal of controlled

release : official journal of the Controlled Release Society. 2009;134(3):158-68.

274. Kean T, Thanou M. Biodegradation, biodistribution and toxicity of chitosan. Adv Drug Deliv Rev. 2010;62(1):3-11.

275. Cheung RC, Ng TB, Wong JH, Chan WY. Chitosan: An Update on Potential Biomedical and Pharmaceutical Applications. Mar Drugs. 2015;13(8):5156-86.

276. Chandy T, Sharma CP. Chitosan--as a biomaterial. Biomater Artif Cells Artif Organs. 1990;18(1):1-24.

277. Yilmaz E. Chitosan: a versatile biomaterial. Adv Exp Med Biol. 2004;553:59-68.

278. Mao S, Sun W, Kissel T. Chitosan-based formulations for delivery of DNA and siRNA. Adv Drug Deliv Rev. 2010;62(1):12-27.

279. Fernandes JC, Qiu X, Winnik FM, Benderdour M, Zhang X, Dai K, et al. Low molecular weight chitosan conjugated with folate for siRNA delivery in vitro: optimization studies. Int J Nanomedicine. 2012;7:5833-45.

280. Alameh M, Dejesus D, Jean M, Darras V, Thibault M, Lavertu M, et al. Low molecular weight chitosan nanoparticulate system at low N:P ratio for nontoxic polynucleotide delivery. Int J Nanomedicine. 2012;7:1399-414.

281. Prabaharan M. Chitosan-based nanoparticles for tumor-targeted drug delivery. Int J Biol Macromol. 2015;72:1313-22.

282. Nascimento AV, Singh A, Bousbaa H, Ferreira D, Sarmento B, Amiji MM. Combinatorial-Designed Epidermal Growth Factor Receptor-Targeted Chitosan Nanoparticles for Encapsulation and Delivery of Lipid-Modified Platinum Derivatives in Wild-Type and Resistant Non-Small-Cell Lung Cancer Cells. Mol Pharm. 2015;12(12):4466-77.

283. Mao Z, Ma L, Yan J, Yan M, Gao C, Shen J. The gene transfection efficiency of thermoresponsive N, N, N-trimethyl chitosan chloride-g-poly (N-isopropylacrylamide) copolymer. Biomaterials. 2007;28(30):4488-500.

284. Corbet C, Ragelle H, Pourcelle V, Vanvarenberg K, Marchand-Brynaert J, Préat V, et al. Delivery of siRNA targeting tumor metabolism using non-covalent PEGylated chitosan nanoparticles: Identification of an optimal combination of ligand structure, linker and grafting method. Journal of Controlled Release. 2016;223:53-63.

285. Scheeren LE, Nogueira DR, Macedo LB, Vinardell MP, Mitjans M, Infante MR, et al. PEGylated and poloxamer-modified chitosan nanoparticles incorporating a lysine-based surfactant for pH-triggered doxorubicin release. Colloids and Surfaces B: Biointerfaces. 2016;138:117-27.

286. Gill KK, Kaddoumi A, Nazzal S. Mixed micelles of PEG(2000)-DSPE and vitamin-E TPGS for concurrent delivery of paclitaxel and parthenolide: enhanced chemosenstization and antitumor efficacy against non-small cell lung cancer (NSCLC) cell lines. European journal of pharmaceutical sciences : official journal of the European Federation for Pharmaceutical Sciences. 2012;46(1-2):64-71.

287. Maya S, Kumar LG, Sarmento B, Rejinold NS, Menon D, Nair SV, et al. Cetuximab conjugated O-carboxymethyl chitosan nanoparticles for targeting EGFR overexpressing cancer cells. Carbohydrate polymers. 2013;93(2):661-9.

288. Nascimento AV, Singh A, Bousbaa H, Ferreira D, Sarmento B, Amiji MM. Mad2 checkpoint gene silencing using epidermal growth factor receptor-targeted chitosan nanoparticles in non-small cell lung cancer model. Mol Pharm. 2014;11(10):3515-27.

289. Zhao Y, Lu H, Yan A, Yang Y, Meng Q, Sun L, et al. ABCC3 as a marker for multidrug resistance in non-small cell lung cancer. Scientific reports. 2013;3:3120.

290. Nascimento AV, Bousbaa H, Ferreira D, Sarmento B. Non-small Cell Lung Carcinoma: An Overview on Targeted Therapy. Current drug targets. 2014.

291. Saad M, Garbuzenko OB, Minko T. Co-delivery of siRNA and an anticancer drug for treatment of multidrug-resistant cancer. Nanomedicine (Lond). 2008;3(6):761-76.

292. Ashihara E, Kawata E, Maekawa T. Future prospect of RNA interference for cancer therapies. Current drug targets. 2010;11(3):345-60.

293. Bora RS, Gupta D, Mukkur TK, Saini KS. RNA interference therapeutics for cancer: challenges and opportunities (review). Molecular medicine reports. 2012;6(1):9-15.

294. Kim DH, Rossi JJ. Strategies for silencing human disease using RNA interference. Nature reviews Genetics. 2007;8(3):173-84.

295. Sotillo R, Hernando E, Diaz-Rodriguez E, Teruya-Feldstein J, Cordon-Cardo C, Lowe SW, et al. Mad2 overexpression promotes aneuploidy and tumorigenesis in mice. Cancer cell. 2007;11(1):9-23.

296. Choi JW, Kim Y, Lee JH, Kim YS. High expression of spindle assembly checkpoint proteins CDC20 and MAD2 is associated with poor prognosis in urothelial bladder cancer. Virchows Archiv : an international journal of pathology. 2013;463(5):681-7.

297. Yu L, Liu S, Guo W, Zhang B, Liang Y, Feng Q. Upregulation of Mad2 facilitates in vivo and in vitro osteosarcoma progression. Oncology reports. 2012;28(6):2170-6.

298. Wang L, Yin F, Du Y, Chen B, Liang S, Zhang Y, et al. Depression of MAD2 inhibits apoptosis and increases proliferation and multidrug resistance in gastric cancer cells by regulating the

activation of phosphorylated survivin. Tumour biology : the journal of the International Society for Oncodevelopmental Biology and Medicine. 2010;31(3):225-32.

299. Fung MK, Cheung HW, Wong HL, Yuen HF, Ling MT, Chan KW, et al. MAD2 expression and its significance in mitotic checkpoint control in testicular germ cell tumour. Biochimica et biophysica acta. 2007;1773(6):821-32.

300. Cheung HW, Jin DY, Ling MT, Wong YC, Wang Q, Tsao SW, et al. Mitotic arrest deficient 2 expression induces chemosensitization to a DNA-damaging agent, cisplatin, in nasopharyngeal carcinoma cells. Cancer research. 2005;65(4):1450-8.

301. Aigner A. Applications of RNA interference: current state and prospects for siRNA-based strategies in vivo. Applied microbiology and biotechnology. 2007;76(1):9-21.

302. Ganesh S, Iyer AK, Morrissey DV, Amiji MM. Hyaluronic acid based self-assembling nanosystems for CD44 target mediated siRNA delivery to solid tumors. Biomaterials. 2013;34(13):3489-502.

303. Ganesh S, Iyer AK, Gattacceca F, Morrissey DV, Amiji MM. In vivo biodistribution of siRNA and cisplatin administered using CD44-targeted hyaluronic acid nanoparticles. Journal of controlled release : official journal of the Controlled Release Society. 2013;172(3):699-706.

304. Ganesh S, Iyer AK, Weiler J, Morrissey DV, Amiji MM. Combination of siRNA-directed Gene Silencing With Cisplatin Reverses Drug Resistance in Human Non-small Cell Lung Cancer. Molecular therapy Nucleic acids. 2013;2:e110.

305. Jean M, Alameh M, De Jesus D, Thibault M, Lavertu M, Darras V, et al. Chitosan-based therapeutic nanoparticles for combination gene therapy and gene silencing of in vitro cell lines relevant to type 2 diabetes. European journal of pharmaceutical sciences : official journal of the European Federation for Pharmaceutical Sciences. 2012;45(1-2):138-49.

306. Jean M, Smaoui F, Lavertu M, Methot S, Bouhdoud L, Buschmann MD, et al. Chitosan-plasmid nanoparticle formulations for IM and SC delivery of recombinant FGF-2 and PDGF-BB or generation of antibodies. Gene therapy. 2009;16(9):1097-110.

307. Koppolu BP, Smith SG, Ravindranathan S, Jayanthi S, Suresh Kumar TK, Zaharoff DA. Controlling chitosan-based encapsulation for protein and vaccine delivery. Biomaterials. 2014;35(14):4382-9.

308. Scherliess R, Buske S, Young K, Weber B, Rades T, Hook S. In vivo evaluation of chitosan as an adjuvant in subcutaneous vaccine formulations. Vaccine. 2013;31(42):4812-9.

309. Agnihotri SA, Mallikarjuna NN, Aminabhavi TM. Recent advances on chitosan-based micro- and nanoparticles in drug delivery. Journal of controlled release : official journal of the Controlled Release Society. 2004;100(1):5-28.

310. Park JH, Saravanakumar G, Kim K, Kwon IC. Targeted delivery of low molecular drugs using chitosan and its derivatives. Advanced drug delivery reviews. 2010;62(1):28-41.

311. Schafer A, Pahnke A, Schaffert D, van Weerden WM, de Ridder CM, Rodl W, et al. Disconnecting the yin and yang relation of epidermal growth factor receptor (EGFR)-mediated delivery: a fully synthetic, EGFR-targeted gene transfer system avoiding receptor activation. Human gene therapy. 2011;22(12):1463-73.

312. Milane L, Duan ZF, Amiji M. Pharmacokinetics and biodistribution of lonidamine/paclitaxel loaded, EGFR-targeted nanoparticles in an orthotopic animal model of multi-drug resistant breast cancer. Nanomedicine : nanotechnology, biology, and medicine. 2011;7(4):435-44.

313. Milane L, Duan Z, Amiji M. Development of EGFR-targeted polymer blend nanocarriers for combination paclitaxel/lonidamine delivery to treat multi-drug resistance in human breast and ovarian tumor cells. Molecular pharmaceutics. 2011;8(1):185-203.

314. Xu J, Singh A, Amiji MM. Redox-responsive targeted gelatin nanoparticles for delivery of combination wt-p53 expressing plasmid DNA and gemcitabine in the treatment of pancreatic cancer. BMC cancer. 2014;14:75.

315. Ganta S, Singh A, Patel NR, Cacaccio J, Rawal YH, Davis BJ, et al. Development of EGFR-Targeted Nanoemulsion for Imaging and Novel Platinum Therapy of Ovarian Cancer. Pharmaceutical research. 2014.

316. Milane L, Duan Z, Amiji M. Therapeutic efficacy and safety of paclitaxel/lonidamine loaded EGFR-targeted nanoparticles for the treatment of multi-drug resistant cancer. PLoS One. 2011;6(9):e24075.

317. Xu J, Gattacceca F, Amiji M. Biodistribution and pharmacokinetics of EGFR-targeted thiolated gelatin nanoparticles following systemic administration in pancreatic tumor-bearing mice. Molecular pharmaceutics. 2013;10(5):2031-44.

318. Li Z, Zhao R, Wu X, Sun Y, Yao M, Li J, et al. Identification and characterization of a novel peptide ligand of epidermal growth factor receptor for targeted delivery of therapeutics. FASEB journal : official publication of the Federation of American Societies for Experimental Biology. 2005;19(14):1978-85.

319. Malmo J, Sandvig A, Varum KM, Strand SP. Nanoparticle mediated P-glycoprotein silencing for improved drug delivery across the blood-brain barrier: a siRNA-chitosan approach. PloS one. 2013;8(1):e54182.

320. Fan Z, Lu Y, Wu X, Mendelsohn J. Antibody-induced epidermal growth factor receptor dimerization mediates inhibition of autocrine proliferation of A431 squamous carcinoma cells. The Journal of biological chemistry. 1994;269(44):27595-602.

321. Maya S, Sarmento B, Lakshmanan VK, Menon D, Seabra V, Jayakumar R. Chitosan cross-linked docetaxel loaded EGF receptor targeted nanoparticles for lung cancer cells. International journal of biological macromolecules. 2014.

322. Howard KA, Rahbek UL, Liu X, Damgaard CK, Glud SZ, Andersen MO, et al. RNA interference in vitro and in vivo using a novel chitosan/siRNA nanoparticle system. Molecular therapy : the journal of the American Society of Gene Therapy. 2006;14(4):476-84.

323. Huang M, Khor E, Lim LY. Uptake and cytotoxicity of chitosan molecules and nanoparticles: effects of molecular weight and degree of deacetylation. Pharmaceutical research. 2004;21(2):344-53.

324. Hirsch FR, Scagliotti GV, Langer CJ, Varella-Garcia M, Franklin WA. Epidermal growth factor family of receptors in preneoplasia and lung cancer: perspectives for targeted therapies. Lung Cancer. 2003;41 Suppl 1:S29-42.

325. Scagliotti GV, Selvaggi G, Novello S, Hirsch FR. The biology of epidermal growth factor receptor in lung cancer. Clinical cancer research : an official journal of the American Association for Cancer Research. 2004;10(12 Pt 2):4227s-32s.

326. Kurai J, Chikumi H, Hashimoto K, Yamaguchi K, Yamasaki A, Sako T, et al. Antibody-dependent cellular cytotoxicity mediated by cetuximab against lung cancer cell lines. Clinical cancer research : an official journal of the American Association for Cancer Research. 2007;13(5):1552-61.

327. Proske D, Blank M, Buhmann R, Resch A. Aptamers--basic research, drug development, and clinical applications. Applied microbiology and biotechnology. 2005;69(4):367-74.

328. Prabha S, Zhou WZ, Panyam J, Labhasetwar V. Size-dependency of nanoparticle-mediated gene transfection: studies with fractionated nanoparticles. International journal of pharmaceutics. 2002;244(1-2):105-15.

329. Langlois MA, Boniface C, Wang G, Alluin J, Salvaterra PM, Puymirat J, et al. Cytoplasmic and nuclear retained DMPK mRNAs are targets for RNA interference in myotonic dystrophy cells. The Journal of biological chemistry. 2005;280(17):16949-54.

330. Robb GB, Brown KM, Khurana J, Rana TM. Specific and potent RNAi in the nucleus of human cells. Nature structural & molecular biology. 2005;12(2):133-7.

331. Berezhna SY, Supekova L, Supek F, Schultz PG, Deniz AA. siRNA in human cells selectively localizes to target RNA sites. Proceedings of the National Academy of Sciences of the United States of America. 2006;103(20):7682-7.

332. Guang S, Bochner AF, Pavelec DM, Burkhart KB, Harding S, Lachowiec J, et al. An Argonaute transports siRNAs from the cytoplasm to the nucleus. Science. 2008;321(5888):537-41.

333. Liu X, Howard KA, Dong M, Andersen MO, Rahbek UL, Johnsen MG, et al. The influence of polymeric properties on chitosan/siRNA nanoparticle formulation and gene silencing. Biomaterials. 2007;28(6):1280-8.

334. Xu D, McCarty D, Fernandes A, Fisher M, Samulski RJ, Juliano RL. Delivery of MDR1 small interfering RNA by self-complementary recombinant adeno-associated virus vector. Molecular therapy : the journal of the American Society of Gene Therapy. 2005;11(4):523-30.

335. Lee SM. Is EGFR expression important in non-small cell lung cancer? Thorax. 2006;61(2):98-9.

336. Siegel R, Ma J, Zou Z, Jemal A. Cancer statistics, 2014. CA: A Cancer Journal for Clinicians. 2014;64(1):9-29.

337. Islam KM, Jiang X, Anggondowati T, Lin G, Ganti AK. Comorbidity and Survival in Lung Cancer Patients. Cancer Epidemiology, Biomarkers & Prevention. 2015;24(7):1079-85.

338. Chen J, Solomides C, Parekh H, Simpkins F, Simpkins H. Cisplatin resistance in human cervical, ovarian and lung cancer cells. Cancer Chemotherapy and Pharmacology. 2015;75(6):1217-27.

339. Ganguly A, Cabral F. New insights into mechanisms of resistance to microtubule inhibitors. Biochimica et Biophysica Acta. 2011;1816(2):164-71.

340. Rivera E, Cianfrocca M. Overview of neuropathy associated with taxanes for the treatment of metastatic breast cancer. Cancer Chemotherapy Pharmacology. 2015;75(4):659-70.

341. Swain SM, Arezzo JC. Neuropathy associated with microtubule inhibitors: diagnosis, incidence, and management. Clinical Advances in Hematology and Oncology 2008;6(6):455-67.

342. Huang M, Shen A, Ding J, Geng M. Molecularly targeted cancer therapy: some lessons from the past decade. Trends in Pharmacological Sciences. 2014;35(1):41-50.

343. Silva P, Barbosa J, Nascimento AV, Faria J, Reis R, Bousbaa H. Monitoring the fidelity of mitotic chromosome segregation by the spindle assembly checkpoint. Cell Proliferation. 2011;44(5):391-400.

344. Teixeira JH, Silva P, Faria J, Ferreira I, Duarte P, Delgado ML, et al. Clinicopathologic significance of BubR1 and Mad2 overexpression in oral cancer. Oral Diseases. 2015;21(6):713-20.

345. Kim Y, Choi JW, Lee JH, Kim YS. MAD2 and CDC20 are upregulated in high-grade squamous intraepithelial lesions and squamous cell carcinomas of the uterine cervix. International Journal of Gynecological Pathology. 2014;33(5):517-23.

346. Choi JW, Kim Y, Lee JH, Kim YS. High expression of spindle assembly checkpoint proteins CDC20 and MAD2 is associated with poor prognosis in urothelial bladder cancer. Virchows Archiv. 2013;463(5):681-7.

347. Nascimento AV, Singh A, Bousbaa H, Ferreira D, Sarmento B, Amiji MM. Mad2 checkpoint gene silencing using epidermal growth factor receptor-targeted chitosan nanoparticles in non-small cell lung cancer model. Molecular pharmaceutics. 2014;11(10):3515-27.

348. Burgess A, Rasouli M, Rogers S. Stressing mitosis to death. Frontiers in Oncology. 2014;4:140.

349. Michel L, Diaz-Rodriguez E, Narayan G, Hernando E, Murty VV, Benezra R. Complete loss of the tumor suppressor MAD2 causes premature cyclin B degradation and mitotic failure in human somatic cells. Proceedings of the National Academy of Sciences of the United States of America. 2004;101(13):4459-64.

350. Borna H, Imani S, Iman M, Azimzadeh Jamalkandi S. Therapeutic face of RNAi: in vivo challenges. Expert Opinion on Biological Therapy. 2015;15(2):269-85.

351. Haussecker D. Current issues of RNAi therapeutics delivery and development. Journal of Controlled Release. 2014;195:49-54.

352. Chaturvedi K, Ganguly K, Kulkarni AR, Kulkarni VH, Nadagouda MN, Rudzinski WE, et al. Cyclodextrin-based siRNA delivery nanocarriers: a state-of-the-art review. Expert Opinion on Drug Delivery. 2011;8(11):1455-68.

353. Eloy JO, Petrilli R, Lopez RF, Lee RJ. "Stimuli-responsive nanoparticles for siRNA delivery". Current Pharmaceutical Design. 2015.

354. Hattori Y, Nakamura A, Arai S, Kawano K, Maitani Y, Yonemochi E. siRNA delivery to lung-metastasized tumor by systemic injection with cationic liposomes. Journal of Liposome Research. 2015;25(4):1-8.

355. Kim MJ, Park JS, Lee SJ, Jang J, Park JS, Back SH, et al. Notch1 targeting siRNA delivery nanoparticles for rheumatoid arthritis therapy. Journal of Controlled Release. 2015;216:140-8.

356. Ngamcherdtrakul W, Morry J, Gu S, Castro DJ, Goodyear SM, Sangvanich T, et al. Cationic Polymer Modified Mesoporous Silica Nanoparticles for Targeted SiRNA Delivery to HER2+ Breast Cancer. Advanced Functional Materials. 2015;25(18):2646-59.

357. Yhee JY, Song S, Lee SJ, Park SG, Kim KS, Kim MG, et al. Cancer-targeted MDR-1 siRNA delivery using self-cross-linked glycol chitosan nanoparticles to overcome drug resistance. Journal of Controlled Release. 2015;198:1-9.

358. Zhao Y, Li H, Wu R, Li S, Wang P, Wang H, et al. Antitumor Effects of Oncolytic Adenovirus-Carrying siRNA Targeting Potential Oncogene EphA3. PLoS One. 2015;10(5):e0126726.

359. Andrade F, Antunes F, Nascimento AV, da Silva SB, das Neves J, Ferreira D, et al. Chitosan formulations as carriers for therapeutic proteins. Current Drug Discovery Technologies. 2011;8(3):157-72.

360. Croisier F, Jérôme C. Chitosan-based biomaterials for tissue engineering. European Polymer Journal. 2013;49(4):780-92.

361. Smith J, Wood E, Dornish M. Effect of chitosan on epithelial cell tight junctions. Pharmaceutical Research. 2004;21(1):43-9.

362. Rai M. Natural antimicrobials in food safety and quality: CABI; 2011.

363. Kim S-K. Chitin and chitosan derivatives: Advances in drug discovery and developments: CRC Press; 2013.

364. Lai WF, Lin MC. Nucleic acid delivery with chitosan and its derivatives. Journal of Controlled Release. 2009;134(3):158-68.

365. Nehoff H, Parayath NN, Domanovitch L, Taurin S, Greish K. Nanomedicine for drug targeting: strategies beyond the enhanced permeability and retention effect. International Journal of Nanomedicine. 2014;9:2539-55.

366. Prabhakar U, Maeda H, Jain RK, Sevick-Muraca EM, Zamboni W, Farokhzad OC, et al. Challenges and key considerations of the enhanced permeability and retention effect for nanomedicine drug delivery in oncology. Cancer Research. 2013;73(8):2412-7.

367. Zhong Y, Meng F, Deng C, Zhong Z. Ligand-directed active tumor-targeting polymeric nanoparticles for cancer chemotherapy. Biomacromolecules. 2014;15(6):1955-69.

368. Gaber R, Watermann I, Kugler C, Reinmuth N, Huber RM, Schnabel PA, et al. Correlation of EGFR expression, gene copy number and clinicopathological status in NSCLC. Diagn Pathol. 2014;9:165.

369. Ganta S, Singh A, Patel NR, Cacaccio J, Rawal YH, Davis BJ, et al. Development of EGFR-targeted nanoemulsion for imaging and novel platinum therapy of ovarian cancer. Pharm Res. 2014;31(9):2490-502.

370. Singh A, Xu J, Mattheolabakis G, Amiji M. EGFR-Targeted Gelatin Nanoparticles for Systemic Administration of Gemcitabine in an Orthotopic Pancreatic Cancer Model. Nanomedicine. 2015.

371. Rusnak DW, Alligood KJ, Mullin RJ, Spehar GM, Arenas-Elliott C, Martin AM, et al. Assessment of epidermal growth factor receptor (EGFR, ErbB1) and HER2 (ErbB2) protein

expression levels and response to lapatinib (Tykerb, GW572016) in an expanded panel of human normal and tumour cell lines. Cell Prolif. 2007;40(4):580-94.

372. Turner PV, Brabb T, Pekow C, Vasbinder MA. Administration of substances to laboratory animals: routes of administration and factors to consider. Journal of the American Association for Laboratory Animal Science: JAALAS. 2011;50(5):600.

373. Li J, Makrigiorgos GM. Anti-primer quenching-based real-time PCR for simplex or multiplex DNA quantification and single-nucleotide polymorphism genotyping. Nature protocols. 2007;2(1):50-8.

374. Ganesh S, Iyer AK, Gattacceca F, Morrissey DV, Amiji MM. In vivo biodistribution of siRNA and cisplatin administered using CD44-targeted hyaluronic acid nanoparticles. Journal of Controlled Release. 2013;172(3):699-706.

375. Holder DJ. Comments on Nedelman and Jia's extension of Satterthwaite's approximation applied to pharmacokinetics. J Biopharm Stat. 2001;11(1-2):75-9.

376. Nedelman JR, Jia X. An extension of Satterthwaite's approximation applied to pharmacokinetics. J Biopharm Stat. 1998;8(2):317-28.

377. Kean T, Thanou M. Biodegradation, biodistribution and toxicity of chitosan. Advanced drug delivery reviews. 2010;62(1):3-11.

378. Alexis F, Pridgen E, Molnar LK, Farokhzad OC. Factors affecting the clearance and biodistribution of polymeric nanoparticles. Molecular pharmaceutics. 2008;5(4):505-15.

379. Rao J, Dragulescu-Andrasi A, Yao H. Fluorescence imaging in vivo: recent advances. Curr Opin Biotechnol. 2007;18(1):17-25.

380. Zhang X, Bloch S, Akers W, Achilefu S. Near-infrared molecular probes for in vivo imaging. Curr Protoc Cytom. 2012;Chapter 12:Unit12 27.

381. Yi X, Wang F, Qin W, Yang X, Yuan J. Near-infrared fluorescent probes in cancer imaging and therapy: an emerging field. Int J Nanomedicine. 2014;9:1347-65.

382. Luo S, Zhang E, Su Y, Cheng T, Shi C. A review of NIR dyes in cancer targeting and imaging. Biomaterials. 2011;32(29):7127-38.

383. Qi L, Xu Z. In vivo antitumor activity of chitosan nanoparticles. Bioorganic & Medicinal Chemistry Letters. 2006;16(16):4243-5.

384. Jayakumar R, Muzzarelli R, Prabaharan M. Chitosan for Biomaterials I: Springer-Verlag Berlin Heidelberg; 2011.

385. Wang J, Sui M, Fan W. Nanoparticles for tumor targeted therapies and their pharmacokinetics. Curr Drug Metab. 2010;11(2):129-41.

386. Leucuta SE. Subcellular drug targeting, pharmacokinetics and bioavailability. J Drug Target. 2014;22(2):95-115.

387. Yamashita F, Hashida M. Pharmacokinetic considerations for targeted drug delivery. Advanced drug delivery reviews. 2013;65(1):139-47.

388. Cabral H, Matsumoto Y, Mizuno K, Chen Q, Murakami M, Kimura M, et al. Accumulation of sub-100 nm polymeric micelles in poorly permeable tumours depends on size. Nature Nanotechnology. 2011;6(12):815-23.

389. Choi KY, Min KH, Yoon HY, Kim K, Park JH, Kwon IC, et al. PEGylation of hyaluronic acid nanoparticles improves tumor targetability in vivo. Biomaterials. 2011;32(7):1880-9.

390. Tobin LA, Xie Y, Tsokos M, Chung SI, Merz AA, Arnold MA, et al. Pegylated siRNA-loaded calcium phosphate nanoparticle-driven amplification of cancer cell internalization in vivo. Biomaterials. 2013;34(12):2980-90.

391. Chen S, Yang K, Tuguntaev RG, Mozhi A, Zhang J, Wang PC, et al. Targeting tumor microenvironment with PEG-based amphiphilic nanoparticles to overcome chemoresistance. Nanomedicine: Nanotechnology, Biology and Medicine. 2015.

392. Ganta S, Singh A, Kulkarni P, Keeler AW, Piroyan A, Sawant RR, et al. EGFR Targeted Theranostic Nanoemulsion for Image-Guided Ovarian Cancer Therapy. Pharm Res. 2015;32(8):2753-63.

393. Talekar M, Trivedi M, Shah P, Ouyang Q, Oka A, Gandham S, et al. Combination wt-p53 and MicroRNA-125b Transfection in a Genetically-Engineered Lung Cancer Model using Dual CD44/EGFR Targeting Nanoparticles. Mol Ther. 2015.

394. Siegel RL, Miller KD, Jemal A. Cancer statistics, 2015. CA Cancer J Clin. 2015;65(1):5-29.

395. Torre LA, Bray F, Siegel RL, Ferlay J, Lortet-Tieulent J, Jemal A. Global cancer statistics, 2012. CA Cancer J Clin. 2015;65(2):87-108.

396. Du L, Morgensztern D. Chemotherapy for Advanced-Stage Non-Small Cell Lung Cancer. Cancer J. 2015;21(5):366-70.

397. Smit E, Moro-Sibilot D, de Castro Carpeño J, Lesniewski-Kmak K, Aerts J, Villatoro R, et al. Cisplatin and carboplatin-based chemotherapy in the first-line treatment of non-small cell lung cancer: analysis from the European FRAME study. Lung Cancer. 2015.

398. Dasari S, Tchounwou PB. Cisplatin in cancer therapy: molecular mechanisms of action. Eur J Pharmacol. 2014;740:364-78.

399. Mueller S, Schittenhelm M, Honecker F, Malenke E, Lauber K, Wesselborg S, et al. Cell-cycle progression and response of germ cell

tumors to cisplatin in vitro. Int J Oncol. 2006;29(2):471-9.

400. Wang D, Lippard SJ. Cellular processing of platinum anticancer drugs. Nat Rev Drug Discov. 2005;4(4):307-20.

401. Lawrence KS, Chau T, Engebrecht J. DNA damage response and spindle assembly checkpoint function throughout the cell cycle to ensure genomic integrity. PLoS Genet. 2015;11(4):e1005150.

402. Galluzzi L, Vitale I, Michels J, Brenner C, Szabadkai G, Harel-Bellan A, et al. Systems biology of cisplatin resistance: past, present and future. Cell Death Dis. 2014;5:e1257.

403. More SS, Akil O, Ianculescu AG, Geier EG, Lustig LR, Giacomini KM. Role of the copper transporter, CTR1, in platinum-induced ototoxicity. J Neurosci. 2010;30(28):9500-9.

404. Sancho-Martinez SM, Prieto-Garcia L, Prieto M, Lopez-Novoa JM, Lopez-Hernandez FJ. Subcellular targets of cisplatin cytotoxicity: an integrated view. Pharmacol Ther. 2012;136(1):35-55.

405. Gao Y, Shen JK, Milane L, Hornicek FJ, Amiji MM, Duan Z. Targeted cancer therapy; nanotechnology approaches for overcoming drug resistance. Curr Med Chem. 2015;22(11):1335-47.

406. Amer MH. Gene therapy for cancer: present status and future perspective. Mol Cell Ther. 2014;2:27.

407. Mc Gee MM. Targeting the Mitotic Catastrophe Signaling Pathway in Cancer. Mediators Inflamm. 2015;2015:146282.

408. Choi M, Kim W, Cheon MG, Lee CW, Kim JE. Polo-like kinase 1 inhibitor BI2536 causes mitotic catastrophe following activation of the spindle assembly checkpoint in non-small cell lung cancer cells. Cancer Lett. 2015;357(2):591-601.

409. Dotiwala F, Harrison JC, Jain S, Sugawara N, Haber JE. Mad2 prolongs DNA damage checkpoint arrest caused by a double-strand break via a centromere-dependent mechanism. Curr Biol. 2010;20(4):328-32.

410. Magiera MM, Gueydon E, Schwob E. DNA replication and spindle checkpoints cooperate during S phase to delay mitosis and preserve genome integrity. J Cell Biol. 2014;204(2):165-75.

411. Shi Q, Hu M, Luo M, Liu Q, Jiang F, Zhang Y, et al. Reduced expression of Mad2 and Bub1 proteins is associated with spontaneous miscarriages. Mol Hum Reprod. 2011;17(1):14-21.

412. Castedo M, Perfettini JL, Roumier T, Andreau K, Medema R, Kroemer G. Cell death by mitotic catastrophe: a molecular definition. Oncogene. 2004;23(16):2825-37.

413. Floor SL, Dumont JE, Maenhaut C, Raspe E. Hallmarks of cancer: of all cancer cells, all the time? Trends Mol Med. 2012;18(9):509-15.

414. Deng Y, Wang CC, Choy KW, Du Q, Chen J, Wang Q, et al. Therapeutic potentials of gene silencing by RNA interference: principles, challenges, and new strategies. Gene. 2014;538(2):217-27.

415. Miele E, Spinelli GP, Miele E, Di Fabrizio E, Ferretti E, Tomao S, et al. Nanoparticle-based delivery of small interfering RNA: challenges for cancer therapy. Int J Nanomedicine. 2012;7:3637-57.

416. Akhtar S, Benter IF. Nonviral delivery of synthetic siRNAs in vivo. J Clin Invest. 2007;117(12):3623-32.

417. Rudzinski WE, Aminabhavi TM. Chitosan as a carrier for targeted delivery of small interfering RNA. International journal of pharmaceutics. 2010;399(1):1-11.

418. Nascimento AV, Singh A, Bousbaa H, Ferreira D, Sarmento B, Amiji MM. Combinatorial-Designed Epidermal Growth Factor Receptor-Targeted Chitosan Nanoparticles for Encapsulation and Delivery of Lipid-Modified Platinum Derivatives in Wild-Type and Resistant Non-Small-Cell Lung Cancer Cells. Mol Pharm. 2015.

419. Andersen MO, Howard KA, Kjems J. RNAi using a chitosan/siRNA nanoparticle system: in vitro and in vivo applications. Methods Mol Biol. 2009;555:77-86.

420. Gref R, Lück M, Quellec P, Marchand M, Dellacherie E, Harnisch S, et al. 'Stealth'corona-core nanoparticles surface modified by polyethylene glycol (PEG): influences of the corona (PEG chain length and surface density) and of the core composition on phagocytic uptake and plasma protein adsorption. Colloids and Surfaces B: Biointerfaces. 2000;18(3):301-13.

421. Tiera MJ, Shi Q, Barbosa HF, Fernandes JC. Polymeric systems as nanodevices for siRNA delivery. Curr Gene Ther. 2013;13(5):358-69.

422. O'Grady S, Finn SP, Cuffe S, Richard DJ, O'Byrne KJ, Barr MP. The role of DNA repair pathways in cisplatin resistant lung cancer. Cancer treatment reviews. 2014;40(10):1161-70.

423. Galluzzi L, Senovilla L, Vitale I, Michels J, Martins I, Kepp O, et al. Molecular mechanisms of cisplatin resistance. Oncogene. 2012;31(15):1869-83.

424. Tao W. The mitotic checkpoint in cancer therapy. Cell Cycle. 2005;4(11):1495-9.

425. Zhong H, Simons JW. Direct comparison of GAPDH, β-actin, cyclophilin, and 28S rRNA as internal standards for quantifying RNA levels under hypoxia. Biochemical and biophysical research communications. 1999;259(3):523-6.

426. Radonić A, Thulke S, Mackay IM, Landt O, Siegert W, Nitsche A. Guideline to reference gene selection for quantitative real-time PCR. Biochemical and biophysical research communications. 2004;313(4):856-62.

427. Hirsch M, Helm M. Live cell imaging of duplex siRNA intracellular trafficking. Nucleic acids research. 2015;43(9):4650-60.

428. Kalantari R, Chiang C-M, Corey DR. Regulation of mammalian transcription and splicing by Nuclear RNAi. Nucleic Acids Research. 2015:gkv1305.

429. Mathieu A, Remmelink M, D'Haene N, Penant S, Gaussin JF, Van Ginckel R, et al. Development of a chemoresistant orthotopic human nonsmall cell lung carcinoma model in nude mice: analyses of tumor heterogenity in relation to the immunohistochemical levels of expression of cyclooxygenase-2, ornithine decarboxylase, lung-related resistance protein, prostaglandin E synthetase, and glutathione-S-transferase-alpha (GST)-alpha, GST-mu, and GST-pi. Cancer. 2004;101(8):1908-18.

430. Talekar M, Ouyang Q, Goldberg MS, Amiji MM. Cosilencing of PKM-2 and MDR-1 Sensitizes Multidrug-Resistant Ovarian Cancer Cells to Paclitaxel in a Murine Model of Ovarian Cancer. Molecular cancer therapeutics. 2015;14(7):1521-31.

431. Meacham CE, Morrison SJ. Tumour heterogeneity and cancer cell plasticity. Nature. 2013;501(7467):328-37.

432. Lavi O. Redundancy: a critical obstacle to improving cancer therapy. Cancer research. 2015;75(5):808-12.

433. Xu X, Ho W, Zhang X, Bertrand N, Farokhzad O. Cancer nanomedicine: from targeted delivery to combination therapy. Trends in molecular medicine. 2015;21(4):223-32.

434. Deng X, Cao M, Zhang J, Hu K, Yin Z, Zhou Z, et al. Hyaluronic acid-chitosan nanoparticles for co-delivery of MiR-34a and doxorubicin in therapy against triple negative breast cancer. Biomaterials. 2014;35(14):4333-44.

435. Jia F, Liu X, Li L, Mallapragada S, Narasimhan B, Wang Q. Multifunctional nanoparticles for targeted delivery of immune activating and cancer therapeutic agents. Journal of controlled release : official journal of the Controlled Release Society. 2013;172(3):1020-34.

436. Singh A, Talekar M, Tran T-H, Samanta A, Sundaram R, Amiji M. Combinatorial approach in the design of multifunctional polymeric nano-delivery systems for cancer therapy. J Mater Chem B. 2014;2(46):8069-84.

437. Mukerjee A, Ranjan AP, Vishwanatha JK. Combinatorial nanoparticles for cancer diagnosis and therapy. Current medicinal chemistry. 2012;19(22):3714-21.

438. Andrade F, Goycoolea F, Chiappetta DA, das Neves J, Sosnik A, Sarmento B. Chitosan-grafted copolymers and chitosan-ligand conjugates as matrices for pulmonary drug delivery. International Journal of Carbohydrate Chemistry. 2011;2011.

439. Alves NM, Mano JF. Chitosan derivatives obtained by chemical modifications for biomedical and environmental applications. International journal of biological macromolecules. 2008;43(5):401-14.

440. Prabaharan M. Review paper: chitosan derivatives as promising materials for controlled drug delivery. Journal of biomaterials applications. 2008;23(1):5-36.

441. Cai K, Liu W, Li F, Yao K, Yang Z, Li X, et al. Modulation of osteoblast function using poly (D, L-lactic acid) surfaces modified with alkylation derivative of chitosan. Journal of Biomaterials Science, Polymer Edition. 2002;13(1):53-66.

442. Martel B, Devassine M, Crini G, Weltrowski M, Bourdonneau M, Morcellet M. Preparation and sorption properties of a β-cyclodextrin-linked chitosan derivative. Journal of Polymer Science Part A: Polymer Chemistry. 2001;39(1):169-76.

443. Ganta S, Singh A, Rawal Y, Cacaccio J, Patel NR, Kulkarni P, et al. Formulation development of a novel targeted theranostic nanoemulsion of docetaxel to overcome multidrug resistance in ovarian cancer. Drug delivery. 2014:1-13.

444. Rieter WJ, Pott KM, Taylor KM, Lin W. Nanoscale coordination polymers for platinum-based anticancer drug delivery. Journal of the American Chemical Society. 2008;130(35):11584-5.

445. Dhar S, Gu FX, Langer R, Farokhzad OC, Lippard SJ. Targeted delivery of cisplatin to prostate cancer cells by aptamer functionalized Pt(IV) prodrug-PLGA-PEG nanoparticles. Proceedings of the National Academy of Sciences of the United States of America. 2008;105(45):17356-61.

446. Banerjee SS, Aher N, Patil R, Khandare J. Poly(ethylene glycol)-Prodrug Conjugates: Concept, Design, and Applications. Journal of drug delivery. 2012;2012:103973.

447. Ali Khan SR, Huang S, Shamsuddin S, Inutsuka S, Whitmire KH, Siddik ZH, et al. Synthesis, characterization and cytotoxicity of new platinum(IV) axial carboxylate complexes: crystal structure of potential antitumor agent [PtIV(trans-1R,2R-diaminocyclohexane)trans(acetate)2Cl2]. Bioorg Med Chem. 2000;8(3):515-21.

448. Khokhar AR, Deng Y, Kido Y, Siddik ZH. Preparation, characterization, and antitumor activity of new ethylenediamine platinum(IV) complexes containing mixed carboxylate ligands. J Inorg Biochem. 1993;50(2):79-87.

449. Black PN, DiRusso CC. Transmembrane movement of exogenous long-chain fatty acids: proteins, enzymes, and vectorial esterification. Microbiology and molecular biology reviews : MMBR. 2003;67(3):454-72, table of contents.

450. Baldrick P. The safety of chitosan as a pharmaceutical excipient. Regulatory toxicology and pharmacology : RTP. 2010;56(3):290-9.

451. Son YJ, Jang JS, Cho YW, Chung H, Park RW, Kwon IC, et al. Biodistribution and anti-tumor efficacy of doxorubicin loaded glycol-chitosan nanoaggregates by EPR effect. Journal of controlled release : official journal of the Controlled Release Society. 2003;91(1-2):135-45.

452. Porter AG, Janicke RU. Emerging roles of caspase-3 in apoptosis. Cell Death Differ. 1999;6(2):99-104.

453. Vermes I, Haanen C, Steffens-Nakken H, Reutelingsperger C. A novel assay for apoptosis. Flow cytometric detection of phosphatidylserine expression on early apoptotic cells using fluorescein labelled Annexin V. Journal of immunological methods. 1995;184(1):39-51.

454. Eljack ND, Ma HY, Drucker J, Shen C, Hambley TW, New EJ, et al. Mechanisms of cell uptake and toxicity of the anticancer drug cisplatin. Metallomics : integrated biometal science. 2014;6(11):2126-33.

455. Jemal A, Center MM, DeSantis C, Ward EM. Global patterns of cancer incidence and mortality rates and trends. Cancer epidemiology, biomarkers & prevention : a publication of the American Association for Cancer Research, cosponsored by the American Society of Preventive Oncology. 2010;19(8):1893-907.

456. Dass CR, Choong PF. The use of chitosan formulations in cancer therapy. J Microencapsul. 2008;25(4):275-9.